

SEMI-ACTIVE CONTROL OF POST-TENSIONED STEEL FRAMES



by

Yasser Eljajeh

**A thesis submitted to
the Faculty of Engineering
of The University of Sheffield
in partial fulfilment of the requirements for
the degree of Doctor of Philosophy**



Department of Civil and Structural Engineering
THE UNIVERSITY OF SHEFFIELD

October 2013

Copyright © 2013

بِسْمِ اللَّهِ الرَّحْمَنِ الرَّحِيمِ

أَفْرَأُ بِاسْمِ رَبِّكَ الَّذِي خَلَقَ * خَلَقَ الْإِنْسَانَ مِنْ عَلَقٍ * أَفْرَأُ وَرَبُّكَ الْأَكْرَمُ * الَّذِي عَلَّمَ بِالْقَلَمِ * عَلَّمَ
* الْإِنْسَانَ مَا لَمْ يَعْلَمْ

سورة العلق (1-5)

TO

MY MOTHER

For being the light of my life ...

&

MY WIFE

As a humble way to express my love ...

ABSTRACT

After the Northridge 1994 earthquake it was found that failures in steel frame buildings were mainly concentrated in beam-column connections. This prompted researchers to work on improvements, mainly focussed on increasing the rotational ductility capacity in connections. Most of these improvements however did not eliminate the residual deformations in the connections. To overcome this weakness, researchers introduced post-tensioned steel connections, composed of post-tensioned steel strands and energy dissipating devices.

In this research, a single-element model of post-tensioned connection was developed and incorporated in a new computer program for non-linear dynamic frame analysis, which was then used to investigate the effects of the level of post-tensioning forces on seismic behaviour of frame buildings. When used in moment resisting frames, post-tensioned connections reduce residual displacements and prevent development of plastic hinges in the beams. The initial stiffness of post-tensioned frames is also similar to conventional moment resisting frames but their energy dissipation capacity is lower. The performance of the structure is sensitive to the level of post-tensioning forces, and in some cases the use of post-tensioned connections leads to increased displacements. The aim of this research was to investigate semi-active control of the post-tensioning forces as an approach for improving the seismic behaviour of multi-storey steel frame buildings.

Three control approaches were proposed to improve the dynamic behaviour of post-tensioned frames: (i) energy dissipation approach which aims to increase the energy dissipation capacity of the frame, (ii) stiffness control approach which aims to change the frequency of the frame by softening or stiffening to avoid excitation by major frequency components of the earthquake and (iii) deformation regulation approach which aims to improve the distribution of deformations along the height of the frame.

The three control approaches showed different results. Increasing energy dissipation in the connections is not an efficient approach for reducing the frame response, especially when large displacements occur in the early stages of loading. The stiffness control approach showed good performance, reducing both floor displacements and force demand on the elements. The deformation regulation approach also improved the response, providing more uniform inter-storey drift distribution. In general, the research presented here shows that semi-active control can be used to improve the seismic performance of post-tensioned steel frames.

ACKNOWLEDGEMENTS

First, I would like to express my deepest and sincere gratitude to my supervisor Dr Mihail Petkovski. His directions, support and encouragement were key reasons of completing this work.

Also, I would like to thank Prof Muhammad Al-Samara from Damascus University for his continuous help and interest in my work.

I am grateful to all my family members, especially my parents, whose support pushed me to work hard. Without their prayers and encouragement, this work would have never finished.

I want to thank all my friends for their valuable support during my studies and most importantly for their priceless friendship.

I would like also to thank my friends in the Concrete and Earthquake Engineering research group at the University of Sheffield for their help and friendly atmosphere.

Finally, I would like to express my deepest gratitude and appreciation to the people of my beloved home Syria. Their heroism and firmness were a big inspiration to me even in difficult times of my work.

TABLE OF CONTENT

ABSTRACT	I
ACKNOWLEDGMENTS	II
TABLE OF CONTENT	III
LIST OF FIGURES	IX
LIST OF TABLES	XXI
LIST OF ABBREVIATIONS	XXIII
LIST OF SYMBOLS	XXV

CHAPTER 1: INTRODUCTION

1.1. Background	1
1.1.1. Conventional Steel Beam-Column Connections	1
1.1.2. Post-Tensioned Steel Beam-Column Connections	2
1.1.3. Behaviour of Post-tensioned Steel Beam-Column Connections	3
1.1.4. Effects of Post-tensioning Forces	4
1.2. Thesis Overview	5

CHAPTER 2: LITERATURE REVIEW

2.1. Pre-Northridge Beam-Column Connections	8
2.2. Post-Northridge Beam-Column Connections	10
2.2.1. Types of Seismic Upgrades of Steel Structures	10
2.2.2. Prequalified Seismic Resistant Connections	12
2.2.3. Conclusion on Prequalified Seismic Resistant Connections	16
2.3. Self-Centring Systems	16
2.3.1. Introduction to Self-Centring Systems	16
2.3.2. Strategies of Structural Self-Centring	17
2.4. Post-tensioned Steel Beam-Column Connections	20
2.4.1. Introduction to Post-tensioned Steel Beam-Column Connections	20

2.4.2. Types of Post-tensioned Steel Beam-Column Connections -----	23
2.4.3. Advantages and Technical Issues of Post-tensioned Steel Beam Column Connections -----	27
2.4.4. Modelling of Post- tensioned Steel Beam-Column Connections -----	31
2.4.5. Design of Post- tensioned Steel Beam-Column Connections -----	33
2.4.6. Parameters Affecting the Behaviour of Steel Beam-Column Post- tensioned Connections -----	34
2.4.7. Conclusions on Post-tensioned Steel Beam-Column Connections ---	38
2.5. Semi-Active Control -----	41
2.5.1. Introduction to Structural Control -----	41
2.5.2. Review of Semi-Active Control for Seismic Protection -----	43
2.5.3. Concluding Remarks on Semi-Active Control -----	50
2.6. Concluding Remarks on Literature Review-----	53

CHAPTER 3: AIMS, OBJECTIVES AND METHODOLOGY OF RESEARCH

3.1. Aims and Objectives -----	54
3.2. Methodology of the Research -----	54
3.2.1. Modelling of a Stand-alone Post-tensioned Connection -----	55
3.2.2. Developing Structural Analysis Program to Incorporate the Connection Model -----	55
3.2.3. Studying Parameters Affecting the Connection and the Passive PT Frame Behaviour -----	56
3.2.4. Developing Semi-Active Control Strategies -----	56
3.2.5. Investigating the Efficiency of the Developed Control Algorithms --	57

CHAPTER 4: PROGRAM FOR 2D FRAME ANALYSIS WITH SEMI- ACTIVE CONTROL (FASAC-2D)

4.1. Operation of FASAC-2D -----	59
4.1.1. Static Analysis in FASAC-2D -----	59
4.1.2. Dynamic Analysis in FASAC-2D -----	60
4.2. Structural Elements in FASAC-2D -----	61
4.2.1. Element 1: Beam-Column Element -----	61

4.2.2. Element 2: Bar Element -----	63
4.2.3. Element 3: Post-tensioned Connection Element -----	65
4.2.4. Element 6: Simple Connection Element -----	65
4.3. Verification of FASAC-2D Results -----	66
4.4. Concluding Remarks on FASAC-2D -----	67

CHAPTER 5: MODELLING, INCORPORATION AND DETAILS OF PT CONNECTION

5.1. Modelling of Standalone Post-tensioned Steel Beam-Column Connection	68
5.1.1. Moment Rotation Relationship -----	68
5.1.2. Transition between Different Stiffness Values of the Post-tensioned Connection Model -----	75
5.1.3. Verification of the Integrated Post-tensioned Connection (IPTC) Model using the Discrete Springs Model -----	75
5.2. Incorporating the Standalone Post-tensioned Connection Model into a 2D Steel Frame -----	76
5.2.1. Geometry and Input Data for Incorporated Post-tensioned Connection (IPTC) Element -----	76
5.2.2. Operation of the Post-tensioned Connection Element incorporated in the frame -----	77
5.2.3. Simulation of dynamic response of post-tensioned steel frame using the IPTC model -----	80
5.3. Connection Details and Application of Semi-active Control on Post-tensioned Steel Frames -----	85
5.3.1. Post-tensioned Connection Details for Passive System -----	85
5.3.2. Application of Semi-active Control on Post-tensioned Steel Frames	87
5.4. Concluding Remarks on Modelling, Incorporation and Details of PT Connection -----	89

CHAPTER 6: CHARACTERISTICS AND DYNAMIC BEHAVIOUR OF PASSIVE POST-TENSIONED STEEL FRAMES

6.1. Effect of Connection Parameters on the Connection Behaviour -----	90
--	----

6.1.1. Rotational Ductility Capacity and Energy Dissipation Capacity -----	91
6.1.2. Ultimate Moment Capacity -----	94
6.1.3. Self-Centring Capacity -----	95
6.1.4. Optimum Ranges of Values for the Connection Parameters in Passively Controlled Post-tensioned Connections -----	96
6.2. Effect of Connection Parameters on the Dynamic Behaviour of Post- tensioned Steel Frames -----	97
6.2.1. Push-over Analyses -----	98
6.2.2. Non-linear Dynamic Analyses-----	100
6.3. Optimal Level of Post-tensioning Forces -----	106
6.4. Conventional MRF Vs. Post-tensioned MRF -----	108
6.4.1. Push-over Analyses -----	108
6.4.2. Dynamic Non-linear Analyses -----	109
6.5. Concluding Remarks on Characteristics and Dynamic Behaviour of Passive PT Frames -----	113

CHAPTER 7: SEMI-ACTIVE CONTROL OF PT FRAMES USING ENERGY DISSIPATION APPROACH

7.1. Introductory Remarks -----	114
7.2. Basics of Energy Dissipation Control Approach -----	115
7.3. Deformation-Based Loading Direction Feedback Algorithm (LDFA) -----	116
7.3.1. Operation of the Deformation-Based LDFA -----	117
7.3.2. Results of Deformation-Based Loading Direction Feedback Control Algorithm -----	117
7.3.3. Disadvantages of the LDFA -----	128
7.3.4. Modified DB-LDFA (MDB-LDFA) -----	131
7.4. Velocity-Based Loading Direction Feedback Control Algorithm -----	133
7.4.1. Operation of the <i>VB-LDFA</i> -----	133
7.4.2. Results of the <i>VB-LDFA</i> -----	134
7.5. Concluding Remarks on Energy Dissipation Approach -----	138

CHAPTER 8: SEMI-ACTIVE CONTROL OF PT FRAMES USING STIFFNESS CONTROL APPROACH

8.1. Basics of Stiffness Control Approach ----- 140

8.2. Excitation Frequency State Feedback Control Algorithm (EFSFA) ----- 141

 8.2.1. Operation of the Control Algorithm ----- 141

 8.2.2. Results of the Control Algorithm ----- 145

8.3. Response Frequency State Feedback Algorithm (RFSFA) ----- 156

 8.3.1. Concept and Operation of the RFSFA ----- 156

 8.3.2. Results of the RFSFA ----- 159

8.4. Filtered Excitation Frequency State Feedback Algorithm (FEFSFA) ----- 161

 8.4.1. Changes from the EFSFA ----- 161

 8.4.2. Results of the FEFSFA ----- 163

8.5. Stiffness Control Approach using Active Variable Stiffness System ----- 166

8.6. Centralisation of Stiffness-Based Control Algorithms ----- 167

8.7. Concluding Remarks on Stiffness Control Approach ----- 169

CHAPTER 9: SEMI-ACTIVE CONTROL OF PT FRAMES USING DEFORMATION REGULATION CONTROL APPROACH

9.1. Basics of the Deformation Regulation Control Approach ----- 171

9.2. Uniform Inter-Storey Drift Algorithm (UIDA) ----- 172

 9.2.1. Operation of the Control Algorithm ----- 172

 9.2.2. Results of the UIDA ----- 173

 9.2.3. Effect of the Drift Threshold on the Algorithm Performance ----- 178

 9.2.4. Centralisation of Control Forces in UIDA ----- 180

 9.2.5. Development of PT forces in UIDA ----- 181

9.3. Simplified Uniform Inter-Storey Drift Algorithm (LUIDA) ----- 182

 9.3.1. Operation of the SUIDA ----- 183

 9.3.2. Results of the of the SUIDA ----- 183

9.4. Concluding Remarks on Deformation Regulation Approach ----- 187

CHAPTER 10: Summary, Conclusions and Recommendations for Future Work

10.1. Summary of Results ----- 188

10.1.1. Summary of Work on Passively Controlled PT Frames -----	188
10.1.2. Summary of Results of Semi-Active Control of PT Frames -----	190
10.2. Conclusions -----	197
10.3. Recommendations for Future Work -----	199
REFERENCES -----	201
APPENDIX A	
FASAC V2.5: FRAME ANALYSIS WITH SEMI-ACTIVE CONTROL- GUIDANCE OF INPUT FILE -----	211
APPENDIX B	
MATLAB SCRIPTS OF CONTROL ALGORITHMS -----	218
APPENDIX C	
ACCELERATION RESPONSE OF CONTROLLED PT FRAMES -----	226

LIST OF FIGURES

Figure 1.1	Solutions proposed to enhance the moment beam-column connection: (a) reduced beam section, (b) added haunches or brackets, (c) T-stubs solution and (d) proprietary side plate connection (FEMA 351, 2000). -----	2
Figure 1.2	Yield-based steel post-tensioned beam-column connections: (a) energy dissipating bars, and (b) top and seat angles (Bruneau M, 2004). -----	2
Figure 1.3	Post-tensioned connections with friction damper (Rojas et al. 2004). -----	3
Figure 1.4	Hysteretic model for post-tensioned connection with energy dissipating bars (Christopoulos et al. 2002): (a) post-tensioned strands, (b) energy dissipating bars and (c) post-tensioned connection (combined action). -----	3
Figure 1.5	Illustration of the full self-centring requirement: (a) sufficient post-tensioning forces and (b) insufficient post-tensioning forces. -----	5
Figure 2.1	Details of early beam-column connections: (a) pinned connection and (b) rigid connection (FEMA 351, 2000). -----	9
Figure 2.2	Pre-Northridge welded-flange-bolted-web connection detail (FEMA 351, 2000). -----	9
Figure 2.3	Post-Northridge recommendations for plastic hinge location in the beam span (FEMA 351, 2000). -----	11
Figure 2.4	Moment rotation relationship of improved welded unreinforced flange connection (FEMA 355D, 2000). -----	12
Figure 2.5	Reduced beam section connection (RBS): (a) connection arrangement and (b) moment-rotation relationship (FEMA 355D, 2000). -----	13
Figure 2.6	Welded top and bottom haunch connection: (a) connection arrangement and (b) moment-rotation relationship (FEMA 355D, 2000). -----	13
Figure 2.7	Welded cover plate flange connection: (a) connection arrangement (FEMA 355D, 2000) and (b) moment-rotation relationship (Engelhardt and Sabol, 1998). -----	14

Figure 2.8	Typical bolted flange plate (BFP) connection: (a) connection arrangement and (b) moment-rotation relationship (FEMA 355D, 2000). -----	15
Figure 2.9	Proprietary side-plate connection (SP): (a) connection arrangement (Houghton, 1997) and (b) moment-rotation relationship (Deylami and Shiravand, 2004). -----	15
Figure 2.10	Idealised pseudo-force–displacement relationship for flag-shape hysteresis (Christopoulos, 2004): α : Post-yielding stiffness ratio, β : energy dissipation factor, x_y : yielding displacement, and f_y : yielding force. -----	17
Figure 2.11	Nickel-Titanium self-centring bracing device (Speicher et a. 2009): (a) internal view and (b) F- Δ response of the device. -----	18
Figure 2.12	Comparison of hysteresis for initial and heated retested beam-column connections with SMA bars (Ocel et al. 2004). -----	18
Figure 2.13	Embodiment of self-centring energy dissipating (SCED) system with steel tubes, tendons, and friction dissipative mechanism (Christopoulos et al. 2008). -----	19
Figure 2.14	Setup for testing of braced frame incorporating SCED brace (Christopoulos et al. 2008). -----	20
Figure 2.15	Hysteretic behaviour of SCVD (Karavasislis, 2010). -----	20
Figure 2.16	Arrangement of the post-tensioned steel beam-column connection: (a) using energy dissipating bars (Christopoulos et al. 2002 ^a), (b) using top and seat angles (Bruneau, 2004) and (c) friction energy dissipater installed at the beam flange (Rojas et al. 2005). -----	21
Figure 2.17	Post-tensioned connection with friction energy dissipater installed at the beam web (Tsai et al. 2008). -----	22
Figure 2.18	Hysteretic model for post-tensioned connection with energy dissipating bars system (Christopoulos et al. 2002 ^a): (a) post-tensioned strands, (b) energy dissipating bars and (c) post-tensioned connection. -----	22
Figure 2.19	Configuration and gap-opening of post-tensioned connection with energy dissipating bars (Christopoulos et al. 2002 ^a). -----	24
Figure 2.20	Behaviour of post-tensioned connection with top and seat angles: (a) configuration and decompression (Bruneau, 2004) and (b) moment-rotation behaviour. -----	25
Figure 2.21	Moment-rotation behaviour of post-tensioned friction damped connection (Rojas et al. 2005). -----	26

Figure 2.22	Post-tensioned steel connections with hourglass shape energy dissipater: (a) frame incorporating the proposed PT connection and exterior PT connection details and (b) Geometry of half a WHP, assumed static system, and internal forces diagrams (Vasdravellis et al. 2013 ^a). -----	26
Figure 2.23	Moment-rotation relationship of PT connections with hourglass web pins energy dissipaters (Vasdravellis et al. 2013 ^a). -----	27
Figure 2.24	Elevation of post-tensioned steel frame: (a) not deformed, (b) deformed (Garlock et al. 2007). -----	28
Figure 2.25	(a) Floor inertia forces on building, (b) plan of hypothetical building, (c) deformation of collector beam, (d) interaction of PT frame with gravity system, (e) beam axial forces on each bay, and (f) idealised moment-rotation plot of the connection (Garlock et al. 2007). -----	29
Figure 2.26	Devices for gravity force transfer devices at self-centred moment resistant frame (Swensen, 2008). -----	30
Figure 2.27	Moment-rotation behaviour of post-tensioned connection with bottom flange friction device (Wolski et al. 2009). -----	30
Figure 2.28	Discrete springs model of post-tensioned connection (Ricles et al. 2001; Dobossy et al. 2006). -----	32
Figure 2.29	Representation of the post-tensioned connection elements in the discrete springs model: (a) gap element (Powel, 1993) and (b) top and seat angles.-----	32
Figure 2.30	Rotational springs model (Dobossy et al. 2006). -----	33
Figure 2.31	Post-yielding to pre-yielding stiffness ratio of post-tensioned connection with energy dissipating bars (Wang, 2004). -----	35
Figure 2.32	Full self-centring requirement for post-tensioned connections: (a) sufficient post-tensioning forces and (b) insufficient post-tensioning forces. -----	36
Figure 2.33	Computation of energy dissipation factor for post-tensioned connections with asymmetric hysteresis (Wolski et al. 2009). -----	37
Figure 2.34	Block diagram of open-loop control system. -----	42
Figure 2.35	Block diagram of close-loop control system. -----	43
Figure 2.36	Block diagram of open-close-loop control system. -----	43
Figure 2.37	Stiffness control device tested by Kobori et al. (1993). -----	44
Figure 2.38	Schematic of electro-rheological damper (Markis and McMahon, 1996). -----	45

Figure 2.39	Shear behaviour of electro-rheological material (Bingham material) (Symans and Constantinou, 1999). -----	45
Figure 2.40	Hysteresis loop of idealised coulomb friction damper (Symans and Constantinou, 1999). -----	46
Figure 2.41	Schematic of semi-active fluid viscous damper (Symans and Constantinou, 1995). -----	46
Figure 2.42	Semi-active actuator (Horvat et al. 1983). -----	47
Figure 2.43	Stress-strain curves for the super-elastic behaviour of SMAs at different temperatures (Weber et al. 2006). -----	48
Figure 3.1	Flowchart of the research methodology. -----	55
Figure 3.2	Semi-active control approaches and corresponding affected parameters. -----	57
Figure 4.1	Moment-rotation behaviour of Element 1: beam-column element. -----	62
Figure 4.2	Stiffness matrix of frame element with no plastic hinges. -----	62
Figure 4.3	Stiffness matrix of frame element with plastic hinge at end <i>i</i> only. -----	63
Figure 4.4	Stiffness matrix of frame element with plastic hinge at end <i>j</i> only. -----	63
Figure 4.5	Stiffness matrix of frame element with plastic hinges at both ends. -----	62
Figure 4.6	Stiffness matrix of bar element with no plastic hinges. -----	64
Figure 4.7	Geometry and behaviour of simple connection element with different direction code. -----	65
Figure 4.8	Portal frame to verify results of FASAC-2D. -----	66
Figure 4.9	Verification of FASAC-2D results with DRAIN-2DX results. Response to Kobe earthquake record (KOB/NIK000): (a) horizontal displacement of node 3, (b) YieldCode for element 2, at node 3, and (c) moment in element 1, at node 3. -----	67
Figure 4.10	Verification of FASAC-2D results with DRAIN-2DX results. Response to Northridge earthquake record (NORTHR/HOS090): (a) horizontal displacement of node 3, (b) YieldCode for element 2, at node 3, and (c) moment in element 1, at node 3. -----	67
Figure 5.1	Moment-rotation relationship of post-tensioned connections: (a) real connection and (b) connection model. -----	69
Figure 5.2	Configuration of post-tensioned connection: (1) post-tensioned strands, (2) energy dissipating bars, (3) shear tab with slotted holes, (4) connection centre of rotation. -----	70

Figure 5.3	Consequences of using finite initial stiffness of the connection: (a) stiffness modification in the gap-opening phase and (b) keeping the same stiffness and carrying the moment error. -----	71
Figure 5.4	Response of post-tensioned connection model for different initial stiffness. ----	71
Figure 5.5	Modelling of the inelastic phase of the post-tensioned connection. -----	72
Figure 5.6	Determining of self-centring angles for positive rotations: (a) $M_{y-new} \leq M_y + M_{Ed}$ and (b) $M_{y-new} > M_y + M_{Ed}$. -----	74
Figure 5.7	Flowchart of modelling the post-tensioned connection element. -----	74
Figure 5.8	(a) Moment calculations when stiffness is changed and (b) points of changing stiffness in the IPTC Model. -----	75
Figure 5.9	Verification of the IPTC model using the discrete springs model. -----	76
Figure 5.10	Schematic of the IPTC element in frame model. -----	77
Figure 5.11	Moment calculation in the connection element: (a) first iteration, (b) second iteration, and (c) flowchart of moment calculation within the time-step. -----	79
Figure 5.12	Post-tensioned connection element in FASAC-2D: (a) undeformed shape, (b) deformed shape and internal displacements, and (c) internal forces.-----	80
Figure 5.13	Model of the portal frame equipped with post-tensioned steel beam-column connections. -----	80
Figure 5.14	Moment-rotation response of the connection element No.1, under four different seismic excitations. -----	81
Figure 5.15	Time history of <code>YieldCode</code> of connection element No.1 for SMART1 earthquake: 0= no gap opening, 1 = gap opening and elastic loading unloading, 2= gap opening and inelastic loading-unloading. -----	81
Figure 5.16	Horizontal displacements of conventional frame and frame with the IPTC (Input: SMART1). -----	82
Figure 5.17	Connection moment compared to column moment. -----	82
Figure 5.18	Error of connection moment when introducing viscous damping to the connection element. -----	83
Figure 5.19	Step-by-step development of damping forces in the IPTC model if $\beta \neq 0$. -----	83
Figure 5.20	Strands deformations due to connection rotation: (a) positive rotation and (b) negative rotation. -----	83
Figure 5.21	Calculation of the tension forces in strands for positive and negative connection rotations. -----	84

Figure 5.22	Tension forces in the strands for SMART1 earthquake. -----	84
Figure 5.23	Illustration of the contact area between the beam and the column in steel post-tensioned beam-column connections: (a) no gap opening and (b) gap opening. -----	86
Figure 5.24	Brass layers in friction-based energy dissipating connections. -----	86
Figure 5.25	Geometry of slotted bolt holes for steel post-tensioned beam-column connections: (a) complete detail and (b) detail of the slotted holes. -----	87
Figure 5.26	Arrangement of external post-tensioned connection equipped for controlling the strands forces. -----	88
Figure 5.27	Arrangement of the master connection and other connections in one storey. ---	88
Figure 6.1	(a) Geometry of post-tensioned connection, (b) loading time history. -----	91
Figure 6.2	Relationship between post-tensioning force (F_{pt}) and energy dissipation factor (β). -----	91
Figure 6.3	Relationship between rotational ductility capacity (μ) and post-tensioning force (F_{pt}). -----	92
Figure 6.4	Relationship between energy dissipation factor (β) and rotational ductility (μ). -----	93
Figure 6.5	Relationship between post-tensioning force (F_{pt}) and normalised energy dissipation capacity (E/E_{max}). -----	94
Figure 6.6	Relationship between the post-tensioning force (F_{pt}) and the ultimate moment capacity of the connection ($M_u/M_{u,max}$). -----	94
Figure 6.7	Behaviour of the post-tensioned connection with energy dissipating bars: (a) sufficient self-centring forces, (b) insufficient self-centring forces. -----	95
Figure 6.8	Derivation of full self-centring requirement of post-tensioned connections with friction energy dissipaters: (a) sufficient self-centring forces, (b) insufficient self-centring forces. -----	96
Figure 6.9	Investigation of post-tensioned steel frame: (a) frame geometry and sections, and (b) idealised model of the frame. -----	98
Figure 6.10	Push-over curves of post-tensioned frame at different levels of post-tensioning: F : base shear, W : weight of the structure, h : height of the frame and Δ : lateral displacement of the top storey. -----	99
Figure 6.11	Ductility of the frame at different levels of initial post-tensioning. -----	100
Figure 6.12	Selected earthquake excitations: (a) acceleration time histories and (b) response spectra of scaled earthquake records. -----	101

Figure 6.13	Effects of variation in post-tensioning forces on frame response at low post-tensioning force. (a) Normalised maximum 3 rd storey displacement, (b) normalised SRSS of 3 rd Storey displacement and (c) normalised residual 3 rd storey displacement. -----	103
Figure 6.14	High residual displacement due to low post-tensioning forces. -----	104
Figure 6.15	Rotations of beams due to columns rotations: (a) conventional MRF and (b) post-tensioned MRF. -----	104
Figure 6.16	Effects of variation in post-tensioning forces on frame response at higher post-tensioning forces: (a) normalised maximum 3 rd storey displacement, (b) normalised SRSS of 3 rd Storey displacement and (c) normalised residual 3 rd storey displacement. -----	105
Figure 6.17	Effect of post-tensioning forces on frame characteristics: (a) secant stiffness of the frame and (b) normalised energy dissipation capacity (E/E_{max}): F : base shear, W : weight of the structure, h : height of the frame and Δ : lateral displacement of the top storey. -----	105
Figure 6.18	Frame response with optimised forces (Input: Mexico City earthquake): (a) top storey displacements and (b) optimum forces time history. -----	107
Figure 6.19	Top storey displacement time histories. -----	107
Figure 6.20	Push-over curves of post-tensioned and conventional frames. -----	109
Figure 6.21	Comparison of top storey displacement for PT frame and conventional MRF. -	110
Figure 6.22	Moment-rotation relationship in PT frame and conventional MRF. -----	111
Figure 6.23	Normalised dissipated energy in PT frame and conventional MRF. -----	111
Figure 6.24	Calculation of dissipated energy: (a) loading phase, (b) unloading phase and (c) schematic time-history. -----	112
Figure 6.25	Effect of post-tensioning force on the frame stiffness during earthquakes. ----	112
Figure 7.1	Modification of $M-\theta$ relationship due to varying post-tensioning forces: (a) $M-\theta$ response with constant PT forces, (b) change in $M-\theta$ response with change of PT forces, and (c) $M-\theta$ response when strands forces are reduced. -----	116
Figure 7.2	Flowchart of the displacement-based $LDFA$. -----	118
Figure 7.3	Three-storey two-bay post-tensioned steel frame. -----	118
Figure 7.4	Top storey displacement time histories. -----	120
Figure 7.5	Energy dissipated through post-tensioned connections. -----	121

Figure 7.6	Details of behaviour of controlled frames with lower total energy dissipation than passive frame: (a) displacements in late stages of loading and (b) energy dissipation in early stages of loading. -----	121
Figure 7.7	Moment-rotation relationships of the master connection of the first storey: (a) complete loop and (b) zoom in. -----	123
Figure 7.8	Inability of the controlled connection to restore initial M_{St} : (a) M_{St} full time-history and (b) zoom into M_{St} time-history. -----	124
Figure 7.9	Artificial earthquake time-histories: (a) low frequency earthquake (0.1 Hz) and (b) high frequency earthquake (3.0 Hz). -----	124
Figure 7.10	Moment-rotation relationships of the master connection of the first storey under artificial earthquakes: (a) low frequency earthquake and (b) high frequency earthquake. -----	124
Figure 7.11	Effect of control force rate on frame behaviour: (a) maximum top storey displacement, (b) SRSS of top storey displacement and (c) energy dissipation in connections. -----	125
Figure 7.12	Best results of the <i>DB-LDFA</i> when $(\Delta f/\Delta t) \neq 0.125 (\Delta f/\Delta t)_{max}$. -----	126
Figure 7.13	<i>LDFA</i> control forces time histories: (a) Northridge 1994 and (b) Kobe 1995. --	127
Figure 7.14	Operation of the <i>LDFA</i> as MIMO system. -----	128
Figure 7.15	Matching scaled records to an elastic response spectrum of Eurocode 8. -----	129
Figure 7.16	Required time for restoring initial PT force: (a) connection moment time-history and (b) finding t_{sci} at each point. -----	129
Figure 7.17	Behaviour of connection with large rate of control force increments: (a) moment-rotation relationship and (b) Variation of normalised M_{st} with loading cycles. -----	130
Figure 7.18	Flowchart of the modified displacement-based <i>LDFA</i> . -----	131
Figure 7.19	PT frame response with <i>DB-LDFA</i> and <i>MDB-LDFA</i> . -----	132
Figure 7.20	Increased energy dissipation in the <i>MDB-LDFA</i> (compared with <i>DB-LDFA</i>). -	132
Figure 7.21	Energy dissipated in frame with <i>DB-LDFA</i> and <i>MDB-LDFA</i> . -----	133
Figure 7.22	Comparison between the deformation-based <i>LDFA</i> and the velocity-based <i>LDFA</i> . -----	134
Figure 7.23	Flowchart of the <i>VB-LDFA</i> . -----	134
Figure 7.24	Comparison of the PT frames response with velocity and displacement-based <i>LDFA</i> . -----	135

Figure 7.25	Energy dissipation time-history. -----	136
Figure 7.26	Moment-rotation relationships of the master connection of the first storey: (a) complete loop and (b) zoom in. -----	137
Figure 7.27	Loss of energy dissipation in velocity-based <i>LDFA</i> . -----	137
Figure 7.28	Moment reduction and negative stiffness when using the velocity-based <i>LDFA</i> . -----	138
Figure 7.29	Backbone curves for passive and velocity-based <i>LDFA</i> controlled frames. ----	138
Figure 8.1	Stiffness values for post-tensioned connections with different energy dissipation mechanisms: (a) friction-based energy dissipation, (b) energy dissipating bars and (c) top and seat energy dissipating angles. -----	141
Figure 8.2	Computation of weighted frequency index for each stiffness pattern from the spectral acceleration diagram. -----	143
Figure 8.3	Repetition of the excitation frequency state feedback algorithm at every control time interval (<i>CtrlTime</i> = 3 sec in this Figure): (a) progress of the ground acceleration record, and (b) spectral acceleration from Fourier transform. -----	144
Figure 8.4	Flowchart of the excitation frequency state feedback control algorithm. -----	145
Figure 8.5	Six-storey post-tensioned steel frame: (a) frame geometry and sections, (b) idealised model of the frame, (c) element and section properties and (d) specifications of rotating motor. -----	146
Figure 8.6	Top storey displacements for passive and <i>EFSSFA</i> -controlled PT frames. -----	147
Figure 8.7	Frequency content of Mexico earthquake with first mode frequency of passive and controlled frames. -----	147
Figure 8.8	Distribution of PT forces in an <i>EFSSFA</i> -controlled frame at the end of the seismic action. -----	148
Figure 8.9	Ranges of frequency for different stiffness patterns and earthquakes. -----	148
Figure 8.10	Top storey displacements for passive frame with high PT forces and <i>EFSSFA</i> -controlled PT frames. -----	149
Figure 8.11	Negative effect of high initial PT forces (Northridge earthquake). -----	150
Figure 8.12	Predominant stiffness patterns of the frame for different earthquakes: (a) finding the predominant stiffness pattern, (b) PT forces of the predominant stiffness pattern and (c) first mode frequency of the predominant stiffness pattern. -----	150

Figure 8.13	Effect of control time interval (<i>CtrlTime</i>) on the <i>EFSFA</i> performance. -----	151
Figure 8.14	Frame response to Landers earthquake for <i>CtrlTime</i> =3.0 sec and <i>CtrlTime</i> =5.0 sec. -----	152
Figure 8.15	Development of the spectral acceleration results for Northridge earthquake. --	154
Figure 8.16	Development of frequency content and PT forces pattern for SMART1 earthquake: (a) earthquake time history, (b) updates of frequency content with time and (c) development of PT forces (actual and target). -----	155
Figure 8.17	Flowchart of the response frequency state feedback control algorithm. -----	157
Figure 8.18	Spectral accelerations of earthquake and response (El Centro). -----	158
Figure 8.19	Frequency content of response acceleration: (a) high effect of second mode and (b) low effect of second mode. -----	159
Figure 8.20	Effect of control time on the <i>RFSFA</i> performance. -----	159
Figure 8.21	Frequency content of input and response accelerations with their final stiffness patterns: (a) Mexico City earthquake and (b) Landers earthquake. -----	160
Figure 8.22	Predominant stiffness patterns of the <i>RFSFA</i> -controlled frame for different earthquakes: (a) finding the predominant stiffness pattern, (b) PT forces of the predominant stiffness pattern and (c) first and second mode frequency of the predominant stiffness pattern. -----	162
Figure 8.23	Design and input data of low-pass filter. -----	163
Figure 8.24	Applying low-pass filter on exciting earthquake (Input: Landers): (a) earthquake time-histories and (b) spectral accelerations. -----	163
Figure 8.25	Flowchart of the filtered excitation frequency state feedback control algorithm. -----	164
Figure 8.26	Effect of control time on the <i>FEFSFA</i> performance. -----	165
Figure 8.27	Similarity in final stiffness pattern between <i>EFSFA</i> and <i>FEFSFA</i> . -----	165
Figure 8.28	Control algorithm proposed by Kobori et al. 1993. -----	166
Figure 8.29	Control effect under the 2 February 1992 earthquake (Kobori et al. 1993). ----	167
Figure 8.30	Centralisation of control forces in stiffness control algorithms: (a) PT forces and switching between k_0 and k_2 and (b) control forces time-histories for the <i>EFSFA</i> (input: Mexico City earthquake). -----	168
Figure 8.31	Operation of stiffness-based control algorithms as SIMO systems. -----	169

Figure 9.1	Illustration of the operation of Uniform Drift Distribution control algorithm (CA1: activation of the algorithm, CA2: new control forces calculated before completion of CA1 sequence). -----	173
Figure 9.2	Flowchart of the uniform inter-storey drift control algorithm. -----	174
Figure 9.3	Top storey displacements for passive and <i>UIDA</i> -controlled PT frames. -----	175
Figure 9.4	Resultant PT forces in <i>UIDA</i> -controlled frame. -----	176
Figure 9.5	Response spectra of Borrego and Mexico City earthquakes. -----	176
Figure 9.6	Top storey displacements for passive frame with high initial PT forces and the <i>UIDA</i> -controlled PT frame. -----	177
Figure 9.7	Standard deviations of the normalised inter-storey drifts. -----	178
Figure 9.8	Effect of the drift threshold on the PT frame response. -----	178
Figure 9.9	Effect of the drift threshold value on resultant PT forces. -----	179
Figure 9.10	Effect of the drift threshold value on the standard deviation of inter-storey drifts. -----	180
Figure 9.11	Control forces in <i>UIDA</i> . -----	181
Figure 9.12	Operation of the <i>UIDA</i> as MIMO systems. -----	181
Figure 9.13	Development of PT forces in <i>UIDA</i> . -----	182
Figure 9.14	Flowchart of the simplified uniform inter-storey drift control algorithm. -----	184
Figure 9.15	Top storey displacements for passive frames with low and high initial PT forces and the <i>SUIDA</i> -controlled PT frame. -----	185
Figure 9.16	Resultant PT forces in <i>SUIDA</i> -controlled frame. -----	185
Figure 9.17	Normalised standard deviation of maximum inter-storey drifts for low passive forces, high passive forces and <i>SUIDA</i> -controlled forces. -----	186
Figure 10.1	Response of <i>LDFA</i> -controlled PT frame normalise to passive PT frame response: (a) top storey maximum displacements, (b) SRSS of top storey displacements and (c) energy dissipation. -----	191
Figure 10.2	Deformations of the frames controlled by stiffness control approach algorithms compared to a passive frame with low initial PT force. -----	193
Figure 10.3	Distribution of the reduction of top storey displacements: (a) reduction in the maximum displacement and (b) reduction in the SRSS of displacements. -----	193

Figure 10.4 Response of deformation regulation controlled PT frame normalised to response of passive frame with low PT force: (a) top storey maximum displacements, (b) SRSS of top storey displacements and (c) standard deviation of inter-storey drifts. -----195

Figure 10.5 Distribution of reduction of top storey displacements in UIDA and SUIDA-controlled frame: (a) reduction in maximum displacement, (b) reduction in SRSS of displacements and (c) Reduction in standard deviation. ----- 196

Figure 10.6 Response of deformation regulation controlled PT frame normalised to response of passive frame with high PT force: (a) top storey maximum displacements, (b) SRSS of top storey displacements and (c) standard deviation of inter-storey drifts. -----197

LIST OF TABLES

Table 2.1	Post-Northridge recommendations for rotation capacity of prequalified connections (FEMA 351, 2000). -----	11
Table 2.2	Summary of work done on steel frames with PT connections. -----	39
Table 2.3	Comparison between passive, active and semi-active control systems. -----	41
Table 2.4	Summary of work done on semi-active control of frame structures. -----	51
Table 4.1	Input data of Element 1 in FASAC-2D. -----	61
Table 4.2	Input data of Element 2 in FASAC-2D. -----	64
Table 4.3	Input data of Element 6 in FASAC-2D. -----	66
Table 4.4	Stiffness matrix of Element 6 for different values of yield code and direction code: (a) dir=1, (b) dir=2 and (c) dir=3. -----	66
Table 5.1	Input data for the IPTC element in FASAC-2D. -----	78
Table 5.2	Connection stiffness matrix for each time step (different YieldCode values). --	78
Table 6.1	Details of earthquake records (Regents of the University of California, 2000). --	100
Table 7.1	Specifications of a rotating motor. -----	118
Table 7.2	Best results using the LDFA. -----	126
Table 8.1	Assembly of the stiffness patterns matrix. -----	142
Table 8.2	Modal properties of the PT frame. -----	146
Table 8.3	Effect of the control time on resultant PT forces in the EFSFA. -----	153
Table 8.4	Optimal stiffness pattern for SMART1 earthquake. -----	154
Table 8.5	Indices of difference between target and actual PT forces. -----	156
Table 10.1	Summary of loading direction feedback algorithms results: DB: displacement-based, MDB: modified displacement-based and VB: velocity based. -----	191
Table 10.2	Deformations of the frames controlled by stiffness control approach algorithms compared to a passive frame with low initial PT force. -----	193
Table 10.3	Results of the stiffness control approach algorithms compared to passive frame with high initial PT force; E: EFSFA, R: RFSFA, F: FEFSFA. -----	194

Table 10.4 Results of the deformation regulation control algorithms compared to passive frame with low PT force. ----- 196

Table 10.5 Results of the deformation regulation control algorithms compared to passive frame with high PT force. ----- 196

LIST OF ABBREVIATIONS

A

AMD: Active Mass Damper.

AVS: Active Variable Stiffness.

B

BFP: Bolted Flange Plate connection.

C

CC: Control Computer.

D

DBE: Design Based Earthquake.

DB-LDFA: Displacement-Based Loading Direction Feedback Algorithm.

E

EFSSFA: Excitation Frequency State Feedback Algorithm.

ER: Electro-rheological Dampers.

F

FASAC-2D: Frame Analysis with Semi-Active Control.

FEFSFA: Filtered Excitation Frequency State Feedback Algorithm.

FFT: Fast Fourier Transform.

I

IWUF: Improved Welded Unreinforced Flange connection.

IPTC: Incorporated Post-tensioned Connection.

L

LDFA: Loading Direction Feedback Algorithm.

LQR: Linear Quadratic Regulator.

M

MCE: Maximum Considered Earthquake.

MDB-LDFA: Modified Displacement-Based Loading Direction Feedback Algorithm.

MRF: Moment Resistant Frame.

N

NI-Ti: Nickel-Titanium

O

OMRF: Ordinary Moment Resisting Frame.

P

PT: Post-tensioned (or Post-tensioning).

R

RBS: Reduced Beam Section connection.

RFSFA: Response Frequency State Feedback Algorithm.

S

SCED: Self-Centring Energy Dissipating system.

SCVD: Self-Centring Viscous Damping device.

SDOF: Single Degree Of Freedom.

SMA: Shape Memory Alloy.

SMRF: Special Moment Resisting Frame.

SP: proprietary Side-Plate connection.

SRSS: Square Root of Sum of Squares.

SUIDA: Simplified Uniform Inter-storey Drift Algorithm.

T

TMD: Tuned Mass Damper.

U

UIDA: Uniform Inter-storey Drift Algorithm.

V

VB-LDFA: Velocity-Based Loading Direction Feedback Algorithm.

W

WBH: connections with Welded Bottom Haunch.

WCPF: Welded Cover Plated Flange connection.

WHP: Web Hourglass Pin.

WTBH: Connections with welded top and bottom haunches.

LIST OF SYMBOLS

A

A : Area of the section.

A_b : Area of one energy dissipating bar.

A_{si} : Area of strand i .

α : Post-yielding stiffness ratio.

B

β : Energy dissipation factor.

C

C : Damping matrix.

C : Initial Stiffness factor.

\hat{C} : Modified damping matrix.

\bar{C} : Damping matrix of the passive control system.

$C(V)$: Voltage dependent damping coefficient.

C_{cap} : Capping ratio of F_{pt} .

D

D : Matrix of the actuators locations.

D_{av} : Average of the inter-storey drifts of all storeys.

D_b : Depth of the beam.

dia : Diameter of energy dissipating bars (only for $EDTY=1$).

dir : direction code of the connection.

d_{si} : Distance of strand i to the centre of rotation.

$ds(1:n)$: Vector of distances of strands to the current centre of rotation.

Δ : Lateral displacement of the top storey.

ΔF : Vector of increment in external forces within time-step.

$\Delta F_{control}$: Drop/increase in the post-tensioning force of each strand.

ΔL : Change in the strands length due to the force drop/ increase.

ΔM_i : Moment increment at time-step i .

$\Delta f/\Delta t$: Increment rate of motor control force.

$(\Delta f/\Delta t)_{max}$: Maximum rate of control force increment of the rotating motor.

$\Delta\varphi$: Rotation angle in the motor due to ΔL .

Δ_{gap} : Gap opening of the post-tensioned frame.

Δ_p : Plastic displacement of the frame at which the first plastic hinge forms in the frame.

$\Delta\theta_i$: Rotation increment at time-step i .

Δ_{st} : Vector of elongations of the strands.

ΔT : Induced force due to the gap opening.

Δ_u : Ultimate lateral displacement of the frame at the point of first yielding in the strands.

$\Delta\ddot{\mathbf{X}}$: Vector of acceleration increment within time-step.

$\Delta\dot{\mathbf{X}}$: Vector of velocity increment within time-step.

$\Delta\mathbf{X}$: Vector of displacement increment within time-step.

E

E : Modulus of elasticity.

E_b : Modulus of elasticity of the energy dissipating bars.

E_s : Modulus of elasticity of the strands.

$EDTY$: Type of the energy dissipater.

e : Error in the moment calculated by the model.

F

F : Vector of external forces.

F : Base shear.

$F_{contHist}$: Time-history of control forces from $t=t_0$ to $t= t_i$.

$F_{control}$: Control force.

F_{fr} : friction force between the beam and the column flange.

$FricLoc$: Location of friction-based damper (only for $EDTY=2$).

F_{pt} : Post-tensioning forces of the connection.

$F_{pt-act(i)}$: Actual post-tensioning force at $t= t_i$.

F_{ptHigh} : Upper limit of post-tensioning forces.

F_{pti} : Initial post-tensioning force.

F_{ptLow} : Lowest PT force to ensure full self-centring ability of the post-tensioned connection.

FR_i : Index of the weighted frequency content of the i^{th} stiffness pattern.

F_{yd} : Slip force of friction-based energy dissipater (only for $EDTY=2$).

$F_{y,beam}$: Axial strength of the beam.

F_{ys} : Yield force of strands.

f_{motor} : Frequency of the rotating motor.

f_i^{if} : Inertial force carried by the PT frame.
 f_i^{cb} : Force resulted from the diaphragm action (collector beam deformation).
 f_x^{cb} : Additional axial forces transferred by the collector beam.
 f_y : Yielding force.
 f_{yb} : Yield stress of energy dissipater (only for $EDTY=1$).

G

Γ : Modal mass participation ratio.
 γ : Shear strain.
 $\dot{\gamma}$: Shear strain rate.

H

h : Height of the frame.
 η : Viscosity coefficient.

I

I : Second moment of inertia about the bending axis.
 \mathbf{Ind} : indicator of self-centring status.
 i_{gap} : Step at which the gap opened.

K

\mathbf{K} : Stiffness matrix.
 $\hat{\mathbf{K}}$: Modified stiffness matrix.
 $\bar{\mathbf{K}}$: Stiffness matrix of the passive control system.
 K_{Conv} : Secant stiffness of the conventional MRF.
 K_i : Stiffness of the connection at time $t=t_i$.
 K_{PT} : Secant stiffness of the post-tensioned frame
 k_0 : Pre-yielding stiffness of the connection.
 k_b : Stiffness of energy dissipating bars.
 k_{b1} : First stiffness of the energy dissipation device.
 k_{b2} : Second stiffness of the energy dissipation device.
 k_{cb} : Stiffness of the collector beam.
 \mathbf{k}_e : Local stiffness matrix of the connection element.
 k_s : Total rotational stiffness of the strands.
 k_{si} : Rotational stiffness of strands i .

L

L : Total length of the strands in one storey.

L_b : Length of the energy dissipating bar.

L_s : Length of the strands.

M

M : Mass matrix.

M_2 : Yielding moment of the connection model.

\hat{M} : Modified mass matrix.

\bar{M} : Mass matrix of the passive control system.

M_{Ed} : Moment provided by the energy dissipation device installed at the connection.

M_p : Plastic moment of the section.

$M_{p,beam}$: Plastic moment of the beam connected to the connection.

M_{R1} : Resisting moment of PT connection before yielding/slipping of energy dissipater.

M_{R2} : Resisting moment of PT connection after yielding/slipping of energy dissipater.

M_{R3} : Resisting moment of PT connection when $\theta_D \leq \theta \leq \theta_C$ (unloading).

M_{R4} : Resisting moment of PT connection when $\theta \leq \theta_D$ (unloading).

M_S : Moment provided by the post-tensioned strands.

M_{Si} : Initial moment provided by the post-tensioned strands.

M_u : Ultimate moment capacity of the connection.

M_y : Yielding moment of the connection.

M_{y-new} : New yielding moment of the connection.

μ : Rotational ductility capacity of post-tensioned connection.

μ_{fr} : Lateral ductility of the frame.

N

N : Normal force.

N_{os} : Number of strands in the post-tensioned connection.

N_s : Number of storeys in the frame.

N_{p+} : Plastic axial force of the section (tension).

N_{p-} : Axial buckling force of the element (compression).

n : Order of the filter.

ν : Coefficient of friction.

P

P : Power of the rotating motor.

P_j : Final force in the post-tensioned strands.

Q

θ : Relative rotation between the column and beam.

θ_j : Rotation of the connection model prior to gap-opening.

θ_B : Rotation angle at which the energy dissipating device starts yielding / slipping.

θ_C : Maximum rotation of the connection.

θ_D : $\theta_C - 2\theta_B$.

θ_{Hist} : Rotation history.

θ_{CS} : Rotation of the connection at the changing stiffness point.

θ_{beam} : Rotation of the connection at the beam end.

θ_{col} : Rotation of the connection at the column end.

θ_{el} : Rotation angle at which the energy dissipating device yields or slips.

θ_i : Rotation at time-step i .

θ_{i+1} : Rotation at time-step $i+1$.

θ_O : Median drift angle capacity for immediate occupancy performance level.

θ_U : Median drift angle at which connection loses gravity load carrying capacity.

θ_{ult} : Ultimate rotation angle of the connection.

θ_{sc} : Self-centring rotation angle of the connection.

θ_{sd} : Median total connection rotation at which the strength degradation starts.

θ_y : Yielding rotation of the connection.

R

R_p : Normalised magnitude at the cut-off frequency.

R_s : Slope of the filter.

r : Radius of the rotating disc.

S

S : Number of possible stiffness patterns of the frame.

sgn : Signum function.

$\sum ds$: Sum of the distances of all strands from the centre of rotation of the connection.

T

Thr : Drift threshold at which the *UIDA* starts working.

T_{switch} : Time required for switching between high and low PT forces.

t_{sc} : Time needed for the connection to fully restore its initial M_{St} .

τ : Applied shear stress.

τ_y : Shear yield stress.

U

$U(t)$: Matrix of control forces.

U_{static} : Vector of global static displacements.

V

V : Voltage command of the servo-valve.

W

W : Weight of the structure.

W_p : Frequency of bandpass edge.

ω : Rotating velocity of the motor.

X

$\ddot{\mathbf{x}}(t)$: Vector of accelerations.

$\dot{\mathbf{x}}(t)$: Vector of velocities.

\dot{x} : Velocity of the motion.

$\mathbf{x}(t)$: Vector of displacements.

$\ddot{\mathbf{x}}_g(t)$: earthquake acceleration.

x_y : Yielding displacement.

Y

$\Psi_{i,n}$: Spectral acceleration of the of the n^{th} mode of vibration for the i^{th} stiffness pattern.

CHAPTER 1

INTRODUCTION

In this Chapter is presented an introduction to the research work of this thesis. A brief background of the research subject is presented first, followed by an introduction to the research problem. At the end is given the layout of thesis, including a brief description of the work presented in each chapter.

1.1. Background

1.1.1. Conventional Steel Beam-Column Connections

Failures of steel frames during Northridge 1994 earthquake prompted researchers to improve the behaviour of beam-column connections where most of the fractures occurred. The most important reason for failures of the pre-Northridge steel connections was the low ductility associated with the fully welded connections (Christopoulos et al. 2002^a) as well as the heterogeneity in the weld-steel combination. In order to enhance the characteristics of the beam-column connection, SAC venture, a comprehensive research programme, was initiated (SAC Report No. 94-01). This programme referred the weaknesses of pre-Northridge beam-column connections to two reasons: (a) low rotational ductility of the connection and (b) inability to restore large residual deformations after the event of earthquake. A set of remedies were suggested to retrofit the existing connections and to avoid these failures in new connections. Among the proposed solutions were using Reduced Beam Section –RBS (Figure 1-a), haunches and brackets (Figure 1-b), T-stubs (Figure 1-c) and proprietary side plate connections (Houghton, 1997) (Figure 1-d). The main objective of all these solutions was locating the plastic hinges outside the connection. These solutions could provide a plastic hinge with high rotational ductility but they could not eliminate the residual deformations of the connection. (Christopoulos et al.2002^a).

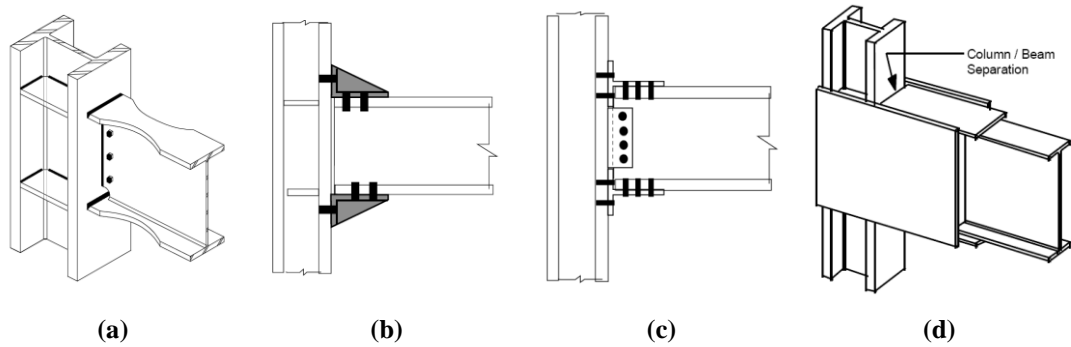


Figure 1.1: Solutions proposed to enhance the moment beam-column connection: (a) reduced beam section, (b) added haunches or brackets, (c) T-stubs solution and (d) proprietary side plate connection (FEMA 351, 2000).

1.1.2. Post-Tensioned Steel Beam-Column Connections

In parallel with the SAC venture project, and inspired by the pre-stressed concrete beam-column connections, researchers introduced post-tensioned steel connections (Ricles et.al 2001) as a solution for avoiding residual deformations. The expected advantages of using post-tensioned steel connections were: (i) avoiding shop welding which was a main reason for low ductility of the beam-column connection, (ii) easiness of erection and construction, (iii) high energy dissipation and self-centring and (iv) confining the damage anticipated in the frame to energy dissipaters installed in these connections.

The two main components of the connection were post-tensioned strands, which provide self-centring and eliminate residual drifts, and energy dissipation device installed in the connection. Energy dissipation devices were either yielding bars or top and seat angles (Figure 1.2), or friction elements (Figure 1.3).

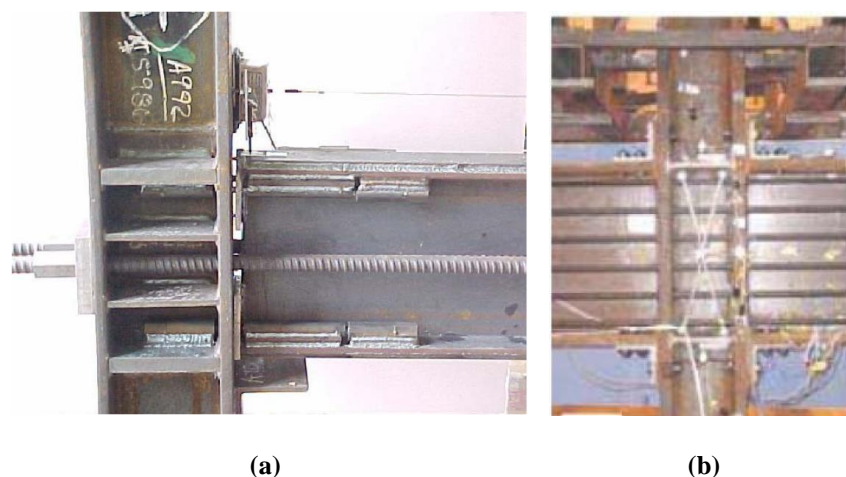


Figure 1.2: Yield-based steel post-tensioned beam-column connections: (a) energy dissipating bars, and (b) top and seat angles (Bruneau M, 2004).

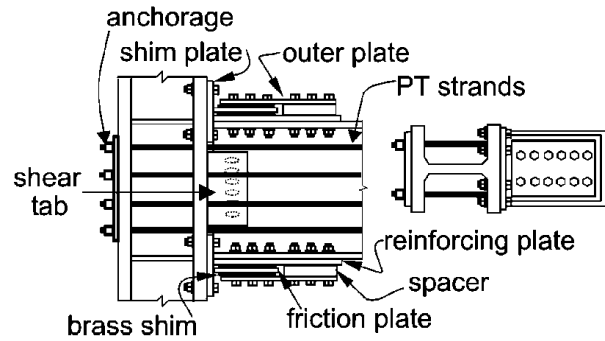


Figure 1.3: Post-tensioned connections with friction damper (Rojas et al. 2004).

1.1.3. Behaviour of Post-tensioned Steel Beam-Column Connections

Post-tensioned connections are characterised by their flag-shaped hysteretic behaviour (Figure 1.4, Christopoulos et al. 2002^a). After experiencing inelastic deformations in its energy dissipater, the connection returns back to its original position due to the effect of post-tensioning forces.

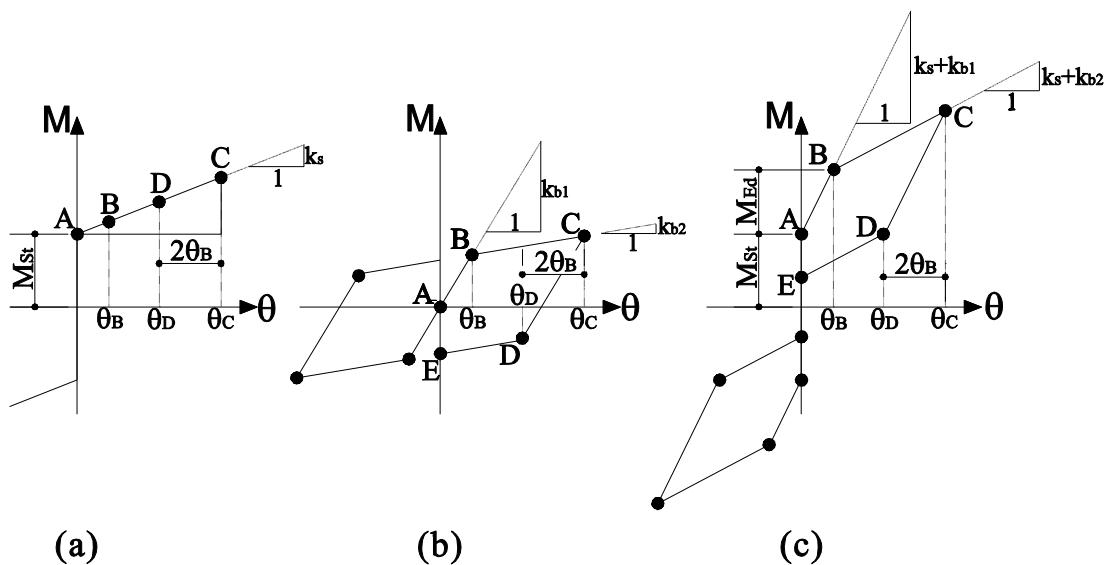


Figure 1.4: Hysteretic model for post-tensioned connection with energy dissipating bars (Christopoulos et al. 2002): (a) post-tensioned strands, (b) energy dissipating bars and (c) post-tensioned connection (combined action).

The moment-rotation behaviour of post-tensioned steel connections can be described for different phases of loading (Figure 1.4). As long as the applied moment is less than the moment provided by the post-tensioned strands ($M_{St}=M_A$ - Figure 1.4-c), the connection behaves as a rigid connection experiencing no relative rotations between the beam and the column. Once the applied moment overcomes M_{St} , a gap opens between the beam and the column and the energy dissipating device starts contributing to the resisting moment of the connection. In this stage (A-B) the resisting moment of the connection can be calculated from:

$$M_{R1} = M_{St} + (k_s + k_{b1}) \theta, \quad (1.1)$$

where k_s is stiffness of the strands, k_{b1} is pre yielding/slipping stiffness of the energy dissipating device, and θ is the angle of rotation between the column and beam.

When the applied moment exceeds the yield/slip force of the energy dissipating device (stage B-C), the resisting moment of the connection is:

$$M_{R2} = M_{R1} + (k_s + k_{b2}) (\theta - \theta_B), \quad (1.2)$$

where k_{b2} is the second stiffness of the energy dissipating device and θ_B is the rotation angle at which the energy dissipating device starts yielding/slipping. If the energy dissipating device is friction based, the second stiffness is zero.

Unloading the connection is characterised by two stages. The first stage (C-D) takes place when $\theta_D \leq \theta \leq \theta_C$ where $\theta_D = \theta_C - 2\theta_B$. The resisting moment of the connection in this stage is:

$$M_{R3} = M_{R2} + (k_s + k_{b1}) (\theta - \theta_C), \quad (1.3)$$

The second unloading stage (D-E) starts when $\theta \leq \theta_D$ and the resisting moment can be obtained from:

$$M_{R4} = M_{R3} + (k_s + k_{b1}) (\theta - \theta_D), \quad (1.4)$$

The effects of the energy dissipating device installed in the connection are considered by defining the energy dissipation factor (β). This factor shows the contribution of the energy dissipating device to the moment capacity of connection, and can be given as: $\beta = M_{Ed}/M_{St}$, where M_{Ed} is moment provided by the energy dissipation device installed at the connection and M_{St} is moment provided by post-tensioned strands before opening the gap.

1.1.4. Effects of Post-tensioning Forces

In order to achieve the best performance of post-tensioned connections, the post-tensioning force and energy dissipation factor should be adjusted to specific values to provide the optimum energy dissipation capacity, the highest rotational ductility and the best self-centring capability (Christopoulos et al. 2002^b).

In this study, simulations were performed to examine the effects of the post-tensioning force on the behaviour of a post-tensioned steel beam-column connection and to optimise the range of post-tensioning forces that would result in the best behaviour of the connection in terms of moment capacity, rotational ductility, energy dissipation and self-centring.

These simulations showed that the upper limit of post-tensioning force is imposed by the failure mode of the post-tensioned connection or other frame elements. Using very high values of post-tensioning force leads to brittle failure characterised by yielding of the strands. The lower limit is imposed by the requirement of full self-centring of the connection (Figure 1.5) where M_{st} is the moment provided by post-tensioned strands. For lower values of post-tensioning forces, the connection experiences residual rotations.

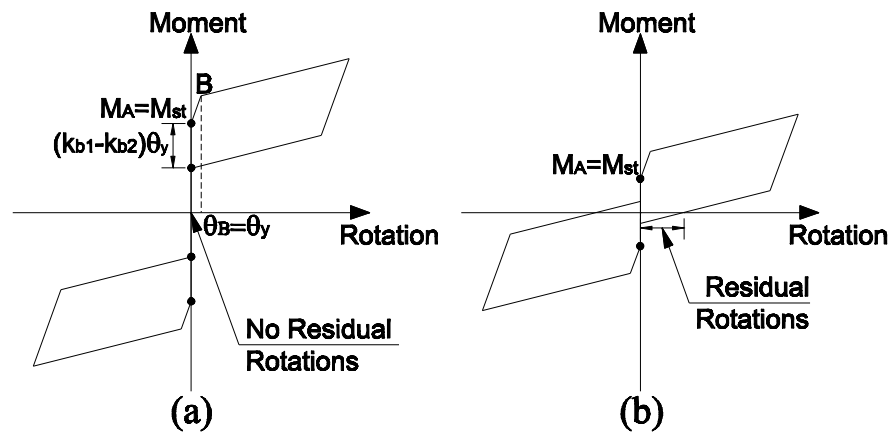


Figure 1.5: Illustration of the full self-centring requirement: (a) sufficient post-tensioning forces and (b) insufficient post-tensioning forces.

The results of simulations of seismic response of a post-tensioned steel frame with incorporated post-tensioned connections showed that imposing different levels of post-tensioning forces on the strands results in different stiffness, energy dissipation and ductility of the frame. These changes in the frame characteristics lead to differences in the dynamic response. Hence, the level of post-tensioning force can be used as a parameter for controlling the dynamic response of the frame under seismic excitations.

1.2. Thesis Overview

A literature review is presented in Chapter 2. Areas covered in the literature review include: (a) reasons that led to developing and using the new generation of beam-column connections from reviewing the preliminary solutions proposed for post-Northridge beam-column connections, (b) potential advantages of using self-centring systems generally and post-tensioned steel connections in particular, (c) limitations and practical issues associated with using post-tensioned beam-column connections and (d) basic principles of various types of control of structural dynamic response, especially those based on semi-active control. A conclusion from the literature review is drawn to determine the aim and objectives of this work.

Chapter 3 presents the aims and objectives of this research. The main aim is to investigate the possibility of controlling the structural dynamic response of post-tensioned steel frame by varying the post-tensioning forces of the beam-column connections. Also, the key steps of the research methodology are introduced in this chapter.

Chapter 4 describes the frame analysis program developed for this research (FASAC-2D). The operation of the program and the list of elements along with their nonlinear dynamic behaviour are all described in this chapter. Finally, verifications of the results of FASAC-2D performed through comparison with results of DRAIN-2DX (Prakash et al. 1993) are presented.

To facilitate the investigation of seismic response of post-tensioned steel frames with passive and semi-active control systems, the steel post-tensioned beam-column connection is modelled as a simple two-node element: Integrated Post-Tensioned Connection element (IPTC). The IPTC model is presented and explained in Chapter 5. This chapter includes modelling, behaviour and incorporation of the IPTC element in a single-storey steel frame. Also presented in Chapter 5 are details of the connection used for this research, including devices and arrangements needed for both passive and semi-active control of post-tensioning forces. These devices and their structural arrangements are responsible for ensuring safe and smooth performance of the connection including semi-active variation of post-tensioning forces.

The effect of the initial post-tensioning force (F_{pt}) is investigated in Chapter 6. This effect is studied at both connection and frame levels. At the connection level, the effects of post-tensioning forces on ultimate moment, energy dissipation capacity, and rotational ductility of the connection is examined. The effects of post-tensioning forces on the frame level are studied through analysing the variations of the structural dynamic response due to different initial post-tensioning forces. In this chapter is included a comparison between the response of conventional MRF and passive post-tensioned (PT) frame to detect weaknesses and strengths of passive PT frames.

Chapter 7 presents the first semi-active control approach adopted for controlling the dynamic response of post-tensioned steel frames. This control approach is based on increasing the energy dissipation capacity of the PT frame. Basics of the energy dissipation approach are first introduced, and then three control algorithms using this approach are proposed and investigated by simulating the dynamic response of a PT frame under a set of earthquake excitations and comparing the results with those obtained for passive PT frame.

The second approach, based on stiffness control, is presented in Chapter 8. This approach aims to avoid large dynamic magnification (resonance frequency state) of the PT frame by changing its dynamic characteristics. The frequency state feedback algorithm is proposed in three forms, using different input data. Investigations of the frame response with applied stiffness control algorithms are carried out on six-storey frames and compared to the seismic response of corresponding passive PT frame with different (constant) post-tensioning forces.

In Chapter 9 is presented the third (and last) control approach which is the deformation regulation control approach. The main objective of this control approach is to regulate the structure displacements in order to achieve a more uniform maximum inter-storey drift distribution. The results of applying this approach are investigated using six-storey post-tensioned steel frame. In order to reduce the computational costs of the control process, a simplified algorithm that aims to achieve uniform inter-storey drifts with minimum control action is also proposed and investigated in this chapter.

Chapter 10 provides a summary of the key results of all semi-active control approaches of post-tensioned steel frames. Different performance indices were used to compare the performance of semi-actively controlled frames with the corresponding passive PT frames.

Chapter 11, the last chapter, presents the conclusions from the work and recommendations for future work in this research area.

CHAPTER 2

LITERATURE REVIEW

In this chapter is presented a review of the up-to-date research on key issues related to this dissertation. The first section is a brief review of pre-Northridge beam-column steel connections including a short description of arrangements used in pre-Northridge beam-column connections, list of types of damage in these connections and analysis of the reasons for damage in pre-Northridge connections. The second section reviews preliminary solutions proposed to improve the seismic performance of beam-column steel connections (prequalified post-Northridge beam-column connections) and highlights weaknesses in the proposed solutions.

Weaknesses of the prequalified post-Northridge beam-column connections prompted researchers to consider the use of self-centring systems. A review of different types of self-centring systems is introduced in the third section. This review includes the introduction of post-tensioned steel beam-column connections which is the focus of this study. Development, mechanisms and practical issues in incorporating the post-tensioned steel beam-column connections in multi-storey frame buildings are presented in the fourth section.

The final part of this review (fifth section) is an introduction of various aspects of seismic semi-active control. The review of semi-active control is based on categorising control devices and algorithms from different aspects. This includes a critical review of these types accompanied by conclusions about the possibility of using these types in controlling the dynamic response of post-tensioned steel frames.

2.1. Pre-Northridge Beam-Column Connections

Many arrangements of beam-column connection have been considered since the start of steel construction. In the early times of steel construction, engineers provided bolted connections with different detailing of pinned and fixed connections as shown in Figure 2.1 (FEMA 351, 2000).

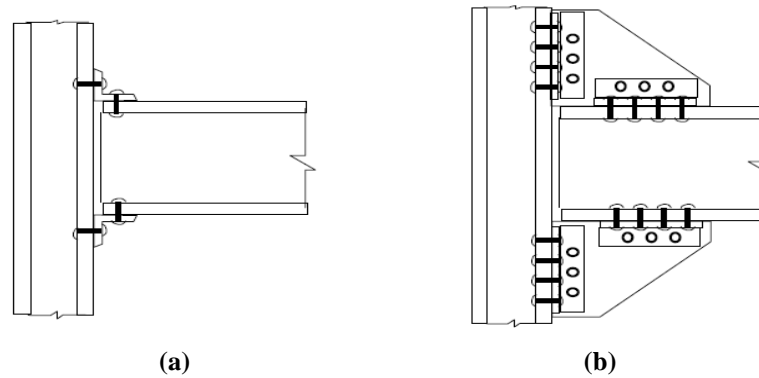


Figure 2.1: Details of early beam-column connections: (a) pinned connection and (b) rigid connection (FEMA 351, 2000).

In the late 1950s welded-flange-bolted-web connections (Figure 2.2) replaced earlier connections. Speed of erection and cost-efficiency were among the reasons that led to wide use of this connection detail (FEMA 351, 2000; FEMA 355D, 2000).

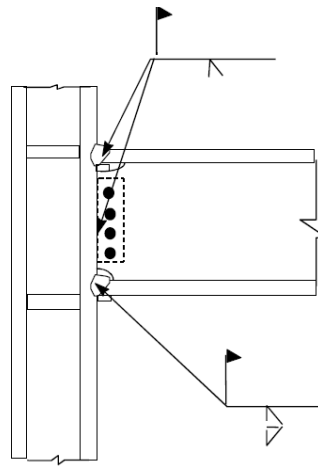


Figure 2.2: Pre-Northridge welded-flange-bolted-web connection detail (FEMA 351, 2000).

Prior to the major earthquake of Northridge, welded-flange-bolted-web connections were considered the most seismic resistant detail of any beam-column connection based on experimental work conducted at Lehigh University and University of California at Berkeley which proved their good cyclic behaviour (Popov and Pinkney, 1969; Popov and Stephen, 1970; Krawinkler et al. 1971). The experimental work showed that this connection can withstand high plastic rotations, especially for welded-flange-welded-web connection (FEMA 355D, 2000). These results led to widespread use of welded-flange-bolted-web connections in the 1980s (FEMA 351, 2000).

The Northridge earthquake (17th January 1994) caused extensive damage to many structures and changed the general idea about steel structures. Despite the fact that some experimental research predicted this damage (Popov and Stephen, 1970; Krawinkler and Popov, 1982), pre-Northridge steel structures were considered as highly earthquake-resistant structures. A

research paper published a few weeks before the earthquake (Engelhardt and Husain, 1993) raised the concerns about the safety of steel frames, but there was no time for any improvements.

A detailed description of the damage observed in pre-Northridge steel beam-column connections was presented in FEMA 351 (2000) and categorised as: (i) weld damage, (ii) girder damage, (iii) column damage, (iv) panel zone damage and (v) shear tab damage.

Causes of the connection damage could not be separated in all cases, and in most cases one factor led to few types of damage. This variety of damage types prompted researchers and governmental agencies to initiate *SAC venture Phase I* to observe damage occurred at pre-Northridge beam-column steel connections and figure out its reasons. The results of this assessment showed that most of the damage occurred due to low quality of detailing in general, and especially low quality of welding (FEMA 351, 2000). Supporting results were already obtained from the work of Krawinkler and Popov (1980) and Engelhardt and Husain (1993). Poor detailing and execution of welding resulted in defects in flange welds which were among the main reasons of connection failures (FEMA 351, 2000; FEMA 355D, 2000).

In general, it can be concluded that the primary reasons for failure of pre-Northridge steel frames were poor detailing and lack of construction quality, which resulted in low energy dissipation capacity and small rotational ductility capacity of the beam-column connections.

2.2. Post-Northridge Beam-Column Connections

2.2.1. Types of Seismic Upgrades of Steel Structures

Solutions for the observed damage in pre-Northridge steel beam-column joints were summarised in the Seismic Upgrade of Steel Structures (SAC Report No. 94-01). Three upgrade strategies were proposed (Roeder, 2002^b) to ensure good seismic performance of beam-column connections:

- Evaluating the force path in the connection so that the stiffness, strength and ductility of the connection can be controlled.
- Providing a designed fuse adjacent to the connection to bring forces to a known path so that the connection can be protected.
- Strengthening or reinforcing the connection using other elements to increase the confidence in the connection performance.

The chosen strategy for the connection upgrade depended on two criteria (FEMA 351, 2000): (i) location of plastic hinges and (ii) drift angle capacity.

2.2.1.1. Location of Plastic Hinges

Figure 2.3 shows the plastic hinge locations recommended by FEMA (FEMA 351, 2000), which are in contrast with the previous AISC (1994) provisions. According to the new recommendations, inelastic energy dissipation through plastic hinge formation was expected to take place away from the column face. This provision can be satisfied by using cover plates, haunches and any similar detailing. Plastic hinges should not form at the panel zone because it increases the susceptibility to brittle fracture. Most importantly, reinforcing the connection should not result in weak-column-strong-connection. It is worth remembering that formation of plastic hinges is not completely benign to the connection performance. Beams experiencing high plastic rotations exhibit large buckling and yielding deformations leading to localised concentrated slab damage (FEMA 351, 2000).

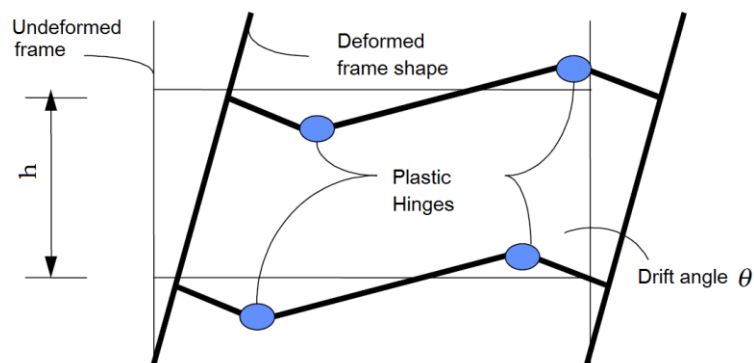


Figure 2.3: Post-Northridge recommendations for plastic hinge location in the beam span (FEMA 351, 2000).

2.2.1.2. Drift Angle Capacity

Another recommendation was that the connection should withstand the total rotation (elastic and plastic) of the frame induced by the earthquake. Three rotation angles were defined in order to determine the drift angle capacity (or rotational capacity) of the connection (FEMA 351, 2000): (i) the median total connection rotation (due to drift) at which the strength degradation starts (θ_{sd}), (ii) the median drift angle capacity for immediate occupancy performance level (θ_{IO}) and (iii) the median drift angle at which connection loses gravity load carrying capacity which is the limit state for collapse prevention (ultimate) performance level (θ_U). Prequalified connections should satisfy rotation capacities given in Table 2.1.

Frame Type	θ_{sd} (radians)	θ_U (radians)
OMRF	0.02	0.03
SMRF	0.04	0.06

Table 2.1: Post-Northridge recommendations for rotation capacity of prequalified connections (FEMA 351, 2000).

None of the welded-flange-bolted-web connections tested by Engelhardt and Husain (1993) satisfied the rotation capacity specified in Table 2.1, which confirmed the lack of rotational ductility of most of the pre-Northridge steel beam-column connections.

2.2.2. Prequalified Seismic Resistant Connections

Design recommendations were reflected in a set of connection configurations considered as prequalified seismic resistant connections (FEMA 351, 2000). Among these configurations were: (i) improved welded unreinforced flange connection (IWUF), (ii) reduced beam section connection (RBS), (iii) connections with welded haunches: top and bottom haunch (WTBH) and bottom haunch (WBH), (iv) welded cover plated flange connection (WCPF), (v) bolted flange plate connection (BFP) and (vi) Proprietary side-plate connection (SP).

2.2.2.1. Improved Welded Unreinforced Flange Connection (IWUF)

This configuration is a retrofitted form of a pre-Northridge welded-flange-bolted-web connection. In this arrangement flange welds were required to possess high toughness and be detailed carefully (Roeder, 2002^a). It was also recommended to provide welding access holes to facilitate the welding process and result in a better full penetration weld (Ricles et al. 2002^a). Energy dissipation capacity of the connection increased significantly when using supplemental weld at the shear tab (FEMA 355 D, 2000; Roeder, 2002^a; Ricles et al. 2002^a). When recommended modifications were accommodated in this connection, it had a very stable hysteretic behaviour (Figure 2.4; FEMA 355D, 2000). It was able to develop the full plastic moment capacity of the connected beam and exhibited high capacity of plastic rotations up to 0.035 rad.

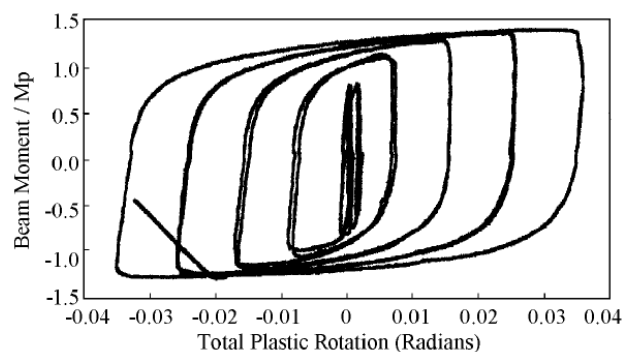


Figure 2.4: Moment rotation relationship of improved welded unreinforced flange connection (FEMA 355D, 2000).

2.2.2.2. Reduced Beam Section Connection (RBS)

This configuration of the reduced beam section connection (Figure 2.5-a) utilised the strategy of creating a fuse to form the plastic hinge at pre-determined distance from the

column face (FEMA 355D, 2000; Roeder, 2002^b). AISC (1994) however did not recommend the reduced beam section connection and stated that this type of connection was very susceptible to brittle failures; which contradicted the post-Northridge design guidelines. This connection showed good ductile behaviour with high rotational capacity, but with some strength degradation when the beam buckled at the reduced section (Figure 2.5-b).

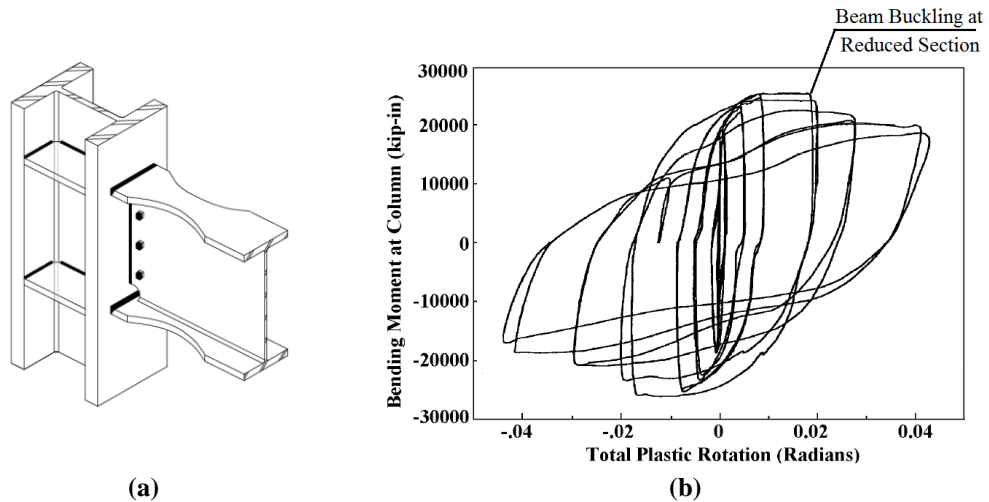


Figure 2.5: Reduced beam section connection (RBS): (a) connection arrangement and (b) moment-rotation relationship (FEMA 355D, 2000).

2.2.2.3. Connections with Welded Haunches: Top and Bottom Haunch (WTBH) and Bottom Haunch (WBH)

Using this reinforcement technique (Figure 2.6-a), the plastic hinge is forced to form at the end of the haunch (FEMA 355D, 2000; Di Sarno and Elnashai, 2002).

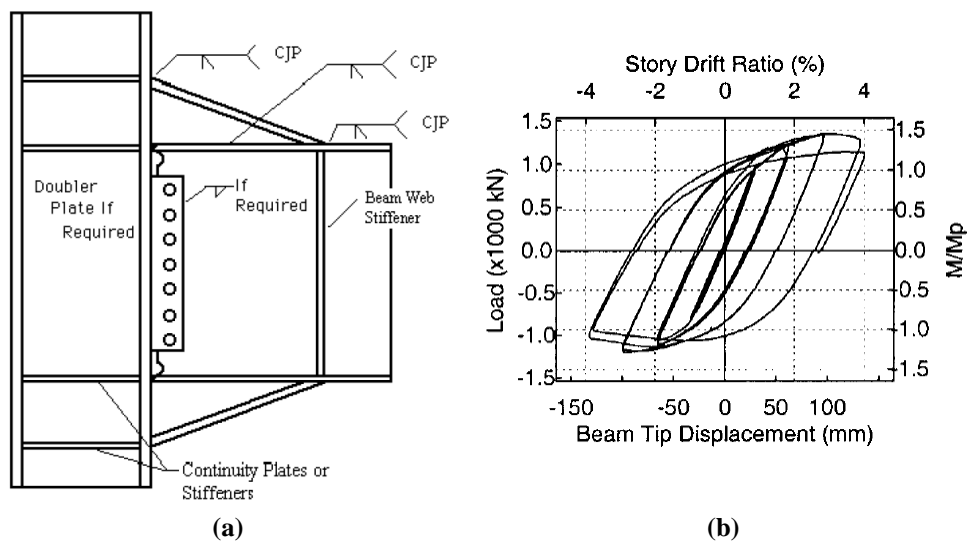


Figure 2.6: Welded top and bottom haunch connection: (a) connection arrangement and (b) moment-rotation relationship (FEMA 355D, 2000).

These connections however were very expensive and therefore, they were appropriate only as retrofit of existing connections. Since most of the brittle fractures initiated at the bottom flange welds, it was proposed to use the welded haunch at the bottom flange only (FEMA 351, 2000), thus reducing the connection cost.

Cyclic testing indicated that haunch connections could provide stable hysteretic behaviour with high rotational ductility capacity (FEMA 355D, 2000; Uang et al. 2000). The connection was able to develop the full plastic moment of the connected beam with no strength degradation (Figure 2.6-b).

2.2.2.4. Welded Cover Plated Flange (WCPF) Connection

This configuration (Figure 2.7-a) is easily executable and cheaper than haunch connections (FEMA 355D, 2000). Pre-Northridge and more recent studies have shown that this beam-column connection configuration exhibited very stable hysteretic behaviour (Krawinkler and Popov, 1980). However, Engelhardt and Sabol (1998) found that the connection strength degraded once the beam started yielding. Yet, the degradation was not severe and did not decrease the connection strength (Figure 2.7-b).

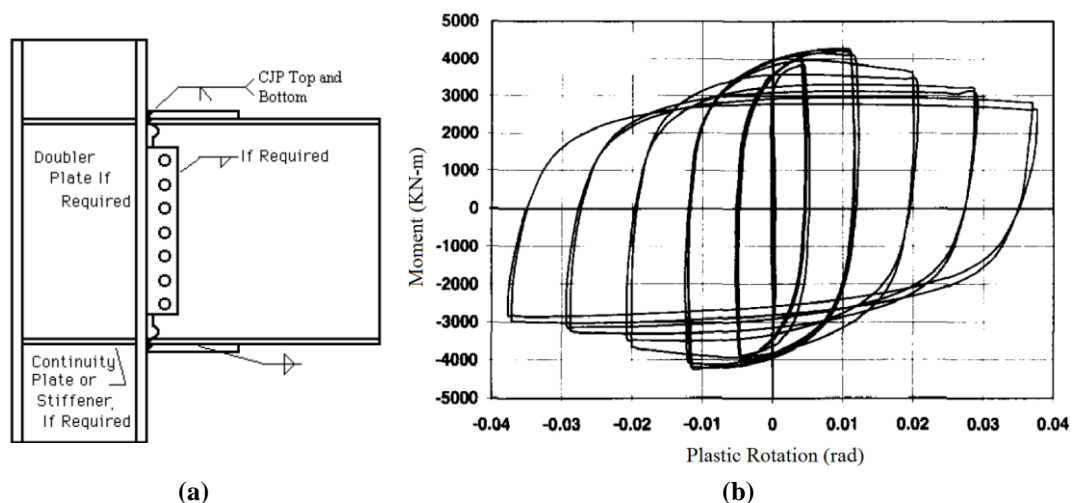


Figure 2.7: Welded cover plate flange connection: (a) connection arrangement (FEMA 355D, 2000) and (b) moment-rotation relationship (Engelhardt and Sabol, 1998).

2.2.2.5. Bolted Flange Plate Connection (BFP)

This configuration of beam-column connections aimed to increase the energy dissipation capacity of the connection by attaching the cover plate to beam flange using bolts instead of welding (Figure 2.8-a). Krawinkler and Popov (1980) reported a very complicated moment-rotation relationship of the Bolted Flange Plate connection due to buckling of flange plates. Yet, post-Northridge experimental work showed that this connection could dissipate significant amount of energy and all of the connection components contributed to the

yielding mechanisms of the connection as shown in Figure 2.8-b. The behaviour was eventually deteriorated by the slip of the bolts (Schneider and Teeraparbowng, 2002), but this connection still exhibited very high rotational ductility and developed the full plastic moment of the beam.

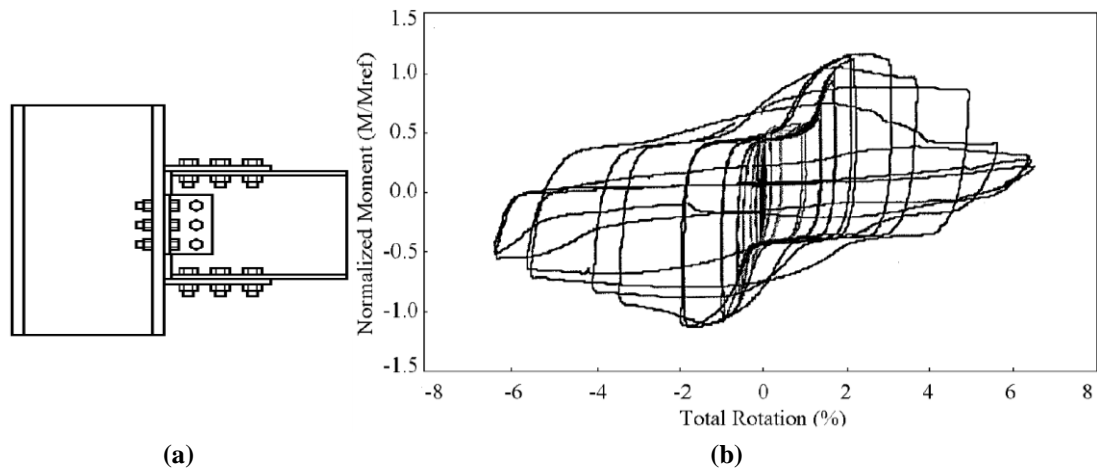


Figure 2.8: Typical bolted flange plate (BFP) connection: (a) connection arrangement and (b) moment-rotation relationship (FEMA 355D, 2000).

2.2.2.6. Proprietary Side-plate (SP) Connection

To avoid premature fractures occurring at the flange weld, this connection employed a gap between the beam and column flanges (Houghton, 1997). Imposed forces are transferred through fillet-welded side plates as shown in Figure 2.9-a. Moment-rotation relationship of this connection was found to be stable and had high reliability and ductility (Figure 2.9-b) which enabled the connection to be used for both retrofitted and new steel frame (Houghton, 1997; Deylami and Shiravand, 2004).

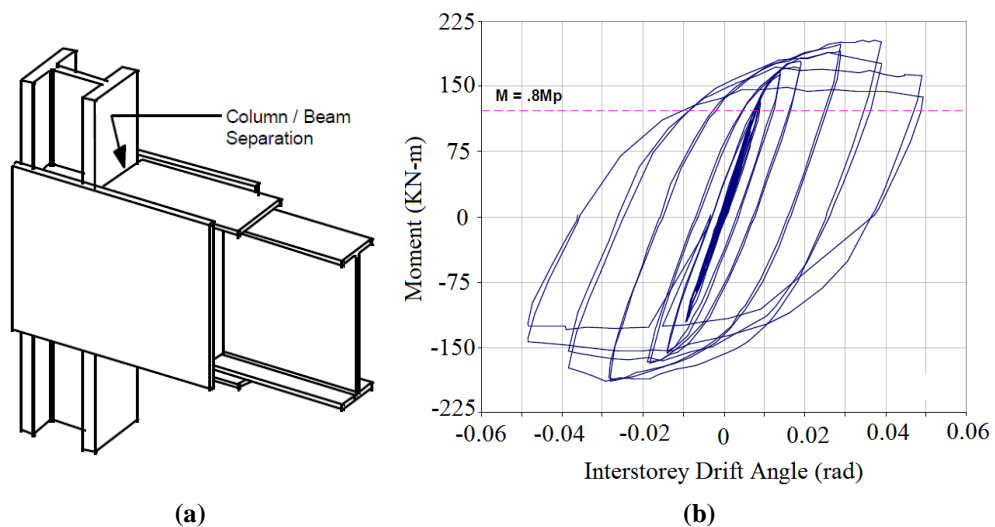


Figure 2.9: Proprietary side-plate connection (SP): (a) connection arrangement (Houghton, 1997) and (b) moment-rotation relationship (Deylami and Shiravand, 2004).

2.2.3. Conclusion on Prequalified Seismic Resistant Connections

The proposed solutions for improving the pre-Northridge earthquake steel beam-column connections were able to eliminate the defects that resulted from poor detailing and lack of construction quality, leading to significant improvement in rotational ductility and relatively reliable cyclic behaviour. However, all these solutions introduced relatively complicated and expensive detailing (especially connections with haunches and the proprietary side-plate connection) which made them suitable only for retrofit of existing structures.

On the other hand, reinforcing the connection with cover plates or haunches resulted in increased demand on the panel zone of the connection which led to complicated and expensive details for the panel zone without eliminating local or global residual drifts after the earthquake. Therefore, researchers were prompted to investigate new solutions that would overcome these defects in the post-Northridge connection details. Among these solutions was the use of self-centring systems in steel structures.

2.3. Self-Centring Systems

2.3.1. Introduction to Self-Centring Systems

To avoid structural failures and performance weaknesses resulting from local (at connection level) and global (at structure level) residual drifts, researchers came up with the idea of using self-centring systems. In fact, using structural techniques to restore residual deformations was not completely new. Aiken et al. (1993) tested a self-centring system when evaluating the structural performance of passive energy dissipating systems. It was explained that the use of Fluor-Daniel energy dissipation restraint would eliminate residual drifts existing after the cyclic testing of beam-column subassemblies. Preloading was vital for these systems to behave in the desired manner (Aiken et al. 1993; Ocel et al. 2004; Song et al. 2006). The preloading type depended on the self-centring system, but all self-centring systems were able to restore their initial characteristics upon unloading. The ability to eliminate plastic deformations was ensured because of either material (e.g. shape memory alloys) or mechanical (e.g. post-tensioning) properties.

The behaviour of self-centring systems was characterised by nearly zero residual deformations at the end of cyclic loading tests (Aiken et al. 1993), in which the system was also able to dissipate energy. The only type of behaviour which ensured these two abilities was the flag-shaped hysteresis behaviour. This idealised behaviour (Figure 2.10) was almost the same for all self-centring systems including shape memory alloys (SMAs, Aiken et al. 1993; Dolce and Cardone, 2001; Ocel et al. 2004; Song et al. 2006) and post-tensioned

connections (Ricles et al. 2001; Christopoulos et al. 2002^a). Also, it was found that self-centring systems change the stiffness and, consequently, the frequency of the base structure (Aiken et al. 1993).

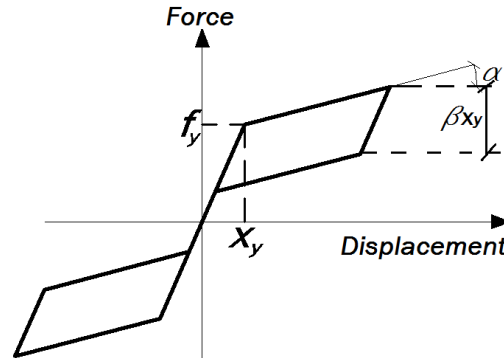


Figure 2.10: Idealised pseudo-force–displacement relationship for flag-shape hysteresis (Christopoulos, 2004): α : Post-yielding stiffness ratio, β : energy dissipation factor, x_y : yielding displacement, and f_y : yielding force.

2.3.2. Strategies of Structural Self-Centring

Two main self-centring strategies have been proposed so far: (i) using shape memory alloys (SMAs) and (ii) using post-tensioning forces

2.3.2.1. Self-Centring by Using Shape Memory Alloys (SMAs)

This strategy relies on the material properties of the self-centring system. It utilises the micro-structural characteristics of Shape Memory Alloys (SMAs) such as Nickel-Titanium alloy which possesses high ability of restoring inelastic deformations upon heating or changing strain (Aiken et al. 1993; Dolce and Cardone, 2001; Ocel et al. 2004; Song et al. 2006, Weber et al. 2006). Research has shown that the use of *SMAs* involved numerous advantages (Song et al. 2006, Weber et al. 2006), including high damping capacity, durability and fatigue resistance. These advantages encouraged engineers to integrate *SMAs* in passive energy dissipation systems at bracing, cable stays, beam-column connections or base isolation. All these forms have proven simplicity, versatility, strong self-centring capacity and good energy dissipation capability. Also, *SMAs* could be used in semi-active control of structures as heating increased the stiffness of the host structure and helped tuning its frequency to avoid resonance.

The behaviour of *SMAs* has been extensively studied (Dolce and Cardone, 2001; Ocel et al. 2004; Janke et al. 2005; Song et al. 2006). The key element in this behaviour was found to be the transformation temperature of the alloy. *SMAs* showed high ability to recover large deformations when heated above its transformation temperature. Characteristics of *SMAs* varied and exhibited unique characteristics at different temperatures. The behaviour of *SMAs*

was both thermal and mechanical as the increase in stress was equivalent to decrease in heating temperature (Ocel et al. 2004). The damping capacity of *SMA*s was dependent upon temperature, loading frequency and number of loading cycles (Dolce and Cardone, 2001, Janke et al. 2005).

A centring device that can take tension and compression forces was used in braced frames (Speicher et al. 2009; Yang et al. 2010). The device included helical Nickel-Titanium springs (NI-TI springs) or Belleville NI-TI washers (Figure 2.11-a) and showed very good self-centring and increased damping ratios, especially for the NI-TI springs (Figure 2.11-b).

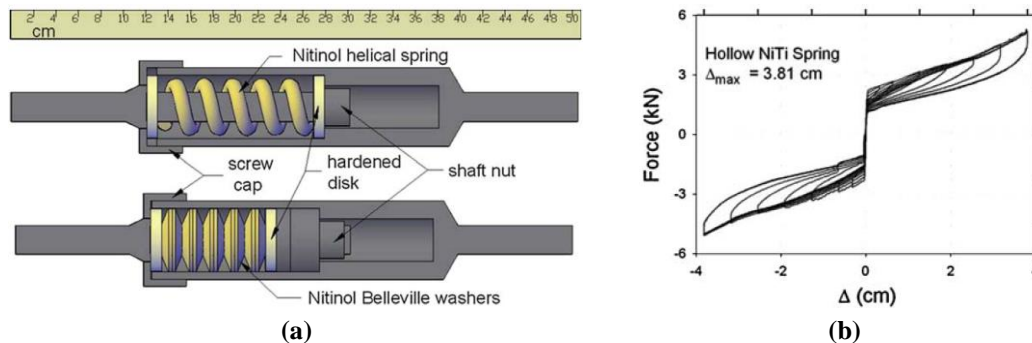


Figure 2.11: Nickel-Titanium self-centring bracing device (Speicher et al. 2009): (a) internal view and (b) F - Δ response of the device.

Attempts to utilise the characteristics of *SMA*s in a beam-column connection subassembly were made by Ocel et al. (2004) and Speicher et al. (2011). The proposed connection included four bars of Nickel-Titanium alloy used to dissipate energy and restore inelastic deformations upon heating after the cyclic testing. The performance of the connection was very good as *SMA* bars were able to restore about 75% of the inelastic deformations when heated. In addition, it was shown that moment-rotation relationship of the heated connection was almost identical to the initial behaviour (Figure 2.12). Also, deformations and energy dissipation were concentrated at the *SMA* bars and no significant yielding was noticed in the beam. Numerical modelling, evaluation and incorporation of these connections in multi-storey composite frames were investigated by Hu and Leon (2011) and Hu et al. (2011).

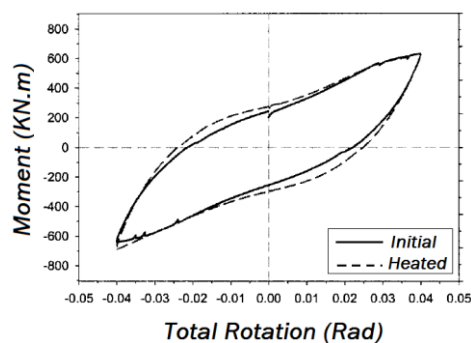


Figure 2.12: Comparison of hysteresis for initial and heated retested beam-column connections with *SMA* bars (Ocel et al. 2004).

2.3.2.2. Self-Centring by Using Post-tensioning Forces

This strategy utilises a mechanical technique represented by pre-stressing the structure before imposing loads instead of relying on the material properties to recover inelastic deformations induced on the structure. Applying post-tensioning forces was found to be a very reliable way to pull the structure back to its original position. Inspired by the pre-stressed concrete structures (Priestley, 1996), researchers came up with a similar technique to utilise pre-stressing in self-centring systems of steel structures. From the structural arrangement point of view, post-tensioning forces can be incorporated in two ways: (1) self-centring of braced structures, and (2) post-tensioned steel beam-column connections.

1. Self-centring of Braced Structures

A subassembly, originally proposed by Christopoulos et al. (2008), was introduced to provide self-centring of braced frames. The device utilised friction bolts to provide energy dissipation and post-tensioned tendons to ensure the self-centring capability of the frame (Figure 2.13).

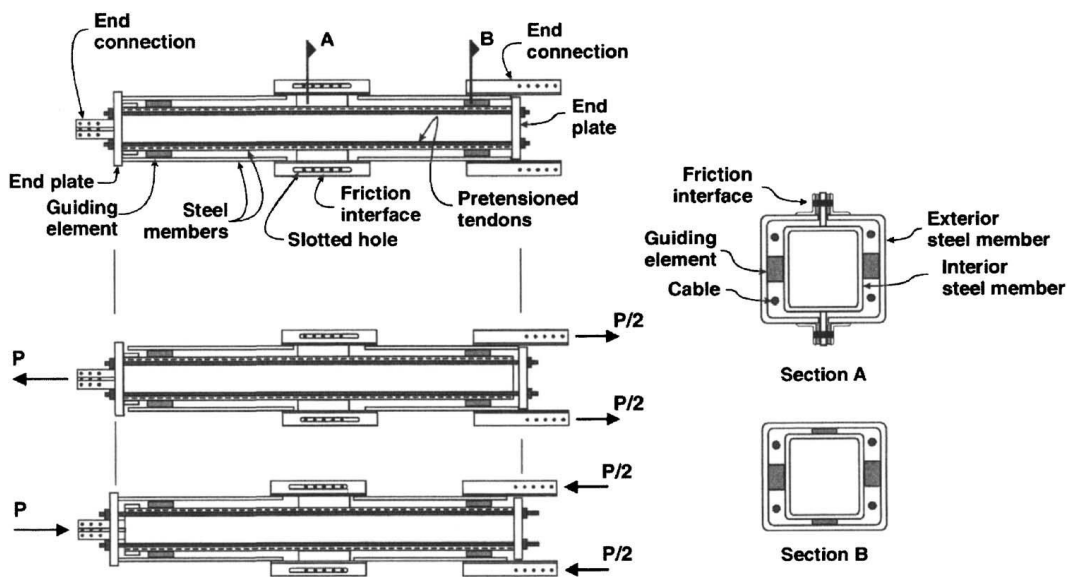


Figure 2.13: Embodiment of self-centring energy dissipating (SCED) system with steel tubes, tendons, and friction dissipative mechanism (Christopoulos et al. 2008).

This self-centring device was installed in the bracing of the frame (Figure 2.14) and exhibited very stable energy dissipating behaviour and very reliable self-centring capacity. However, since the energy dissipation device is displacement-based, this self-centring device was activated only at large deformations.

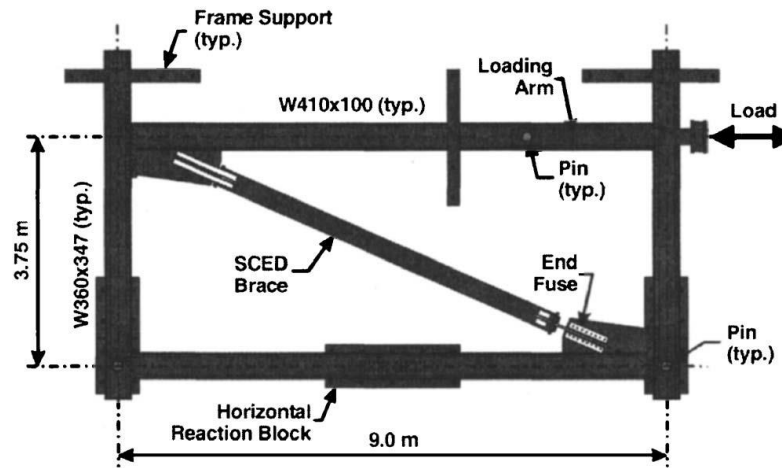


Figure 2.14: Setup for testing of braced frame incorporating SCED brace (Christopoulos et al. 2008).

Karavasilis et al. (2011) proposed the use of self-centring system incorporating a viscous damper together with the friction damper. The new system was able to dissipate energy at different levels of deformations (Figure 2.15). The system was velocity-based under small to moderate deformation amplitudes and displacement-based under large amplitudes. Hence, the system was able to dissipate more energy than the SCED. Incorporation and numerical simulations of the element behaviour in braced steel frames was presented by Karavasilis et al. (2011).

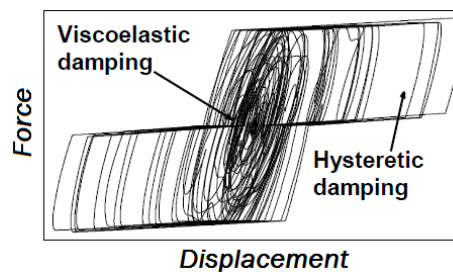


Figure 2.15: Hysteretic behaviour of SCVD (Karavasilis, 2010).

2. Post-tensioned Steel Beam-Column Connections

This system is a key subject of this research. Issues related to post-tensioned beam-column connections are thoroughly discussed in the next section.

2.4. Post-tensioned Steel Beam-Column Connections

2.4.1. Introduction to Post-tensioned Steel Beam-Column Connections

In parallel with the SAC venture project, and inspired by the pre-stressed concrete beam-column connections, researchers introduced the post-tensioned steel connections (Ricles et al. 2001; Christopoulos et al. 2002^a). The connection included two main components: (a) post-tensioned strands which provided the self-centring capacity of the connection and (b) energy

dissipation devices installed in the connection to provide energy dissipation. In the proposed arrangement, high tensile strands passed through the frame columns and ran parallel to the beam web along all spans for different types of energy dissipaters (Figure 2.16). Energy dissipaters were installed in each connection and took various forms. Energy dissipation in post-tensioned steel beam-column connection was mainly either yield-based or friction-based.

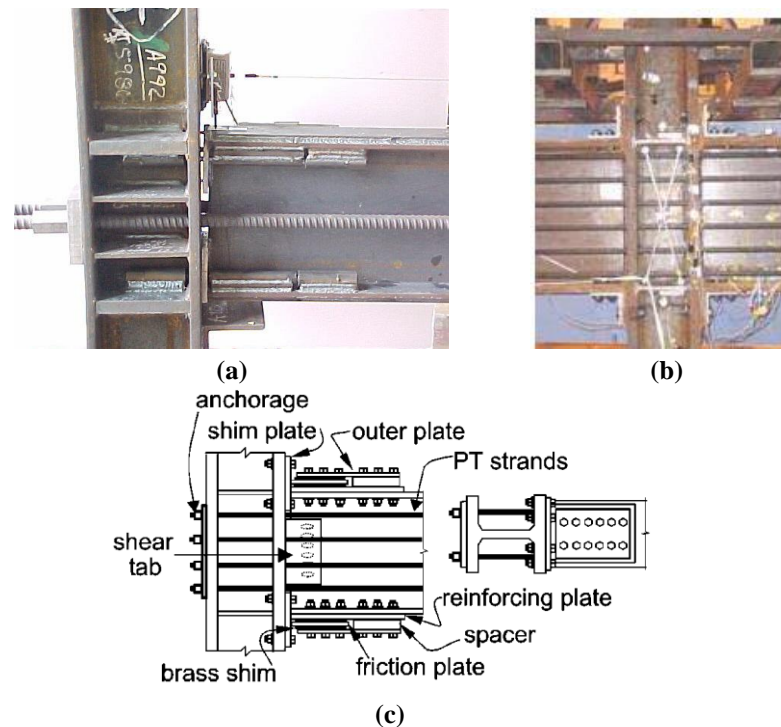


Figure 2.16: Arrangement of a post-tensioned steel beam-column connection: (a) using energy dissipating bars (Christopoulos et al. 2002^a), (b) using top and seat angles (Bruneau, 2004) and (c) friction energy dissipater installed at the beam flange (Rojas et al. 2004).

Several types of energy dissipaters for post-tensioned connections have been proposed so far. Christopoulos et al. (2002^a) proposed the use of replaceable energy dissipating bars to dissipate energy upon yielding (Figure 2.15-a). Independently, researchers at Lehigh University employed top and seat angles to provide energy dissipation mechanism through inelastic bending of the angles (Figure 2.15-b). Top and seat angles formed plastic hinges upon the loading of the connection and energy was dissipated via the rotation of these plastic hinges. Both types of energy dissipaters proved high reliability and energy dissipation capability. However, yield-based energy dissipaters were required to be replaced after experiencing plastic deformations. A more durable energy dissipater, which is friction-based, was proposed to avoid the need to replace yield-based dissipaters (Rojas et al. 2005). This friction energy dissipater (Figure 2.15-c) employed brass layers in friction surfaces (increasing the energy dissipation capacity) and clamping bolts (providing the normal force).

Another configuration of post-tensioned connection with friction energy dissipater was proposed to employ a shear tab energy dissipater. The friction damper was equipped with slotted holes allowing for bolts slippage (Tsai et al. 2008) as shown in Figure 2.17.

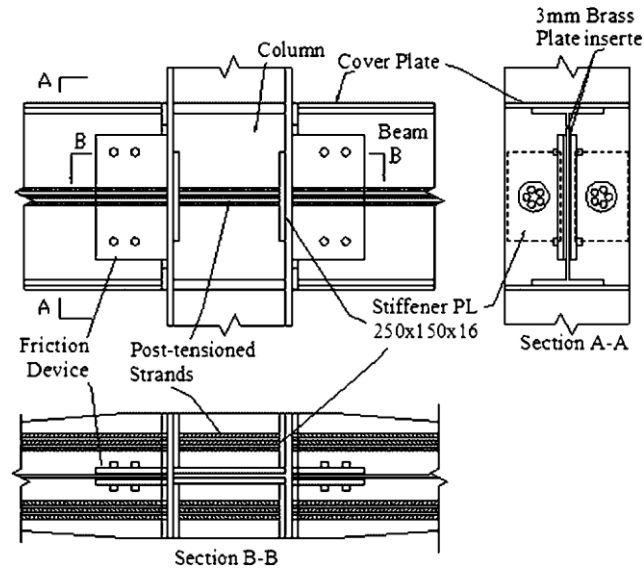


Figure 2.17: Post-tensioned connection with friction energy dissipater installed at the beam web (Tsai et al. 2008).

Regardless of the type of the energy dissipater installed in the connection, all post-tensioned connections shared similar behaviour. Post-tensioned connections were characterised by their flag-shaped hysteretic behaviour (Figure 2.18; Christopoulos et al. 2002^a).

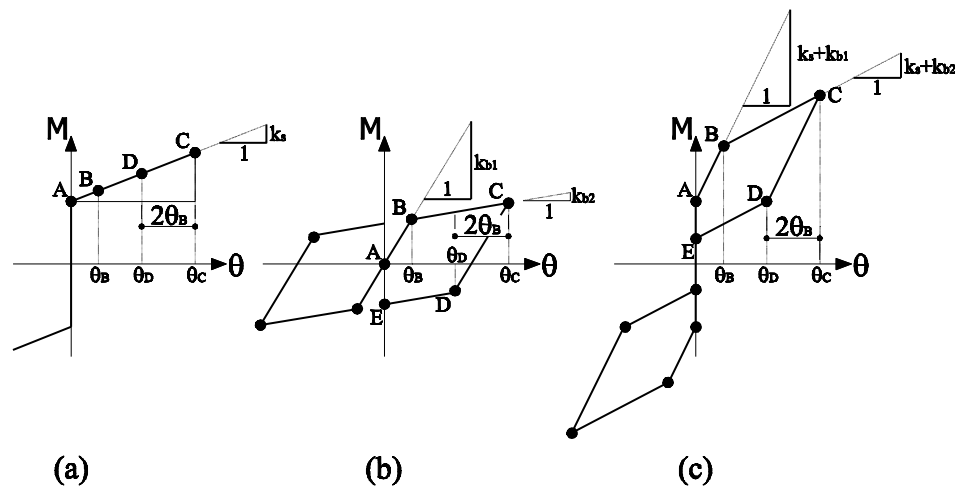


Figure 2.18: Hysteretic model of post-tensioned connection with energy dissipating bars (Christopoulos et al. 2002^a): (a) post-tensioned strands, (b) energy dissipating bars and (c) post-tensioned connection

The key point in the behaviour of post-tensioned connections was the gap opening (Ricles et al. 2001; Christopoulos et al. 2002^a). The equations describing the connection behaviour were very similar for all types of energy dissipation mechanisms adopted in the connection. This set of equations was derived from Figure 2.18 showing that as long as the applied

moment was less than the moment provided by the post-tensioned strands (M_{St}), the connection behaved as fully rigid connection experiencing no relative rotations between the beam and the column. Once the applied moment exceeded M_{St} , a gap started opening between the beam and the column and the energy dissipating device started contributing to the resisting moment of the connection. The resisting moment of the connection is calculated from:

$$M_{R1} = M_{St} + (k_s + k_{b1}) \theta, \quad (2.4)$$

where k_s is stiffness of the strands, k_{b1} is first stiffness of the energy dissipation device and θ is the relative rotation between the column and beam.

When the applied moment exceeds the yield/slip force of the energy dissipating device, the resisting moment of the connection is given as:

$$M_{R2} = M_{R1} + (k_s + k_{b2}) (\theta - \theta_B), \quad (2.5)$$

where k_{b2} is the second stiffness of the energy dissipating device and θ_B is the rotation angle at which the energy dissipation device starts yielding/slipping. Unloading the connection was characterised by two phases. The first phase took place when $\theta_D \leq \theta \leq \theta_C$ where $\theta_D = \theta_C - 2\theta_B$. The resisting moment of the connection at this phase is given in Equation (2.6). If the energy dissipating device was friction based, the second stiffness would be zero.

$$M_{R3} = M_{R2} + (k_s + k_{b1}) (\theta - \theta_C), \quad (2.6)$$

The second unloading phase started when $\theta \leq \theta_D$ and the resisting moment could be obtained from:

$$M_{R4} = M_{R3} + (k_s + k_{b2}) (\theta - \theta_D). \quad (2.7)$$

Although equations (2.4) through (2.7) describe the general behaviour of post-tensioned connections quite well, discrepancies in the hysteretic behaviour did exist depending on the type of the energy dissipater. Also, the resistance of the connection to shear forces and bending moment depended on the energy dissipating device.

2.4.2. Types of Post-tensioned Steel Beam-Column Connections

A Summary of the differences between post-tensioned connections with different energy dissipaters was presented by Eljajeh (2010). The comparison was based upon three main points: (a) energy dissipaters and dissipating mechanism, (b) connection resistance to shear forces and bending moment and (c) hysteretic behaviour of the connection.

2.4.2.1. Post-tensioned Connections with Energy Dissipating Bars

Figure 2.19 shows the configuration of a post-tensioned connection with energy dissipating bars. Replaceable steel bars were installed in the connection and confined with steel cylinders to avoid buckling (Ricles et al. 2001; Christopoulos et al. 2002^a; Christopoulos et al. 2002^b; Esposito, 2008). Upon gap opening of the connection, these bars elongate and yield to dissipate energy. The resistance of the bending moment in this connection is provided by dual action of the post-tensioned strands and the energy dissipating bars (Christopoulos et al. 2002^a; Wang, 2004). Shear resistance was provided by friction at the interface between the beam and the column flange. However, shear resistance of the connection dropped substantially upon gap opening as the contact area between beam and column became very small. Therefore, it was recommended to provide a separate mechanism to transfer shear forces.

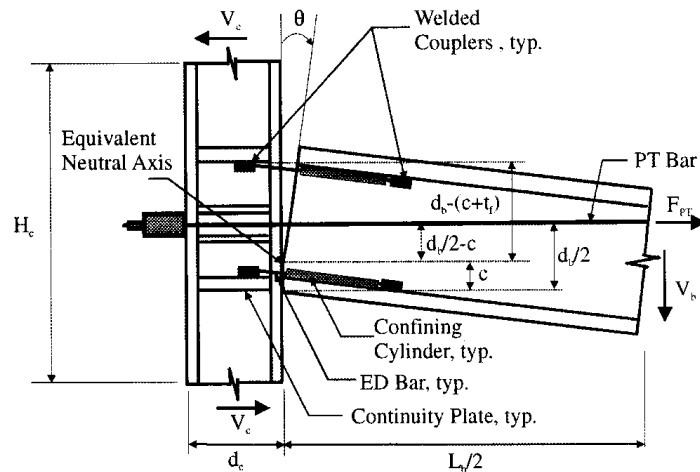


Figure 2.19: Configuration and gap-opening of post-tensioned connection with energy dissipating bars (Christopoulos et al. 2002^a).

The hysteretic behaviour of the post-tensioned connection with energy dissipating bars is shown in Figure 2.18. As the energy dissipating bars have bi-linear behaviour, they contributed to the moment resistance in two stages, having a first stiffness prior to yielding and second stiffness in the post-yielding stage.

2.4.2.2. Post-tensioned Connections with Top and Seat Angles

Top and seat angles provided at each connection were used to provide an energy dissipation mechanism to these systems. Upon the gap opening, seat angles deformed plastically and formed plastic hinges at the top and bottom (Figure 2.20-a). The bending moment resistance in this connection was provided by dual action of the post-tensioned strands and the seat angles. Shear resistance was provided by friction at the interface between the beam and the

column flange. In this arrangement seat angles were designed to contribute to the shear resistance (Garlock et al. 2007; Garlock and Li, 2008; Garlock et al. 2008).

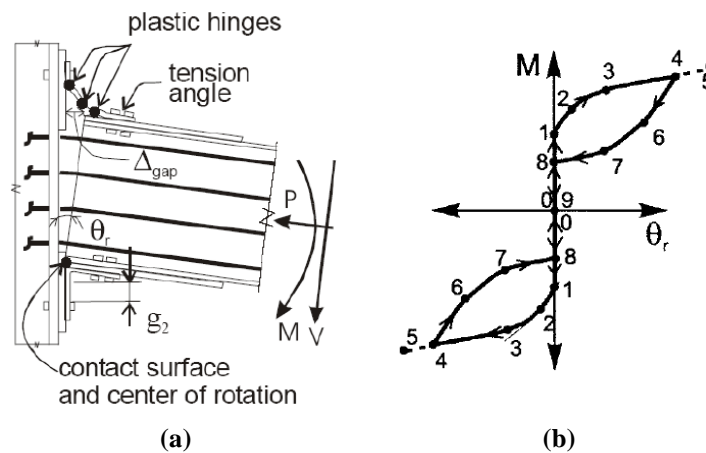


Figure 2.20: Behaviour of post-tensioned connection with top and seat angles: (a) configuration and decompression (Bruneau, 2004) and (b) moment-rotation behaviour.

The hysteretic behaviour of post-tensioned connections with top and seat angles is illustrated in Figure 2.20-b. As several plastic hinges formed during decompression and gap opening of the connection, the hysteretic behaviour took a curved shape characterised by a change of slope at the formation of each plastic hinge.

2.4.2.3. Post-tensioned Connections with Friction Damper

This connection utilised a friction mechanism to provide a system with high capability of energy dissipation. The connection was provided with a brass layer between two layers of steel and installed at the beam flange (Figure 2.15-c) or at the beam web (Figure 2.16). The connection was supplied with slotted holes which allowed the bolts to slip and dissipate energy (Rojas et al. 2004; Rojas et al. 2005; Tsai et al. 2008; Kim and Christopoulos, 2008).

Moment resistance of the connection was provided by the post-tensioned strands as well as the friction forces in the friction device. Shear resistance was provided by friction at the interface between the beam and the column flange (Lin et al. 2008). If the friction device is installed at the beam web, it is used to provide shear resistance when the gap opens and the contact area between the beam and the column flange is reduced.

Moment-rotation behaviour of post-tensioned connections with friction energy dissipaters is shown in Figure 2.21. Since most of friction energy dissipaters have rigid-plastic behaviour, the gap-opening phase cannot be distinguished. However, actual gap-opening of the beam starts at point (1). Also, since the post-slip stiffness is zero, friction forces do not contribute to the moment resistance after the bolts slip.

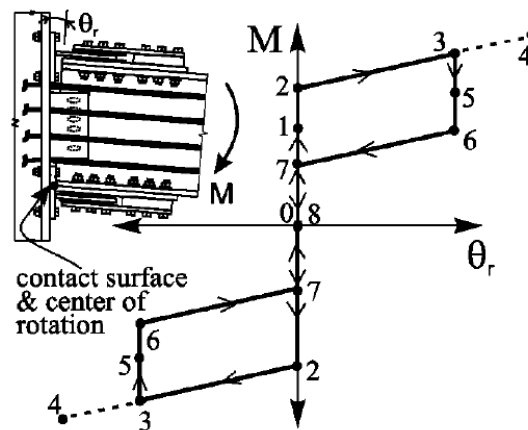


Figure 2.21: Moment-rotation behaviour of post-tensioned friction damped connection (Rojas et al. 2005).

2.4.2.4. Post-tensioned Connections with Web Hourglass Shape Energy Dissipaters

A newly developed yield-based energy dissipater was recently proposed for the use in post-tensioned steel connections. This energy dissipater took the shape of hourglass and was placed on the beam web to avoid interference with the slab (Figure 2.22; Vasdravellis et al. 2013^a). The structural identification and the experimental results of post-tensioned connections with hourglass shape pins, including determining the rotational stiffness and plastic design of the hourglass pins were carried out by Vasdravellis et al. 2013^{a,b} and Dimopoulos et al. 2013.

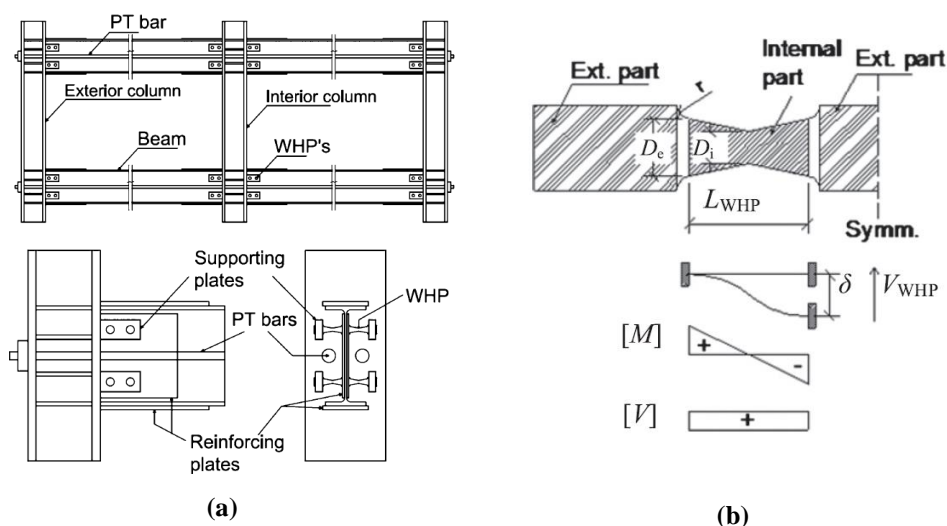


Figure 2.22: Post-tensioned steel connections with hourglass shape energy dissipater: (a) frame incorporating the proposed PT connection and exterior PT connection details and (b) Geometry of half a WHP, assumed static system, and internal forces diagrams (Vasdravellis et al. 2013^a).

Moment resistance of the connection was provided by both the PT strands and the energy dissipating pins. The energy dissipating pins could help also in the shear resistance but it was

recommended to provide a separate shear mechanism such as a shear tab or seat angles because the vertical shear strength of the hourglass pins was reduced when they experienced horizontal shear as a result of moment development in the connection.

The moment-rotation relationship of this type of post-tensioned connections (Figure 2.23) is characterised by four different stiffnesses: (i) before gap-opening (*infinite* stiffness), (ii) after gap-opening with no yielding in the hourglass pins (K_1), (iii) gap-opening with yielding of one hourglass pin at θ_2 (K_2) and (iv) gap-opening with yielding of the two hourglass pins at θ_3 (K_3).

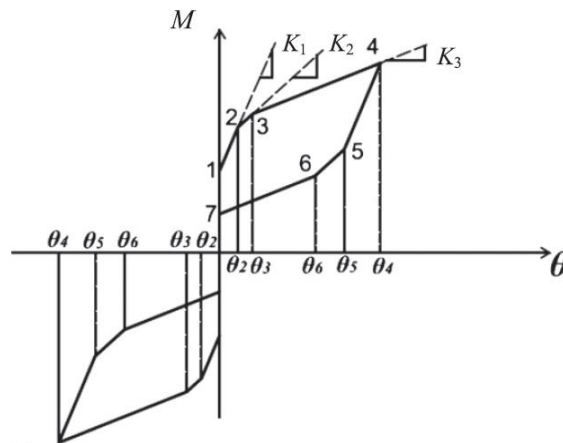


Figure 2.23: Moment-rotation relationship of PT connections with hourglass web pins energy dissipaters (Vasdravellis et al. 2013^a).

2.4.3. Advantages and Technical Issues of Post-tensioned Steel Beam-Column Connections

The use of the post-tensioned steel connections incorporates several potential advantages (Ricles et al. 2001; Christopoulos et al. 2002^a; Ricles et al. 2002^b; Rojas et al. 2004; Bruneau, 2004; Wang, 2004; Bruneau et al. 2005; Suase et al. 2005; Chou and Lai, 2009):

- No need for field welding which was a main reason of the low ductility of beam-column connections,
- Simple erection and construction as the connection was made with conventional materials and skills,
- High self-centring capacity which ensured small local and global residual drifts,
- Initial stiffness of post-tensioned connections similar to the fully welded connections in Moment Resistant Frames,
- Confining the damage anticipated in the frame to the energy dissipaters installed in these connections and therefore, reducing the damage in the beam,

- Incorporating the nonlinear characteristics of yielding structures and therefore, limiting the induced seismic forces and providing additional damping,
- Element sizes in post-tensioned steel frames were the same as those in conventional frames,
- Controlling the lateral force demand due to a softening in the force- displacement behaviour under earthquake loads. This softening was caused by gap opening rather than structural damage, and
- High ductility capacity as the ductility was not governed completely by the ductility of the structural elements (beams/columns).

The use of post-tensioned connections however, raised a few technical issues regarding the performance of these systems in composite steel frames. Two major issues were associated with the use of post-tensioned connections: (a) influence of the composite slab on the post-tensioned connection (Garlock et al. 2007; Garlock and Li, 2008; Swensen, 2008; Chou et al. 2008), and (b) replacement of energy dissipaters that had experienced plastic deformations during severe earthquake (Chou and Lai, 2009; Wolski et al. 2009).

Interference of the composite slab with the post-tensioned connection affects the performance of the connection adversely. As the gap opening event is a critical factor for the performance of the post-tensioned connection, it was not allowed for the composite slab to interfere or obstruct the gap opening (Swensen, 2008; Chou et al. 2008). When subjected to lateral loads, the post-tensioned frame deformed and therefore, the distance between the beam-column nodes extended as shown in Figure 2.24.

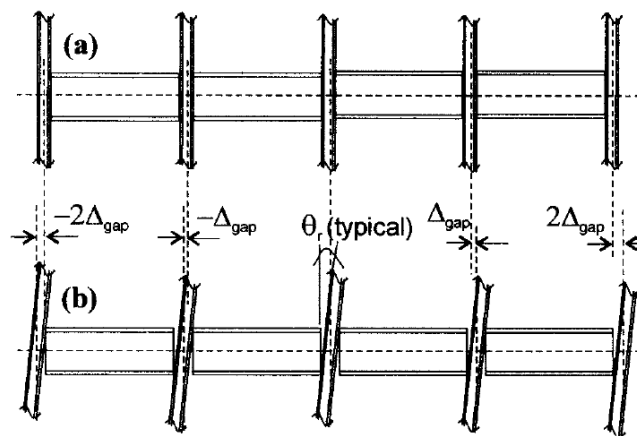


Figure 2.24: Elevation of post-tensioned steel frame: (a) not deformed, (b) deformed (Garlock et al. 2007).

When the gap opens, the floor restrains the frame from developing the gap which imposed more axial forces on the beam in addition to the post-tensioning forces. To avoid this malfunction of the post-tensioned system, a collector beam was needed to take the

deformation from the composite floor and transfer it to the post-tensioned frame. Additional axial forces applied to the collector beam and transferred to the frame can be estimated from:

$$f_x^{cb} = k_{cb} \Delta_{gap}, \quad (2.8)$$

where f_x^{cb} is the additional axial force transferred by the collector beam, k_{cb} is the stiffness of the collector beam and Δ_{gap} is the gap opening of the post-tensioned frame.

Although collector beams were connected to the interior columns only, applied seismic forces were distributed over all spans as axial forces. Consequently, axial forces varied over spans (Figure 2.25; Garlock et al. 2007).

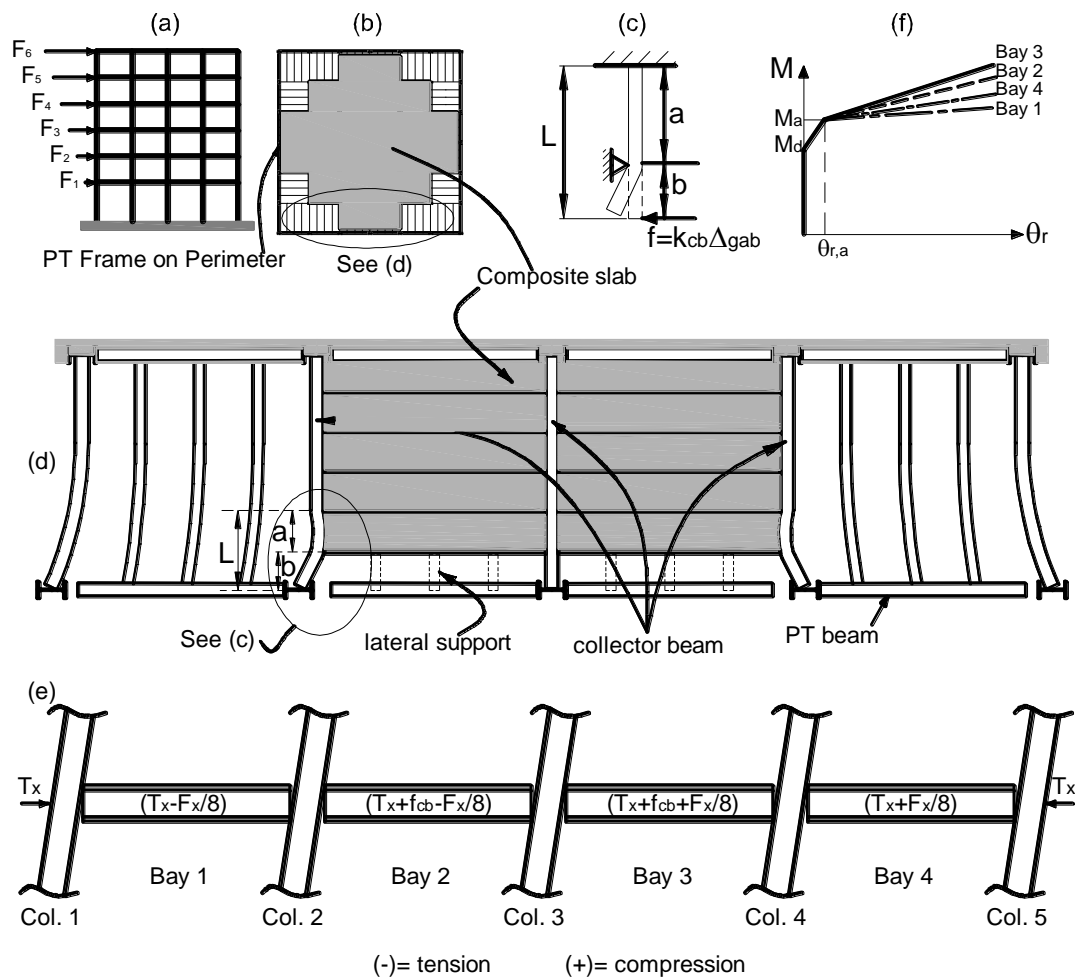


Figure 2.25: (a) Floor inertia forces on building, (b) plan of hypothetical building, (c) deformation of collector beam, (d) interaction of PT frame with gravity system, (e) beam axial forces in each bay, and (f) idealised moment-rotation relationship of the connection (Garlock et al. 2007).

A system to transfer gravity loads to the post-tensioned frame and accommodate the gap opening using the collector beam was proposed by Swensen (2008). The proposed system, shown in Figure 2.26, transferred gravity loads reliably and did not intervene with post-tensioned strands.

Another solution was proposed by Chou et al. (2008) to avoid the slab interference with the post-tensioned connection by using discontinuous composite slab at the column centreline so that the gap opening can be properly accommodated. The behaviour of post-tensioned connections with discontinuous composite slab was very similar to the behaviour of post-tension connection in a continuous slab system.

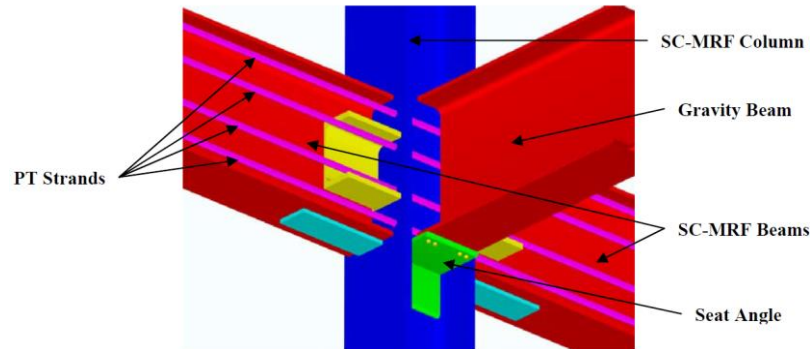


Figure 2.26: Devices for gravity force transfer in self-centred moment resistant frame (Swensen, 2008).

Replacement of energy dissipaters installed in the connection was also a subject of concern. Energy dissipaters were expected to experience plastic deformations after the event of severe earthquake. The interaction between the floor slab and energy dissipaters installed at the top flange of the beam makes it difficult to replace these energy dissipaters (Tsai et al. 2008; Wolski et al. 2009). One of the proposed solutions was the use of a bottom flange friction device (Wolski et al. 2009). The result was asymmetric hysteretic behaviour obtained from the different lever arm of the bottom flange friction device for positive and negative moments (Figure 2.27). Post-tensioned frames equipped with bottom flange friction devices exhibit asymmetric moment capacity and hence require the beam to be deeper or to increase the post-tensioning forces.

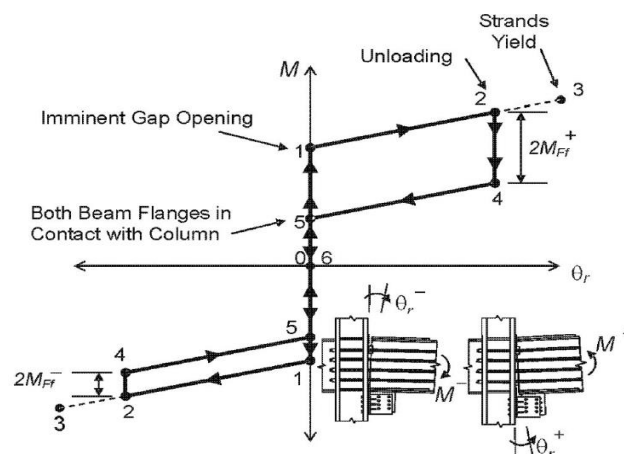


Figure 2.27: Moment-rotation behaviour of post-tensioned connection with bottom flange friction device (Wolski et al. 2009).

A better technique was proposed to install the friction dissipater at the beam web rather than the flange (Tsai et al. 2008). This solution showed reliable symmetric hysteretic behaviour. This configuration provided a safe mechanism to transfer shear forces by employing a web channel to act as (i) energy dissipater supplied with slotted bolt holes and layers of brass and (ii) a shear tab to transfer shear forces. Furthermore, web friction channels were not required to be replaced as they remain linear elastic. Brass layers could be easily maintained and replaced if needed.

2.4.4. Modelling of Post-tensioned Steel Beam-Column Connections

After the introduction of post-tensioned steel beam-column connection, three approaches have been proposed to analyse their behaviour (Kim and Christopoulos, 2009): (a) discrete springs model, (b) integrated single rotational spring model, and (c) finite element model. The detailed finite element model (Esposito, 2008; Vasdravellis et al. 2013^b) was used to investigate the behaviour of connection components: post-tensioning strands and energy dissipating (friction or yield) elements.

The finite element modelling was used to study stresses and expected failure modes of post-tensioned steel beam-column connections. The results of this study showed that the finite element approach provides a detailed representation of deformations and stress-states of all elements involved in the connection, as well as different types of failures (such as beam buckling and bearing action of shim plates) that cannot be captured when using other techniques. The accuracy of the FE simulations was verified by comparison with experimental results (Christopoulos et al. 2002^a; Ricles et al. 2002^b; Vasdravellis et al. 2013^a). This approach is however very expensive from a computational point of view and detailed FE models would be only suitable for a standalone connection, but not for incorporating the model into full frame analysis.

The discrete springs model (Ricles et al. 2001; Dobossy et al. 2006, Dimopoulos et al. 2013) aimed at enabling the user to incorporate the connection model into a full frame model. It represented the connection behaviour well, but incorporating the connection model into a full frame required using a large number of nodes to represent the connection accurately. An attempt was made by Christopoulos et al. (2002^a) to provide a simple model by using only one rotational spring, but this model was not able to capture the gap opening event (Dobossy et al. 2006).

In the discrete springs model proposed by Ricles et al. (2001), the connection is represented by a set of compression only springs and truss elements (Figure 2.28). The gap opening of the connection is represented by gap elements which are compression only springs. These

elements have a very high stiffness when subjected to compression and zero stiffness under tension (Figure 2.29-a; Powel, 1993). Truss elements are used for energy dissipating bars. Stiffness of the panel zone can be computed as proposed by Castro et al. (2005) and assigned to a rotational spring. Master and slave nodes are selected and assigned to ensure the stability and compatibility of deformations of the connection.

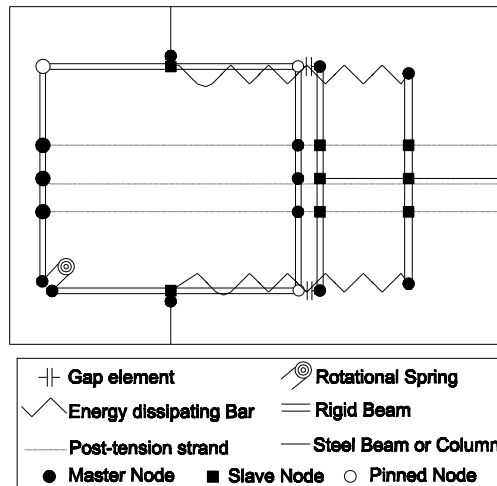


Figure 2.28: Discrete springs model of post-tensioned connection (Ricles et al. 2001; Dobossy et al. 2006).

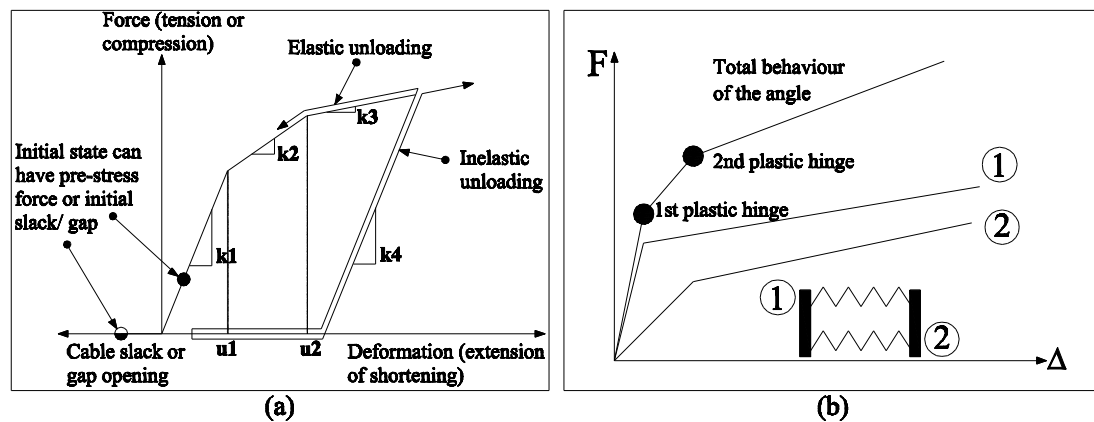


Figure 2.29: Representation of the post-tensioned connection elements in the discrete springs model: (a) gap element (Powel, 1993) and (b) top and seat angles.

Type and computational model of the truss element representing the energy dissipater varies depending on the behaviour of the energy dissipater. Energy dissipating bars (Christopoulos et al. 2002^a; Wang, 2004) are represented using bilinear elasto-plastic truss elements with suitable post-yielding stiffness. If the energy dissipating device installed in the connection is friction based (Tsai et al. 2008; Kim and Christopoulos, 2008; Wolski et al. 2009), it is represented by rigid – ideal plastic truss element models having the same slip force as the friction dissipater. Top and seat angle dissipaters (Garlock et al. 2007; Garlock and Li, 2008; Garlock et al. 2008) are more complicated and cannot be represented by a single element.

Ricles et al. (2001) used two parallel bilinear truss elements to simulate the force-displacement behaviour of the angle (Figure 2.29-b). The model was based on a pushover analysis of a fibre model of a steel angle and all plastic hinges were represented properly.

The advantage of discrete springs approach over other FE models is that it enables the user to incorporate the model of the post-tensioned connection into frame analysis software without further development. However, the model of each connection requires a large number of nodes (25 nodes in case of the connection shown in Figure 2.28) which means that incorporating the model into full frame models of larger structures, with many such connections, would be cumbersome and increase the computational costs of the analysis.

Post tensioned connections can be easily incorporated in 2D frame models if it is represented by a single rotational spring (Christopoulos et al. 2002^a; Dobossy et al. 2006- Figure 2.30). This model did not capture the gap opening event and its moment-rotation relationship showed noticeable differences from relationships obtained in experimental investigations (Christopoulos et al. 2002^a) and by the detailed discrete springs models (Ricles et al. 2001). While the response of frames modelled using single rotational springs was very similar to the one obtained by discrete springs model (Dobossy et al. 2006), this single spring model (Christopoulos et al. 2002^a) did not provide direct information on the forces in the post-tensioning strands and dissipation elements.

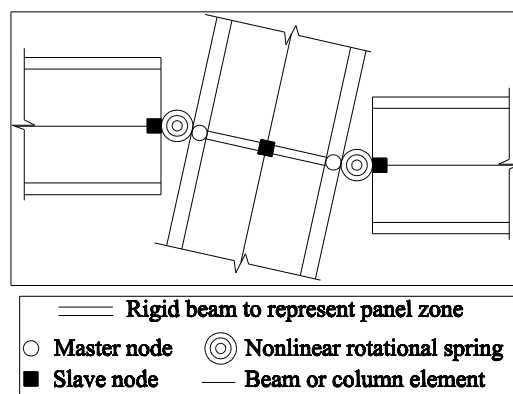


Figure 2.30: Rotational springs model (Dobossy et al. 2006).

2.4.5. Design of Post-tensioned Steel Beam-Column Connections

Design of post-tensioned beam-column connections has been the subject of an extensive research (Christopoulos et al. 2002^a; Rojas et al. 2004; Garlock et al. 2007; Tsai et al. 2008; Garlock et al. 2008; Chou et al. 2008; Chou and Lai, 2009; Kim and Christopoulos, 2009). Any design approach was required to satisfy two main criteria: (i) strength of the post-tensioned connection and (ii) performance demand at local and global levels.

Christopoulos et al. (2002^a) proposed the strength-based design approach for post-tensioned connections with energy dissipating bars. This approach was based on the sectional analysis of the connection with iterative procedure to estimate strains and stress in the connection components. However, it did not determine any performance criteria for the post-tensioned connection.

The performance based design approach (FEMA 350; 2000) for the post-tensioned connections included the following performance levels (Garlock et al. 2007; Tsai et al. 2008):

- Fully Operational Level under Design Earthquake having 50% probability of being exceeded within 50 years. For this level the whole system remains elastic, without gap opening or yielding in the energy dissipating device.
- Immediate Occupancy Level under Design Based Earthquake (DBE) having 10% probability of being exceeded within 50 years. The rotational demand of the post-tensioned connection for this level is less than 0.035 rad. Gap opening develops and energy dissipaters undergo plastic deformations.
- Collapse Prevention Level under Maximum Considered Earthquake (MCE) having 2% probability of being exceeded within 50 years. The rotational demand of the post-tensioned connection for this level is less than 0.05 rad. The connection undergoes significant plastic deformations and post-tensioned strands may yield.

Based on these performance levels, Chou et al. (2008) proposed the following steps as design procedure for a standalone post-tensioned connection:

1. Select the target design drift (i.e. 4% close to gap-opening angle of 0.03 rad for Immediate Occupancy performance level) and compute the corresponding beam moment and moment provided by the energy dissipaters.
2. Determine the area of strands based on the expected proportion of moment contribution by the strands from the total moment.
3. Calculate stresses in the strands at the target gap-opening angle by considering the initial post-tensioning forces, elongation of the strands and beam shortening. If the tensile stress is greater than the limit, it is suggested to increase the area of the strands.

2.4.6. Parameters Affecting the Behaviour of Steel Beam-Column Post-tensioned Connections

The main parameters controlling the behaviour of post-tensioned connections are: (i) post-yielding to pre-yielding stiffness ratio (α); (ii) energy dissipation factor (β); and (iii) post-tensioning forces of the connection (F_{pt}) (Christopoulos et al. 2002^b; Christopoulos, 2004;

Wang, 2004; Garlock et al. 2007; Garlock and Li, 2008). In addition, Garlock et al. (2008) studied the influence of other parameters including the strength of the panel zone and the increased connection strength in the upper floors of post-tensioned steel frame on the global response of the frame. However, post-yielding stiffness, energy dissipating factor and initial post-tensioning force in the connection were found to have far stronger effect on the behaviour of the connection itself and the post-tensioned steel frame as a whole.

2.4.6.1. Post-Yielding to Pre-Yielding Stiffness Ratio (α)

The post-yielding to pre-yielding stiffness ratio (α) is a characteristic of the energy dissipation device installed in the post-tensioned connection (Figure 2.31). This ratio can be defined for the hysteretic behaviour of the post-tensioned connections with energy dissipating bars or friction energy dissipaters. Post-tensioned connections with top and seat angles develop numerous plastic hinges, resulting in gradual changes in post-yielding stiffness (i.e. tangent stiffness rather than a single post-yielding stiffness ratio).

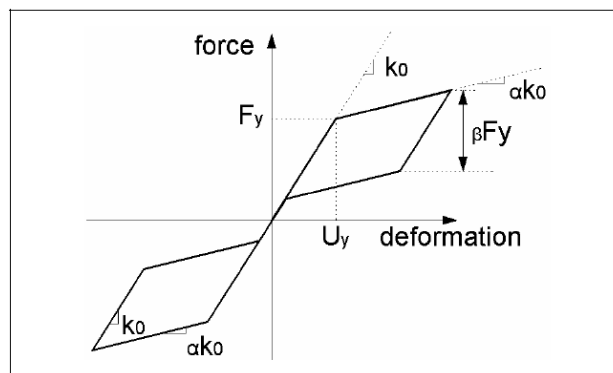


Figure 2.31: Post-yielding to pre-yielding stiffness ratio of post-tensioned connection with energy dissipating bars (Wang, 2004).

A study conducted by Christopoulos et al. (2002^b) concluded that post-yielding to pre-yielding stiffness ratio has a significant effect on the response of post-tensioned connections in terms of ductility, energy dissipation and acceleration under seismic loading. These results were confirmed by Christopoulos (2004) when the response of the post-tensioned connection was studied in the frequency domain. Wang (2004) showed that post-yielding stiffness ratio for self-centring systems can reach 0.35 which is high in comparison with post-yielding stiffness ratios of elasto-plastic systems, which are typically about 0.02. These results indicated that large difference in response between self-centring systems and elasto-plastic systems can be noticed under the same loading conditions. For friction-based energy dissipaters the post-yielding stiffness ratio was related to the strands stiffness only as the post-slip stiffness of friction dissipaters is generally zero. In contrast, the cross-sectional area of the energy dissipating bars had high contribution in the post-yielding stiffness of the

post-tensioned connection as their second stiffness contributed to the post-yielding stiffness of the connection (Wang, 2004).

2.4.6.2. Energy Dissipation Factor (β)

The energy dissipation factor of post-tensioned steel beam-column connections is defined as:

$$\beta = \frac{M_{Ed}}{M_{St}}, \quad (2.9)$$

where M_{Ed} is moment provided by the energy dissipation device installed in the connection and M_{St} is moment provided by post-tensioned strands before gap opening.

Thorough investigations of the effect of energy dissipation factor on the response of the post-tensioned connections were conducted by Christopoulos et al. (2002^b). The research showed that (β) had high influence on the response in terms of ductility, moment capacity, energy dissipation capacity and self-centring characteristics of the post-tensioned connection. Recommended values for β have been proposed in many research papers. Christopoulos (2004) showed that values of energy dissipation factor should lie within the range [0, 1]. When $\beta = 0$, the system behaved as bilinear elastic system and β was required to be less than 1 to ensure full self-centring of the connection (Figure 2.32).

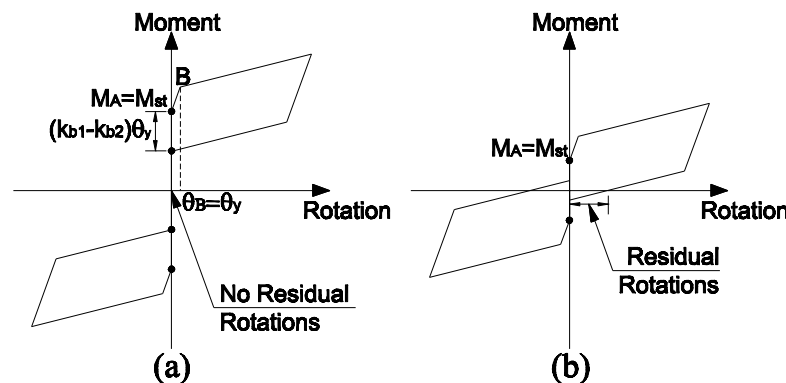


Figure 2.32: Full self-centring requirement for post-tensioned connections: (a) sufficient post-tensioning forces and (b) insufficient post-tensioning forces.

Other research indicated that the full self-centring requirement, shown in Figure 2.30, is associated with $\beta < 0.5$ (Wolski et al. 2009). More refined ranges were proposed for β to lie within the range [0.2, 0.3] to provide enough self-centring, high ductility and reliable energy dissipation capacity (Wang, 2004; Chou et al. 2008; Chou and Lai, 2009). Regarding asymmetric hysteresis of post-tensioned connections supplied with bottom flange friction energy dissipaters, Wolski et al. (2009) proposed calculating two values of β and taking the mean as effective value of energy dissipation factor of the connection as shown in Figure 2.33.

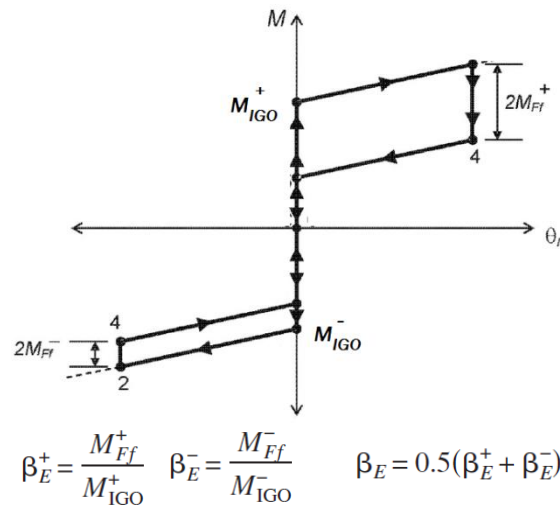


Figure 2.33: Computation of energy dissipation factor for post-tensioned connections with asymmetric hysteresis (Wolski et al. 2009).

The energy dissipation factor is directly related to the post-tensioning forces as it is inversely proportional to the moment provided by the post-tensioned strands. Therefore, determining of a correct (or optimum) energy dissipation factor requires more investigations of the effect of post-tensioning forces on the behaviour of the connection.

2.4.6.3. Post-tensioning Forces (F_{pt})

Post-tensioning forces applied on the strands in PT steel beam-column connections are the main parameter that determines the behaviour of the connection. Characteristics including self-centring capacity, moment resistance and rotational ductility of the connection are closely related to post-tensioning forces applied on the strands. Therefore, considerable effort has been spent to study the influence of post-tensioning forces on the behaviour of the connection and to specify their applicable ranges (Garlock et al. 2007; Tsai et al. 2008; Garlock and Li, 2008; Lin et al. 2008). The basic requirement for post-tensioning forces is to provide the connection with full self-centring capability. Christopoulos et al. (2002^b) showed that the lower bound of post-tensioning forces can be obtained from:

$$M_{St} \geq (k_{b1} - k_{b2}) \theta_B, \quad (2.10)$$

where θ_B is rotation angle at which energy dissipating device starts yielding/slipping, k_{b1} is the first stiffness of the energy dissipating device and k_{b2} is the second stiffness of the energy dissipating device.

The total post-tensioning force in the strands is chosen to cause neither local buckling in the beam nor yielding of the strands. The total force in the strands is composed of few components (Garlock and Lai, 2008):

$$P_i = F_{pt} + \Delta T + f_i^{cb} + f_i^{if}, \quad (2.11)$$

where P_i is the final force in the post-tensioned strands, F_{pt} is the initial post-tensioning force, ΔT is the induced force due to the gap opening, f_i^{cb} is force resulting from the diaphragm action (collector beam deformation) and f_i^{if} is the inertial force carried by the PT frame.

For inter-storey drifts less than 0.05, Garlock and Lai (2008) proposed closed forms to calculate each component of P_i and their test results showed the following ratios for the contribution of each component to the total force:

$$0.5 < \frac{F_{pt}}{P_i} < 1.0, \quad 0 < \frac{\Delta T}{P_i} < 0.3, \quad 0 < \frac{f_i^{cb}}{P_i} < 0.2, \quad 0 < \frac{f_i^{if}}{P_i} < 0.1$$

Among these components, the initial post-tensioning force is the only controllable one. Recommended values for the initial post-tensioning force were between 40% and 50% of the yield force of strands F_{ys} (so $P_i < 0.8 F_{ys}$) so that the strands remain elastic (Lin et al. 2008). In fact, criteria including ductility and energy dissipation capacity of the connection should be taken into account as well. It was shown that increasing the initial post-tensioning force in the connection would result in lower energy dissipating capability for the same loading and performance level (Eljajeh, 2010). The effect on the ductility of the connection was found to be similar (Eljajeh, 2010).

At the structural level, the dynamic response of post-tensioned steel frames varies for different levels of post-tensioning forces. At different levels of post-tensioning forces, the stiffness of post-tensioned connection varies and hence, the stiffness of the frame changes as well (Eljajeh, 2010).

2.4.7. Conclusions on Post-tensioned Steel Beam-Column Connections

The two key parameters of the post-tensioned connection behaviour are the post-tensioning force applied to the strands (F_{pt}) and the energy dissipation factor (β). The relationship between the post-tensioning forces and the energy dissipation factor is such that increasing one parameter decreases the other. The up-to-date research did not completely cover the effect of these connection parameters on the seismic response of post-tensioned steel frames (Table 2.2-a, b). Also, passive control cannot present a solution for the conflict between the post-tensioning forces and the energy dissipation factor values, as structural parameters are pre-set in advance. This means that semi-active control of post-tensioned steel frames can be considered as a potential strategy for reducing the response of PT frames and optimising the frame characteristics with time.

Reference	Experimental work	Model	Design	technical Issues	Frame response	Earthquakes	Effect of F_{pt}	Conclusions
Ricles et al. (2001)	x	x			x	x		Six-storey frame under 4 earthquakes having similar amplitudes for one soil profile.
Christopoulos et al. (2002 ^a)	x	x	x					Mainly experimental work on connection with energy dissipating bars and no incorporation of the connection in frame.
Christopoulos et al. (2002 ^b)		x				x	x	Parametric study of the connection behaviour with wide range of earthquakes, but no study of frame response.
Rojas et al. (2004) & Rojas et al. (2005)		x	x		x	x		Six-storey frame under 4 earthquakes having similar amplitudes for one soil profile. Shape of the earthquake is not taken into account
Dobossy et al. (2006)		x			x	x		Comparison of two modelling techniques incorporated in six-storey frame subjected to only two earthquake records.
Garlock et al. (2007)			x	x	x	x		six-storey frame with several earthquakes having similar characteristics
Tsai et al. (2008) & Kim and Christopoulos. (2008)	x	x	x					Mainly experimental work on connection with friction device and no incorporation of the connection in frame.
Garlock and Li. (2008)			x	x	x	x		Frame response with collector beam- several earthquakes. Shape of earthquake not taken into account

Table 2.2-a: Summary of work done on steel frames with PT connections

Reference	Experimental work	Model	Design	technical Issues	Frame response	Earthquakes	Effect of F_{pt}	Conclusions
Esposito (2008)		x					x	FEM Modelling of the connection.
Garlock et al. (2008)				x	x	x	x	Response of six-storey frame to 4 earthquakes (similar characteristics). Effect of F_{pt} was studied only for reducing the effect of higher modes.
Swensen. (2008)				x				Studying supplementary parts to transfer gravity loads from PT frames.
Chou et al.(2008)	x		x	x				Experimental work of PT connection with discontinuous composite slabs.
Kim and Chrisopoulos (2009)		x	x					Modelling and incorporation of PT connections.
Chou and Lai. (2009) & Wolski et al. (2009)	x		x	x				Experimental work on PT connection with bottom flange energy dissipater
Karavasilis and Seo (2011)		x				x		A comparison between the seismic behaviour of bilinear systems and self-centring systems for a SDOF with different damping ratios.
Vasdravellis et al. (2013 ^a)	x		x					Experimental work on PT connection with web hourglass pins.
Vasdravellis et al. (2013 ^b)		x	x				x	FEM modelling of PT connections with WHPs.
Dimpoulos et al. 2013	x	x	x		x	x		Design, modelling and frame response of PT frame with connections have WHPs under several earthquake records, but envelop shape of earthquakes was not considered.

Table 2.2-b: Summary of work done on steel frames with PT connections.

2.5. Semi-Active Control

This section presents a review of different types of structural control solutions and reassesses the existing control algorithms that have been proposed for semi-active control of structures.

2.5.1. Introduction to Structural Control

Structural control denotes supplying the base structure with devices that result in reducing its dynamic response (Arfiadi and Hadi, 2000) or providing the structure with the required mechanism to dissipate input energy through inelastic deformations (Symans and Constantinou, 1999). For seismic response of structures, Nishitani (2008) listed the following principles as main objectives of using structural control: (a) reducing the effect of seismic excitation (which is achieved by base isolation for instance); (b) preventing a structure from exhibiting resonance by changing the stiffness of the structure; (c) transferring the vibration of the main structure to a secondary oscillator like a tuned mass damper (TMD); (d) supplying the structure with additional damping; and (e) adding control forces to the structure to balance the acting forces.

Control systems can be divided into three categories: (a) passive control systems (Mahmoodi, 1969), (b) active control systems (Abdel-Rohman and Leipholz, 1979) and (c) semi-active control systems (Horvat et al. 1983; Lane et al.1992). Table 2.4 compares the three types of control systems in terms of features of the system and generation of control forces.

	Passive Control	Active Control	Semi-Active Control
Features of the System.	It does not need either energy supply or control computer but lacks to flexibility and adaptability (Nishitani and Inoue, 2001).	It needs energy supply and control computer, but it is flexible and adaptable as constraints on performance are relaxed (Nishitani and Inoue, 2001).	It combines advantages from both passive and active control systems: it needs less energy than active control but shows more efficiency and better performance than passive control (Nishitani, 2008).
Generation of Control Forces.	Control forces are generated by devices installed in the structure. These forces are dependent on the structural response and location of control devices (Symans and Constantinou, 1999).	Control forces are supplied directly to the structure using force actuators that generate forces opposing the applied forces. Control forces are based on the feedback information of the response and/or the excitation of the structure (Symans and Constantinou, 1999).	Control forces are generated by changing or controlling the characteristics of the structure during the earthquake, based on feedback of the response and/or seismic input (Nishitani, 2008).

Table 2.3: Comparison between passive, active and semi-active control systems.

If the structure is subjected to seismic excitation, the response can be described by the equation of motion (Chopra, 1995):

$$M\ddot{x}(t) + C\dot{x}(t) + Kx(t) = -M\ddot{x}_g(t), \quad (2.12)$$

where M , C , K are matrices of mass, damping and stiffness of the structure respectively, $\ddot{x}(t)$, $\dot{x}(t)$, $x(t)$ are vectors of acceleration, velocity and displacement of the structure respectively; and $\ddot{x}_g(t)$ is the earthquake acceleration.

When passive control system is employed in the structure; the equation of motion is modified to (Constantinou et al.1998):

$$\widehat{M}\ddot{x}(t) + \widehat{C}\dot{x}(t) + \widehat{K}x(t) = -\widehat{M}\ddot{x}_g(t), \quad (2.13)$$

where \widehat{M} , \widehat{C} , \widehat{K} are the modified matrices of mass, damping and stiffness of the structure which can be expressed as:

$$\widehat{M} = M + \bar{M}, \quad \widehat{C} = C + \bar{C}, \quad \widehat{K} = K + \bar{K}; \quad (2.14)$$

here \bar{M} , \bar{C} , \bar{K} are matrices of mass, damping and stiffness of the passive control system.

For structures supplied with active control systems, the change in the equation of motion is applied to the excitation rather than the characteristics of the structure as (Li et al. 2001):

$$M\ddot{x}(t) + C\dot{x}(t) + Kx(t) = -M\ddot{x}_g(t) + DU(t), \quad (2.15)$$

where D is a matrix denoting the location of the actuators and $U(t)$ is a matrix denoting the controlling forces.

In general, control algorithms can be classified in three categories (Doyle et al. 1990; Glad and Ljung, 2000): (i) open-loop control algorithms, (ii) close-loop control algorithms and (iii) open-close-loop control algorithms.

In open-loop control algorithms, control gains (control forces) of the control system are obtained from the external excitation only (Figure 2.34). This means that the characteristics of the structure are not included when making the control decision. This type of control is used when data about the excitation are more reliable than data about the structure (e.g. controlling vibrations from a rotating machine on a foundation constructed on inhomogeneous soil).

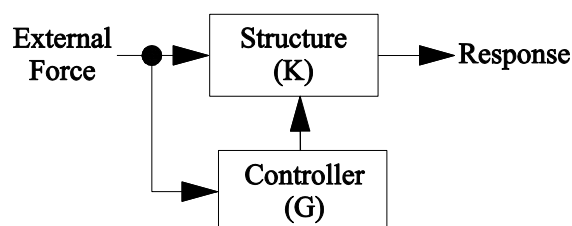


Figure 2.34: Block diagram of open-loop control system.

When close-loop control algorithms are used, control gains are obtained on the basis of structural characteristics which are well defined. Therefore, input data of the control system are the response of the controlled structure (Figure 2.35). Characteristics of the exciting forces are not included here as they are random or unreliable. The control of seismic response of structure lies mostly in this category. Here, the structural characteristics (mass and stiffness) are well known whereas exciting forces are random.

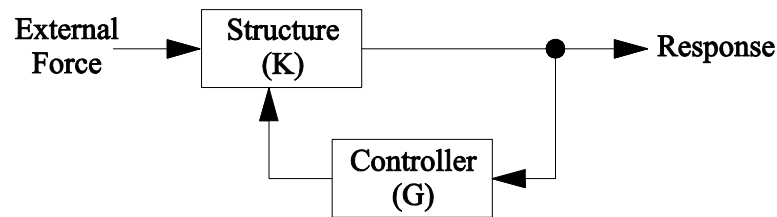


Figure 2.35: Block diagram of close-loop control system.

Open-close-loop control systems make their control decisions based on both the (input) external forces and the output response of the structure (Figure 2.36). In this type of control system, the structure characteristics and the exciting force are deterministic and can be used to generate the control gains.

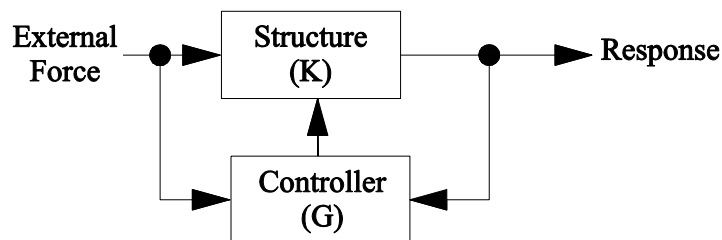


Figure 2.36: Block diagram of open-close-loop control system.

2.5.2. Review of Semi-Active Control for Seismic Protection

2.5.2.1. Types of Semi-Active Control Devices

In contrast to active control devices, semi-active control devices do not apply forces to the structure. These devices adjust the structure characteristics and, therefore do not excite the structure directly (Spencer Jr et al. 1998; Spencer Jr and Nagarajaiah 2003; Xu et al. 2003).

Although the use of semi-active systems in the containment of machines and vehicles vibrations can be traced back to 1920s, the first employment of semi-active control for structural seismic protection was proposed in 1983 (Symans and Constantinou, 1999) when a semi-active tuned mass damper was utilised to mitigate the dynamic response of frame structures under seismic excitations (Horvat et al. 1983). Since then, many types of semi-active devices have been proposed and tested.

The efficiency of semi-active control of structures has been a subject of debate. Although many previous research papers stated that semi-active control is superior to passive control (Dyke and Spencer Jr, 1997; Sadek and Mohraz, 1998), a recent research paper by Chae et al. (2013) showed that this superiority can be proved only when a limited number of earthquakes is used in the structural simulations. It was stated in this paper that when a large number of earthquakes is used, passive control can show similar results to semi-active control.

Reviews of semi-active devices (Symans and Constantinou, 1999; Kurata et al. 2002; Weber et al. (2006) classified them as: (i) stiffness control devices, (ii) electro-rheological dampers, (iii) magneto-rheological dampers, (iv) friction control devices, (v) fluid viscous dampers, (vi) tuned mass dampers and tuned liquid dampers and (vii) controlled shape memory alloys.

(i) Stiffness Control Devices.

The performance of these devices relies on modifying the stiffness of the structure and thus the natural vibration characteristics. The main objective of stiffness control devices is to save the structure from resonance by altering its stiffness. This can be achieved by activating and deactivating the frame bracing at specific time instants (Yao, 1972). Djajakesukma et al. (2002) reported significant reduction in the structural response when using these devices under various seismic inputs with different control laws. Figure 2.37 shows the configuration of a stiffness control device tested by Kobori et al. (1993).

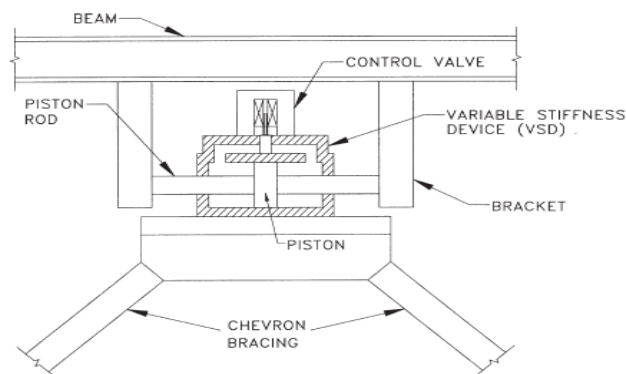


Figure 2.37: Stiffness control device tested by Kobori et al. (1993).

(ii) Electro-rheological Dampers.

An electro-rheological damper consists of dielectric particles contained in a cylinder which is filled with oil (Figure 2.38). The change in the strength of the electric field applied to the ER material polarises these particles and causes the shear resistance to increase or decrease.

The shear stress of electro-rheological materials within ER dampers is given as:

$$\tau = \tau_y \text{sgn}(\dot{\gamma}) + \eta \dot{\gamma}, \quad (2.18)$$

where τ is the applied shear stress, τ_y is the yield stress, γ is the shear strain, η is the viscosity coefficient, $\dot{\gamma}$ is the shear strain rate and sgn is the signum function (Figure 2.39).

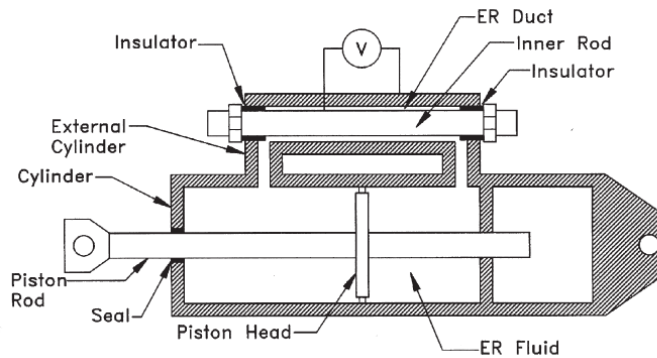


Figure 2.38: Schematic of electro-rheological damper (Markis and McMahon, 1996).

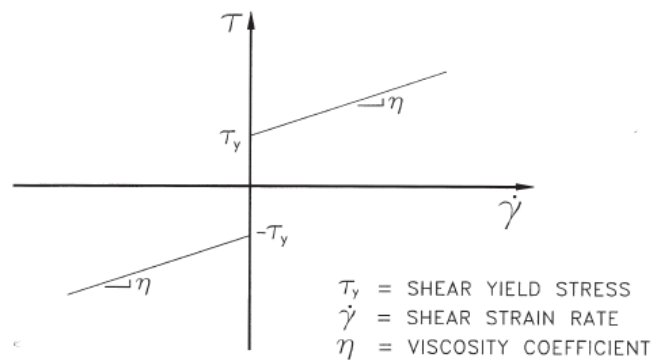


Figure 2.39: Shear behaviour of electro-rheological material (Bingham material) (Symans and Constantinou, 1999).

(iii) Magneto-rheological Dampers.

Magneto-rheological dampers are very similar to electro-rheological dampers except that the particles in the piston are polarised by a change in the magnetic field rather than the electric field. Beside the controlling input (magnetic or electric), magneto-rheological dampers can provide higher damping than electro-rheological dampers for the same size of the damper. This qualified magneto-rheological dampers to be used in the vibration mitigation of large civil structures (Weber et al. 2006).

(iv) Friction Control Devices.

Since seismic forces are not definite due to many factors, the design of passive damper with fixed slip force would be inappropriate. The potential solution is to vary the slip force of the damper in an *intelligent* way to obtain the optimum damping ratio (Nishitani et al. 2003; Lu,

2004; Ng and Xu, 2007). An ideal friction damper may be considered to behave as a Coulomb element (Symans and Constantinou, 1999):

$$F = vNs\text{gn}(\dot{x}), \quad (2.19)$$

where F is the output force, v is coefficient of friction, N is the normal force and \dot{x} is velocity of the motion. The ideal hysteresis of a conventional friction damper is shown in Figure 2.40.

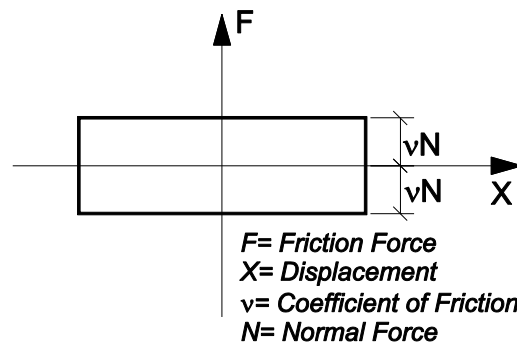


Figure 2.40: Hysteresis loop of idealised coulomb friction damper (Symans and Constantinou, 1999).

When the normal force of a semi-active friction damper increases, the force-displacement hysteresis expands in the vertical direction and the amount of energy dissipated varies at each cycle leading to increasing or decreasing the structural damping and thus, controlling the dynamic response of the structure.

(v) Fluid Viscous Dampers.

Fluid viscous dampers utilise the flow of a viscous liquid (usually oil) through controllable orifices to increase or decrease the structural damping. The damper is supplied with a servo-valve that controls the velocity of the oil flow (Figure 2.41).

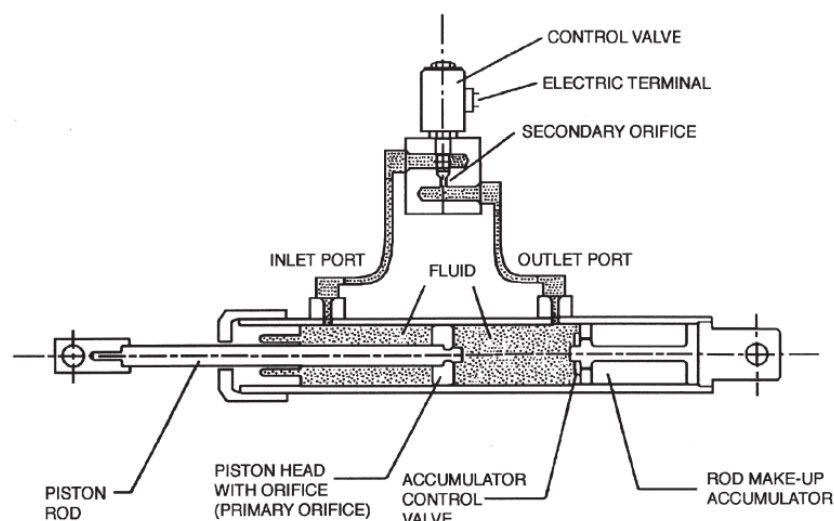


Figure 2.41: Schematic of semi-active fluid viscous damper (Symans and Constantinou, 1995).

The force output of the device is given from:

$$F = C(V)\dot{x}, \quad (2.20)$$

where \dot{x} is the relative velocity of the piston head with respect to the damper housing, V is the voltage command of the servo-valve and $C(V)$ is the voltage dependent damping coefficient. Among others, Sadek and Mohraz (1998) presented a comprehensive investigation and analysis of the performance of dampers with variable damping forces for single and multi-degree of freedom systems.

(vi) Tuned Mass Dampers and Tuned Liquid Dampers.

A tuned mass damper is a SDOF mass located at the top of the structure. It can perform semi-actively as proposed by Horvat et al. (1983) by altering damping within a specific range. Semi-active dampers, shown in Figure 2.42, are supplied with time varying controllable damping.

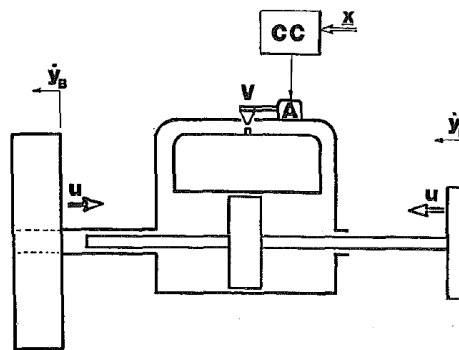


Figure 2.42: Semi-active actuator (Horvat et al. 1983).

The operation of semi-active damper includes two modes:

- Passive mode where the valve is stationary and partially open (no external power is required).
- Semi-active mode where electrical signals from the Control Computer (CC) initiate control valve actuator action which results in the motion of the valve. The control computer measures the damper force $u(t)$ and compares it with the reference force. The requirement for the semi-active damper to be activated is that the product of the damper force and the relative velocity between the structure and the damper is negative.

Advantages of the semi-active TMD over other types of dampers as summarised by Horvat et al. (1983):

- Simplicity of hardware requirements (no need for pumps and accumulators).
- Lower capital and operational costs.

- Stable and reliable behaviour that characterises passive devices.

Tuned liquid dampers are very similar to tuned mass dampers except that the mass-spring damper is replaced by container filled with fluid.

(vii) Controlled Shape Memory Alloys

The effect of the shape memory alloys falls in two categories (Weber et al. 2006): (a) pseudo plasticity which results from the mechanical action on the alloy and (b) pseudo or super elasticity which results from the thermal action on the alloy.

The pseudo plasticity of the shape memory alloy can produce high damping but its hysteresis is too complicated to be used in damping devices (Otsuka and Wayman (1999)).

On the other hand, the pseudo elasticity effect is more utilisable. It can result in different stress levels and elastic moduli of the alloy (Figure 2.43). Therefore, this effect can be used in variable damping control devices. Various characteristic of the damper can be produced by applying different heating and cooling patterns to the alloy (Rustighi et al. 2005; Williams et al. 2002).

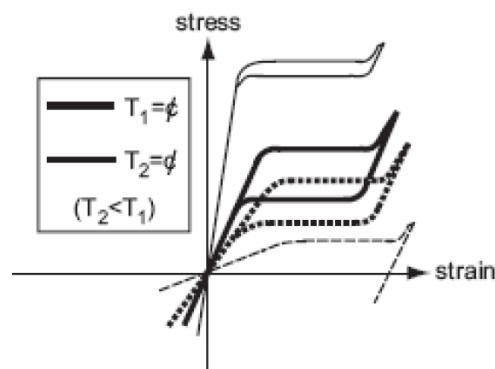


Figure 2.43: Stress-strain curves for the super-elastic behaviour of SMAs at different temperatures (Weber et al. 2006).

2.5.2.2. Control Algorithms for Seismically Excited Structures

The alteration of structural characteristics in semi-active control at specific time instants is based on some predetermined control schemes (Control Algorithms). Many control algorithms for active and semi-active control have been proposed so far. Most of the control algorithms aim to minimise an objective function (Datta, 2003).

For earthquake excitations, the load duration is very short and control algorithms taking a long time for the device to learn and operate would render the control ineffective. Control algorithms for seismic control should be simple and effective to operate quickly and mitigate the dynamic response of the structure. A summary of major semi-active control algorithms was presented by Dyke and Spencer Jr. (1997) and Datta (2010).

Control algorithms based on formulating the equation of motion of the frame-control system in a state-space form such as Lyapunov stability approach (Borgan, 1991; Leitmann, 1994) and optimal and clipped optimal control (Dyke et al. 1996^a; Dyke et al. 1996^b; Dyke, 1996; Shing et al. 1996) depended on finding the control gains matrix. Therefore, the system should be linear so it can be solved using the general solution of state-space equation. This means that these control algorithms cannot be used in frame structures subjected to high nonlinearity under seismic actions.

Control algorithms utilising the increase in energy dissipation capacity using variable slip force friction dampers (Nishitani et al. 2003; Lu, 2004; Ng and Xu, 2007) such as the modulated homogeneous control (Inaude, 1997), have been used to achieve significant reductions in structural response. However, these approaches do not offer big reduction in the early stages of the dynamic response as they need a relatively long time to build up the energy dissipation and mitigate the response. It can be shown that if the earthquake imposes its highest load reversals in the early stages, these algorithms would become significantly less effective. Walsh et al. (2008) used a hybrid algorithm incorporating the linear quadratic regulator (LQR) to increase the energy dissipation through hysteresis. A linearization of the system was needed before applying the LQR (Jinping and Hui, 2009); therefore the nonlinear properties of the spring system were ignored.

It worth reminding that none of the mentioned control algorithms considered the possible changes in structure due to the likely damage during earthquake (Bitaraf et al. 2010).

Fuzzy semi-active control has been widely used because of its simple logic, accumulated knowledge of the controller and ability to overcome nonlinearities (Bhardwaj and Datta, 2006; Wilson and Abdullah, 2010). Research has shown that this controller is efficient in reducing the seismic response of frame structures, but the desired performance of the controller is achieved only when the design parameters are well designed which requires a full knowledge of the system behaviour (Zhou et al. 2003). This understanding is not always achievable for highly nonlinear structures. Also, the performance of the fuzzy controller varies for different membership functions and hence, additional techniques are needed to determine the suitable membership functions. Several techniques have been investigated such as the use of neural networks (Schurter and Roschke, 2001) and genetic algorithms (Bitaraf et al. 2010). These requirements make fuzzy control challenging and difficult to implement.

Frequency-dependant control algorithms were used to achieve non-resonant case of the frame (Kobori et al.1993; Iskhakov and Ribakov, 2008; Duerr et al. 2013). These stiffness-based control algorithms showed good performance in reducing the dynamic response of

structures. However, most of these algorithms required very fast action with continuous change of the frame stiffness status which is not always achievable. Also, parameters of these control algorithms used to switch stiffness of the structure from one state to another are not well determined. If the modal energy transference algorithm was used to optimise the stiffness of the structure (Nemir et al. 1994), the control would be suitable for linear systems only as this algorithm is based on the modal decomposition of the equation of motion to find the modal energy of the structure at any time.

In Table 2.5-a, b is presented a summary of the up-to-date research on semi-active control of multi-storey frames based on the adopted control approach. This summary also shows the used control algorithms and simulations of the seismic response with brief critical comments on the work.

2.5.3. Concluding Remarks on Semi-Active Control

The post-tensioning forces of PT steel connections represent a key element that rules the behaviour of both the connection and the structure. If these forces are used as a parameter for semi-active control of the seismic response of PT frames, new control algorithms should be proposed due to the following reasons:

- (1) Most of the up-to-date semi-active control algorithms proposed in the literature are based on supplying the structure with incorporated dampers where the damping forces can be varied (Datta, 2010). This is not the case in post-tensioned steel frames where damping devices are installed in the beam-column connections as friction-based or yielding-based dissipaters. The damping provided from these energy dissipaters is constant and difficult to be varied. Hence, new control algorithms utilising the post-tensioning forces of the post-tensioned beam-column connections are needed to suit post-tensioned steel frames without adding new incorporated dampers to the base structure.
- (2) The characteristics and performance of semi-active control devices are highly nonlinear. Therefore, each control device should be associated with its own control algorithms which may not be suitable for other control devices (Dyke and Spencer Jr, 1997).
- (3) Classical control strategies were applied and have been suitable for linear and time-invariant systems (Weber et al. 2006). Post-tensioned steel frames are characterised by their non-linear behaviour once energy dissipaters are activated. Hence, these control algorithms do not fit these structures.

Reference	Control approach		Frame	Earthquakes	Control Algorithm	Conclusions
	Added Dampers	Energy dissipation				
Horvat et al. (1983)			Tall buildings	(wind load)	Linear Quadratic (LQ)	Semi-active TMD for wind loads.
Kobori et al. (1993)			3-storey	3 earthquake in Tokyo	Evaluative response indices	Checked for 3 earthquake records with similar characteristics. Response indices are not well-determined. Control actions were applied in too short time interval (4 msec).
Nemir et al. (1994)			Truss structure	---	Modal energy transference	System should be linear to use the modal analysis and find the modal energy.
Leitmann (1994)			---	---	Lyapunov stability	Investigating Lyapunov stability on structures with ER dampers (Linear systems).
Dyke et al. (1996 ^a) & Dyke et al. (1996 ^b)			3 and 5 storeys	EI Centro record only.	Optimal clipped (LQR)	Checking seismic response with MR dampers and optimal clipped control.
Shing et al. (1996)			10-storey	4 records	LQR and nonlinear clipped control.	Work done for linear structures only.
Inuade (1997)			6-storey	EI Centro only.	Prior local peak operator	Variable friction slip-force. Linearization of the system was required.
Sadek and Mohraz. (1998)			3-storey isolated.	20 records	LQR and acc.-disp.-domain algorithm	Investigating variable damping on isolated structures.
Djajakesukma et al. (2002)			5-storey	4 reduced records scaled to 0.1g _r	Bang-bang and LQR	Control laws and earthquake records are for linear systems only.
Nishitani et al. (2003)			20-storey	EI Centro record only.	Constant ductility of factor of damper.	Frame modelled as a stick model, and the algorithm was investigated for one earthquake excitation only.
Zhou et al. (2003)			3-storey	EI Centro record only.	Fuzzy with Lyapunov stability	Single dampers should be used to keep the system working as SISO. Control parameters are updated every time-step. Damping nonlinearity was not considered. Checked for EI Centro earthquake only.

Table 2.4-a: Summary of work done on semi-active control of frame structures.

Reference	Control approach			Frame	Earthquakes	Control Algorithm	Conclusions
	Added Dampers	Energy dissipation	Stiffness control				
Lu. (2004)		x		3-storey	4 records ¹	Bang-bang based on LQR	Modelled for linear behaviour. Control time intervals made at 1msec.
Gavin and Alhan. (2005)	x			3-storeys	-	Bang-bang.	Investigating the transmissibility of semi-active systems with ER dampers at low frequencies.
Bhardwaj and Datta, 2006	x				El Centro record only.	Fuzzy control algorithm.	Efficiency of the algorithm was checked only for linear systems under one earthquake record only.
Ng and Xu. (2007)		x		complex	4 records ¹	Different algorithms	A comparison between different control algorithms for friction damper with variable slip force
Iskhakov and Ribakov. (2008)			x	6-storey	4 records	Trial and Error	Control algorithm not suitable for real time control as it causes significant time delay as it attempts all schemes and chooses the best one.
Walsh et al. (2008)			x	8-storey	4 records ¹	Hybrid: LQR and acc.-disp.-domain.	Linearization of the system was required to represent the frame in state-space.
Bitaraf et al. (2010)	x			6-storey	4 records	Fuzzy with genetic algorithm	Earthquakes scaled down to keep the structure working in the linear range.
Wilson and Abdullah. (2010)	x			SDOF systems (rigid frames)	4 records ¹	Self-tuning fuzzy algorithm	Complex and difficult to implement control algorithm. Checked only for SDOF systems.
Duerr et al. (2013)		x	x	4-storey	10 scaled records	Smart spring with bang-bang algorithm	Suitable for retrofitting. Nonlinearity was not considered and the frame was modelled as mass, spring and dashpot system.

Table 2.4-b: Summary of work done on semi-active control of frame structures.

¹ The same records were used in these research papers: 1. El Centro NS 1940, 2. Hachinohe NS 1968, 3. Northridge NS 1994 and 4. Kobe NS 1995.

2.6. Concluding Remarks on Literature Review

This chapter presented a state-of-the-art review of topics related to the work of this thesis including: (i) post-Northridge pre-qualified steel beam-column connections, (ii) post-tensioned steel beam-column connections and (iii) semi-active control strategies and devices.

The previous work on post-Northridge pre-qualified steel beam-column connections showed that these connections possessed high rotational ductility but they were not able to restore residual deformations after an earthquake event even though they were expensive to execute and detail (Section 2.2.3).

The work done on post-tensioned steel beam column connections showed that the connection parameters F_{pt} and β have significant influence on the seismic response of PT frames. However, the values of these parameters have not been determined for different frames and earthquake excitations (Section 2.4.7).

The final section of this chapter provided a review of the previous work on semi-active control systems including their devices and algorithms. It is concluded that new control algorithms are required to incorporate semi-active control techniques in post-tensioned steel frames (Section 2.5.3).

CHAPTER 3

AIMS, OBJECTIVES AND METHODOLOGY OF RESEARCH

This chapter presents the aim of this research together with objectives that need to be accomplished to achieve the aim. Also presented in this chapter is the adopted research methodology.

3.1. Aims and Objectives

The aim of the presented research was to investigate the effectiveness of an innovative method of controlling the structural response of multi-storey post-tensioned steel frames by adjusting the characteristics of post-tensioned connections during the earthquake (semi-active control).

In order to achieve the aim, the following objectives were fulfilled:

1. The effect of the level of initial post-tensioning force on the dynamic response of the structure (passive system) was examined.
2. The effectiveness of post-tensioned connections with variable characteristics of the semi-active system for control of the seismic response of multi-storey steel frames was investigated.
3. The most effective feedback control algorithm based on the relationship between variations of post-tensioning force and the structural response was found.

3.2. Methodology of the Research

In order to achieve specified objectives, the following methodology was adopted in this research: (1) developing of a model of a stand-alone post-tensioned connection, (2) developing structural analysis program to incorporate the connection model, (3) studying parameters affecting the connection and the frame behaviour, (4) developing semi-active control strategies, and (5) investigating the efficiency of the developed control algorithms. The methodology of this research is illustrated in Figure 3.1.

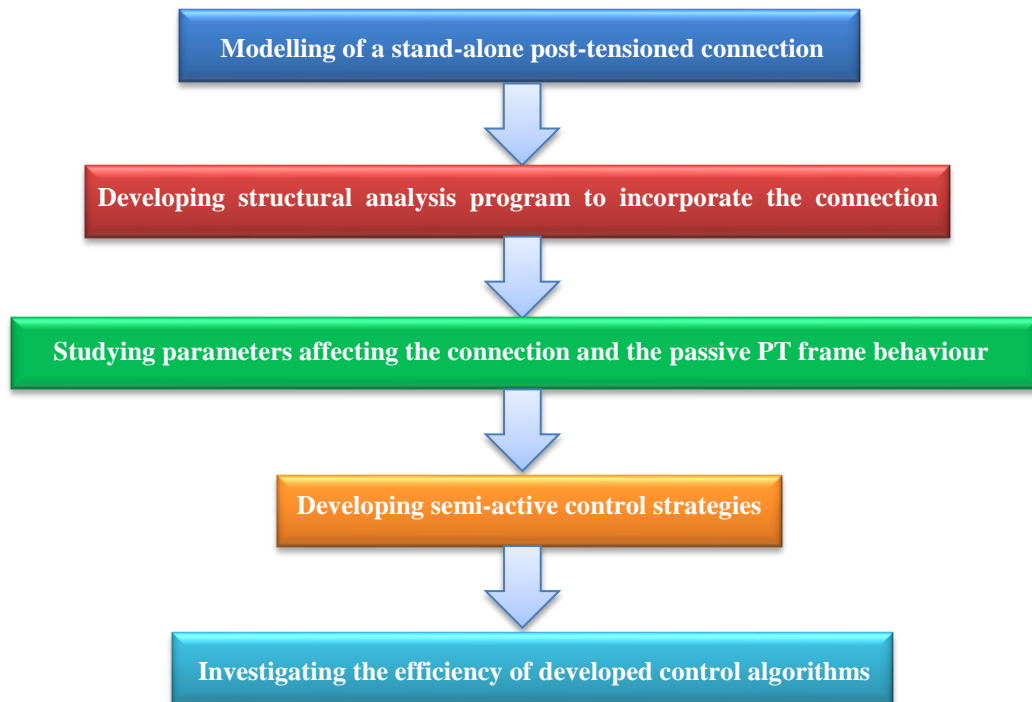


Figure 3.1: Flowchart of the research methodology.

3.2.1. Modelling of a Stand-alone Post-tensioned Connection

In order to study the behaviour of the post-tensioned connection and to investigate effects of the range of values for the connection parameters, a simple yet effective mathematical model of the connection is proposed. The connection element proposed for this research is a single rotational spring defined as a simple two-node element with six-degrees of freedom. This element can be easily incorporated in frame analysis software and, at the connection level, it captures all the important events of the post-tensioned steel beam-column connection.

3.2.2. Developing Structural Analysis Program to Incorporate the Connection Model

A new structural analysis program for simulating the dynamic response of steel frames with post-tensioned connections was developed for this study. This program was used to incorporate the newly developed connection element (Objective 1) and embed the control algorithms for semi-active control of the seismic response of post-tensioned frame buildings (Objectives 2 and 3).

Incorporating the connection element in an existing structural frame analysis program (and also embedding semi-active control algorithms) requires significant interventions in the source code. While adding new element modules (in this case a new connection element) is possible in some publicly available codes (such as DRAIN 2DX (Prakash et al.1993)) but

introducing semi active control algorithms would be very difficult. In this research the new structural analysis program (FASAC-2D, *Frame Analysis with Semi-Active Control*) was developed using MATLAB.

The new structural analysis program can perform static and dynamic, linear and nonlinear analyses, incorporating the connection element developed for this research. The program was designed to perform semi-active control of the inelastic, dynamic response, by including modules with different control algorithms. New elements and control algorithms can be added to the program by adding new modules.

3.2.3. Studying Parameters Affecting the Connection and the Passive PT Frame Behaviour

The behaviour of steel post-tensioned beam-column connection with different parameters (Objective 1) can be investigated by using the connection element developed for this research (Section 3.2.1). The performance of the connection was assessed in terms of moment capacity, rotational ductility and energy dissipation capacity. Optimum ranges for the connection parameters (initial post-tensioning forces and energy dissipation factor) were determined by the means of parametric analysis, using simulations of moment-rotation behaviour under cyclic loading.

The connection parameters were further varied in order to investigate their effect on the dynamic response of a passive multi-storey post-tensioned steel frame. A three-storey, two-bay post-tensioned steel frame was used for this purpose.

The behaviour of the post-tensioned steel frame (with parameters within optimum ranges) was compared with a conventional moment resisting frame having the same geometry and element properties. The comparison was based on the behaviour of the two frames obtained in nonlinear-static (pushover) and nonlinear-dynamic analyses using a set of earthquakes with different characteristics. The behaviour was assessed on the basis of displacements, residual drifts, and energy dissipation of the two frames. This comparison highlighted the advantages that well-designed post-tensioned steel frame can offer. Also, it indicated the limitations of these structures.

3.2.4. Developing Semi-Active Control Strategies

Development of semi-active control strategies for post-tensioned steel frames (Objectives 2 and 3) aimed at improving the behaviour of the frame by keeping the advantages of the passive system and reducing (or eliminating) its limitations. Three approaches were

proposed to control the behaviour of post-tensioned steel frames: (i) energy dissipation approach, (ii) stiffness control approach and (iii) deformation regulation approach.

Figure 3.2 shows the adopted control approaches and the expected affected parameters due to using each of them.

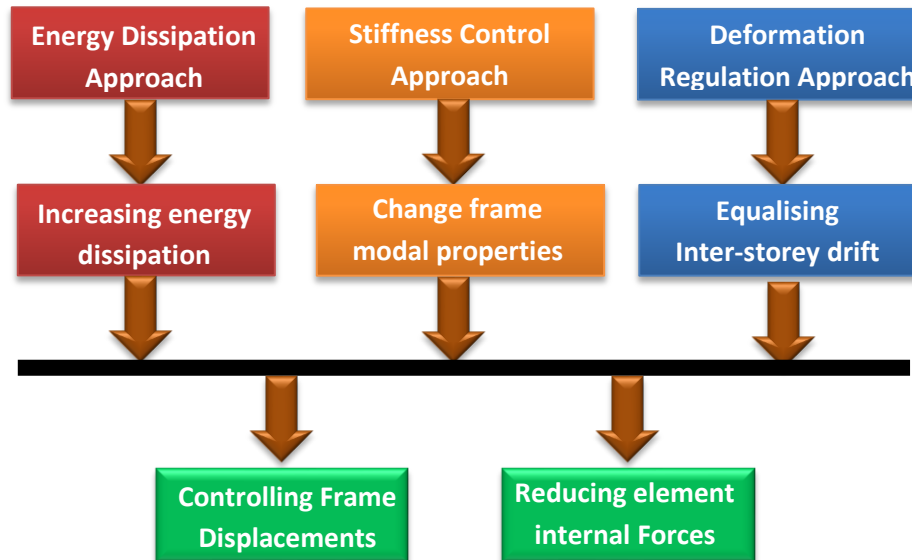


Figure 3.2: Semi-active control approaches and corresponding affected parameters.

3.2.5. Investigating the Efficiency of the Control Algorithms

The efficiency of the proposed semi-active control algorithms (Objective 3) was investigated by simulating their responses and comparing them to passively controlled post-tensioned steel frames. The seismic response with passive and semi-active control systems was investigated on two post-tensioned steel frames with 3 and 6 storeys.

There were two reasons for the selection of the investigated post-tensioned frames with 3 and 6 storeys:

- (i) Post-tensioned steel frames were proposed as a replacement of conventional moment resisting frames (MRFs), which are usually used for low to medium-high structures. Conventional MRFs are not used for high and very high structures as they become too flexible if not supplied with bracing or shear walls.
- (ii) Low and medium-high steel frames are the most affected by seismic excitations due to their modal characteristics. High and very high steel frames are characterised by their long period (very low frequency) and the earthquake loading combination is usually not critical in their design. Hence, they are designed for wind loading combinations.

For the energy dissipation control approach (both deformation-based and velocity-based), a three-storey-two-bay steel frame is used as a passively controlled post-tensioned steel frame. Then, the frame is assumed to be equipped with rotation motors that can be used to change the post-tensioning force in the strands, thus allowing controlled variations in the behaviour of the connections.

The investigation of the other two control approaches (stiffness control and deformation regulation) was carried out on a six-storey-one-bay steel frame. Using six-storey steel frame for the centralised control approaches aimed to increase the control options for the stiffness control approach (by increasing the number of possible stiffness patterns) and show how control forces in different storeys are applied simultaneously, which is not clear for three-storey frames.

To keep the computational cost of the analysis of the six-storey frame similar to the one required for the three-storey-two-bay frame, the number of bays of the six-storey frame was reduced to one.

CHAPTER 4

PROGRAM FOR 2D FRAME ANALYSIS WITH SEMI-ACTIVE CONTROL (FASAC-2D)

FASAC-2D is a MATLAB-based structural analysis program that performs linear and nonlinear static and dynamic analyses of two dimensional frames with incorporated post-tensioned connections. The program also includes semi-active control algorithms developed for this research.

4.1. Operation of FASAC-2D

FASAC-2D uses the direct stiffness method to perform both static and dynamic analyses. The program (i) generates the element stiffness matrices in local coordinates, (ii) transforms element matrices from local to global coordinates, (iii) assembles the global stiffness matrix of the frame, (iv) determines the deformations in global coordinates (by solving either static or dynamic equations), (v) calculates the element forces in local coordinates, (vi) changes the local stiffness matrices of elements in which the forces exceeded elastic limits, (vii) reassembles the global stiffness matrix, (viii) re-calculates the deformations in global coordinates (steps vii and viii are repeated until the two successive solutions are equal), and (ix) the analysis progresses to a new loading step.

It is worth mentioning that a few important features are not included in FASAC-2D: (i) gravity columns and P-Delta effects, (ii) M-N interaction in columns and (iii) deformations of panel zones. Ignoring these features results in some limitations to the structural analysis performed using FASAC-2D. However, these limitations do not invalidate the results of the frame analyses within the scope of this thesis.

4.1.1. Static Analysis in FASAC-2D

The static analysis is performed by the following equation:

$$\{\mathbf{F}\} = [\mathbf{K}] \cdot \{\mathbf{U}_{\text{static}}\}, \quad (4.1)$$

where $\{\mathbf{F}\}$ is vector of external forces, $[\mathbf{K}]$ is the global stiffness matrix of the frame, and $\{\mathbf{U}_{\text{static}}\}$ is a vector of global static displacements. These are used by FASAC-2D to calculate displacements and forces in the elements in local coordinates.

If the analysis is nonlinear, loads are applied incrementally, in small steps defined as input in the program. The program compares internal forces with pre-defined yield forces of each element in every loading step. Then FASAC-2D determines the yield code of the element at each step and calls the local stiffness matrix based on the plastic hinge status of the element. The local stiffness matrix is used to assemble the global stiffness matrix of the next loading step. As a part of the static-nonlinear analysis, FASAC-2D can perform push-over analysis and generate the $F-\Delta$ curve of the frame (base shear versus top storey displacement).

4.1.2. Dynamic Analysis in FASAC-2D

For dynamic analysis the solution is obtained by solving the dynamic equation in each time step:

$$[\mathbf{M}]\{\Delta\ddot{\mathbf{X}}\} + [\mathbf{C}]\{\Delta\dot{\mathbf{X}}\} + [\mathbf{K}]\{\Delta\mathbf{X}\} = \{\Delta\mathbf{F}\}, \quad (4.2)$$

where $[\mathbf{M}]$ is the mass matrix of the frame, $[\mathbf{C}]$ is the damping matrix of the frame, $[\mathbf{K}]$ is the global stiffness matrix of the frame, $\{\Delta\ddot{\mathbf{X}}\}$ is the vector of acceleration increment within time-step, $\{\Delta\dot{\mathbf{X}}\}$ is the vector of velocity increment within time-step, $\{\Delta\mathbf{X}\}$ is the vector of displacement increment within time-step, and $\{\Delta\mathbf{F}\}$ is vector of increment in external forces within time-step.

Equation 4.2 is solved for both linear and nonlinear dynamic analysis by using the Newmark numerical integration method (Chopra, 1995), using either constant or linear acceleration, which is controlled by the values of two input parameters (α and δ). In linear analysis, the solution is a direct application of Equation 4.2. The nonlinear dynamic analysis includes an iterative procedure when the global stiffness matrix changes due to inelastic behaviour of elements. In FASAC-2D the change in the stiffness of each element is recorded as a yield-code, which takes values of 0 and 1 for the frame elements, and 0, 1 and 2 for the post-tensioned connection element. These codes are stored in a yield-code vector. In each time step, iterations are performed until the yield-code vector (i.e. the global stiffness matrix) remains unchanged in two consecutive iterations. The maximum number of iterations in any time-step can be limited by an input parameter. If this number is exceeded, the time-step is reduced and the iteration process is repeated.

4.2. Structural Elements in FASAC-2D

FASAC-2D is a modular program which can incorporate different structural elements with different inelastic behaviour by adding new modules. So far, four inelastic elements have been incorporated in the program: (a) Element 1: beam-column element (2 nodes, 6 DOFs) with bi-linear moment-rotation behaviour, (b) Element 2: bar (or truss) element (2 nodes, 2 DOFs) with bilinear axial load-deformation behaviour, (c) Element 3: post-tensioned steel beam-column connection element (2 nodes, 6 DOFs) with complex inelastic behaviour (described in the next chapter) and (d) Element 6: simple connection element (2 nodes, 2 DOFs) with bilinear general force-deformation behaviour.

4.2.1. Element 1: Beam-Column Element

Element 1 is a beam-column element that is used to represent structural elements subjected to pure bending or bending combined with axial forces. Plastic hinges form when the applied moment exceeds the given yielding moment of the element.

4.2.1.1. Input Data

All input data of Element 1 are defined in the input file. These data include geometry information and section properties to compute the element stiffness and section resistance. The properties matrix (Table 4.1) includes data to set stiffness and resistance characteristics of the element.

Notation	Description
E	modulus of elasticity
A	area of the section
I	second moment of inertia about the bending axis
M_p	plastic moment of the section
k_1/k_0	ratio of the post-yielding stiffness to the pre-yielding stiffness
β	stiffness ratio for Reighley damping

Table 4.1: Input data of Element 1 in FASAC-2D.

4.2.1.2. Inelastic Behaviour: Moment-Rotation Relationship

The element is designed to behave as linear elastic under axial and shear load, and to yield only under moment action. The inelastic behaviour is represented by bi-linear moment-rotation relationship, defined by the plastic moment M_p and the ratio between the pre-yielding and the post-yielding stiffness k_1/k_0 (Table 4.1). In the pre-yielding phase, the deformations of the element are recoverable and residual deformations are zero. Once the plastic moment is exceeded, the element undergoes irrecoverable plastic deformations. Figure 4.1 shows the moment-rotation behaviour of Element 1.

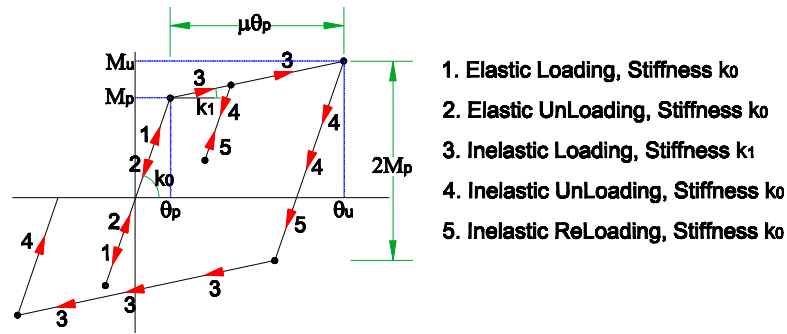


Figure 4.1: Moment-rotation behaviour of Element 1: beam-column element.

4.2.1.3. Yield-Code and Stiffness Matrix

Two values of the yield-code at each end of the element are recognised: (0) loading/unloading follows the pre-yielding stiffness (k_0), and (1) loading follows the post-yielding stiffness (k_1). If the value of the yield code is 0, it does not necessarily mean that the element has not yielded, but rather that the current loading stiffness is k_0 which can occur at various points of the hysteresis.

The element stiffness matrix depends on the values of the yield codes in the two nodes (i and j). Four cases are distinguished (Cheng, 2001): (0,0), (1,0), (0,1) and (1,1).

First Case: No yielding at both ends

In FASAC-2D, the first case is a matrix for an element with no yielding (elastic case), when **YieldCode** at end $i = 0$, and **YieldCode** at end $j = 0$, shown in Figure 4.2.

Terms of the matrix shown in Figure 4.2 are given in Equation 4.3.

$$aa = \frac{EA}{l}, a = \frac{4EI}{l}, b = \frac{2EI}{l}, c = \frac{6EI}{l^2}, d = \frac{12EI}{l^3} \quad (4.3)$$

$$[k_e] = \begin{bmatrix} aa & 0 & 0 & -aa & 0 & 0 \\ 0 & d & c & 0 & -d & c \\ 0 & c & a & 0 & -c & b \\ -aa & 0 & 0 & aa & 0 & 0 \\ 0 & -d & c & 0 & d & -c \\ 0 & -c & b & 0 & -c & a \end{bmatrix}$$

Figure 4.2: Stiffness matrix of frame element with no plastic hinges.

Second Case: Plastic hinge formed at node i only

The second case is for a beam-column element where a plastic hinge forms only in i node (Figure 4.3). Yield-code in FASAC-2D for this case is: **YieldCode** at end $i = 1$ and **YieldCode** at end $j = 0$.

Terms of the element stiffness matrix shown in Figure 4.3 are presented in Equations 4.3 and 4.4.

$$g = \frac{3EI}{l^3}, f = \frac{3EI}{l^2}, e = \frac{3EI}{l}, p = \frac{k_1}{k_0}, q = 1 - p \quad (4.4)$$

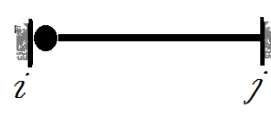
$$[k_e] = \begin{bmatrix} aa & 0 & 0 & -aa & 0 & 0 \\ 0 & pd + qg & pc & 0 & -(pd + qg) & pc + qf \\ 0 & pc & pa & 0 & -pc & pb \\ -aa & 0 & 0 & aa & 0 & 0 \\ 0 & -(pd + qg) & -pc & 0 & pd + qg & -(pc + qf) \\ 0 & pc + qf & pb & 0 & -(pc + qf) & pa + qe \end{bmatrix}$$


Figure 4.3: Stiffness matrix of frame element with plastic hinge at end i only.

Third Case: Plastic hinge is forming at end (j) only

This case represents an element where the plastic hinge is formed only at node j (Figure 4.4). Yield-code of the element in FASAC-2D for this case is: **YieldCode** at end $i = 0$ and **YieldCode** at end $j = 1$. In this case, element stiffness matrix is given from Figure 4.4:

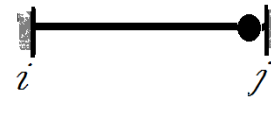
$$[k_e] = \begin{bmatrix} aa & 0 & 0 & -aa & 0 & 0 \\ 0 & pd + qg & pc + qf & 0 & -(pd + qg) & pc \\ 0 & pc + qf & pa + qe & 0 & -(pc + qf) & pb \\ -aa & 0 & 0 & aa & 0 & 0 \\ 0 & -(pd + qg) & -(pc + qf) & 0 & pd + qg & -pc \\ 0 & pc & pb & 0 & -pc & pa \end{bmatrix}$$


Figure 4.4: Stiffness matrix of frame element with plastic hinge at end j only.

Fourth Case: Plastic hinges form at both ends

When plastic hinges are formed at the two ends (i and j) as in Figure 4.5, Yield-code in FASAC-2D is given as: **YieldCode** at end $i = 1$ and **YieldCode** at end $j = 1$. In this case, element stiffness matrix can be given as the element stiffness matrix for the element in the first case (acting elastically, **YieldCode** at end $i = 0$ and **YieldCode** at end $j = 0$) reduced by $p = k_1/k_0$ as in Figure 4.5.

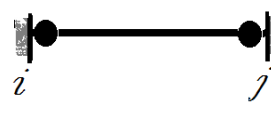
$$[k_e] = p * \begin{bmatrix} aa & 0 & 0 & -aa & 0 & 0 \\ 0 & d & c & 0 & -d & c \\ 0 & c & a & 0 & -c & b \\ -aa & 0 & 0 & aa & 0 & 0 \\ 0 & -d & -c & 0 & d & -c \\ 0 & c & b & 0 & -c & a \end{bmatrix}$$


Figure 4.5: Stiffness matrix of frame element with plastic hinges at both ends.

4.2.2. Element 2: Bar Element

Element 2 is a bar element (or truss element) that is used to represent elements which can take only axial forces. Yielding in this element occurs when the applied axial force exceeds the yielding force.

4.2.2.1. Input Data

The input data for Element 2, geometry information and section properties to compute the element stiffness and section resistance are given in Table 4.2.

Notation	Description
E	modulus of elasticity
A	area of the section
N_{p+}	plastic axial force of the section (tension)
N_{p-}	axial buckling force of the element (compression)
k_1/k_0	ratio of the post-yielding stiffness to the pre-yielding stiffness
β	stiffness ratio for Reighley damping

Table 4.2: Input data of Element 2 in FASAC-2D.

4.2.2.2. Force-Deformation Relationship

The force-deformation relationship adopted for Element 2 in FASAC_2D is bilinear, and is identical to the $M-\theta$ hysteresis defined for Element 1, shown in Figure 4.1.

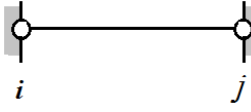
4.2.2.3. Yield Code and Stiffness Matrix

Two values for the yield-code of the element are recognised: 0 and 1. When the value of the yield-code is zero, the loading/ unloading is following the pre-yielding stiffness (k_0). When it is one, the loading is following the post-yielding stiffness (k_1). If the value of the yield-code is 0, it does not necessarily mean that the element has not undergone inelastic deformations, but that the current loading stiffness is k_0 .

Two cases are distinguished for the yield-code of Element 2: (0) or (1).

First Case: No yielding or buckling

Element 2 behaves elastically when no yielding or buckling is recorded. In this case **YieldCode** = 0 and element stiffness matrix is given in Figure 4.6:

$$[k_e] = \begin{bmatrix} aa & 0 & 0 & -aa & 0 & 0 \\ 0 & 0 & 0 & 0 & 0 & 0 \\ 0 & 0 & 0 & 0 & 0 & 0 \\ -aa & 0 & 0 & aa & 0 & 0 \\ 0 & 0 & 0 & 0 & 0 & 0 \\ 0 & 0 & 0 & 0 & 0 & 0 \end{bmatrix}$$


The diagram shows a horizontal bar element with two nodes, labeled 'i' and 'j', at its ends. Each node is represented by a small circle with a vertical line passing through its center, indicating a hinge or connection point.

Figure 4.6: Stiffness matrix of bar element with no plastic hinges.

Second Case: Yielding in tension or buckling in compression

When Element 2 undergoes nonlinearity resulted from yielding in tension or buckling in compression, the **YieldCode** = 1. In this case, element stiffness matrix is given as:

$$[k_e] = p \times \begin{bmatrix} aa & 0 & 0 & -aa & 0 & 0 \\ 0 & 0 & 0 & 0 & 0 & 0 \\ 0 & 0 & 0 & 0 & 0 & 0 \\ -aa & 0 & 0 & aa & 0 & 0 \\ 0 & 0 & 0 & 0 & 0 & 0 \\ 0 & 0 & 0 & 0 & 0 & 0 \end{bmatrix}, \quad (4.3)$$

where $p = \frac{k_1}{k_0}$.

4.2.3. Element 3: Post-tensioned Connection Element

The post-tensioned beam-column connection is one of the key components of this research. The connection model (Element 3), its load-deformation behaviour and the incorporation of the model in FASAC-2D are presented in detail in a separate chapter (Chapter 5).

4.2.4. Element 6: Simple Connection Element

Element 6 is a zero-length element that is used to model simple nonlinear connections. This element takes loads in one direction only. To combine loads in different directions, different elements should be used. The force-deformation relationship of Element 6 is bilinear (elastic-plastic behaviour), with yielding point corresponding to a pre-defined yield force (F_y), and pre and post-yielding stiffnesses k_0 and k_1 , identical to the $M-\theta$ hysteresis defined for Element 1 (Figure 4.1).

Figure 4.7 shows simple connection elements with different direction codes and their yield forces.

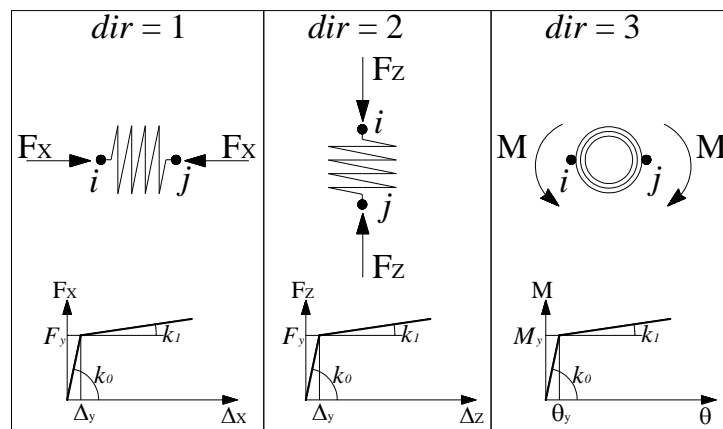


Figure 4.7: Geometry and behaviour of simple connection element with different direction code.

4.2.4.1. Input Data

Input data of the simple connection element are initial stiffness, post-yielding stiffness ratio, direction code and yield force (Table 4.3).

Notation	Description
k_0	pre-yielding stiffness of the connection
k_1/k_0	ratio of post-yielding stiffness to pre-yielding stiffness
dir	direction code of the connection (Figure 4.7): 1= X –translation, 2= Z –translation, 3= Rotation.
F_y	yield force of the connection(or M_y if $dir=3$, Figure 4.7).

Table 4.3: Input data of Element 6 in FASAC-2D.

4.2.4.2. Yield Code and Stiffness Matrix

Yield code of Element 6 can take two values: 0 when the force in the connection is less than the yield force and 1 when the force of the connection is greater than the yield force. The stiffness matrix of the element depends on: (i) the direction code of the element and (ii) the value of the yield code of the element (Table 4.4).

$[k_e] = \begin{bmatrix} k_r & 0 & 0 & -k_r & 0 & 0 \\ 0 & 0 & 0 & 0 & 0 & 0 \\ 0 & 0 & 0 & 0 & 0 & 0 \\ -k_r & 0 & 0 & k_r & 0 & 0 \\ 0 & 0 & 0 & 0 & 0 & 0 \\ 0 & 0 & 0 & 0 & 0 & 0 \end{bmatrix}$ <p>YieldCode = 0 $\rightarrow k_r = k_0$ YieldCode = 1 $\rightarrow k_r = k_1$</p>	$[k_e] = \begin{bmatrix} 0 & 0 & 0 & 0 & 0 & 0 \\ 0 & k_r & 0 & 0 & -k_r & 0 \\ 0 & 0 & 0 & 0 & 0 & 0 \\ 0 & 0 & 0 & 0 & 0 & 0 \\ 0 & -k_r & 0 & 0 & k_r & 0 \\ 0 & 0 & 0 & 0 & 0 & 0 \end{bmatrix}$ <p>YieldCode = 0 $\rightarrow k_r = k_0$ YieldCode = 1 $\rightarrow k_r = k_1$</p>	$[k_e] = \begin{bmatrix} 0 & 0 & 0 & 0 & 0 & 0 \\ 0 & 0 & 0 & 0 & 0 & 0 \\ 0 & 0 & k_r & 0 & 0 & -k_r \\ 0 & 0 & 0 & 0 & 0 & 0 \\ 0 & 0 & 0 & 0 & 0 & 0 \\ 0 & 0 & -k_r & 0 & 0 & k_r \end{bmatrix}$ <p>YieldCode = 0 $\rightarrow k_r = k_0$ YieldCode = 1 $\rightarrow k_r = k_1$</p>
(a)	(b)	(c)

Table 4.4: Stiffness matrix of Element 6 for different values of yield code and direction code: (a) $dir=1$, (b) $dir=2$ and (c) $dir=3$.

4.3. Verification of FASAC-2D Results

The results of a nonlinear dynamic analysis of a portal frame (Figure 4.8) calculated with FASAC-2D are very close with those obtained by using DRAIN-2DX (Prakash et al.1993). The verification of results for Kobe and Northridge earthquakes are shown in Figures 4.9 and 4.10.

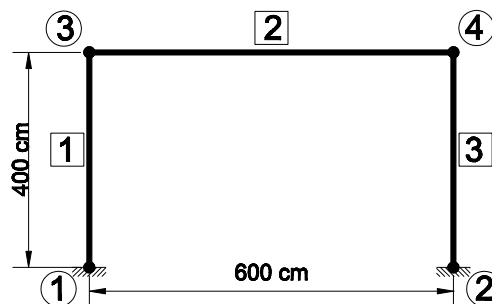


Figure 4.8: Portal frame to verify results of FASAC-2D.

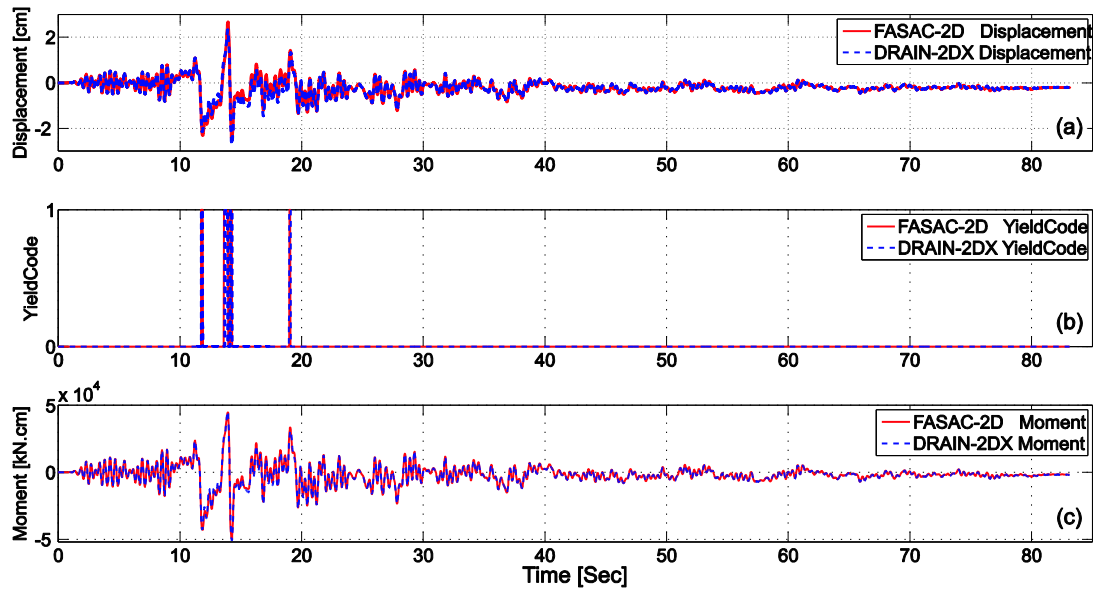


Figure 4.9: Verification of FASAC-2D results with DRAIN-2DX results. Response to Kobe earthquake record (KOBE/HIK000): (a) horizontal displacement of node 3, (b) YieldCode for element 2, at node 3, and (c) moment in element 1, at node 3.

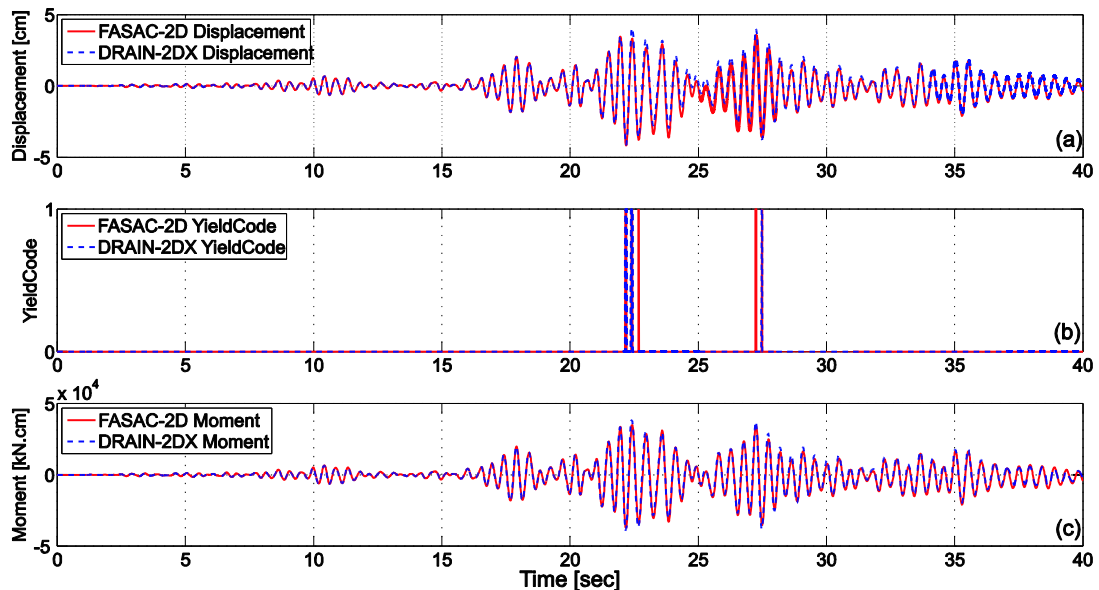


Figure 4.10: Verification of FASAC-2D results with DRAIN-2DX results. Response to Northridge earthquake record (NORTHR/HOS090): (a) horizontal displacement of node 3, (b) YieldCode for element 2, at node 3, and (c) moment in element 1, at node 3.

4.4. Concluding Remarks on FASAC-2D

This chapter presented the program for Frame Analysis with Semi-Active Control (FASAC-2D) which was developed to incorporate the PT connection element and embed semi-active control algorithms. The operation, structural elements and limitations of FASAC-2D are described and illustrated. Also, verifications of the nonlinear dynamic analysis of FASAC-2D with DRAIN-2DX were presented and showed close agreement between the results of the two programs.

CHAPTER 5

MODELLING, INCORPORATION AND DETAILS OF PT CONNECTION

This chapter introduces the modelling and incorporation of the idealised model of the post-tensioned steel beam-column connection. This model was developed in order to facilitate the processing and control of post-tensioning forces. Also, details of the post-tensioned connection for both passive and semi-active systems are presented. Although the detailed design of the connection and the control system are not among the main objectives of this dissertation, practical solutions are proposed in Section 5.3 in order to demonstrate that semi-active control of post-tensioned connections can be achieved in practice. These serve only as illustrations and they are not necessarily the best connection details and control mechanism solutions.

5.1. Modelling of Standalone Post-tensioned Steel Beam-Column Connection

The connection model (IPTC) is built to generate the moment-rotation relationship of any standalone post-tensioned connection. The connection model is driven by the rotation time-history of the connection. This facilitates incorporation of the connection into a 2D frame model, as the direct stiffness method computes first the element displacements which are then used to compute the internal element forces. The model computes the connection moment at time-step $t=t_{i+1}$ using the rotation and moment input at time-step $t=t_i$. The set $[\theta_i, M_i]$ and the loading or unloading condition represented by rotation increment $\Delta\theta_i = \theta_{i+1} - \theta_i$ determine the stiffness of the connection k_{i+1} (k_0 , k_1 or k_2).

5.1.1. Moment Rotation Relationship

5.1.1.2. Elastic Phase

Figure 5.1-a shows that the behaviour of post-tensioned steel beam-column connections when subjected to dynamic loading is characterised by two main phases: elastic phase and

inelastic phase. The rotation of the connection is zero when the gap is closed, for applied moments (M_c) lower than the moment supplied by the post-tensioned strands (M_{St}). When the gap opens, the connection behaves as elastic as long as the applied moment is less than the moment causing yielding/ slipping of the energy dissipating device (M_y). The rotation θ_y corresponds to applied moment equal to the sum of moments provided by post-tensioned strands and energy dissipating device at the point of yielding/ slipping of the energy dissipating device.

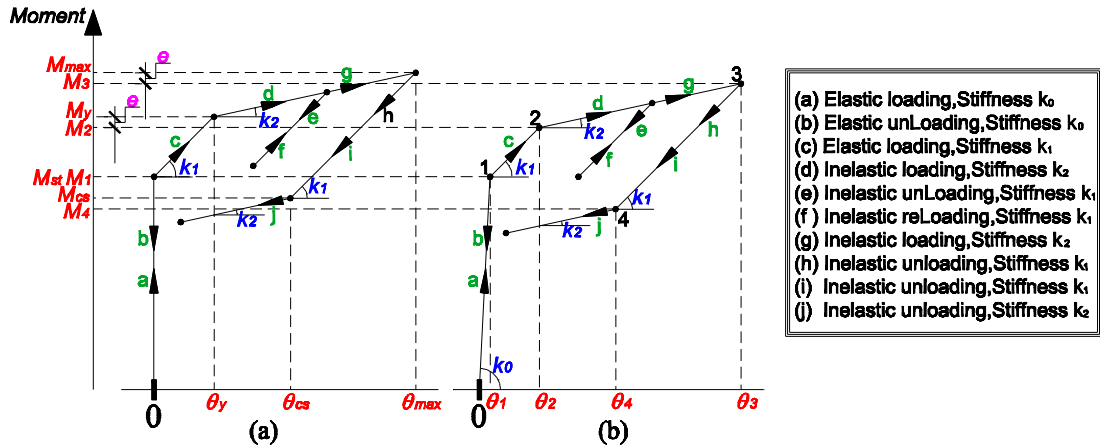


Figure 5.1: Moment-rotation relationship of post-tensioned connections: (a) real connection and (b) connection model.

When $M_c < M_{St}$ the stiffness of the connection (k_0) is *infinite*. Once M_{St} is exceeded, the stiffness reduces to k_1 ($k_1 \ll k_0$). The stiffness k_1 is a sum of the total rotational stiffnesses of the strands (k_s) and the stiffness of the energy dissipating device (k_b). The total rotational stiffness of the strands (k_s) is a sum of the stiffnesses of individual strands k_{si} , which is calculated from:

$$k_{si} = E_s A_{si} d_{si}^2 / L_s, \quad (5.1)$$

here E_s is the modulus of elasticity of the strands, A_{si} is the area of strand i , d_{si} is the distance of strand i to the centre of rotation, and L_s is the length of the strands (Figure 5.2). The total stiffness of post-tensioned strands resulted by using Equation (5.1) is higher than this proposed by Garlock and Li (2008). The difference in the connection stiffness is however insignificant as the simplified model proposed here does not account for stiffness added to the connection due to the diaphragm action.

The stiffness of energy dissipating bars (k_b) is obtained from:

$$k_b = E_b A_b D_b^2 / L_b, \quad (5.2)$$

where E_b is modulus of elasticity of the energy dissipating bars, A_b is area of one energy dissipating bar, D_b is depth of the beam (an approximation of the centre-to-centre distance

from the energy dissipating device to the centre of rotation), and L_b is the length of the energy dissipating bar. For connections supplied with friction dampers, k_b is the in-plane stiffness of the connected plates, which compared to other stiffnesses in the connection, is a very large value (*infinite stiffness*).

In the connection model, for numerical reasons, the infinite connection stiffness prior to the gap-opening event is replaced by a finite initial stiffness k_0 (Equation 5.3). This results in a small rotation of the connection before the gap-opening (θ_1), which does not exist in reality (Figure 5.1-b).

$$k_0 = C k_s, \quad (5.3)$$

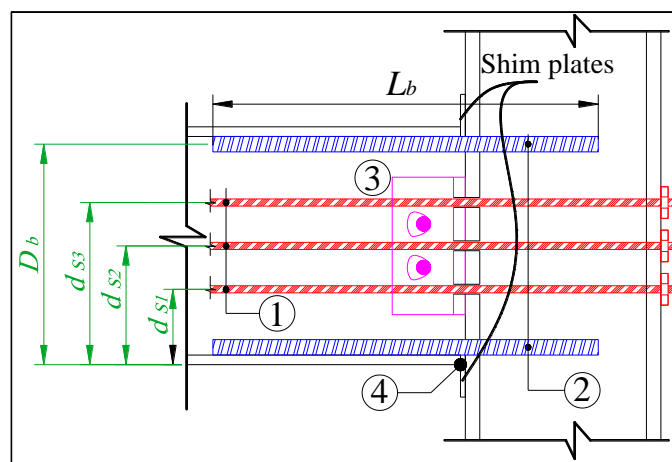


Figure 5.2: Configuration of post-tensioned connection: (1) post-tensioned strands, (2) energy dissipating bars, (3) shear tab with slotted holes, (4) connection centre of rotation.

The introduction of initial rotation (θ_1) would affect either the yielding rotation of the connection (θ_y) or the yielding moment M_y . The correct yielding rotation ($\theta_y = \theta_2$; Figure 5.3) can be maintained by either (i) increasing the stiffness in the elastic phase $k_1' > k_1$ (Figure 5.3-a) or (ii) reducing the yielding moment $M_2 < M_y$ (Figure 5.3-b).

When the first approach is used (Figure 5.3-a), the post-yielding moments in the IPTC model are identical to these in the real connection. Modifying the stiffness of the connection in the elastic phase however, results in an intervention in the response of the frame as the modification introduced to the connection stiffness will be passed to the global stiffness matrix of the post-tensioned frame.

When the second approach is used (Figure 5.3-b), the error in the moment calculated by the model ($e = M_y - M_2$), is carried out throughout the analysis. This approach however, maintains the correct stiffness of the connection through all the phases following the gap opening and does not introduce any further changes in the frame response. This approach was adopted for the model presented here.

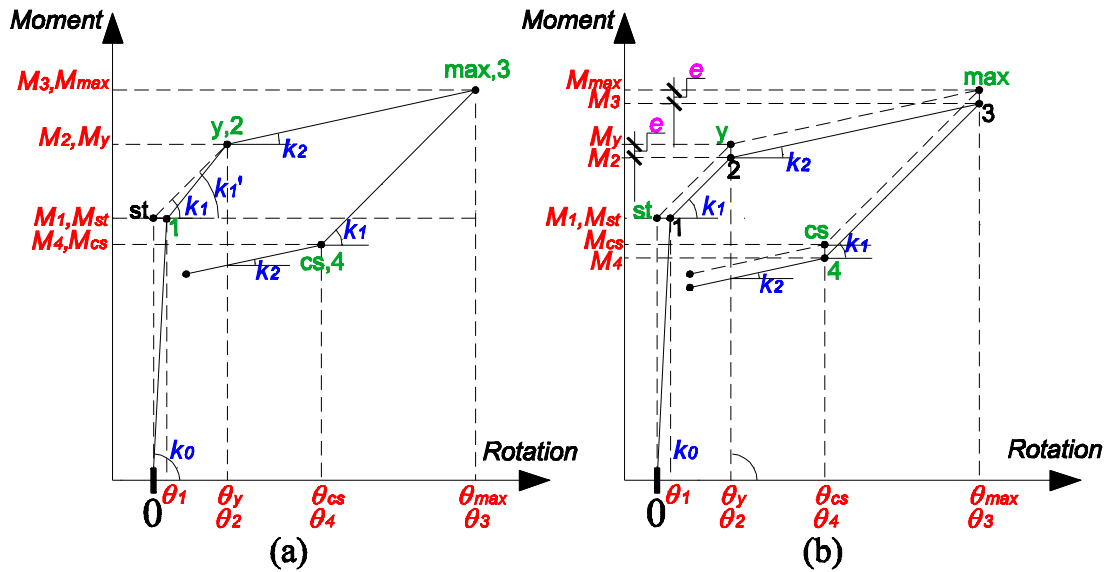


Figure 5.3: Consequences of using finite initial stiffness of the connection: (a) stiffness modification in the gap-opening phase and (b) keeping the same stiffness and carrying the moment error.

To investigate the effect of the initial stiffness on the performance of the standalone post-tensioned connection model, the initial stiffness (k_0) was varied between factors 1 and 35 times the stiffness of the beam. The response of the connection under harmonic loading with initial post-tensioning force ($F_{pt} = 300$ kN) at different initial stiffness levels is shown in Figure 5.4.

The simulations show that for all initial stiffness values higher than ten times the beam stiffness, the response of the connection is very similar, with very small differences in yielding moments. If initial stiffness is too high, it may lead to computational errors when the connection is incorporated into a post-tensioned frame structure. Therefore, the value of k_0 should be carefully selected to avoid numerical instability and provide acceptable accuracy.

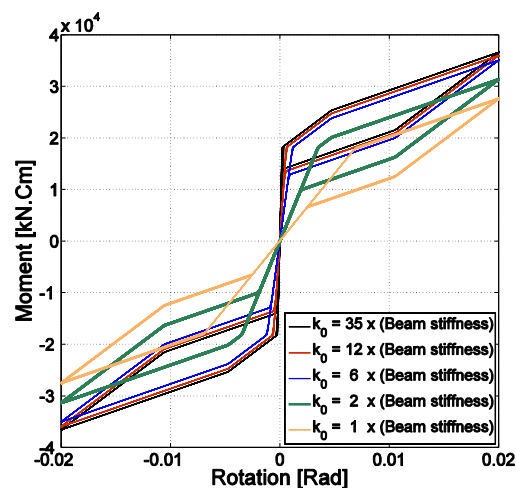


Figure 5.4: Response of post-tensioned connection model for different initial stiffness.

5.1.1.3. Inelastic Phase (Post-yielding)

The connection behaviour becomes inelastic when the yielding moment (M_y) is exceeded. The stiffness of the connection in this phase depends on the loading/ unloading status of the connection. In order to specify the stiffness of the connection during the inelastic phase, the yield-status-time-increment technique is used (Cheng, 2001). In this technique, the stiffness of the connection in the new step and the new yielding moment (M_{y-new}) depend on (i) whether the connection is subjected to loading, unloading or reloading, (ii) the values of moment and rotation in the previous step, and (iii) the previous characteristic points in the moment-rotation history (points 3 and 4 in Figure 5.5). This means that M_y is a special case of M_{y-new} , for a point at which the energy dissipating device reaches yielding for the first time.

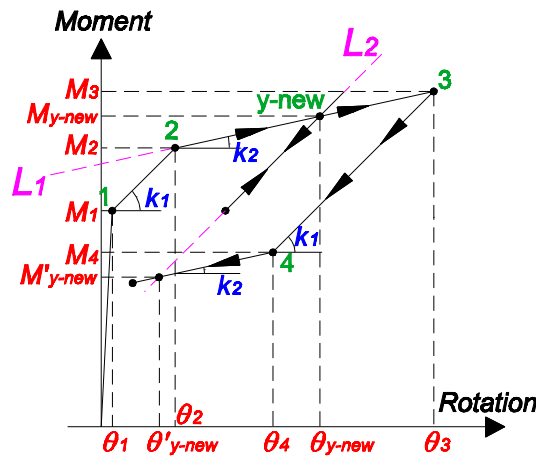


Figure 5.5: Modelling of the inelastic phase of the post-tensioned connection.

Figure 5.5 shows that the inelastic phase starts when loading is beyond point 2 (θ_2, M_2). The point of changing stiffness $y-new$ ($\theta_{y-new}, M_{y-new}$) may vary during the response history. This point is determined as a point of intersection between the two lines L_1 and L_2 :

$$L_1: \quad (M - M_2) = k_2(\theta - \theta_2), \quad (5.4)$$

$$L_2: \quad (M - M_1) = k_1(\theta - \theta_1), \quad (5.5)$$

The intersection between the two lines gives:

$$\theta_{y-new} = [(M_2 - M_1) + k_1\theta_1 - k_2\theta_2] / (k_1 - k_2), \quad (5.6)$$

The corresponding moment M_{y-new} can be obtained by substituting Equation 5.6 in Equation 5.5:

$$M_{y-new} = k_1(\theta_{y-new} - \theta_1) + M_1, \quad (5.7)$$

When the connection is loading, the stiffness is equal to k_1 if $M_c < M_{y-new}$. In case of unloading, the stiffness of the connection is equal to k_1 if $M'_{y-new} \leq M_c \leq M_{y-new}$. In all other cases, the stiffness of the connection is equal to k_2 .

5.1.1.4. Modelling of Self-Centring Characteristics of Post-tensioned connection

The most important feature of the connection moment-rotation relationship is its ability to self-centre after it undergoes inelastic deformations. Inelastic deformations of any element are determined from the deformation history. If any rotation/displacement in the deformation time history is greater than the yielding deformation, the structural element undergoes inelastic (residual) deformations. For conventional structural elements, once the element has undergone inelastic deformations, it cannot go back to its elastic phase. Elements with self-centring ability can switch between elastic and inelastic phases. The element may undergo inelastic deformations, and then self-centre upon unloading and return back to the elastic phase.

The first step in the modelling of self-centring in the post-tensioned connection is determining the rotation angle at which the connection self-centres. In real post-tensioned connections, this angle is zero, but having introduced the non-infinite initial stiffness k_0 , the self-centring rotation angle takes a non-zero value $\theta_{sc} < +\theta_l$, determined by intersecting lines L_3 and L_4 (Figure 5.6).

After yielding in the connection, the self-centring angles change and depend on the loading status and plastic deformations. If the unloading starts at $M_{y_new} < M_{Ed} + M_y$, the unloading stiffness is k_1 and the self-centring angle θ_{sc} is in the intersection of L_3 and L_4 (Figure 5.6-a). If the unloading starts at moment at $M_{y_new} \geq M_{Ed} + M_y$, the unloading stiffness changes from k_1 to k_2 at the intersection of L_4 and L_5 , and θ_{sc} is at the intersection of L_3 and L_5 (Figure 5.6-b). If either of these cases is followed by negative rotation, the self-centring angle is equal to $-\theta_l$. The same process applies when situation is reversed (negative rotations followed by positive rotations).

The self-centring status of the connection is included in the algorithm through a variable **Ind** (indicator of self-centring status). The initial value of the indicator is **Ind**=1. In a computational step i : (a) if the connection is self-centred ($\theta_i \leq \theta_{sc}$) the indicator increases (**Ind** = i), (b) when the gap is open ($\theta_i > \theta_{sc}$) the value of the indicator remains constant (**Ind** = i_{gap}), where i_{gap} is the step at which the gap opened. Once the connection re-self-centres, the indicator takes the new value of the computation step and increments while the connection remains self-centred. Hence, the rotation history (θ_{Hist}) contains only rotations from **Ind** to the current computation step i (rotations prior to the last self-centring event are eliminated from the history). Figure 5.7 shows the flowchart of the complete algorithm used for modelling a standalone post-tensioned connection element.

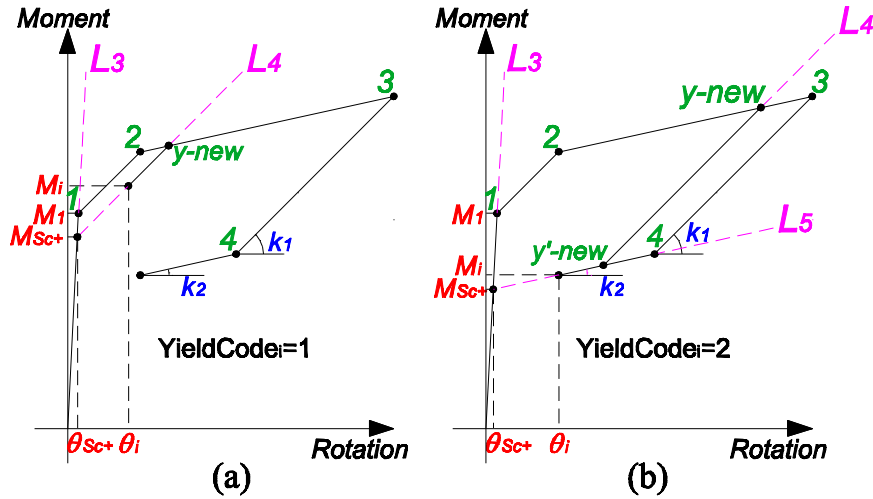


Figure 5.6: Determining of self-centring angles for positive rotations: (a) $M_{y-new} \leq M_y + M_{Ed}$ and (b) $M_{y-new} > M_y + M_{Ed}$.

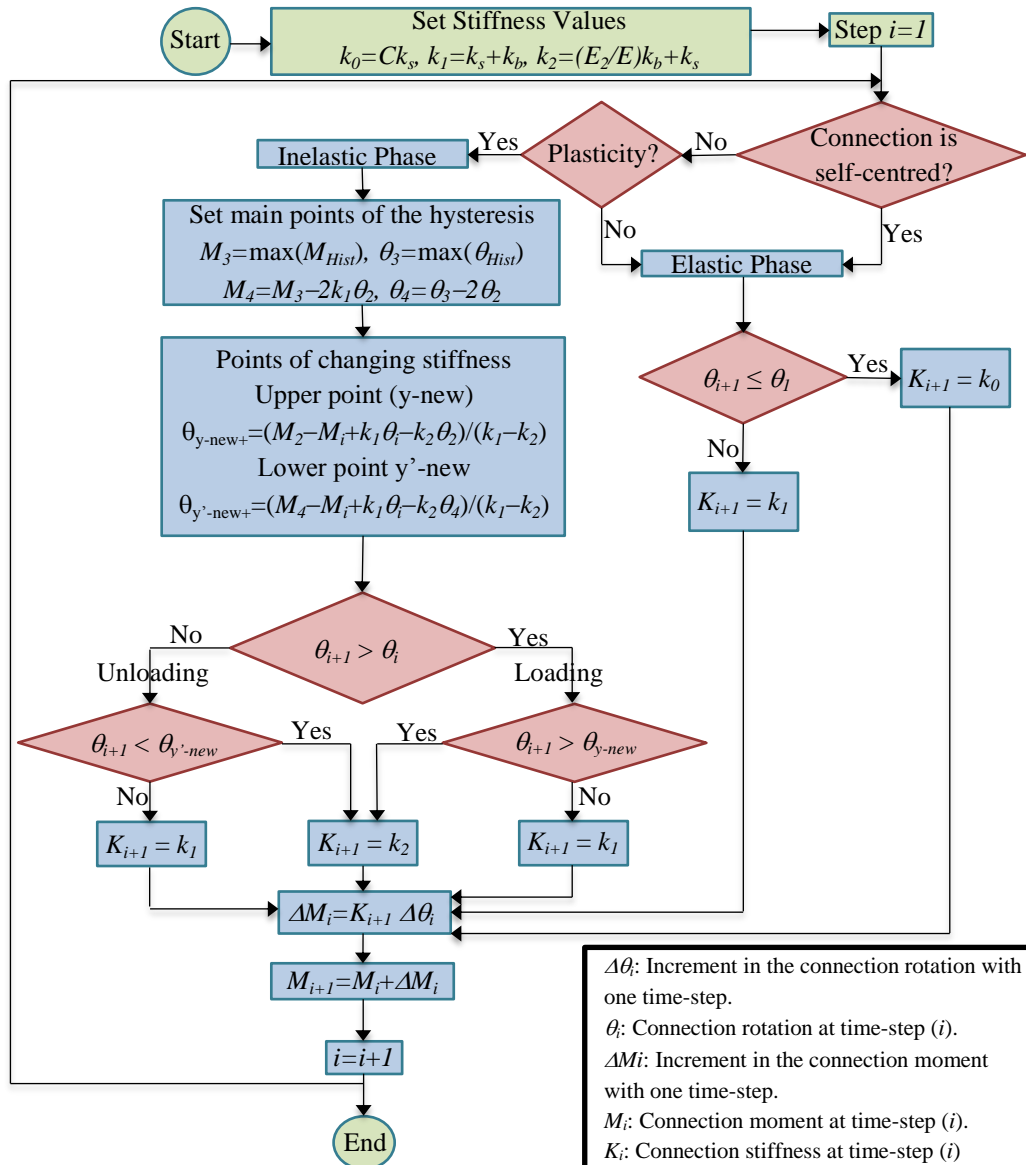


Figure 5.7: Flowchart of modelling the post-tensioned connection element.

5.1.2. Transition between Different Stiffness Values of the Post-tensioned Connection Model

In each step the model returns a moment increment calculated by multiplying the rotation increment by the current stiffness of the connection. When the stiffness changes within a rotation increment (Figure 5.8-a), the moment calculated by using either stiffness value is not correct. The largest error occurs at the transition from and to the initial stiffness k_0 (hence its value is limited, Figure 5.4).

In the IPTC model this error is avoided by taking into account the stiffness change in the connection. When stiffness of the connection at step $i+1$ is different from that at time-step i , the calculation of the moment increment is divided into two or more parts:

$$\Delta M_i = K_i (\theta_{CS} - \theta_i) + K_{i+1} (\theta_{i+1} - \theta_{CS}), \quad (5.8)$$

where ΔM_i is the moment increment, K_i stiffness of the connection at time $t=t_i$ and θ_{CS} is the rotation of the connection at the changing stiffness point.

In case of large rotation increments, the stiffness of the connection may change more than once. In such cases, the model counts the number of points at which the stiffness changes within the rotation step (θ_{CS1} , θ_{CS2} etc, Figure 5.8-b), and calculates the corresponding moment increment using the concept given in Equation 5.8.

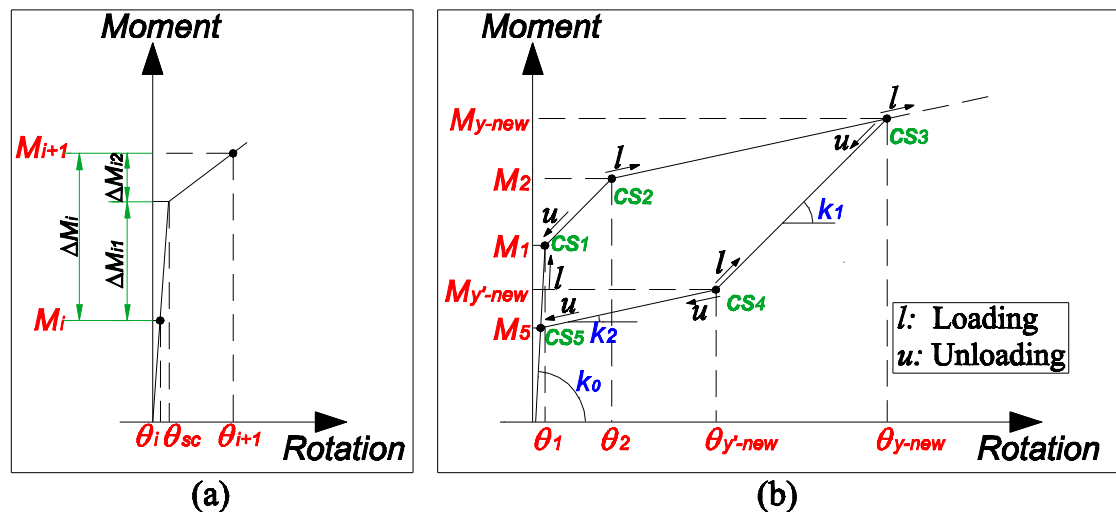


Figure 5.8: (a) Moment calculations when stiffness is changed and (b) points of changing stiffness in the IPTC Model.

5.1.3. Verification of the Integrated Post-tensioned Connection (IPTC) Model using the Discrete Springs Model

To verify the new IPTC model, its performance was compared with a discrete springs model, using DRAIN 2DX (Prakash et al.1993). The simulations were carried out for a post-

tensioned connection between beam UB 610x305x179 and column UB 686x254x170, energy dissipating bars $\phi 20$; $f_y = 240$ MPa, strands with area $A_s = 560$ mm² and post-tensioning force $F_{pt} = 300$ kN. The initial stiffness of the connection in the integrated model (k_θ) was taken as 80 times the beam stiffness. The moment-rotation relationships from the IPTC model and the discrete springs model (in DRAIN 2DX), under the same harmonic loading, are shown in Figure 5.9.

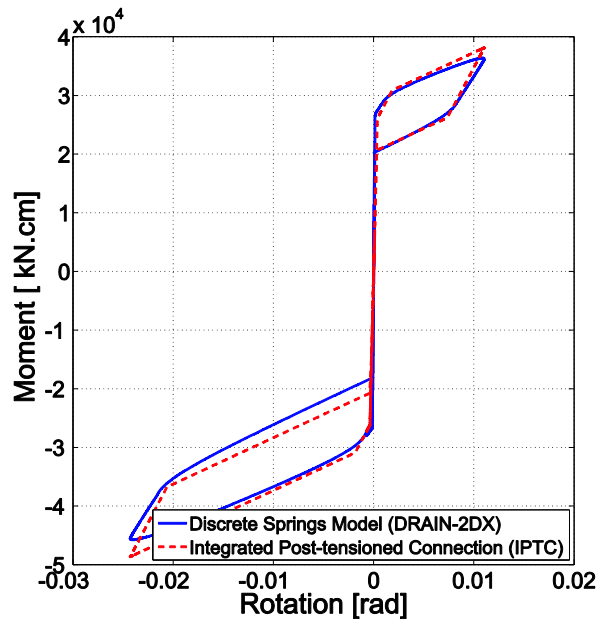


Figure 5.9: Verification of the IPTC model using the discrete springs model.

The gap-opening moments and the maximum rotations obtained from the two models were almost identical, and the moments at which the energy dissipating bars start yielding were very similar (Figure 5.9). The difference in the maximum moments between the two models was about 5%, whereas the difference between the energy dissipated in each model was about 8%. These differences are due to the interaction between the 8 discrete elements in the DRAIN model (gaps, axial and rotational springs) all defined with different, approximate initial stiffnesses, yield points and post-yield stiffness. This comparison suggests that the IPTC model gives an acceptable level of accuracy and can be used in simulations.

5.2. Incorporating the Standalone Post-tensioned Connection Model into a 2D Steel Frame

5.2.1. Geometry and Input Data for Incorporated Post-tensioned Connection (IPTC) Element

Element 3, the post-tensioned steel beam-column connection in FASAC-2D, is a zero-length element that connects the beam to the column (Figure 5.10). The two nodes of Element 3 have the same coordinates.

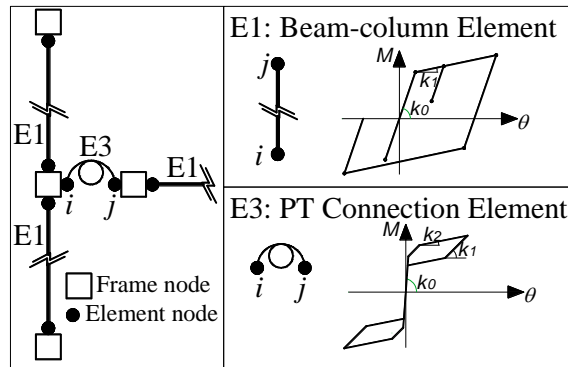


Figure 5.10: Schematic of the IPTC element in frame model.

Beam-column elements shown in Figure 5.10 are modelled using the plastic hinge element which does not accurately simulate the behaviour of beams and columns in this case. A fibre element could be used instead, but this would increase the computational cost of the analysis. Input data for the IPTC element are shown in Table 5.1.

5.2.2. Operation of the Post-tensioned Connection Element Incorporated in the Frame

In a dynamic analysis, the initial value of `YieldCode` is zero, which means that there is neither gap-opening nor yielding in the connection. The initial rotational stiffness of the connection is assumed to be very high (it is calculated using Equation 5.3) and the stiffness matrix of the connection element $[k_e]$ for `YieldCode=0` is:

$$[k_e] = \begin{bmatrix} k_0 & 0 & 0 & -k_0 & 0 & 0 \\ 0 & k_0 & 0 & 0 & -k_0 & 0 \\ 0 & 0 & k_0 & 0 & 0 & -k_0 \\ -k_0 & 0 & 0 & k_0 & 0 & 0 \\ 0 & -k_0 & 0 & 0 & k_0 & 0 \\ 0 & 0 & -k_0 & 0 & 0 & k_0 \end{bmatrix}, \quad (5.9)$$

Axial and shear stiffness of the connection are assumed to be as high as the rotational stiffness, which at this stage is a reasonable assumption.

After solving the dynamic equation, the global deformations of the frame are used to calculate the element deformations in local coordinates.

For the connection element, the rotation is calculated from the rotations of its ends:

$$\theta = \theta_{beam} - \theta_{col} \quad (5.10)$$

where θ is rotation of the post-tensioned connection, θ_{beam} is rotation of the connection at the beam end and θ_{col} is rotation of the connection at the column end.

Parameter	Variable	Description	Unit	Value for simulation [kN-cm]
Energy Dissipation Type	$EDTY$	Type of the energy dissipater: 1. yielding, and 2. friction.	---	1
Energy Dissipation Properties	D_b	Depth of the beam	[L]	40.26
	E_b	Modulus of elasticity of the energy dissipater (only for $EDTY=1$)	[F.L ⁻²]	21000
	f_{yb}	Yield stress of energy dissipater (only for $EDTY=1$)	[F.L ⁻²]	24
	F_{yd}	Slip force of friction-based energy dissipater (only for $EDTY=2$)	[F]	---
	L_b	Length of energy dissipating bars (only for $EDTY=1$)	[L]	100
	dia	Diameter of energy dissipating bars (only for $EDTY=1$)	[L]	2.00
	E_2/E	Ratio between post-yielding and pre-yielding stiffness of the energy dissipating bars (only for $EDTY=1$. If $EDTY=2$ it will be taken automatically as zero)	---	0.20
	C	Initial stiffness factor	---	80
	$FricLoc$	Location of friction-based damper: (1) installed at flanges, and (2) installed at web (only for $EDTY=2$).	---	---
Post-tensioned Strands Properties	N_{os}	Number of strands in the post-tensioned connection	---	3
	E_s	Modulus of elasticity of strands	[F.L ⁻²]	19650
	f_{ys}	Yield stress of strands	[F.L ⁻²]	186
	A_s	Area of strand cross section	[L ²]	5.60
	L_s	Length of strands adjacent to the connection (length of the frame span)	[L]	300
	F_{pt}	Post-tensioning force applied to the connection	[F]	300

Table 5.1: Input data for the IPTC element in FASAC-2D.

$$[k_e] = \begin{bmatrix} k_0 & 0 & 0 & -k_0 & 0 & 0 \\ 0 & k_0 & 0 & 0 & -k_0 & 0 \\ 0 & 0 & k_r & 0 & 0 & -k_r \\ -k_0 & 0 & 0 & k_0 & 0 & 0 \\ 0 & -k_0 & 0 & 0 & k_0 & 0 \\ 0 & 0 & -k_r & 0 & 0 & k_r \end{bmatrix}$$

$YieldCode=0 \dots k_x = k_0$
 $YieldCode=1 \dots k_x = k_1$
 $YieldCode=2 \dots k_x = k_2$

Table 5.2: Connection stiffness matrix for each time step (different *YieldCode* values).

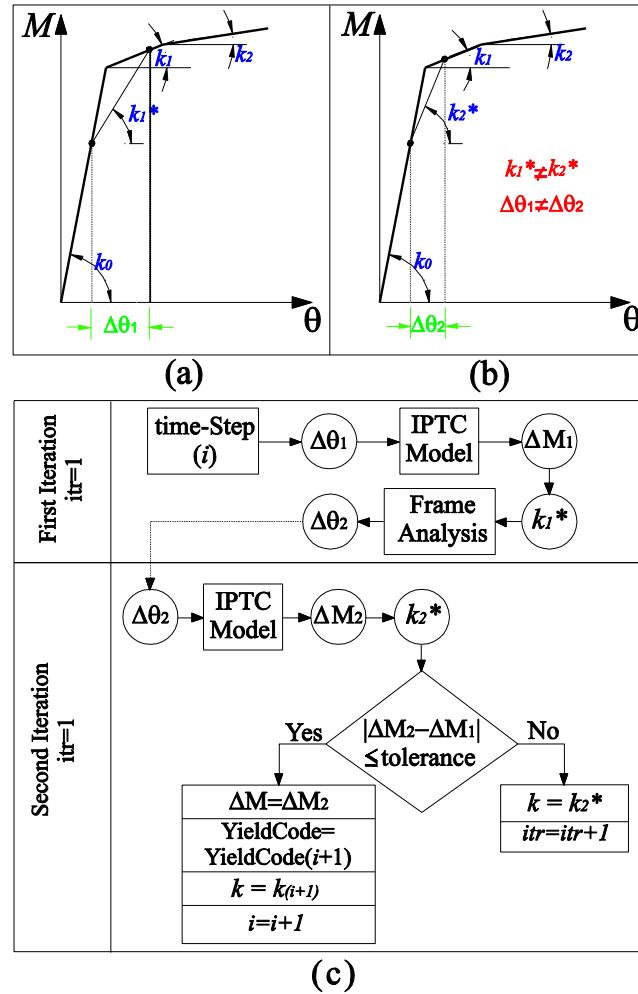


Figure 5.11: Moment calculation in the connection element: (a) first iteration, (b) second iteration, and (c) flowchart of moment calculation within the time-step.

The sign convention and calculation of the internal forces of the post-tensioned steel beam-column connection are shown in Figure 5.12. The axial and shear forces in the connection are calculated directly from the local stiffness matrix of the connection element. In reality, when the gap opens the connection undergoes axial deformations, resulting in elongation of the strands. For simplicity, the axial stiffness in the IPTC model is kept constant (k_0), which means that the axial and shear deformations of the element are not calculated correctly. However, the model returns correct forces in the strands, because they are calculated directly from the rotation of the connection, and not from the axial deformations. An improved model can be developed to include the axial deformations.

The connection model does not exactly represent the real behaviour of PT frames as it does not: (i) capture the true axial force in the PT beam-column interface, (ii) take the effect of the diaphragmatic action from slabs, (iii) simulate the expansion of the frame and (iv) include the effect of column restraint on the frame expansion. All these features however, do not

severely affect the results of the frame response under seismic excitations which is the main focus of this work.

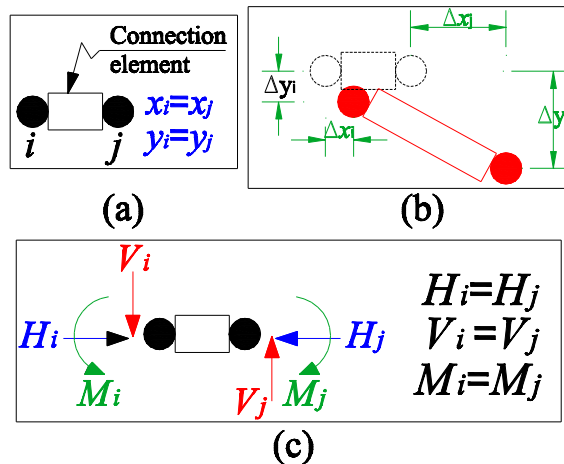


Figure 5.12: Post-tensioned connection element in FASAC-2D: (a) undeformed shape, (b) deformed shape and internal displacements, and (c) internal forces.

5.2.3. Simulation of dynamic response of post-tensioned steel frame using the IPTC model

In order to study the response of a structure equipped with post-tensioned steel beam-column connections, the frame shown in Figure 3.15 (Chapter 3) was supplied with IPTC elements (Figure 5.13). The cross sections chosen for frame elements are UB 457x191x82, with plastic moment of $M_p = 842$ kNm, for columns, and UB 406x178x54, with $M_p = 375$ kNm, for the beam. The properties assigned to the post-tensioned steel beam-column connection elements are given in Table 5.1. The frame was analysed by using a set of four earthquake scaled records: El Centro 1940, SMART1 1983, Northridge 1994 and Kobe 1995.

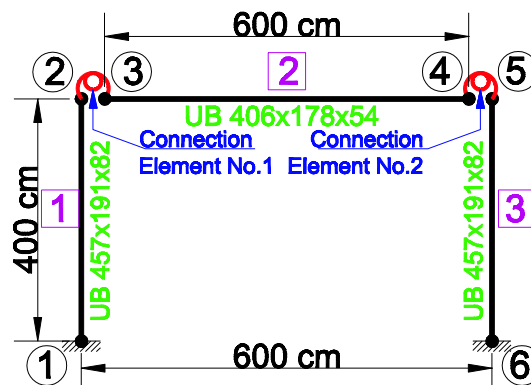


Figure 5.13: Model of the portal frame equipped with post-tensioned steel beam-column connections.

Results of the simulations are analysed in terms of moment-rotation relationship of the post-tensioned steel beam-column connections, global response of the frame,

moment in the connection, and tension forces in the strands of the connection element.

5.2.3.2. Moment-Rotation Relationship of the Post-tensioned Steel Beam-Column

Connections

The moment-rotation response of connection element No.1 (Figure 5.13) for the four earthquake excitations shows the expected flag-shaped behaviour (Figure 5.14), in which the three response stages have been mobilised: (k_0) before gap opening, (k_1) elastic with gap opening starting at rotation angle $\theta_2 = 4.3 \times 10^{-4}$ Rad and moment $M_1 = 181$ kNm, and (k_2) inelastic phase starting at $\theta_2 = 2.8 \times 10^{-3}$ Rad and $M_2 = 219$ kNm. In all cases the connection self-centres at the end of the simulation (as expected), and shows no residual rotations.

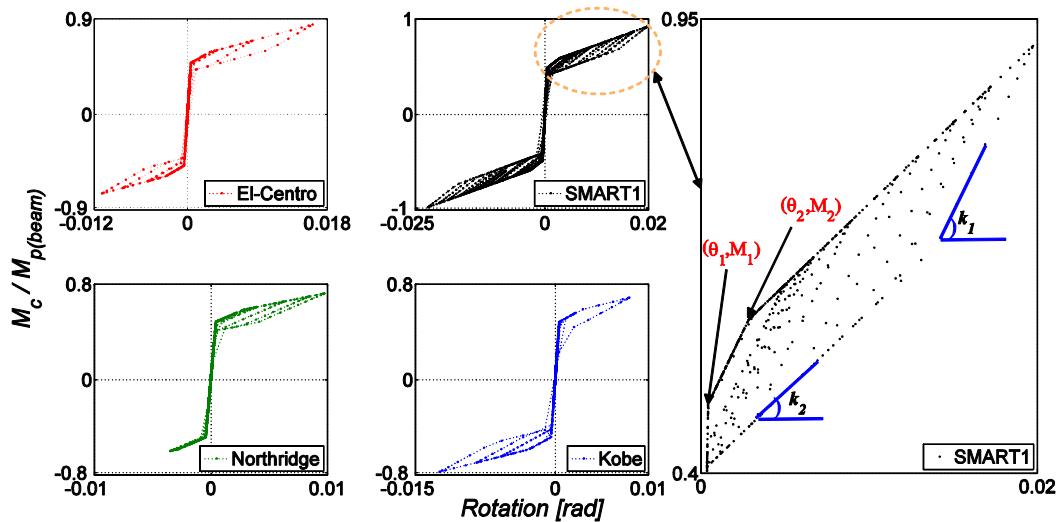


Figure 5.14: Moment-rotation response of the connection element No.1, under four different seismic excitations.

Figure 5.15 shows the yield code of the connection element No.1. It could be noticed that during the simulations with the four earthquakes, the connection performed several cycles of loading and unloading and maintained its self-centring behaviour.

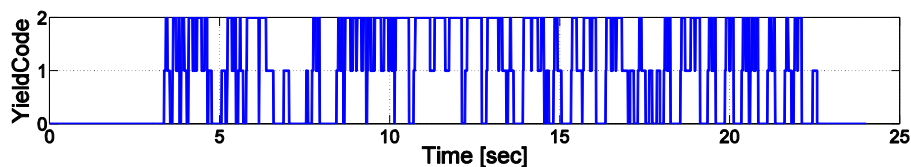


Figure 5.15: Time history of `YieldCode` of connection element No.1 for SMART1 earthquake: 0= no gap opening, 1 = gap opening and elastic loading-unloading, 2= gap opening and inelastic loading-unloading.

5.2.3.3. Global Response of the Frame

The comparison of horizontal displacements of the conventional frame and the frame equipped with the IPTC model under SMART1 earthquake (Figure 5.16) shows that the IPTC reduces the residual displacements of the frame from 14.5 mm to 2.5 mm (83%).

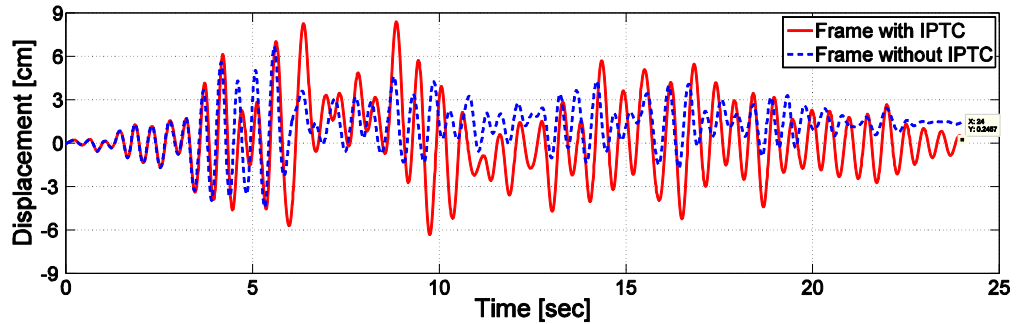


Figure 5.16: Horizontal displacements of conventional frame and frame with the IPTC (Input: SMART1).

5.2.3.4. Moment in the Connection

Figure 5.17 shows that the connection moment and the column moment are very close. The differences were within the given error tolerance level (see Figure 5.11), in this case 1%. In these simulations, by using a combination of 1% tolerance value and a small time step (0.005s), the maximum number of iterations per step was 12.

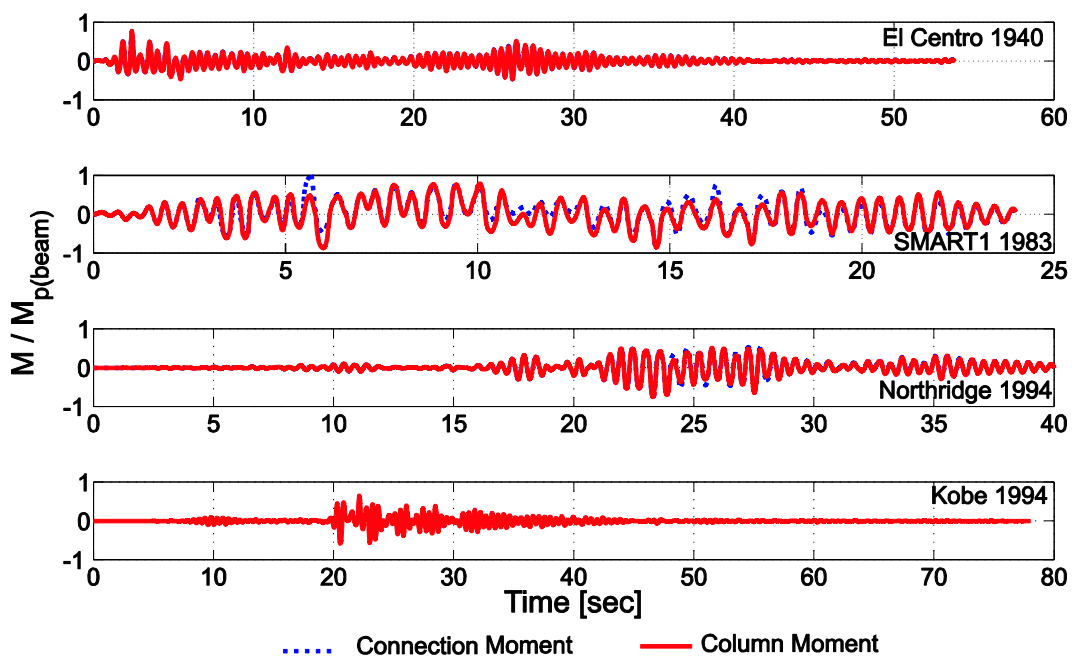


Figure 5.17: Connection moment compared to column moment.

It should be noted that assigning any nonzero value to the factor of viscous damping of the connection results in large differences between the moments in the connection and the column. In Figure 5.18 are shown the moment histories in the connection and the column, when a non-zero stiffness-proportional Rayleigh damping factor $\beta=0.005$ is assigned to the connection element. The difference between the connection and the column moments occurs and accumulates whenever there is a self-centring event in the connection. The reason for this difference is that the self-centring moment is calculated directly from the $M-\theta$ diagram

of the model rather than from the stiffness matrix. The moments in the connection and the frame are balanced after several iterations, but this balancing does not include the viscous damping forces in the connection. This is illustrated in Figure 5.19 which shows the development of damping forces in the IPTC model.

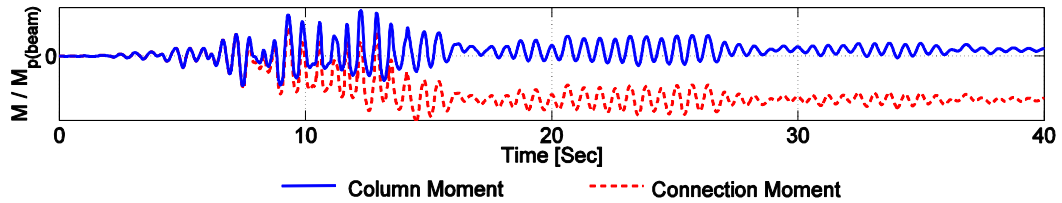


Figure 5.18: Error of connection moment when introducing viscous damping to the connection element.

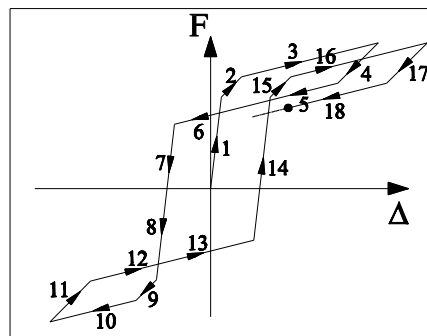


Figure 5.19: Step-by-step development of damping forces in the IPTC model if $\beta \neq 0$.

5.2.3.5. Tension Forces in the Strands at the Connection Element

FASAC-2D can be used to compute the tension forces in each strand of the connection element. The calculation of the tension forces is based on elongation of the strands due to rotation of the connection. Figure 5.20 shows deformations of the strands for positive and negative rotations.

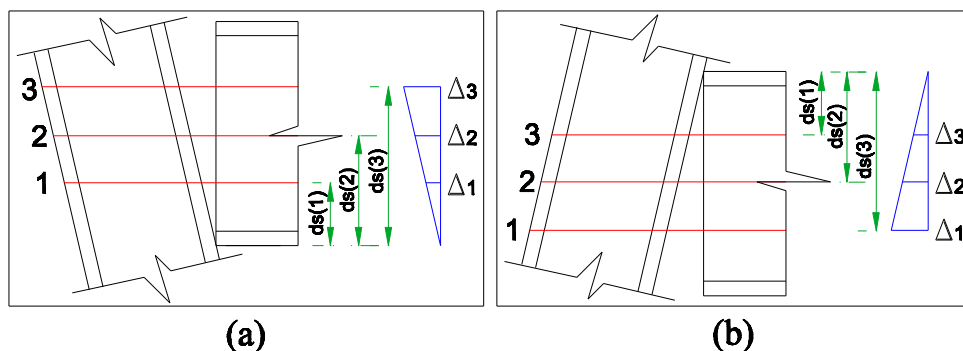


Figure 5.20: Strands deformations due to connection rotation: (a) positive rotation and (b) negative rotation.

The elongation status of each strand is swapped when the rotations change direction (Figure 5.20). In all cases, the deformation of the strands is elongation only and there is no

shortening. The algorithm used to compute tension forces in the strands and take into account the changes of rotation direction is shown in Figure 5.21.

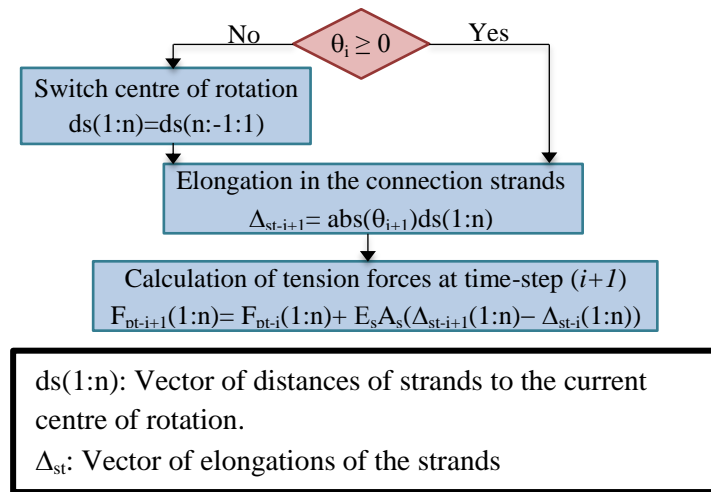


Figure 5.21: Calculation of the tension forces in strands for positive and negative connection rotations.

The values of the tension forces in the strands can be used as a criterion for assessing the failure status of the connection. If the tension force in any strand is higher than the yielding force of the strands, the connection fails. In Figure 5.22 are shown the time histories of tension forces in all strands in the connection element No. 1 for the SMART1 earthquake. The maximum tension force ($F_{t-max} = 550$ kN) is below the yielding force of the strands ($F_{ys} = 1041.6$ kN).

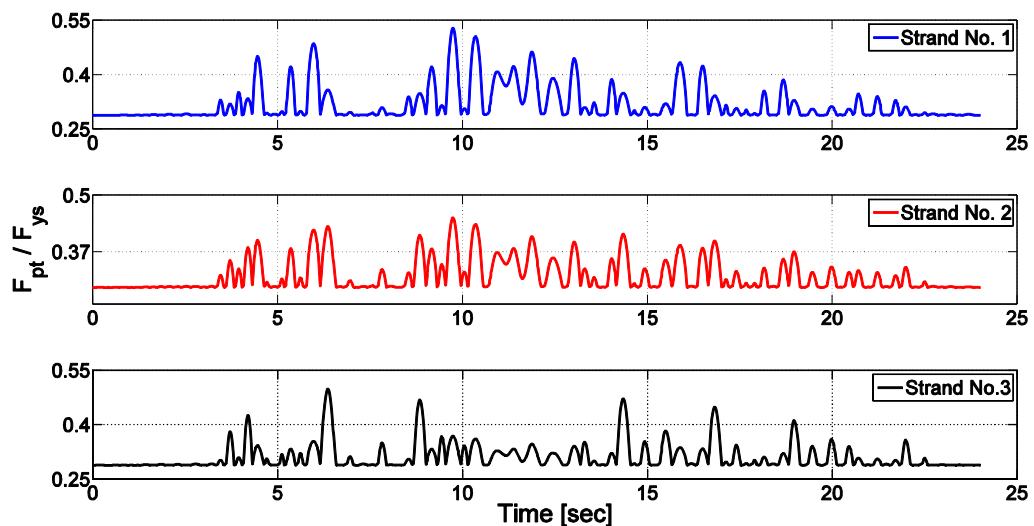


Figure 5.22: Tension forces in the strands for SMART1 earthquake.

5.3. Connection Details and Application of Semi-active Control on Post-tensioned Steel Frames

This section presents steel post-tensioned beam-column connection details adopted in this research. These details are first illustrated for passive system (post-tensioning forces are pre-set and constant). Then, the connection detail is modified to allow for the application of semi-active control of post-tensioning forces.

5.3.1. Post-tensioned Connection Details for Passive System

If the post-tensioned connection works passively, its details are similar to those proposed in previous work (Ricles et al. 2001, Christopoulos et al. 2002^a, and Rojas et al. 2005). The detail depends on the energy dissipating device installed in the connection (energy dissipating bars or friction mechanism).

The connection detail adopted for this research is designed to maintain the main features of steel post-tensioned beam-column connections: high initial stiffness, self-centring and flag-shaped hysteresis. The main difference between the new and the original connection (Christopoulos et al. 2002^a) is the introduction of a mechanism for transferring shear forces instead of relying on the friction between beam and column flange as recommended by Vasdravellis et al. (2013^a).

While the connection is self-centred, friction force (F_{fr}) between the beam and the column flange can be obtained from:

$$F_{fr} = \nu N_{os} F_{pt}, \quad (5.11)$$

where ν is the coefficient of friction between the beam and the column flange (steel to steel - dry surfaces), N_{os} is the number of strands in the connection, and F_{pt} is the post-tensioning force in each strand.

If there is no gap opening in the connection, friction forces are high and sufficient to transfer shear forces from the beam to the column. When the gap opens however, the contact area between the beam and the column face reduces substantially (Figure 5.23). The loss in contact area leads to a drop in friction resistance and they may become insufficient to carry the shear forces.

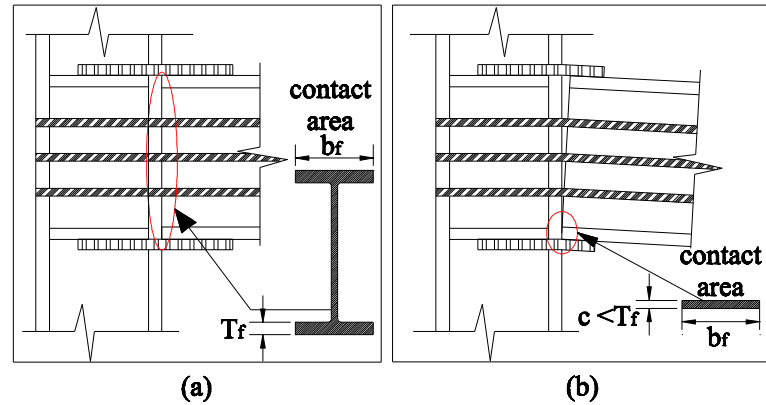


Figure 5.23: Illustration of the contact area between the beam and the column in steel post-tensioned beam-column connections: (a) no gap opening, and (b) gap opening.

To avoid loss in shear capacity of the connection due to drop of contact area, a separate shear element is provided in the connection. This element is a shear tab welded to the column flange and connected to the beam web using bolts. This shear tab is not responsible only for transferring shear forces, but also for dissipating energy in the case of friction-based energy dissipaters. When friction-based energy dissipater is used, a layer of brass (Figure 5.24) can be placed between the shear tab and the beam web to improve the friction cyclic behaviour (Latour et al. 2012).

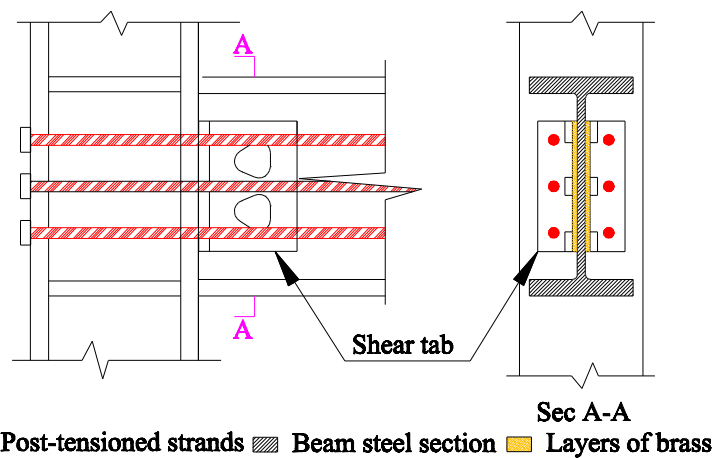


Figure 5.24: Brass layers in friction-based energy dissipating connections.

The bolt holes are slotted and shaped to allow unrestrained rotation of the connection around two centres of rotation when the gap opens. The shape of the holes is such that the shear tab does not bear the bolts or obstruct the rotation of the connection (Figure 5.25). Edges of the hole are rounded with radii equal to the distance between the bolt and the connection centre of rotation. In a special case when only one bolt is required, then the two radii are equal.

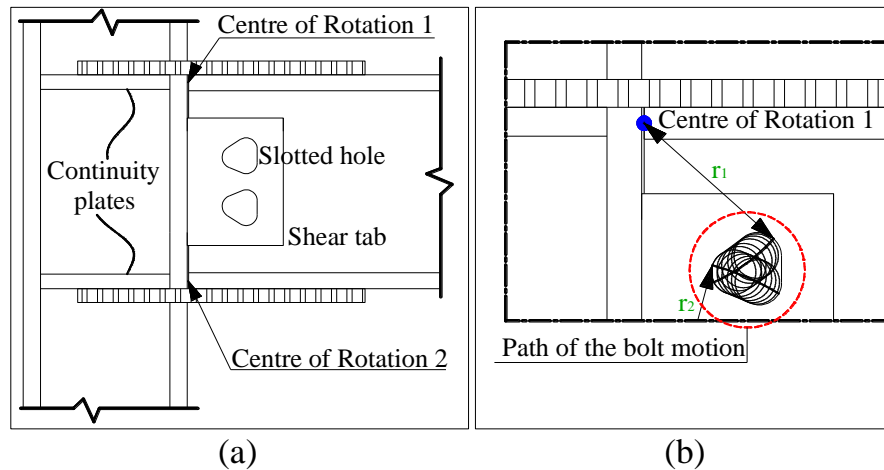


Figure 5.25: Geometry of slotted bolt holes for steel post-tensioned beam-column connections:
(a) complete detail and (b) detail of the slotted holes.

When the gap opens, high compressive stresses forces are concentrated at the centre of rotation (Figure 5.23-b). These high forces may cause local failure of the column such as buckling or yielding of the flange or crushing or buckling of the web. Hence, two column stiffeners are provided at the level of both beam flanges.

5.3.2. Application of Semi-active Control on Post-tensioned Steel Frames

5.3.2.2. Post-tensioned Connection Details for Semi-active System

A possible arrangement for applying the control action to post-tensioned steel frames is shown in Figure 5.26. In this arrangement, the post-tensioned strands (1) are anchored to a collecting plate (2) which is connected to a steel connector (10) and then to a rotating motor (6). Shear forces are transmitted using a shear tab (3), which is provided with bolts with slotted holes to allow gap opening. A limiting element (7) is used to make sure that the rotation of the motor is limited so no slack in the strands occurs during operation. Continuity plates (8) are used to avoid local failures in the column under compressive forces. The relative displacement between the beam and the column face is measured using sensors (9) (linear variable differential transducers). Measures from the sensors are passed to the central controller to apply the semi-active control algorithms.

The arrangement shown in Figure 5.26 is provided only to one connection (master connection) in each storey. The rest of the post-tensioned connections in the storey are conventional post-tensioned connections (with shear tabs and bolts with slotted holes). The measurements from the master connection are enough to apply the control algorithm as the rotation angle of all connections in one storey are the same (Figure 5.27).

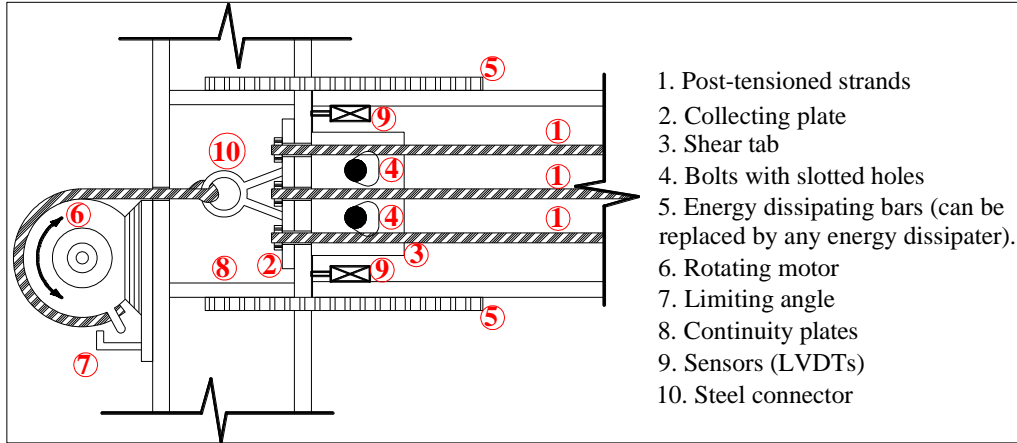


Figure 5.26: Arrangement of external post-tensioned connection equipped for controlling the strands forces.

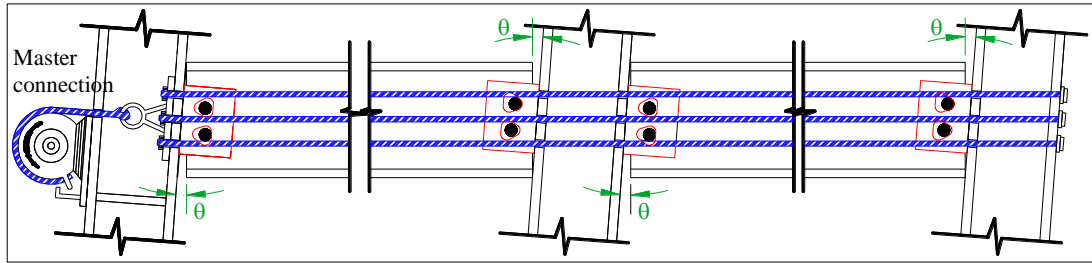


Figure 5.27: Arrangement of the master connection and other connections in one storey.

5.3.2.3. Specifications of the Rotating Motor

Specifications of the rotating motor are determined from the properties of both strands and motor. If the drop/increase in the post-tensioning force of each strand is $\Delta F_{control}$, the change in the strands length is given as:

$$\Delta L = \frac{\Delta F_{control} \times L}{E_s \times A_s} \quad (5.12)$$

here ΔL is the change in the strands length due to the force drop/ increase, L is the total length of the strands in one storey, E_s is the strands modulus of elasticity and A_s is the cross section area of one strand.

If the radius of the rotating disc is r , the rotation angle ($\Delta\phi$) due to ΔL is obtained from:

$$\Delta\phi = \Delta L / r \quad (5.13)$$

If the control force ($\Delta F_{control}$) is applied every time increment (Δt) then the rotating velocity of the motor (ω) is given as:

$$\omega = \Delta\phi / \Delta t \quad (5.14)$$

Using equations (5.12), (5.13) and (5.14) the required frequency of the rotating motor (f_{motor}) can be obtained from:

$$f_{motor} = \frac{\Delta F_{control} \times L}{2\pi \times E_s \times A_s \times r \times \Delta t} \quad (5.15)$$

The power required for the rotating motor (P) can be given from Equation (5.16) with N_{os} is the number of strands in the master connection.

$$P = \frac{\Delta W}{\Delta t} = \frac{\Delta F_{\text{control}} N_{os} r \Delta \phi}{\Delta t} \quad (5.16)$$

By manipulating Equation 5.16, the required power of the motor can be obtained from:

$$P = \frac{\Delta F_{\text{control}}^2 \times N_{os} \times L}{\Delta t \times E_s \times A_s}. \quad (5.17)$$

5.4. Concluding Remarks on Modelling, Incorporation and Details of PT Connection

In this chapter is presented an integrated model of a post-tensioned steel beam-column connection element (IPTC) for simulating the dynamic response of post-tensioned steel frames. This is a three stage model, incorporating gap opening, and yielding or slip (of energy dissipating elements) as well as self-centring upon unloading. The IPTC model captures all the important events in the post-tensioned connections.

In order to incorporate the IPTC model into a 2D frame analysis program, the stiffness matrix of the connection element was derived. When incorporated in a 2D post-tensioned steel frame, the IPTC model shows the expected flag-shaped moment-rotation relationship. The simulations of four earthquake time histories showed self-centring of the frame and reduced residual deformations. The IPTC model also computes the post-tensioning forces in the strands which can be used for designing the connections.

The last section of this chapter discussed possible connection details for both passive and semi-active control systems. The most important feature of the connection detail in passive systems is the detail of the slotted holes of the bolts. These holes should be designed to allow gap opening and avoid bearing from the bolts. The connection detail was developed for semi-active control systems. A rotating motor was added with a special detailing to avoid malfunction of the connection. Formulae describing the motor specifications were presented as well.

CHAPTER 6

CHARACTERISTICS AND DYNAMIC BEHAVIOUR OF PASSIVE POST-TENSIONED STEEL FRAMES

In this chapter is presented a study of the structural characteristics of post-tensioned steel frames and their dynamic behaviour under seismic loads. The characterisation of post-tensioned steel frames was carried out by performing analyses at two levels: (i) connection level and (ii) frame level.

The purpose of investigating the connection performance at the local level is optimising the ranges of action of the connection parameters: post-tensioning force (F_{pt}) and energy dissipation factor (β). The parametric optimisation is based on four criteria: (a) moment capacity, (b) energy dissipation capacity, (c) rotational ductility of the connection, and (d) self-centring capacity.

At the frame level, the effects of the connection parameters on the dynamic response of the structure were investigated. To describe the influence of the connection parameters on the frame behaviour, various aspects of the frame response were inspected: secant stiffness of the structure, maximum displacement, self-centring capacity, energy dissipation capacity, and internal forces in the elements. To complement the structural characterisation of the post-tensioned steel frames, their performance was assessed through comparison with conventional moment resisting steel frames (MRF).

6.1. Effect of Connection Parameters on the Connection Behaviour

The effects of the two parameters, post-tensioning force in the strands (F_{pt}) and energy dissipation factor (β), on the behaviour of the post-tensioned connection were investigated by a parametric analysis similar to the one done by Christopoulos et al. (2002^b).

The post-tensioned connection used for this study is shown in Figure 6.1-a. The connection was analysed for two types of energy dissipating devices: energy dissipating bars and friction-based energy dissipater. The optimum ranges of F_{pt} and β were determined by comparison of the results obtained for these two types of energy dissipaters. The connection was subjected to a displacement-driven cyclic loading (Figure 6.1-b) which increased until failure in the connection. The failure occurred when the tension force in any strand exceeded the yielding force F_{ys} .

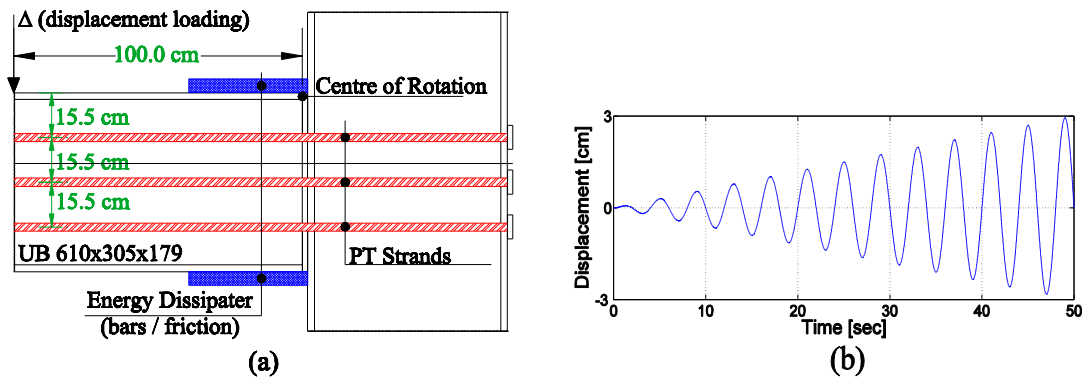


Figure 6.1: (a) Geometry of post-tensioned connection, (b) loading time history.

Since F_{pt} and β are related and cannot be varied independently, the behaviour of the post-tensioned connection was studied by variations of the post-tensioning force in the strands F_{pt} and the moment provided by the energy dissipater M_{Ed} (Figure 6.2).

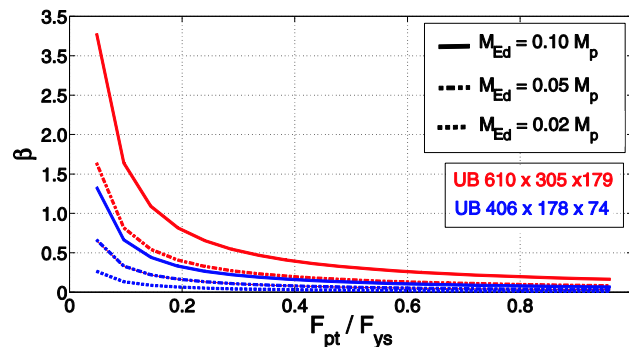


Figure 6.2: Relationship between post-tensioning force (F_{pt}) and energy dissipation factor (β).

6.1.1. Rotational Ductility Capacity and Energy Dissipation Capacity

The rotational ductility capacity of post-tensioned connection (μ) is a ratio between the ultimate rotation angle of the connection θ_{ult} (the collapse is characterised by yielding of the post-tensioned strands) and $\theta_{el} = \theta_2$, the rotation angle at which the energy dissipating device yields or slips (Equation 6.1). It should be noted that θ_{ult} cannot be reached in practice and the connection would fail due to the excessive yielding in the beam and the shim plates before the strands yield.

$$\mu = \frac{\theta_{ult}}{\theta_{el}} \quad (6.1)$$

The ability of post-tensioned connections to provide high rotational ductility is one of the most important characteristics of this connection type. The ductility capacity of the connection varied significantly with the variation of post-tensioning force (Figure 6.3).

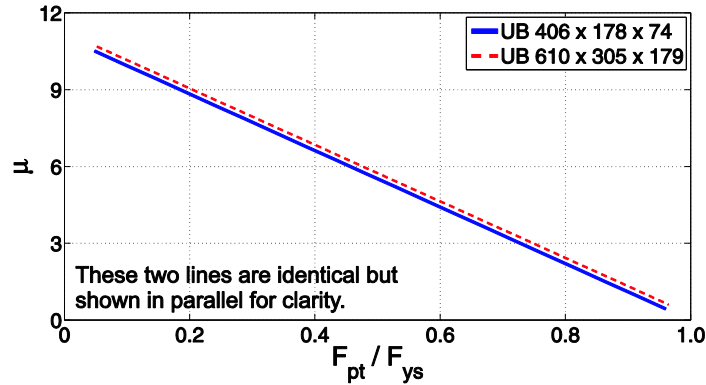


Figure 6.3: Relationship between rotational ductility capacity (μ) and post-tensioning force (F_{pt}).

If the yield force of the post-tensioned strands was F_{ys} , tension forces in the strands would be in the range between F_{pt} and F_{ys} . The higher the post-tensioning force (F_{pt}) the narrower the range of tension forces, and the lower the ultimate rotational angle (θ_{ult}). Hence, the ductility of the connection was reduced when higher post-tensioning forces were used.

It is worth mentioning that the rotational ductility of the post-tensioned connection could be less than 1 (in contrast to other connection types). When a very high post-tensioning force was used, the strands may have yielded and the connection may have failed before reaching the elastic rotation angle (θ_{el}).

Also, Figure 6.3 indicates that the rotational ductility capacity of the post-tensioned connection was dependent only on post-tensioning forces in the strands. As long as the plastic moment of the beam was higher than M_{St} , the size of the beam had no effect on the rotational ductility of the connection (in contrast to conventional beam-column connection types). While conventional beam-column connections exhibited lower ductility for deeper beam sections (FEMA 351, 2000; FEMA 355D, 2000), the gap opening action in the post-tensioned connection made rotation of the beam independent of the rotation of the column and, therefore, connections with different beam section sizes had the same ductility capacity. The independence of rotational ductility of the post-tensioned connection of the beam size led to more stable ductile behaviour of post-tensioned connections than that of conventional beam-column connections.

Stable ductile behaviour of post-tensioned connections could be achieved only if the behaviour of the energy dissipating system was also ductile and stable. When an energy

dissipating bar is subjected to tension, its ductility is about 12.5 for low-ductility steel and about 37.5 for high-ductility steel (Eurocode 2, 2004) which is higher than the maximum ductility capacity provided by the post-tensioned strands. When the bar is subjected to compression, its ductility is deteriorated by buckling actions, and therefore, a mechanism should have been provided to prevent the buckling of the energy dissipating bars. Usually, a cylinder is used to confine the energy dissipating bars and eliminate the probability of having buckling in the bars. Friction-based energy dissipating devices on the other hand offered very stable and ductile behaviour when the friction material was characterised by stable cyclic behaviour such as brass. This stable behaviour was ensured as long as the friction device was provided with sufficiently large slots to accommodate the expected rotation.

The effect of the moment provided by the energy dissipation system (M_{Ed}) on the ductility of the post-tensioned connection could be shown by plotting the relationship between the energy dissipating factor (β) and the rotational ductility (μ) (Figure 6.4). This relationship showed that the maximum ductility capacity was the same for different β values. Also, the rotational ductility increased with the energy dissipation factor because: (i) high energy dissipation factors were associated with smaller post-tensioning forces (Figure 6.2 and Figure 6.3), or (ii) higher energy dissipation factors were results of higher moments provided by the energy dissipating system (M_{Ed}) which resulted in higher moment capacity and therefore higher ultimate rotation angle. Note that beams with larger depth provided higher values of M_{St} and M_{Ed} , resulting in higher dissipation factor β for the same ductility.

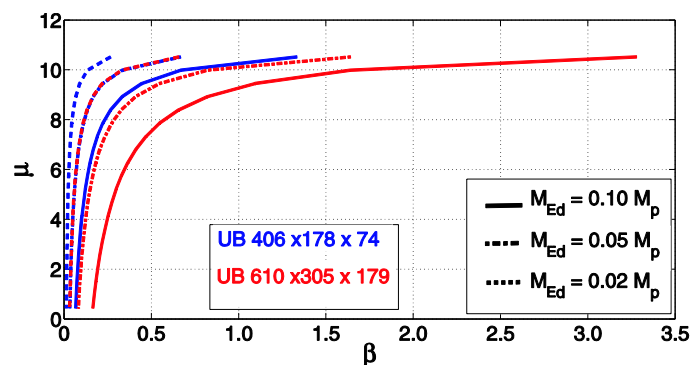


Figure 6.4: Relationship between energy dissipation factor (β) and rotational ductility (μ).

The relationship between the post-tensioning force (F_{pt}) and the normalised maximum energy dissipated before the connection failed is shown in Figure 6.5. In this figure, the energy dissipating capacity of the connection showed a similar behaviour to the connection rotational ductility. When very high post-tensioning forces were used, the connection failed before the energy dissipater was activated. Therefore, at very high levels of post-tensioning, the behaviour of the connection remained elastic and it was characterised by a brittle mode of failure.

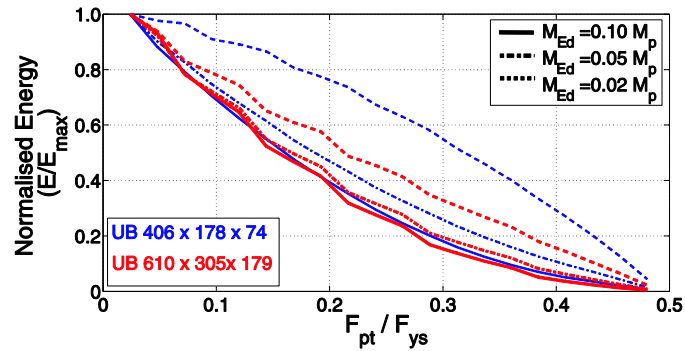


Figure 6.5: Relationship between post-tensioning force (F_{pt}) and normalised energy dissipation capacity (E/E_{max}).

6.1.2. Ultimate Moment Capacity

The effects of post-tensioning force on moment capacity of the connection for two beam sizes (UB 610x305x179 and UB 406x178x74) are presented in Figure 6.6. The graphs show that increasing the post-tensioning forces resulted in a linear increase of the ultimate moment capacity of the connection.

For both beam sizes, and up to the limit of post-tensioning force ($\mu=1$; shown as green line in Figure 6.6), the relationship between the post-tensioning force (F_{pt}) and ultimate moment capacity of the connection (M_u) was linear. The slope of the line depended on the beam size and the moment provided by the energy dissipating device.

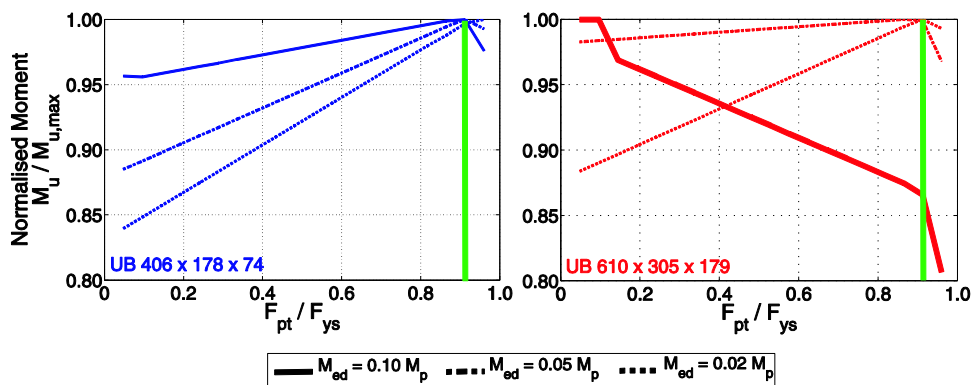


Figure 6.6: Relationship between the post-tensioning force (F_{pt}) and the ultimate moment capacity of the connection ($M_u/M_{u,max}$).

The graphs in Figure 6.6 show that: (i) the slope of the M_u-F_{pt} relationship decreased when the moment provided by the energy dissipating device (M_{Ed}) increased, and (ii) at the same ratio of moment provided by the energy dissipater to the plastic moment of the beam (M_u/M_p), the slope of the relationship was less for the larger beam size. In both cases, the slope of the line was dependent on the moment provided by the energy dissipating device (M_{Ed}) (or the energy dissipating factor β). For small energy dissipating factor, the effect of the moment provided by the post-tensioned strands (M_{S_t}) on the ultimate moment capacity of the

connection was higher than the effect of the moment provided by the energy dissipating device (M_{Ed}). Therefore, the loss in the rotational ductility of the connection due to the increase in the post-tensioning forces was not associated with a loss in the ultimate moment capacity (M_u) as it was compensated by the increase in the moment provided by the strands (M_{St}). This is the case for small beams where the lever arm of the energy dissipating device (D_b) was small. The moment provided by the energy dissipating device is given as:

$$M_{Ed} = F_{yd} \cdot D_b, \quad (6.2)$$

where F_{yd} is the yield/ slip force in the energy dissipating device.

Increasing post-tensioning force beyond the upper limit determined by rotational ductility $\mu=1$ (represented by a green line on Figure 6.6) would decrease the ultimate moment capacity of the connection, regardless of the size of the beam or the value of the energy dissipation factor. It can be noticed in Figure 6.6 that for deeper beam sections and larger values of M_{Ed} ($M_{Ed}=0.1M_p$), the ultimate moment of the connection M_u was achieved for low values of F_{pt} , and increasing F_{pt} resulted in yielding of the strands and reduction of the $M_u/M_{u,max}$, i.e. in negative slope of the $M_u/M_{u,max} - F_{pt}/F_{ys}$ relationship.

6.1.3. Self-Centring Capacity

The connection capacity to fully self-centre and restore its rotation depended mainly on the post-tensioning forces applied to the strands. If small post-tensioning forces were applied to the strands, the connection would not be able to self-centre, and would undergo irretrievable residual rotations (Figure 6.7). It can be noticed from Figure 6.7 that in order to provide the connection with full self-centring ability, the moment provided by the post-tensioned strands (M_{St}) should have satisfied:

$$M_{St} \geq (k_{b1} - k_{b2}) \theta_y, \quad (6.3)$$

where k_{b1} is the first stiffness of the energy dissipating device (elastic), k_{b2} is the second stiffness of the energy dissipating device (post-yield) and θ_y is the rotation angle at which the energy dissipating device yields.

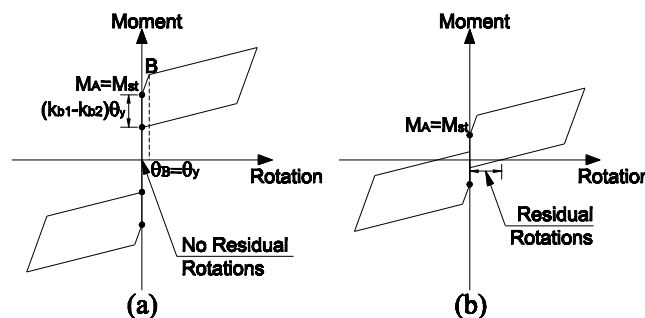


Figure 6.7: Behaviour of the post-tensioned connection with energy dissipating bars: (a) sufficient self-centring forces, (b) insufficient self-centring forces.

The moment provided by the post-tensioned strands (M_{St}) is:

$$M_{St} = F_{pt} \sum ds, \quad (6.4)$$

where F_{pt} is the post-tensioning force and $\sum ds$ is the sum of the distances of all strands from the centre of rotation of the connection. By substituting Equation 6.4 in Inequality 6.3, the lowest post-tensioning force (F_{ptLow}) to ensure full self-centring ability of the post-tensioned connection was defined as:

$$F_{ptLow} = \frac{(k_{b1} - k_{b2})\theta_y}{\sum ds} \quad (6.5)$$

When friction-based energy dissipater was used in the post-tensioned connection, the first stiffness of the energy dissipater (k_{b1} , elastic stiffness before slip) was very high, and could be assumed as infinite, and the second stiffness (k_{b2}) was zero (rigid-ideal plastic behaviour). Therefore, the requirement in Equation 6.5 could not be used. Instead, the lowest post-tensioning force to ensure full self-centring of the connection (F_{ptLow}) was derived from Figure 6.8.

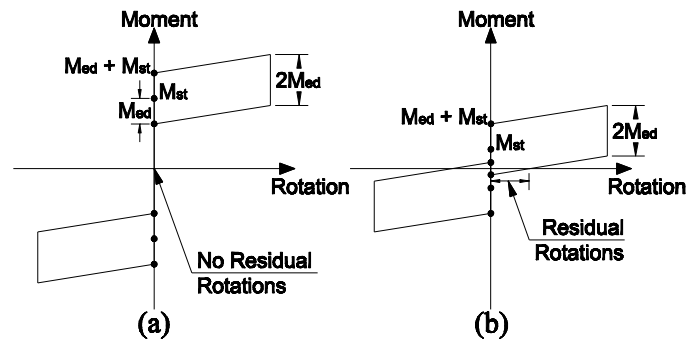


Figure 6.8: Derivation of full self-centring requirement of post-tensioned connections with friction energy dissipaters: (a) sufficient self-centring forces, (b) insufficient self-centring forces.

From Figure 6.8 it can be seen that that full self-centring was satisfied when $M_{St} \geq M_{Ed}$, or when $\beta \leq 1$.

6.1.4. Optimum Ranges of Values for the Connection Parameters in Passively Controlled Post-tensioned Connections

It has been shown in this chapter that the behaviour of a passively controlled post-tensioned connection was heavily dependent on the values of its parameters (i.e. post-tensioning force F_{pt} , and energy dissipation factor β). Values chosen for these two parameters affected the rotational ductility, energy dissipation capacity, ultimate moment capacity, and self-centring ability of the connection. Therefore, in order to obtain the best performance of the post-tensioned connection, these parameters should lie within specific ranges.

The lowest value of the post-tensioning force ($F_{pt,Low}$) can be obtained using Equation 6.5 (or $\beta \leq 1$ for connections with friction-based energy dissipaters) to satisfy the full self-centring requirement (Figures 6.7 and 6.8). The highest value of F_{pt} was chosen to provide the connection with the required levels of rotational ductility, energy dissipation capacity, and moment capacity (Figures 6.5 and 6.6).

The upper limit for the post-tensioning force was the one associated with rotational ductility equal to one (Figures 6.3 and 6.6, $F_{pt,max} = 0.9 F_{ys}$). This value was too high as it treated the connection individually without considering the plastic moments of column and beam connected to it. In fact, the maximum value of the post-tensioning force should not result in strong-connection-weak-column, where the plastic moment of the connection ($M_y = M_{St} + M_{Ed}$) is higher than the plastic moment of the connected column. Also, the post-tensioned connection should work as a fuse to dissipate energy and attract the plastic hinge as permitted in Eurocode 8 (2004). Hence, the upper limit for the post-tensioning force in the connection is the force that produces a yield moment less than the plastic moment of the connected beam ($M_y \leq M_{p,beam}$).

On the other hand, if the post-tensioning force was too low the moment capacity of the connection would be very low. This would result in forming a plastic hinge in the connection at low loading levels, resulting in reduced stiffness and consequently in large deformations of the structure, plastic hinges in the columns and potential structural failure.

There are some recommended values for F_{pt} , given in existing research (Wang, 2004; Garlock et al. 2008), but these are not optimum. The selected value of F_{pt} should result in high moment capacity of the connection, yet its plastic moment should be less than the plastic moment of the connected elements. Also, it should provide the connection with acceptable levels of rotational ductility and energy dissipation capacity. The selection of the post-tensioning force is a complex procedure and requires further investigation that takes into account the properties of the structure as well as the characteristics of the seismic motion. In the following section is presented a limited investigation of the effects of the connection parameters (F_{pt} and β) on the dynamic behaviour of a three-storey frame building under several seismic excitations.

6.2. Effect of Connection Parameters on the Dynamic Behaviour of Post-tensioned Steel Frames

In order to investigate the effect of connection parameters on the dynamic behaviour of post-tensioned steel frames, the behaviour of a passively controlled three-storey two-span post-tensioned steel frame (Figure 6.9) was studied at different levels of post-tensioning force.

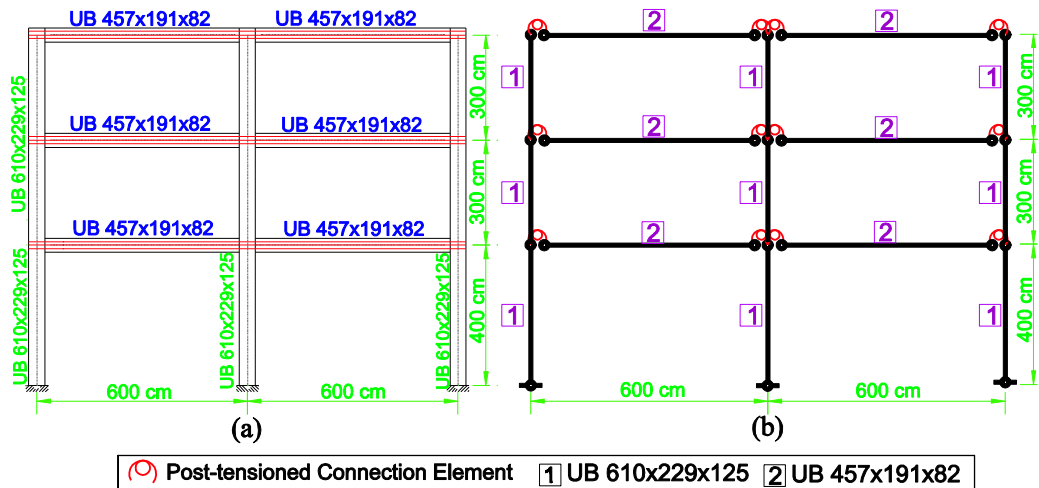


Figure 6.9: Investigation of post-tensioned steel frame: (a) frame geometry and sections, and (b) idealised model of the frame.

The post tensioned frame was designed in accordance with the capacity design principles, by assuming the following strength hierarchy: (1) inelastic deformations in the connection (yielding/slip of dissipaters), (2) plastic hinges at the base of columns, (3) plastic deformations in beams under combined axial load and moment, (4) hinges in columns (above base) and (5) failure of connection (yielding of strands). In order to achieve plastic deformations under moments and axial forces in the beams, they are assumed to be laterally restrained elements made of class 1 sections.

The lower limit for the post-tensioning force in the analysis was assumed to be the force required for full self-centring of the connection (F_{ptLow}). The upper limit of the post-tensioning force was taken as a proportion of the yielding force in the strands ($F_{ptmax}=0.8F_{ys}$), assuming that the axial strength of the beams was $F_{y,beam}=0.8F_{ys}$. The moment provided by the energy dissipating device at each connection was calculated for bars with diameter 20 mm, or about 7% of the plastic moment of the beam. The post-tensioning force was increased gradually from F_{ptLow} to F_{ptmax} in increments $\Delta F_{pt}=0.1F_{ys}$.

The frame behaviour was investigated by using two types of analyses: (i) non-linear static push-over analysis, and (ii) nonlinear dynamic analysis, using a series of seismic excitations.

6.2.1. Push-over Analyses

A set of push-over analyses were performed on the post-tensioned steel frame at different levels of post-tensioning forces. The main aim of these analyses was to investigate the effect of the post-tensioning forces on the ductility capacity and the sequence of plastic hinge development in the frame. The push-over analysis of the frame was controlled by the failure

of any post-tensioned connection. The analyses stopped when the tension force in any strand in the frame exceeded the yield force F_{ys} .

Push-over force-displacement curves were generated for different levels of post-tensioning forces (Figure 6.10). These plots show that by increasing the post-tensioning forces both the ultimate displacement of the frame, characterised by the yield of one strand, and the ultimate lateral force decrease. As a result, post-tensioned frames with higher post-tensioning forces are characterised by lower lateral ductility of the frame (μ_{fr}):

$$\mu_{fr} = \frac{\Delta_u - \Delta_p}{\Delta_p}, \quad (6.7)$$

where Δ_u is the ultimate lateral displacement of the frame at the point of first yielding in the strands and Δ_p is the plastic displacement of the frame, the displacement at which the first plastic hinge forms in the frame (either in the post-tensioned connections or in other frame elements).

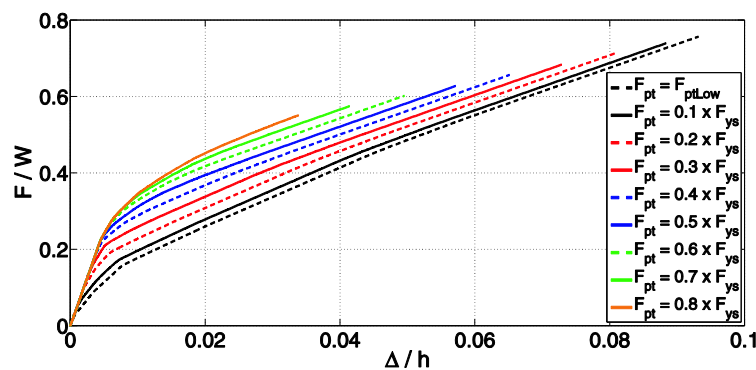


Figure 6.10: Push-over curves of post-tensioned frame at different levels of post-tensioning: F : base shear, W : weight of the structure, h : height of the frame and Δ : lateral displacement of the top storey.

The push-over curves (Figure 6.10) also show that at the same level of displacement, frames with higher level of post-tensioning force can take more load. This indicates that the performance level of the frame (as defined in FEMA 445, 2006) can be improved by applying higher post-tensioning forces in the connections.

The relationship between the ductility capacity and the post-tensioning force (Figure 6.11) shows that the decrease of ductility due to increase in post-tensioning force can be divided in two phases. In the first phase, at relatively low levels of post-tensioning force, the first plastic hinge formed always in the connections (yield or slip of the energy dissipating devices). This means that the plastic displacement (Δ_p) and the ultimate displacement (Δ_u) were both governed by the connection, which is the preferable behaviour of the structure. In the second phase, at higher post-tensioning levels, the plastic deformations were governed by plastic hinges in the columns. In most cases, the plastic hinges formed at the base of the

frame, which is a permitted hinge location, but not the preferable hinge sequence in post-tensioned frames. When post-tensioning forces in the connections were very large, plastic hinges formed in most elements outside the connections and structural failure was a result of either a storey mechanism or instantaneous yielding of strands, without any energy dissipation in the connections. This would result in large residual deformations after an earthquake.

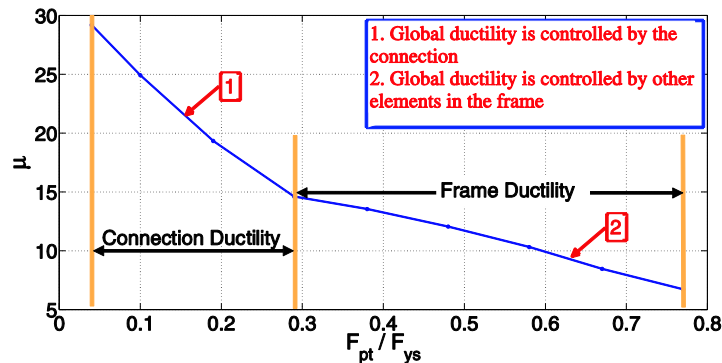


Figure 6.11: Ductility of the frame at different levels of initial post-tensioning.

6.2.2. Non-linear Dynamic Analyses

6.2.2.1. Selection of Earthquake Excitations

In order to characterise the dynamic behaviour of post-tensioned frames at different levels of post-tensioning force, the three-storey-two-bay post-tensioned frame was analysed through simulations of non-linear response to a set of scaled earthquakes (Table 6.1 and Figure 6.12).

The selected earthquake records provide a wide range of characteristics such as: (i) frequency content, (ii) intensity and (iii) distribution of large amplitudes over the earthquake duration (shape of the earthquake envelope).

Earthquake	Year	Country	Record	Δt (sec)	Duration (sec)	Earthquake Scaling
El-Centro	1940	USA	elcn40ns	0.020	53.760	S1
Borrego Mountain	1968	USA	BORREGO/A-ELC180	0.010	40.000	S2
Tabas	1978	Iran	TABAS/BAJ-V1	0.020	39.400	S2
SMART1	1983	Taiwan	SMART1/25C00EW	0.010	24.000	S2
Mexico-City	1985	Mexico	mexico_sct1_021	0.020	180.000	S3
Erzican	1992	Turkey	ERZIKAN/ERZ-NS	0.005	21.325	S2
Landers	1992	USA	LANDERS/H05000	0.020	56.000	S1
Northridge	1994	USA	NORTHR/HOS090	0.010	40.000	S1
Kobe	1995	Japan	KOBE/HIK000	0.020	78.000	S1

Table 6.1: Details of earthquake records (Regents of the University of California, 2000).

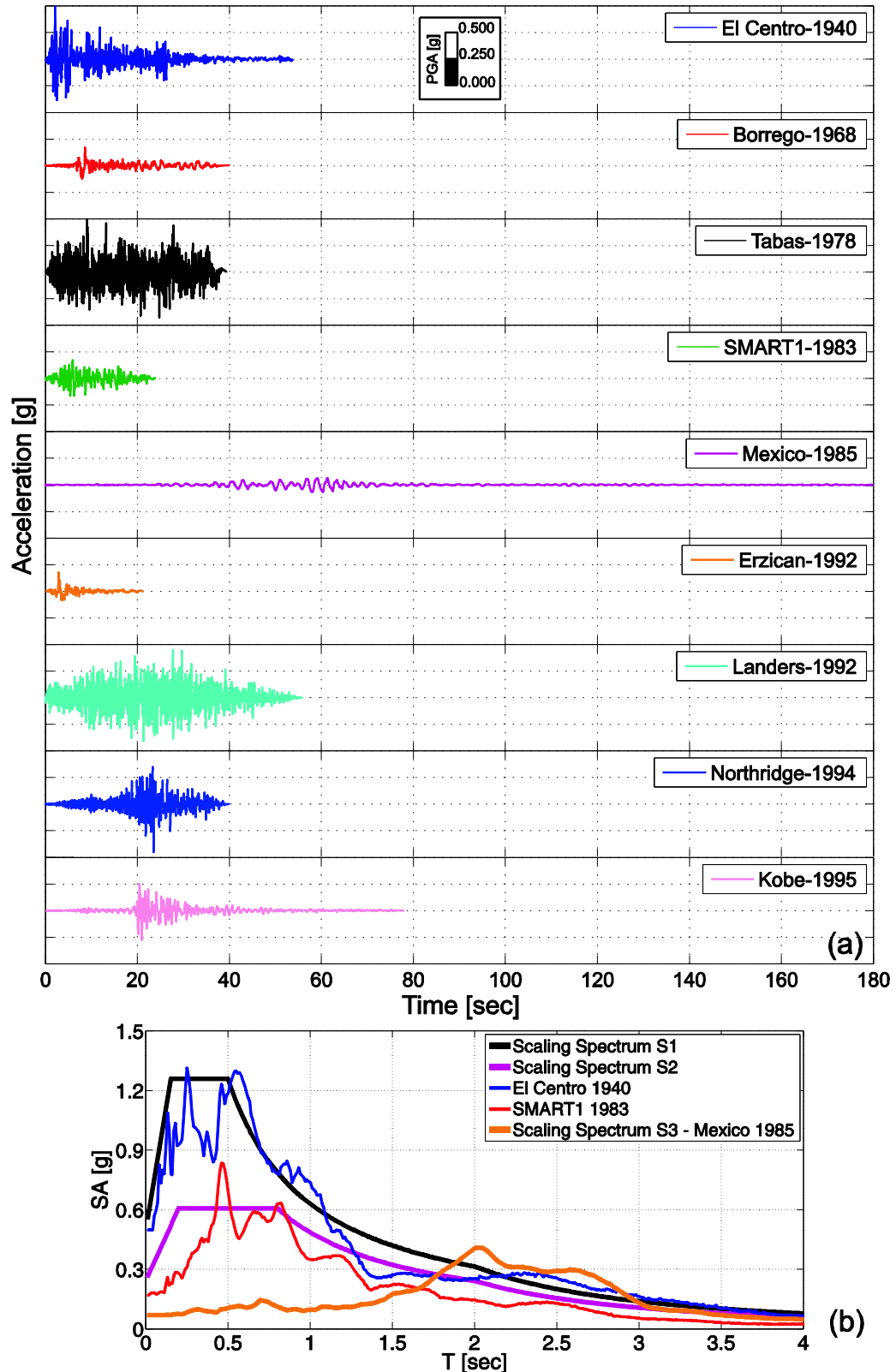


Figure 6.12: Selected earthquake excitations: (a) acceleration time histories and (b) response spectra of scaled earthquake records.

Figure 6.12-b shows that the selected earthquake records are characterised by different frequency content. The frequency content of the selected earthquake excitations varies

gradually from high frequency (earthquakes scaled to spectrum S1) to medium frequency (earthquake scaled to spectrum S2) and low frequency content (Mexico City earthquake).

Different shapes of the earthquake envelopes are provided using the selected earthquakes. These envelopes can be categorised in 3 categories (Carr, 2007):

- (i) Exponential envelope characterised by large amplitudes in early stages of the earthquake followed by long decaying phase, such as El Centro and Erzican earthquakes,
- (ii) Stationary envelope characterised by consistent distribution of the acceleration amplitudes along the earthquake duration, such as Tabas, SMART1 and Landers earthquakes, and
- (iii) Trapezoidal envelope characterised by gradual increase of acceleration amplitudes in the early stages of the earthquake followed by a flat phase and decaying part, such as Mexico City and Northridge earthquakes.

These different types of envelope shape of the earthquake have significant impact on the seismic response of the passive PT frames as well as the semi-active PT frames, as will be shown later. Therefore, despite the fact that the number of earthquake excitations used here is relatively small, these earthquakes were selected to cover a wide range of earthquake excitations characteristics to test the seismic behaviour of conventional and post-tensioned steel frames under different conditions. As these earthquake records do not belong to the same seismic group (seismic location), their intensity would be different for the same peak ground acceleration (PGA). Therefore, these earthquakes were scaled to cause structural response similar to what design based earthquakes (DBE) may cause.

6.2.2.2. Results of the Nonlinear Dynamic Analyses

Simulations of the dynamic behaviour of passive PT frame at different levels of post-tensioning forces provide an insight into the effects of connection parameters on the frame response in terms of maximum displacements, square root of sum of squares (SRSS) of displacements at the top storey, moment-rotation relationships of connections, residual deformations of the frame and energy dissipated in the connections.

The results showed a significant difference between (i) a frame with the lowest post-tensioning forces ($F_{pt} = F_{ptLow} = 0.04F_{ys}$) and (ii) frames with post-tensioning forces in the range between $0.10F_{ys}$ and $0.80F_{ys}$.

a. Dynamic Response of Frame with $F_{pt} = F_{ptLow}$ ($F_{pt}/F_{ys} < 0.1$)

When the post-tensioning force was low ($F_{pt} = F_{ptLow}$), the frame experienced very high displacements and residual deformations (Figure 6.13). In this case the structure behaved as a pinned rather than moment resisting frame due to the small moment resistance of the connections. The connections entered their inelastic phase at low loading levels; the moments were redistributed among the other elements and plastic hinges spread through the structure almost simultaneously. Plastic hinges formed early, first in connections and then, due to moment redistribution, in the columns. The time between the formation of the first plastic hinge in the frame (yield/slip of the energy dissipating elements in the connections) and development of a storey mechanism was very short (< 0.5 sec). The structure failed through development of a mechanism in the storey of the first plastic hinge in a column, followed by plastic hinges in another storey, leading to another storey mechanism and continued until plastic hinges formed in all columns.

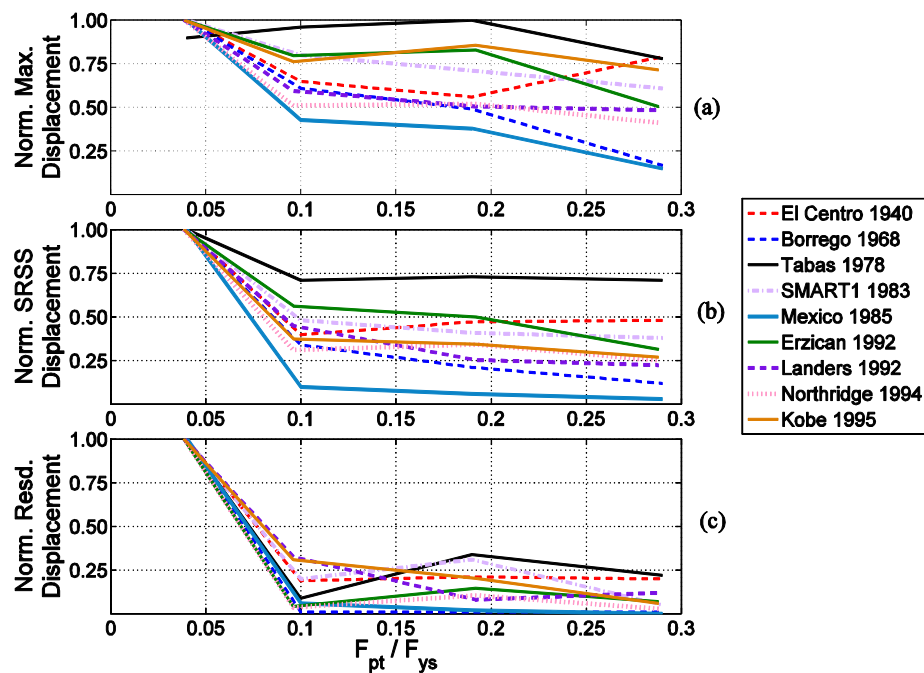


Figure 6.13: Effects of variation in post-tensioning forces on frame response at low post-tensioning force. (a) Normalised maximum 3rd storey displacement, (b) normalised SRSS of 3rd storey displacement and (c) normalised residual 3rd storey displacement.

This behaviour led to: (i) loss of lateral stiffness, (ii) storey mechanisms, and eventually (iii) large residual deformations. Residual deformations were entirely due to the plastic hinges in the columns, as the post-tensioning forces were sufficient to provide full self-centring of the connections. The total energy dissipated in the connections was found to be very high, which resulted in damping of the response in the latter stages, although at this stage storey mechanisms were already developed, and the structure vibrated around a deformed shape.

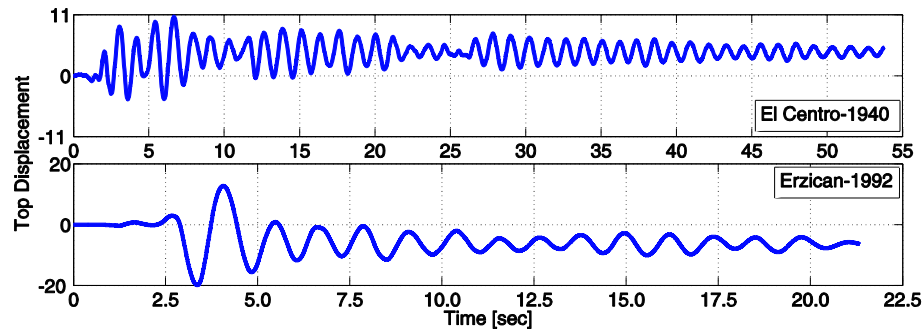


Figure 6.14: High residual displacement due to low post-tensioning forces.

An important feature of seismic response was that plastic hinges formed first in the connections, then in the columns, but not in the beams. The reason for this is that rotations at beam ends in post-tensioned steel frames, in contrast to conventional moment resisting frames, are not the same as the rotations of the adjacent column ends (Figure 6.15). Rotations in the beams are controlled by the gap opening in the connections, and the moments acting on the beams are limited by the post-tensioning forces, yield/slip-forces in the energy dissipaters and ultimately, by the yield forces in the strands. Hence these forces (rather than the moment resistances of the columns) would be used for the capacity design of the beams.

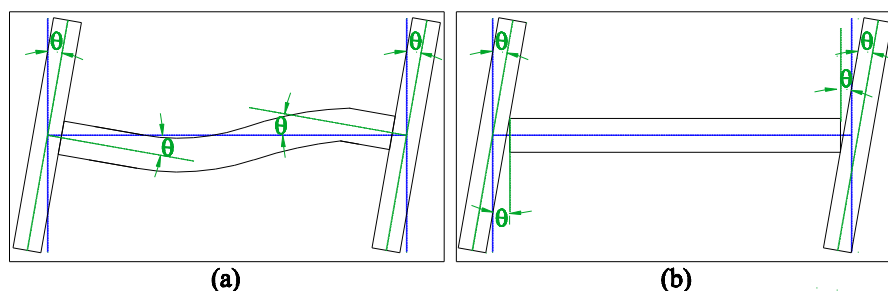


Figure 6.15: Rotations of beams due to columns rotations: (a) conventional MRF and (b) post-tensioned MRF.

b. Dynamic Response of Frame with $F_{pt} > F_{ptLow}$ ($F_{pt}/F_{ys} > 0.1$)

Structures with post-tensioning forces $F_{pt} > F_{ptLow}$ ($F_{pt}/F_{ys} = 0.1 - 0.8$) showed different behaviour from the frame with $F_{pt} = F_{ptLow}$. Plastic hinges formed mainly in the connections, with only few hinges at the bases of the columns. Maximum displacements, square root of sum of squares of displacements (SRSS), and residual deformations (all recorded for the top level; Figure 6.16), show significant differences for (i) different levels of post-tensioning (under the same seismic input), (ii) different seismic input (at same PT levels), and (iii) different response parameters (for the same input and PT level). There are two main reasons for variation of frame response with variations of F_{pt}/F_{ys} ratio: (i) change of frame stiffness and (ii) change of energy dissipation capacity of the frame.

The stiffness of the post-tensioned frame changes due to varying post-tensioning forces. Push-over analysis plots show that an increase in post-tensioning force from $0.1F_{ys}$ to $0.8F_{ys}$ increased the secant stiffness of the frame by about 45%, for a lateral deformation of 2.5% of the frame height (Figure 6.17-a).

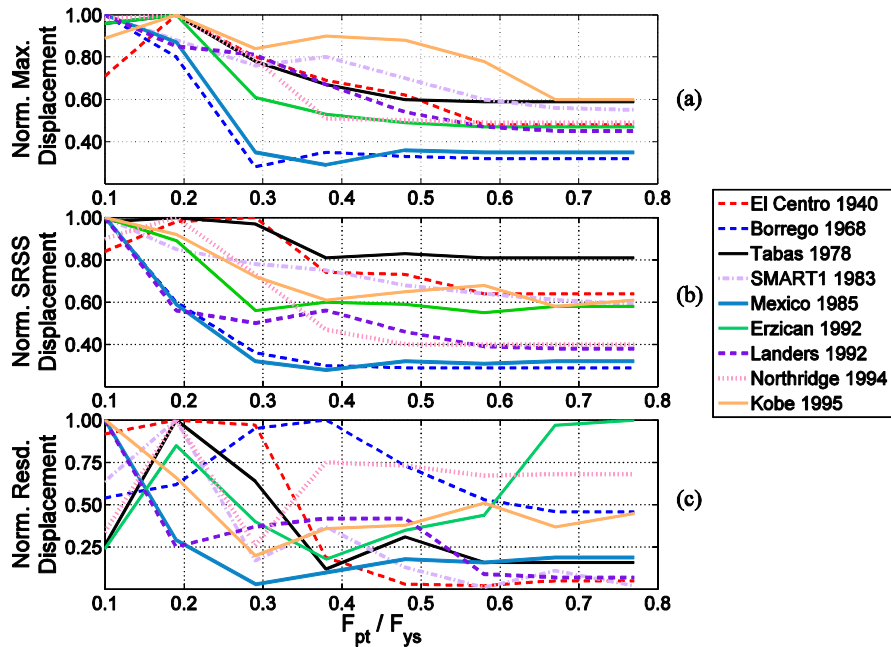


Figure 6.16: Effects of variation in post-tensioning forces on frame response at higher post-tensioning forces: (a) normalised maximum 3rd storey displacement, (b) normalised SRSS of 3rd Storey displacement and (c) normalised residual 3rd storey displacement.

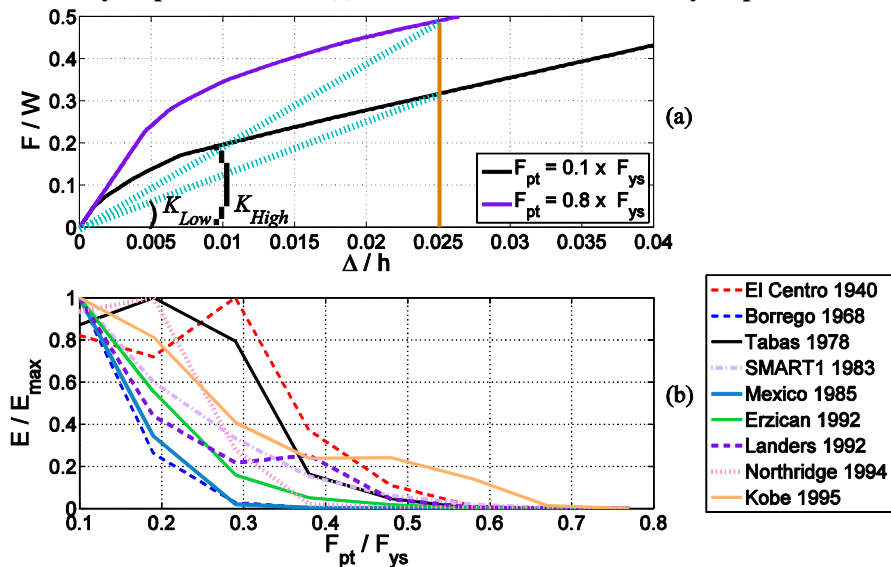


Figure 6.17: Effect of post-tensioning forces on frame characteristics: (a) secant stiffness of the frame and (b) normalised energy dissipation capacity (E/E_{max}): F : base shear, W : weight of the structure, h : height of the frame and Δ : lateral displacement of the top storey.

This effect can also be seen in Figure 6.16 where, for most cases, maximum displacements, SRSS of displacements and residual displacements show very little change when the post-

tensioning forces increase beyond certain, critical values. These are the force levels sufficient to prevent gap opening. This means that there are no changes in the behaviour of the frame for any further increase in PT forces: the structure remains in the elastic range, and there is no gap opening or yielding in connections.

It was shown earlier (Figure 6.5) that the energy dissipation capacity of a standalone connection decreased with the increase in post-tensioning force. The same behaviour can be noticed when connections are incorporated in a frame (Figure 6.17-b). This decrease in the ability of the structure to dissipate energy may lead to an increase in the dynamic response, which may result in plastic hinges forming in columns. Consequently, the structure would experience higher residual deformations (Erzican, Northridge, Kobe, and Mexico City earthquakes, Figure 6.16-c).

It can be concluded that if the structure shows a better response to a given earthquake for higher F_{pt} values, then the response is governed by the frame stiffness. In this case, applying high post-tensioning stiffens up the frame and shifts the frequency of the structure away from the predominant frequencies of the excitation. This is typical for low-frequency earthquakes such as Mexico and Borrego (Figure 6.16). In other cases, the structural response is reduced when the frame dissipates more energy and applying high PT forces increases the response. Examples of this behaviour are the responses to Erzican and Kobe earthquakes (Figure 6.16). This shows that the effect of varying the post-tensioning force differs for different earthquake excitations. Most importantly, these simulations show that the level of post-tensioning has a significant effect on the structural response. This can be utilised to control the seismic response of the structure.

6.3. Optimal Level of Post-tensioning Forces

The results of the seismic response simulations, using one earthquake and different levels of post-tensioning forces, can be used to inspect which value of PT force results in minimum response (e.g. top floor displacement) in each given time-step. This can be used to create time histories of minimum displacement and corresponding PT force (Figure 6.18). This is not a method that gives any indication of the optimum levels of PT force, or a semi-active control strategy, but only an indication of the potential effectiveness of a system for controlling the structural response by varying the post-tensioning forces in the frame.

The minimum top storey displacements obtained in this way are plotted together with those of frames with constant, low and high level PT forces, for 9 seismic inputs (Figure 6.19). These plots show that minimum response is not achieved by using constant post-tensioning forces. This suggests that minimum response may be achieved if the post-tensioning force

was optimised at every time-step during the earthquake. The optimum forces however need to be calculated on the basis of the response using the complex methodologies of active or semi-active control. Also, even if the optimum required PT forces were known, the actual control forces would be limited by factors such as time delay in executing the control algorithm and time delay in the increase of control forces due to limited power of the rotating motor.

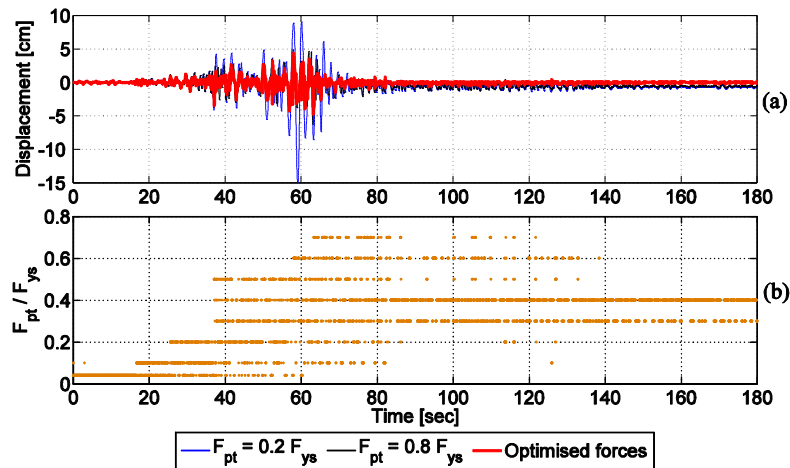


Figure 6.18: Frame response with optimised forces (Input: Mexico City earthquake): (a) top storey displacements and (b) optimum forces time history.

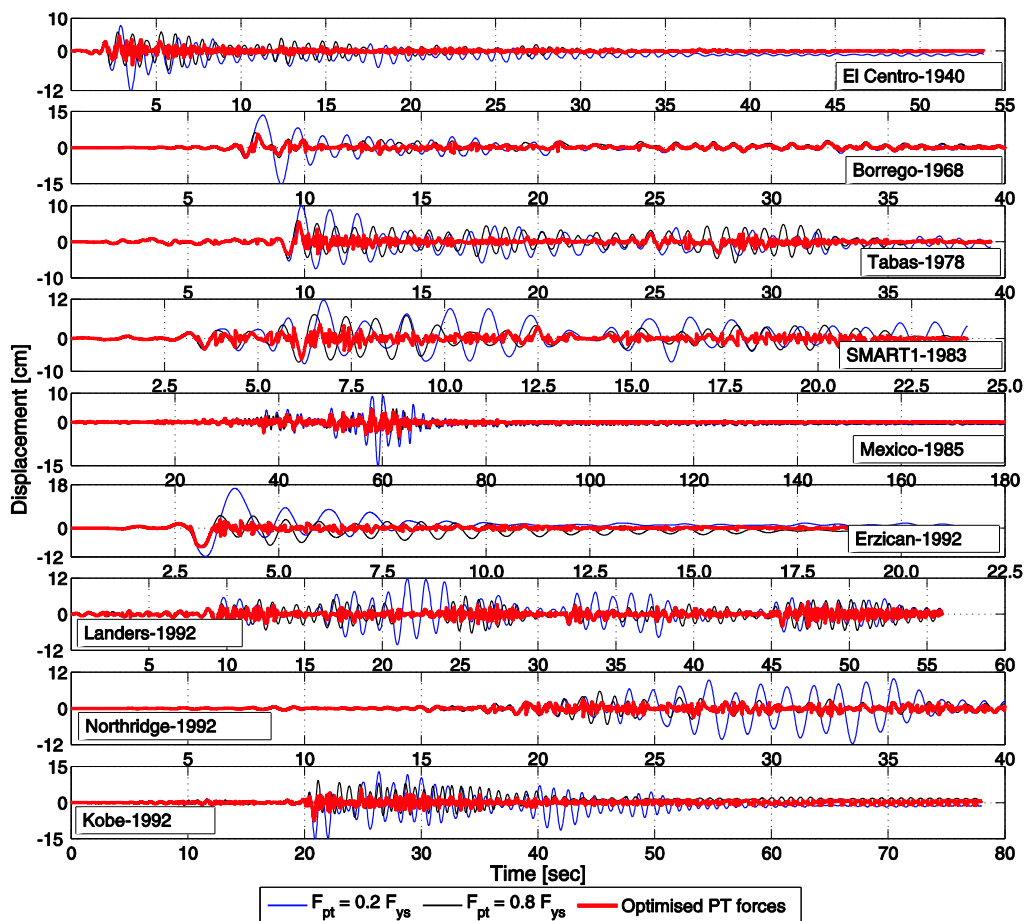


Figure 6.19: Top storey displacement time histories.

6.4. Conventional MRF Vs. Post-tensioned MRF

A comparison between a conventional moment resisting frame and post-tensioned frame is presented to determine the advantages of post-tensioned frames over conventional frames and assess their weaknesses. A three-storey-two-span frame (Figure 6.9) was investigated with and without post-tensioning. The same process used for characterising the effect of post-tensioning forces was used again for this investigation. The two frames were compared using push-over and nonlinear dynamic analyses.

6.4.1. Push-over Analyses

Push-over analyses were performed for a conventional moment resisting frame having the same geometry and section properties as the post-tensioned frame. The failure criterion adopted for the analysis was the rotation of any beam-column connection exceeding the ultimate rotation capacity of a conventional beam-column connection (θ_U). If beam-column connections in the MRF were considered to be pre-qualified post-Northridge beam-column connections, the value of $\theta_U=0.06$ rad was adopted on the basis of two different sources:

- (i) The ultimate rotation required for beam-column connections in SMRFs is $\theta_U=0.06$ rad (Table 2.1, Chapter 2) (FEMA 351, 2000).
- (ii) The ultimate rotation obtained from experimental work done for several types of prequalified beam-column connections was $\theta_U=0.06$ rad (Figure 2.4, Figure 2.5-b, Figure 2.6(b), Figure 2.7-b, Figure 2.8-b, Figure 2.9-b; Chapter 2).

It is worth mentioning that the ultimate rotation of prequalified beam-column connections (θ_U) is based on an assumption that the connection moment-rotation relationship is stable before reaching θ_U . Beam instabilities such as lateral torsional buckling and web or flange local buckling, which result in deterioration in the behaviour of the connection, were not considered for θ_U here. The actual ultimate rotation capacity of prequalified beam-column connections could be less than the values used here.

The comparison was performed between two frames having the same total ductility. It was found that the post-tensioned frame with initial post-tensioning force $F_{pt}=0.6 F_{ys}$ has a very similar ductility to the conventional MRF. Push-over curves of the two frames (Figure 6.20) show that the initial stiffness of both frames is very similar. Also, the elastic displacement (Δ_e), and the location of the first plastic hinge are identical. The difference between the two curves becomes noticeable when the frame enters the inelastic phase. The secant stiffness of the conventional MRF (K_{Conv}), at $\Delta/h=0.04$ rad is 30% higher than the corresponding stiffness of the post-tensioned frame (K_{PT}). This difference is a result of the low post-

yielding stiffness of post-tensioned connections ($k_2 = k_s + k_{b2}$) which is as low as 1% of the post-yielding stiffness of the beam. The similarity in the initial stiffness between the PT frame and the conventional MRF is a result of the simplified model of the PT connection used in the analysis. However, the initial stiffness of the PT frame should be higher than the conventional MRF. Upon gap opening and yielding/slipping of the energy dissipaters, the PT frame softens and its tangent stiffness becomes lower than the tangent stiffness of the conventional MRF (Figure 6.20).

It was shown earlier (Figure 6.10) that by reducing the post-tensioning force the ductility of PT frames increases. Similarly, it can be shown that post-tensioned frames provide higher ductility than conventional MRFs at low level of post-tensioning force. This increase in the frame ductility is however at the expense of reducing the secant lateral stiffness of the frame.

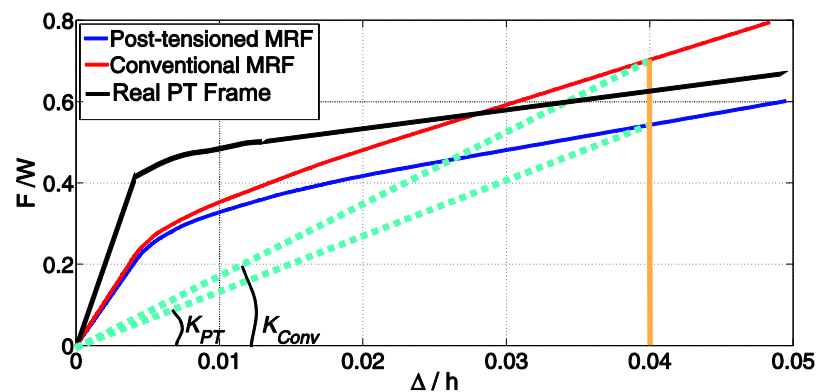


Figure 6.20: Push-over curves of post-tensioned and conventional frames.

6.4.2. Dynamic Non-linear Analyses

The comparison of the dynamic response of post-tensioned and conventional moment resisting frames was carried out by simulating the non-linear dynamic behaviour of the same three-storey-two-span frame using nine earthquake records (Table 6.1).

In Figure 6.21 are shown the time histories of top storey displacements for nine earthquakes, for the MRF frame and a PT frame with $F_{pt}=0.6F_{ys}$, which was chosen because of the similar ductility capacity (Figure 6.20). The results show similar maximum displacements in all earthquakes. Residual displacements in all cases were reduced as expected, when the frame was post-tensioned. Also, it can be seen that at the later phases of the response which was characterised by free vibration response, the post-tensioned frame exhibits reduced displacements due to the self-centring effect of the post-tensioning forces.

For two frames with the same geometry, mass distribution, and initial stiffness the nonlinear dynamic response will depend on the strength distribution and post-elastic behaviour of

elements. These two factors govern the tangent stiffness and the energy dissipation of the frame during the earthquake.

To compare the energy dissipation in the two frames, moment-rotation relationships of the first end of the first-storey beams were plotted for both frame types (Figure 6.22). These plots show that beams in the post-tensioned frames work mostly as elastic elements and they rarely yield. On the other hand, beams of the conventional frame are used as dissipative elements and their moment-rotation relationships seem to undergo several cycles of inelastic loading and unloading during earthquakes.

The total damping of the structure is composed of two components: (i) material (viscous) damping and (ii) hysteretic damping. The material damping, modelled as Rayleigh damping, is assumed to be the same in the two frames, so the same viscous damping coefficients were used in the simulations. Hysteretic damping is proportional to the energy dissipated in the elements.

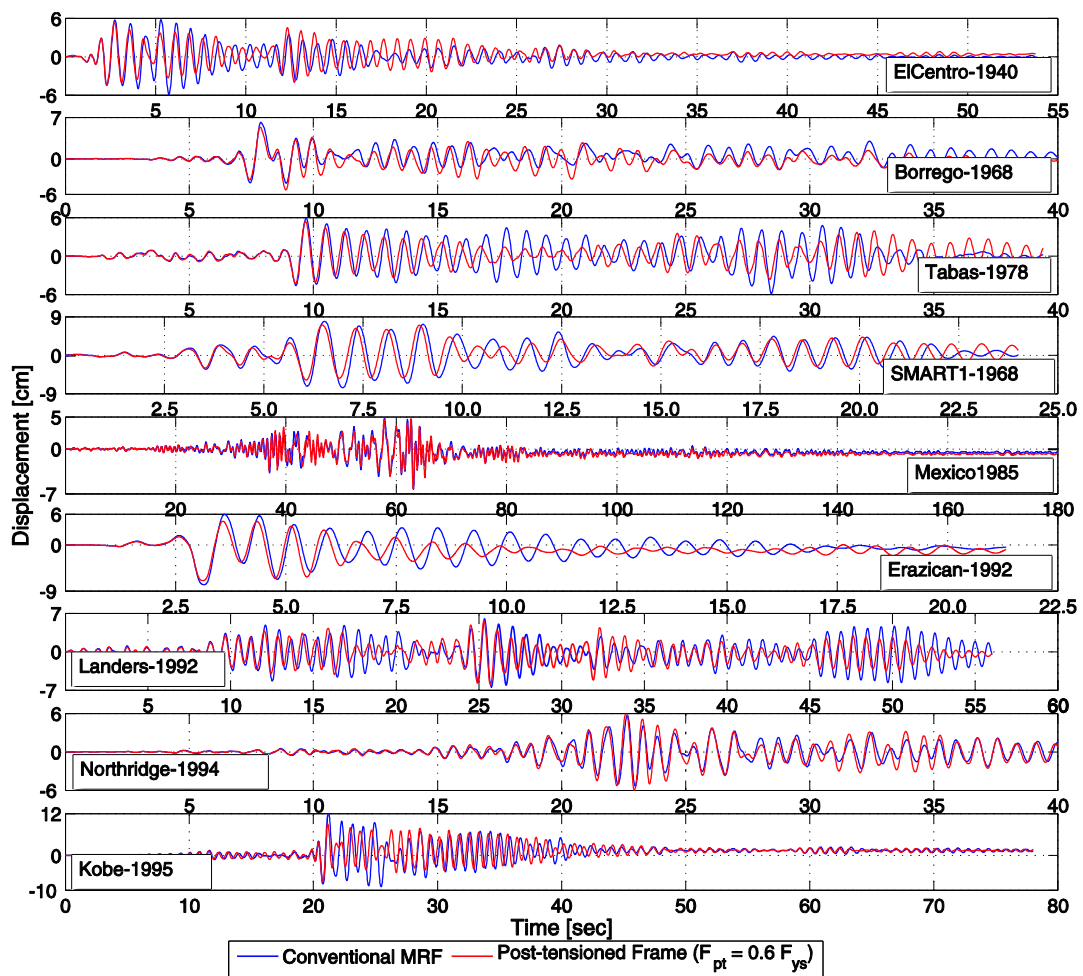


Figure 6.21: Comparison of top storey displacement for PT frame and conventional MRF.

The sources of hysteretic damping of the MRF are the plastic hinges in the beams. In the PT frame, hysteretic damping can be developed both in the beam and in the connections,

although the connections can be designed to yield before beams, and hinges in the beams can be avoided. This is illustrated in Figure 6.22, showing hysteretic damping in the MRF beams and elastic response of the PT beams.

The difference in hysteretic damping of the two frames could be also quantified from the energy dissipation time histories of their dissipative elements (Figure 6.23), where the dissipated energy is computed as the area under the curve of moment-rotation relationship. Conventional MRF show higher energy dissipation than post-tensioned frames, but the mechanisms are different. The increased energy dissipation capacity in conventional frames is a result of inelastic deformations (and damage) in the beams. In PT-frames the sources of energy dissipation are the energy dissipating devices in the connections, which can be easily replaced after the earthquake.

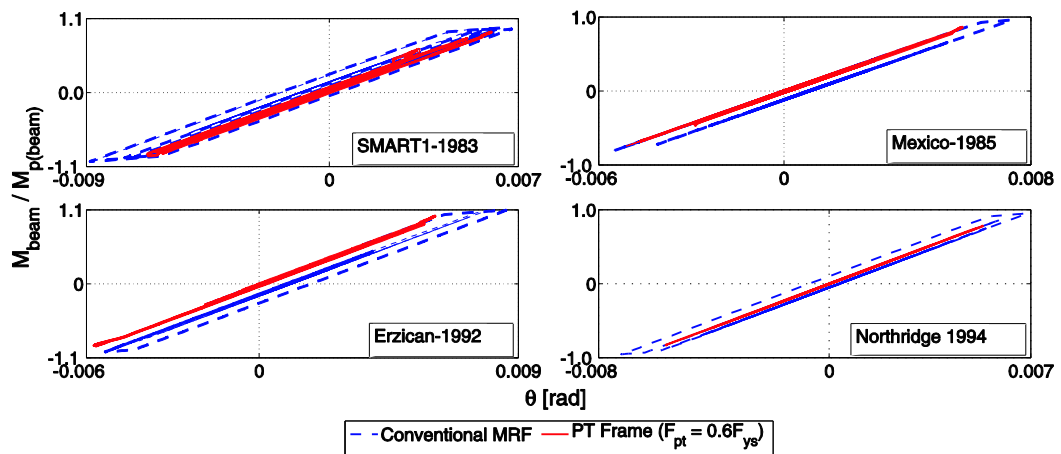


Figure 6.22: Moment-rotation relationship in PT frame and conventional MRF.

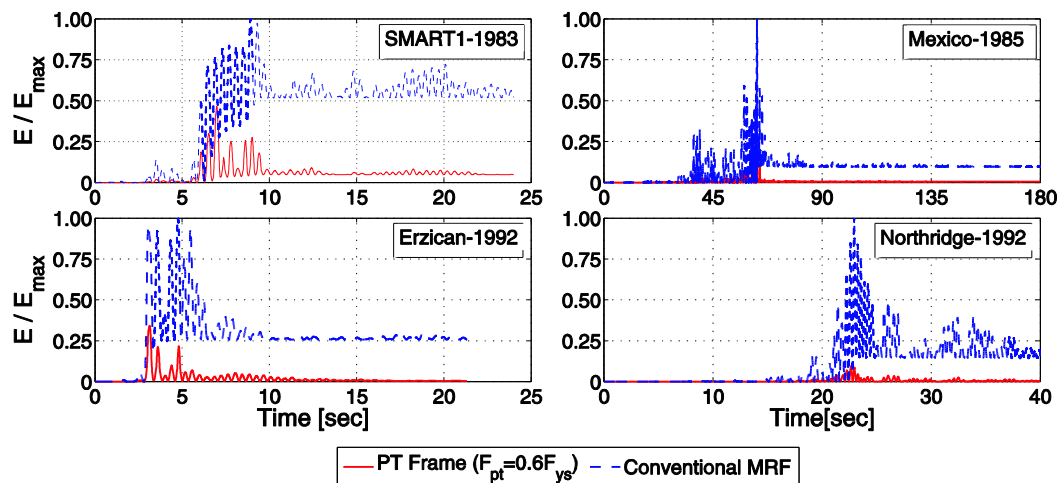


Figure 6.23: Normalised dissipated energy in PT frame and conventional MRF.

Note that the fluctuations in energy dissipation shown in Figure 6.23 are results of the algorithm that calculated the work in each time step (as $M \cdot \theta$), rather than calculating the total energy dissipated in a cycle. This means that the elastic work is included when loading and

subtracted when unloading. The final amount of work, at the end of the response, is therefore accurate (Figure 6.24)

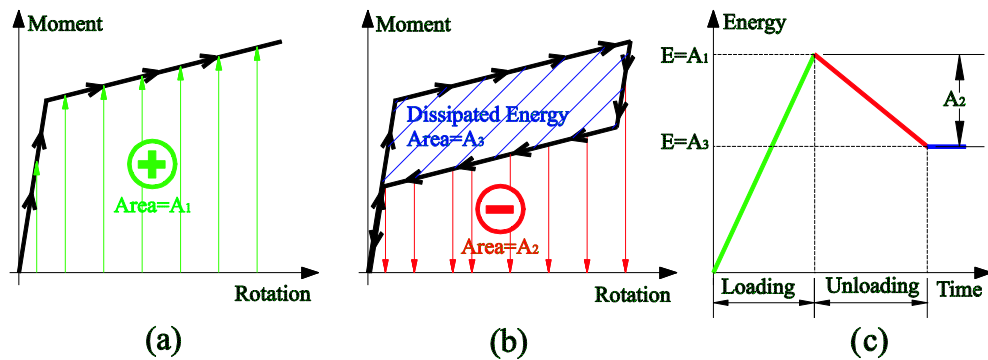


Figure 6.24: Calculation of dissipated energy: (a) loading phase, (b) unloading phase and (c) schematic time-history.

The variations in tangent stiffness of post-tensioned frames during an earthquake depend on the level of post-tensioning forces. This can be illustrated by comparing the frequency content of the response of PT frames with different PT forces (F_{pt}). In Figure 6.25 are shown the amplitude spectra of top floor acceleration of PT frames with three levels of F_{pt} . From the response to El Centro it can be seen that with the increase of force from $0.1 F_{ys}$ to $0.8 F_{ys}$, the predominant frequency increases from 0.86 Hz to 1.23 Hz , approaching the predominant frequency of the conventional MRF (1.28 Hz). This relationship between PT forces and the tangent stiffness can be utilised to adjust the frame stiffness during the earthquake. This can be used for semi-active control of the seismic response of PT frames.

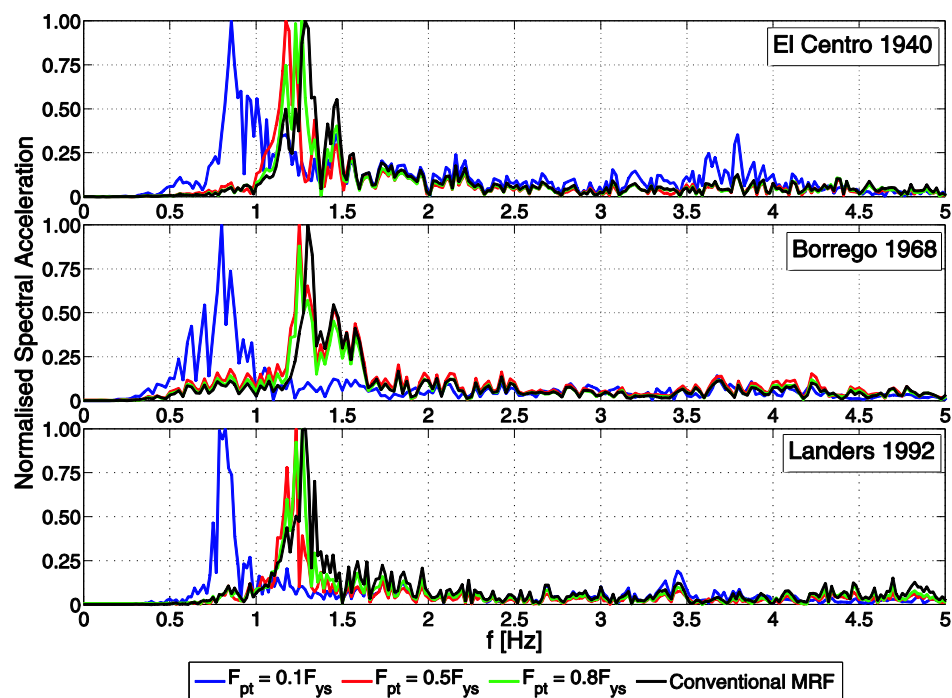


Figure 6.25: Effect of post-tensioning force on the frame stiffness during earthquakes.

6.5. Concluding Remarks on Characteristics and Dynamic Behaviour of Passive PT Frames

Post-tensioning forces represent a key element in the dynamic behaviour of post-tensioned beam-column connections. Varying the post-tensioning forces leads to changing characteristics of post-tensioned steel frames. Stiffness, ductility, and energy dissipation capacity of post-tensioned steel frames are directly related to the post-tensioning forces. Consequently, the dynamic response of a post-tensioned steel frame is strongly influenced by the post-tensioning forces.

The pre-set value of the post-tensioning forces may not be the optimum value throughout the earthquake response. A series of simulations shows that for a given earthquake, different PT forces would result in different deformations of the frame at different times of the response history. This suggests that active control of the post-tensioning forces could be an effective new technique for semi-active control of the dynamic response of post-tensioned steel frames.

The comparison between the response of a conventional MRF and a post-tensioned steel frame to nine earthquake inputs showed:

- Reduced residual displacements in post-tensioned frames in all cases.
- Higher energy dissipation in conventional MR frame. The energy in MRF was dissipated through hysteretic behaviour of its dissipative elements (beams). Beam elements are characterised by large area of moment-rotation relationships, provided that they are able to rotate in a stable manner without deterioration due to instabilities such as local or local buckling.
- Stiffness of PT frames increases with the increase of PT forces, approaching conventional MRF for very high PT values.

If semi-active control of post-tensioning force is to be used, control algorithms should utilise the strengths and minimise the weaknesses of the post-tensioned frames. Low energy dissipating capacity is the main weakness of the post-tensioned frames, and the control strategy or algorithm should be designed to increase it. Low lateral stiffness could be either advantageous or disadvantageous, depending on the frequency content of the excitation. The advantage of PT frames is however, that the secant stiffness (i.e. the stiffness during the earthquake) is different for different levels of PT forces. This can be utilised in a control strategy that will actively change the PT forces and thus alter the secant stiffness of the frame. Therefore, control approaches should attempt to increase energy dissipation capacity and adjust the lateral stiffness of the frame to reduce the structural response.

CHAPTER 7

SEMI-ACTIVE CONTROL OF PT FRAMES USING ENERGY DISSIPATION APPROACH

In this chapter are presented three loading direction feedback algorithms (LDFA) based on an energy dissipation approach for semi-active control of post-tensioning forces in post-tensioned steel frames. The essence of the energy dissipation approach is to increase the energy dissipation in the connection by actively altering the PT forces during the seismic action. The background of the approach is introduced first, and then, the three control algorithms (LDFA) based on this approach are presented: (i) deformation-based (DB-LDFA), (ii) modified deformation-based algorithm (MDB-LDFA) and (iii) velocity based algorithm (VB-LDFA). The investigation of applicability and efficiency of each algorithm is carried out by simulating the seismic response of a controlled frame and comparing the results with a corresponding passive PT frame.

7.1. Introductory Remarks

Control approaches that are applicable to frames depend on the controllable elements in these structures. It was shown in Chapter 6 that key elements of any post-tensioned steel beam-column connection are the energy dissipation factor (β) and the post-tensioning force (F_{pt}). Hence, any control approach should be based on the control usability of the key elements, as well as on the range of adjustments they can offer to the structure.

Energy dissipation factor is a representation of the moment provided by the energy dissipation device installed in the connection. When energy dissipating bars or top and seat dissipating angles are used as energy dissipating mechanism in the connection, this moment cannot be controlled during the earthquake. When friction-based energy dissipation mechanism is used in the post-tensioned connection however, the energy dissipation factor

becomes controllable provided that a variable slip force mechanism (Nishitani et al. 2003; Lu, 2004; Ng and Xu, 2007) is introduced to the connection.

The second key parameter of the connection, post-tensioning forces, is always controllable if the connection is provided with arrangement similar to the one shown in Figure 5.26 (Chapter 5). Also, varying the post-tensioning forces can introduce a wider range of modifications to the structure. These include varying strength of the connections, stiffness of the structure and the total energy dissipation capacity, as discussed in Chapter 6. These three modifications can be used to control the dynamic response of post-tensioned steel frames.

The analysis of the response of passive systems (Chapter 6) showed that the contribution of energy dissipation factor to the total behaviour of both the connection and the post-tensioned steel frame was small in comparison to the contribution of post-tensioning forces. Therefore in this research, only the post-tensioning forces in beam-column connections are considered as control variables.

The control is realised by controlled changes of the PT force: $F_{pt}(t) = F_{pt}(t-\Delta t) + F_{control}(t)$, where $F_{control}(t)$ is the control force, calculated by the control algorithm. In practice, the changes in control force $F_{control}$ are limited by the physical system (motor capacity, losses, etc.), and the control is applied as a rate ($F_{control} / \Delta t$). In this research an attempt was made to keep the rates within realistic limits (see Section 5.3.2).

7.2. Basics of Energy Dissipation Control Approach

The energy dissipation control approach is based on an attempt to strengthen one of the weaknesses in the performance of post-tensioned connections. Steel post-tensioned beam-column connections are characterised by flag-shape hysteresis which has a limited energy dissipation capacity, lower than yield-only connections which can develop full hysteretic loops. It was shown (Christopoulos et al. 2002^b; Wang D, 2004) that high self-centring capacity of the connection is achieved at the expense of reducing the energy dissipating capacity. The range of values for the energy dissipation factor β is restricted by the self-centring requirement and therefore, the energy dissipation capacity of the devices (yielding bars or friction) installed in post-tensioned connections is relatively small. As a result, the hysteretic damping in post-tensioned steel frames is also small, leading to small reduction of the dynamic amplification of seismic excitations.

The main aim of the energy dissipation control approach is to increase the energy dissipation capacity of the connections without undermining the self-centring capability. This is achieved by increasing the area of the hysteresis. If the post-tensioning forces of the strands are varied while the connection is subjected to dynamic loading, the moment-rotation

relationship of the connection will differ from the one with constant post-tensioning forces (Figure 7.1).

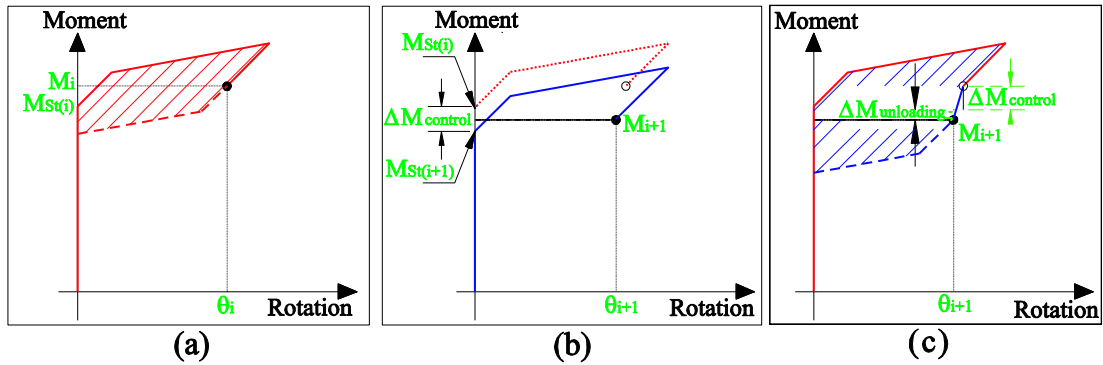


Figure 7.1: Modification of M - θ relationship due to varying post-tensioning forces: (a) M - θ response with constant PT forces, (b) change in M - θ response with change of PT forces, and (c) M - θ response when strands forces are reduced.

At time t_i the moment provided by the strands is $M_{St(i)}$ and the moment-rotation model of the connection follows the graph shown in Figure 7.1-a. If the force in the strands drops by $F_{control(i)}$ (strands are released), the moment provided by the strands at time t_{i+1} will be reduced by $\Delta M_{control}$ to $M_{St(i+1)} < M_{St(i)}$ and the moment-rotation model will follow the curve shown in Figure 7.1-b (solid line). As the moment is reduced further due to unloading of the connection, the total change in moment from time t_i to time t_{i+1} is given as:

$$\Delta M_i = \Delta M_{control(i)} + \Delta M_{unloading(i)} \quad (7.1)$$

The moment-rotation diagram of the combined model of the connection will follow the curve shown in Figure 7.1-a from $t=0$ to $t=t_i$, then the curve shown in Figure 7.1-b from $t=t_i$ to $t=t_{i+1}$, resulting in the combined action shown in Figure 7.1-c. The moment at time $t=t_{i+1}$ can be computed using Equation 7.2. The same concept applies when the connection is loading or when the forces in the strands increase.

$$M_{i+1} = M_i + \Delta M_{control(i)} + \Delta M_{unloading/loading(i)} \quad (7.2)$$

Consequently, the moment-rotation relationship of the connection will be modified, and the area of the hysteresis (dissipated energy) will be changed.

7.3. Deformation-Based Loading Direction Feedback

Algorithm (DB-LDFA)

Deformation-based *LDFA* is a control algorithm designed to increase the energy dissipation capacity of post-tensioned connections by increasing the area of moment-rotation relationship of the connection. Forces in the strands are increased (by tightening the strands)

or reduced (by releasing the strands) according to the loading direction (or status) of the connection: loading, unloading or reloading.

7.3.1. Operation of the Deformation-Based LDFA

The key element in this algorithm is timing the application of force decrease/increase. If the energy dissipating device has not been activated, reducing the strand forces does not increase the area of the moment-rotation loop of the connection. When the energy dissipating device is activated, the post-tensioning forces remain constant until the connection starts unloading. Once the unloading starts, PT forces are reduced gradually (by $\Delta f_i/\Delta t$; where Δf_i is the force increment) in order to increase the area of the hysteresis. The releasing of strands continues while the connection is unloading, provided that post-tensioning forces are still sufficient to ensure self-centring of the connection. This is judged by using $F_{contHist}=\{F_{control(1)}, F_{control(2)}, \dots, F_{control(i)}\}$, the time-history of control forces from the beginning of the earthquake to the current time. The actual current post-tensioning force ($F_{pt-act(i)}$) is given as:

$$F_{pt-act(i)} = F_{pti} + \sum F_{control(i)}, \quad (7.3)$$

where F_{pti} is the initial post-tensioning force in the strands. To ensure that the connection can self-centre at the end of the earthquake, the lowest actual post-tensioning force can be calculated by using Equation 6.5 (Chapter 6) and substituting $M_{Si}=F_{pt}\sum d_{si}$, which finally leads to:

$$F_{ptLow} = \frac{[(k_{b1}-k_{b2})\theta_y]}{\sum ds_i}, \quad (7.4)$$

where d_{si} is distance of strand i to the current centre of rotation of the connection. Therefore, the first criterion for the control force function can be obtained from:

$$\sum F_{control(i)} \geq F_{pti} - F_{ptLow}. \quad (7.5)$$

Once the connection has re-centred, the initial post-tensioning force is retrieved by increasing the post-tensioning forces gradually until (i) the initial post-tensioning force is reached, or (ii) a new gap is opened; whichever occurs first. Figure 7.2 shows the flowchart for the deformation-based loading direction feedback algorithm.

7.3.2. Results of Deformation-Based Loading Direction Feedback Control Algorithm

A three-storey two-bay post-tensioned steel frame was used to investigate the effectiveness of the deformation-based control algorithm. Initial post-tensioning forces in all storeys were assumed as 300 kN. The frame was equipped with three rotating motors (one at each storey)

having specifications as listed in Table 7.1. Details and sections of the frame are shown in Figure 7.3.

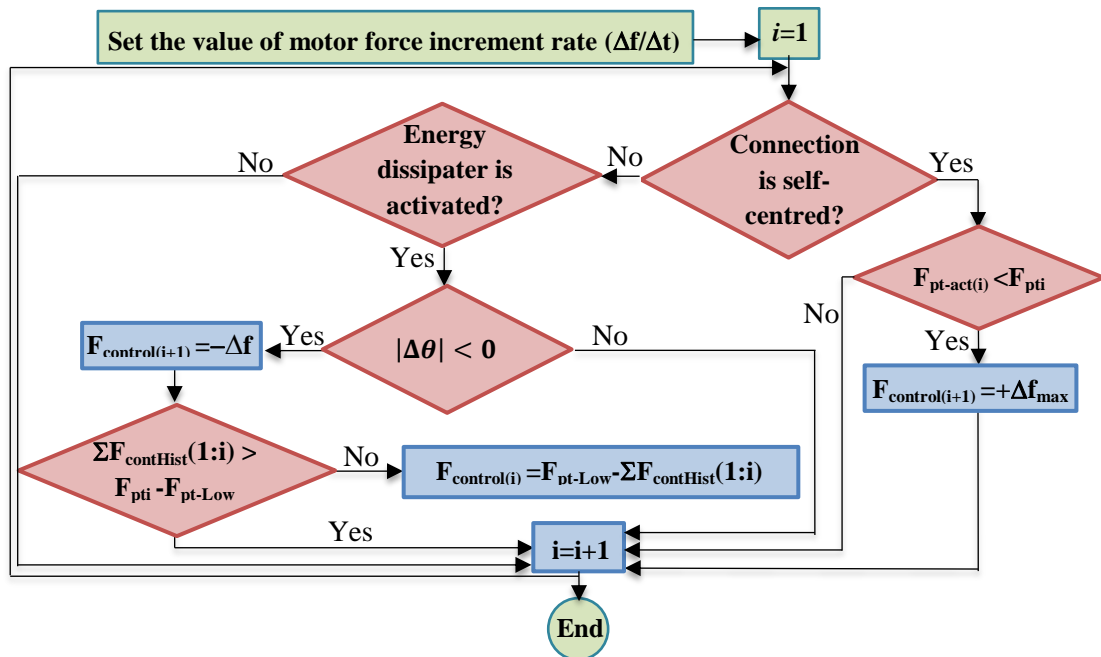


Figure 7.2: Flowchart of the deformation-based LDFA.

Power (kW)	77
Voltage (v)	220/380
Current (A)	134
Speed (r/min)	2970
Efficiency %	93.0

Table 7.1: Specifications of a rotating motor (commercially available at: http://www.alibaba.com/product-gs/579001601/100_copper_wire_synchronous_rotational_motors.html).

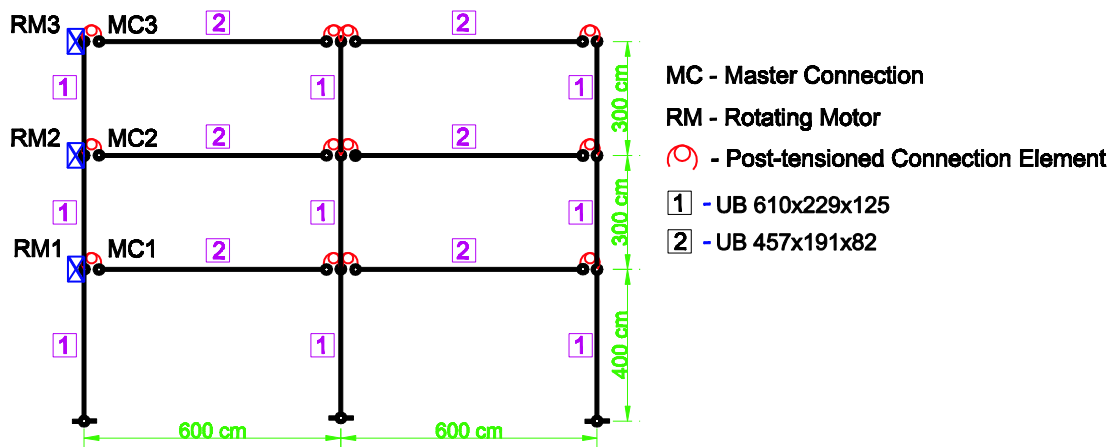


Figure 7.3: Three-storey two-bay post-tensioned steel frame.

7.3.2.1. Response of PT Frame with Deformation-Based LDFA

The simulations of seismic response of a frame structure with applied *DB-LDFA* were performed with systematic increase of PT force rates ($\Delta f/\Delta t$). The purpose of varying the rate of decreasing of post-tensioning force was to analyse the changes in frame behaviour due to the change in the rate of control force ($\Delta f/\Delta t$). The lowest rate of control force used in the simulations was 125 kN/s (12.5% of the motor capacity), and the highest was 1000 kN/s (full motor capacity). The force rate ($-\Delta f/\Delta t$) increases by 12.5% of the motor capacity for each new simulation. When the connection is centred and $F_{pt} < F_{pti}$ the *LDFA* will be retrieving the initial post-tensioning force at rates $+\Delta f/\Delta t = (\Delta f/\Delta t)_{max}$.

a. *DB-LDFA* with small force rate ($\Delta f/\Delta t$)

Top storey displacement time-histories for passive PT frame and semi-actively controlled frame through *LDFA* with decrease in the force rate $-\Delta f/\Delta t = 125 \text{ kN/s}$ (Figure 7.4) show that the effect of applying the control algorithm is different for different earthquakes. While the algorithm shows an improvement in the frame behaviour for El-Centro, SMART1, Landers, Northridge and Kobe earthquakes, it does not for the other earthquakes. The improvement in the frame response includes reduced SRSS of displacements and therefore, better self-centring at the end of the record. Peak displacements seem to be very similar for all earthquakes and no reduction was introduced to the frame through the application of *LDFA*.

The reduction in the top level displacements starts after completing the first loop of the moment-rotation relationship (e.g. El Centro, SMART1, Landers in Figure 7.4.). At this time, the controlled frame has already dissipated more energy than the passive frame. In most cases however, the maximum displacement occurs in the first load reversal, before the connections complete the first loop, and the algorithm starts affecting the response (El-Centro, Tabas, SMART1, Landers and Kobe earthquakes, Figure 7.4). Even when the energy dissipation is similar to that of the passive frame (Figure 7.5), the increased unloading stiffness (Figure 7.7) as well as the better self-centring contributes to reduction of displacements in the later stages of the response (reduced SRSS). The ideal case would be if the frame started dissipating energy before reaching the peak load reversal, as in the case of the Northridge earthquake (Figure 7.4), where the *LDFA* reduced both SRSS and maximum displacements.

The time-histories of dissipated energy (Figure 7.5) can be categorised into two categories. In the first category, the total energy dissipated through PT connections in the controlled frame is higher than that in the passive frame (Borrego, Tabas, Erzican, Landers and Kobe earthquakes), which was the expected result when applying the *LDFA*. In the second

category, the final energy dissipated through connections in the controlled frame is less than that in the passive frame (El-Centro, SMART1 and Northridge earthquakes), which was not expected.

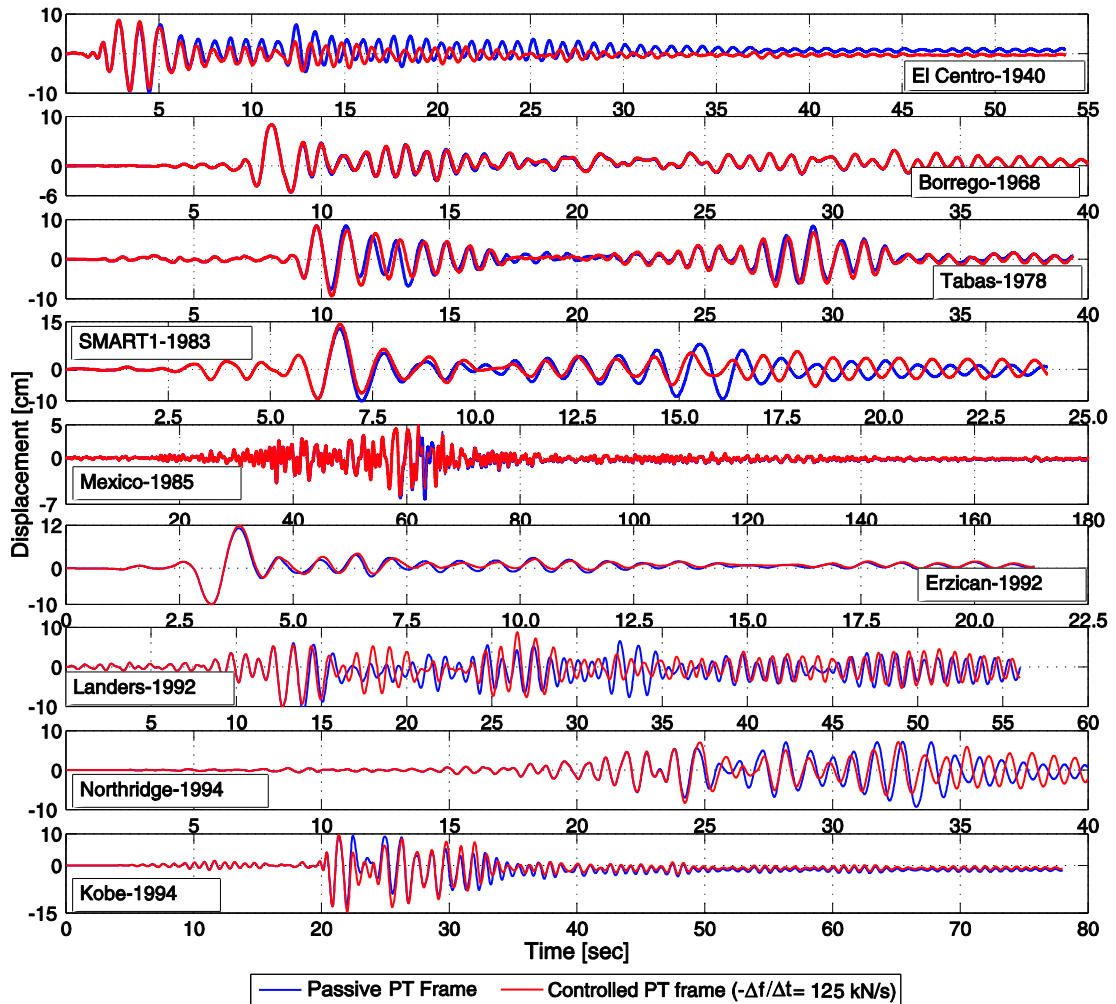


Figure 7.4: Top storey displacement time histories.

Several features can be observed in the response of the cases where the passive frame dissipated more energy than the controlled frame:

- (i) The energy dissipated in the controlled frame is higher in the early stages (large load reversals), whereas in the later stages, when the seismic input diminishes, the energy dissipation in the passive frame increases, while the energy in the controlled frame stabilises (Figure 7.6-b), and
- (ii) Displacements in the controlled frame decay more in the late phase of loading (Figure 7.6-a).

These observations imply that higher energy in the later stage of the response of the passive frame is a result of higher amplitudes of displacement, rather than larger energy dissipation

for the same displacement amplitudes (Figure 7.6). The differences are not large, but this implies that the passive system is less efficient.

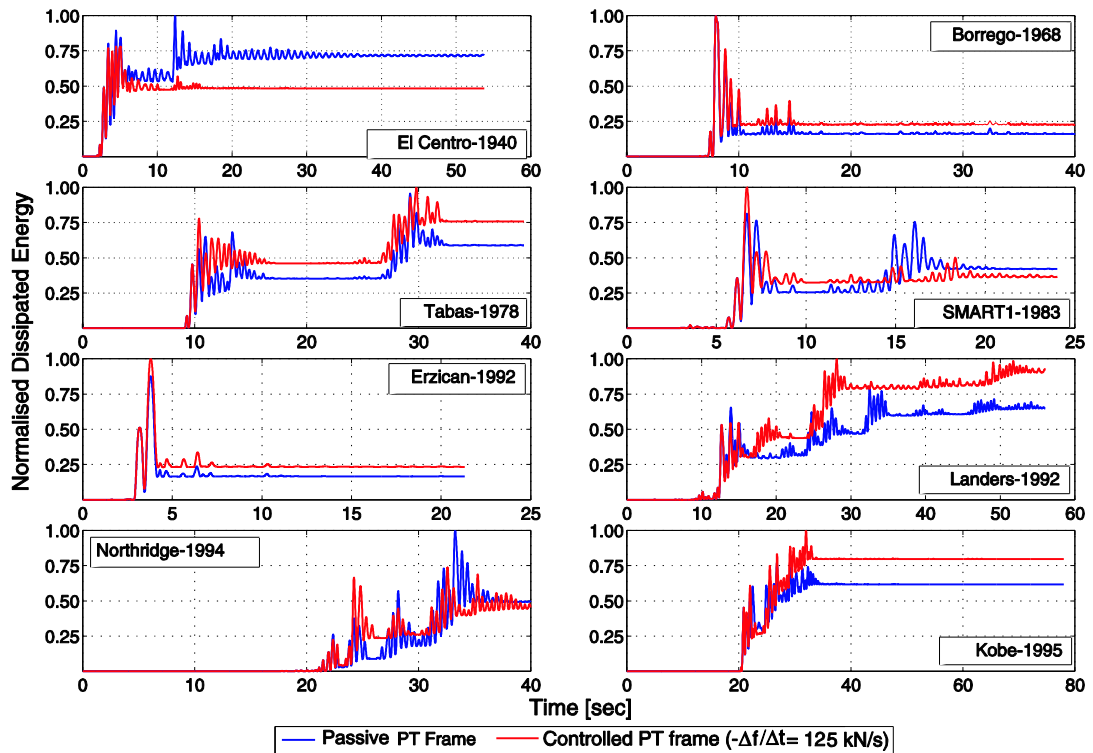


Figure 7.5: Energy dissipated through post-tensioned connections.

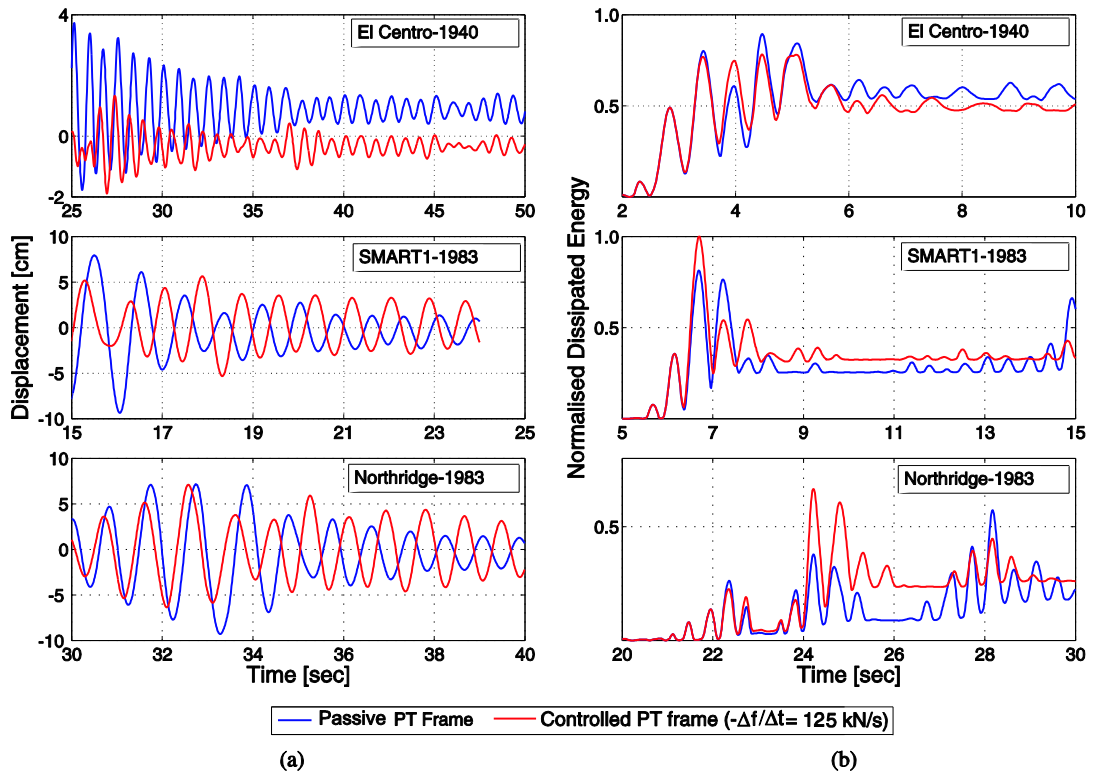


Figure 7.6: Details of behaviour of controlled frames with lower total energy dissipation than passive frame: (a) displacements in late stages of loading and (b) energy dissipation in early stages of loading.

Plots of moment-rotation relationships (Figure 7.7) show how areas of hysteresis loops increased due to releasing the strands while the connection was unloading. The increase in the slope of the unloading path is a result from the unloading action plus the force release action. These two actions result in a larger area of the hysteresis which leads to increased energy dissipation capacity of the connection.

An important observation from moment-rotation relationships (Figure 7.7) is that in some cases the moment provided by the strands (M_{St}) varies and becomes lower than the initial M_{Sti} for latter cycles (Tabas, Landers and Kobe in Figure 7.7). This behaviour indicates that the strands were not able to fully retrieve their initial post-tensioning force (Figure 7.8). In these cases the connection gap started opening at a lower moment than the initial M_{St} .

The inability of the *L DFA*-controlled connection to restore its initial M_{St} is associated with short duration of self-centring. When the connection is self-centred, t_{sc} the time needed for the connection to fully restore its initial M_{St} is calculated from:

$$t_{sc} = \frac{F_{pti} - F_{pt-act(i)}}{(\Delta f / \Delta t)_{max}}, \quad (7.6)$$

where F_{pti} is the initial post-tensioning force, $(\Delta f / \Delta t)_{max}$ is the maximum force rate of the rotating motor and $F_{pt-act(i)}$ is the current post-tensioning force:

$$F_{pt-act(i)} = F_{pti} + \Sigma F_{control}. \quad (7.7)$$

If the self-centring duration was less than t_{sc} , the connection would not be able to restore its initial post-tensioning force. In order to investigate the effect of the self-centring duration, the frame response was simulated using two artificial earthquakes (Figure 7.9). The first one has a very low frequency allowing for a long self-centring duration, and the second one has a very high frequency which reduces the self-centring duration. Both records are long and strong enough to cause several cycles of inelastic loading and unloading of connections.

Moment-rotation relationships of the master connection of the first storey under these two artificial earthquakes (Figure 7.10) show that when subjected to low frequency earthquake (sine wave with $f=0.1$ Hz) the connection completely restores its initial post-tensioning force after each cycle. Therefore, the connection dissipates more energy with stable behaviour and no reduction in the connection strength is noticed (Figure 7.10-a). On the other hand, high frequency earthquakes (sine wave with $f=3.0$ Hz) would result in a reduction in the moment capacity of the connection as the time of self-centring would not be enough to restore the initial post-tensioning force. The connection shows a reduction in M_{St} after each inelastic unloading cycle.

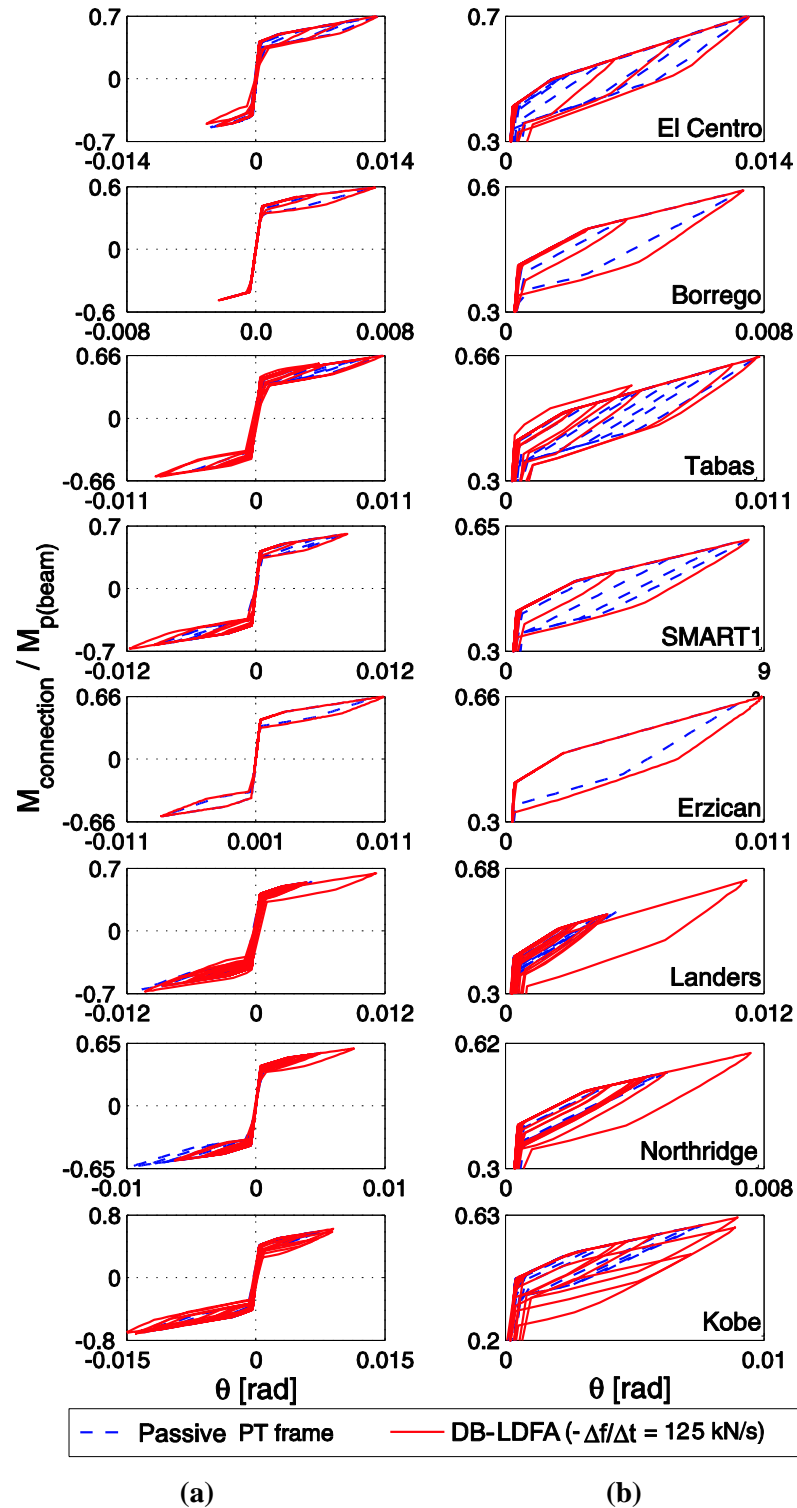


Figure 7.7: Moment-rotation relationships of the master connection of the first storey: (a) complete loop and (b) zoom in.

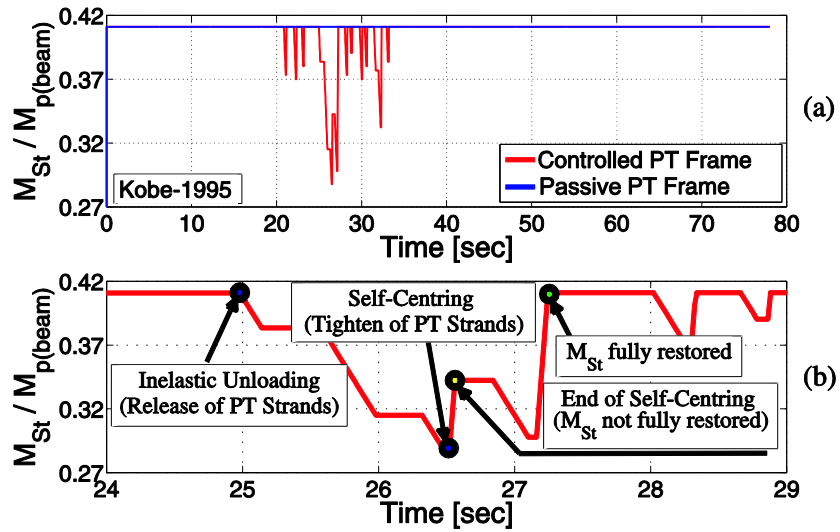


Figure 7.8: Inability of the controlled connection to restore initial M_{St} : (a) M_{St} full time-history and (b) zoom into M_{St} time-history.

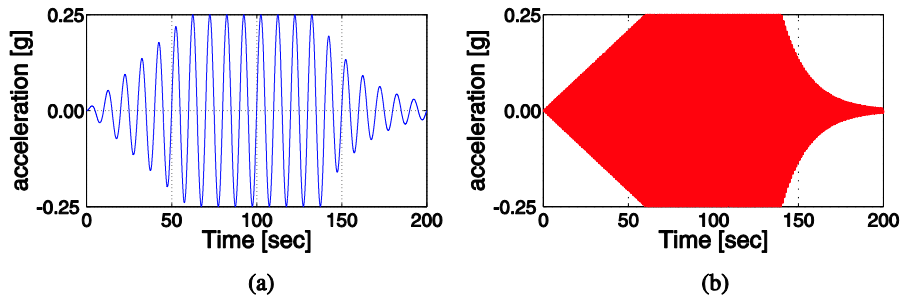


Figure 7.9: Artificial earthquake time-histories: (a) low frequency earthquake (0.1 Hz) and (b) high frequency earthquake (3.0 Hz).

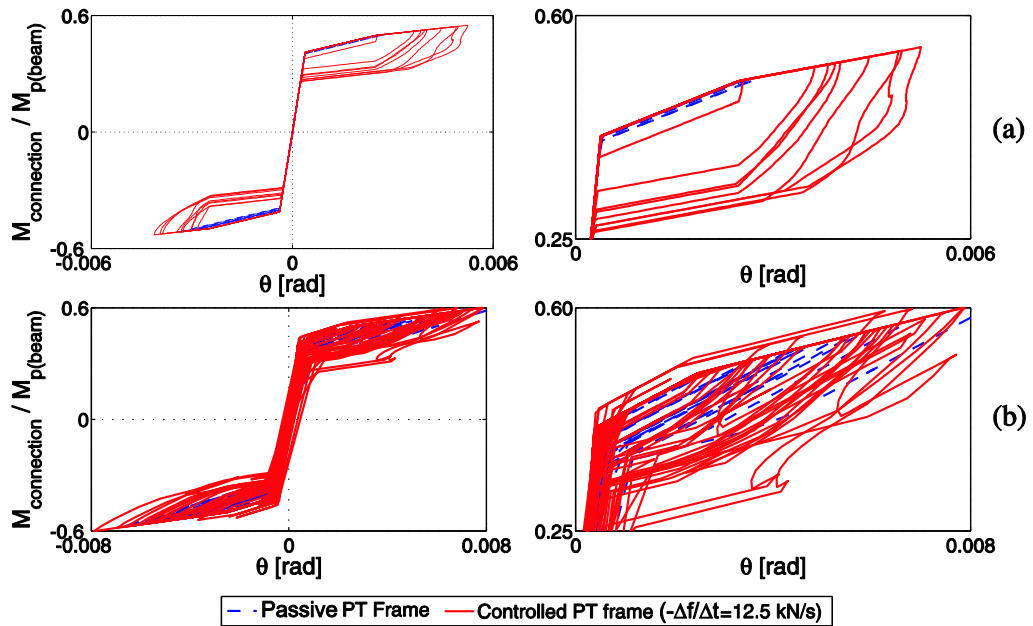


Figure 7.10: Moment-rotation relationships of the master connection of the first storey under artificial earthquakes: (a) low frequency earthquake and (b) high frequency earthquake.

Consequently, the behaviour of the connection with *DB-LDFA* under high frequency earthquakes leads to increasing the frame response instead of reducing it. Also the energy dissipating capacity of the connection will be limited when forces in strands reach their lower limit (F_{ptLow}). Although the connection restores its initial post-tensioning force at late stages of the earthquake, by this time the level of response would be too small to dissipate energy again.

b. *DB-LDFA* with Large Force Variation Rate ($\Delta f/\Delta t$)

Figure 7.11 shows the effect of the control force rate $(\Delta f/\Delta t) / (\Delta f/\Delta t)_{max}$ on the behaviour of the PT frame ($\Delta f/\Delta t=0$ indicates passive PT frame). In most of the cases when $(\Delta f/\Delta t) < 0.25(\Delta f/\Delta t)_{max}$, the *LDFA* reduces the dynamic response of the structure. For higher values of $\Delta f/\Delta t$ the response is higher than the response of the passive PT frame. This is a result of the inability of the controller to restore the initial post-tensioning forces due to the short time for self-centring.

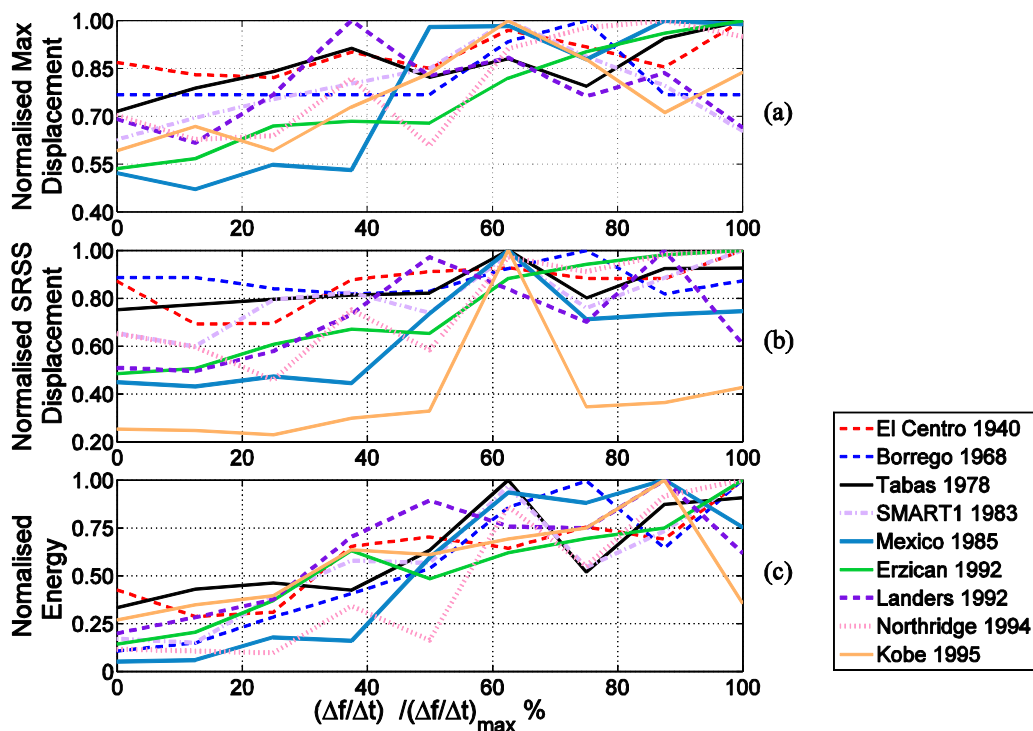


Figure 7.11: Effect of control force rate on frame behaviour: (a) maximum top storey displacement, (b) SRSS of top storey displacement and (c) energy dissipation in connections.

For high values of force rate ($\Delta f/\Delta t$), F_{pt} would have a low value at the end of the unloading interval, and cannot be restored to its initial value (F_{pti}) during the short time of loading in the opposite direction. As a result, F_{pt} starts from a low value in the next cycle (See Equations 7.6 and 7.7), and the connection could not work with its full moment capacity.

This leads to larger deformations in the frame despite the high energy dissipation of the connections for high values of $\Delta f/\Delta t$ (Figure 7.11-c).

In addition, Figure 7.11 shows that the effect of control force increment on the dynamic response of the frame depends also on the characteristics of the excitation. Best results of the *DB-LDFA* for different earthquakes are not associated with the same value of $\Delta f/\Delta t$. In most cases, best results were associated with small force increments $(\Delta f/\Delta t) = 0.125(\Delta f/\Delta t)_{max}$ (Figures 7.5, 7.6 and 7.7). For Borrego Mountain, Northridge and Kobe earthquakes however, best results were not associated with $(\Delta f/\Delta t) = 0.125(\Delta f/\Delta t)_{max}$, but with higher values of $\Delta f/\Delta t$ (Table 7.2). The time histories of response to these three earthquakes, for the corresponding optimum $\Delta f/\Delta t$ values, are shown in Figure 7.12.

Earthquake	Optimum $(\Delta f/\Delta t)/(\Delta f/\Delta t)_{max}$ %	Reduction in Max. displacement %	Reduction in SRSS displacement %
El-Centro	12.5	4.4	20.1
Borrego Mountain	37.5	0.0	8.0
Tabas	12.5	—	—
SMART1	12.5	—	8.6
Mexico City	12.5	9.6	3.6
Erzican	12.5	—	—
Landers	12.5	10.8	2.6
Northridge	25.0	9.0	29.6
Kobe	25.0	—	9.0

Table 7.2: Best results using the *DB-LDFA*.

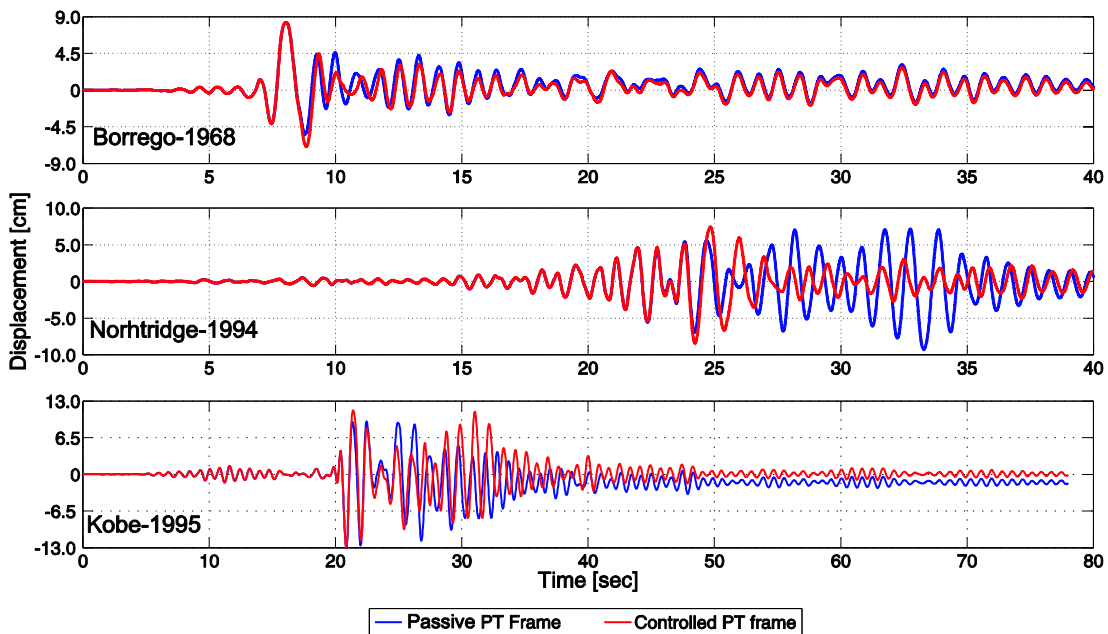


Figure 7.12: Best results of the *DB-LDFA* when $(\Delta f/\Delta t) \neq 0.125(\Delta f/\Delta t)_{max}$.

7.3.2.2. Decentralisation of the Algorithm

In decentralized control, the structure is led by separate independent sub-computers, which do not communicate with each other. The decentralized control was introduced for high multi-storey structures where the response of one storey is treated as completely independent from the response of the other storeys (Nishitani, 2008). This could happen when the contribution of higher vibration modes to the response is significant. The idea behind the decentralised control systems was to provide a set of different feedback control gains which fit the current response of each storey.

The energy dissipation approach shown here is based on a decentralized system, where one master connection per floor responds separately and forces are varied for all the connections in the storey. Post-tensioning forces are not controlled synchronously and therefore, control loading patterns in different storeys are random. The objective of this approach is to increase the energy dissipating capacity of every post-tensioned connection independently. The main aim of the energy dissipation approach however is increasing the energy dissipation capacity of the whole post-tensioned frame.

An example of decentralization of *LDFAs* is shown in the time-histories of control forces in Figure 7.13, where it can be seen that control forces do not increase or decrease for all storeys at the same time.

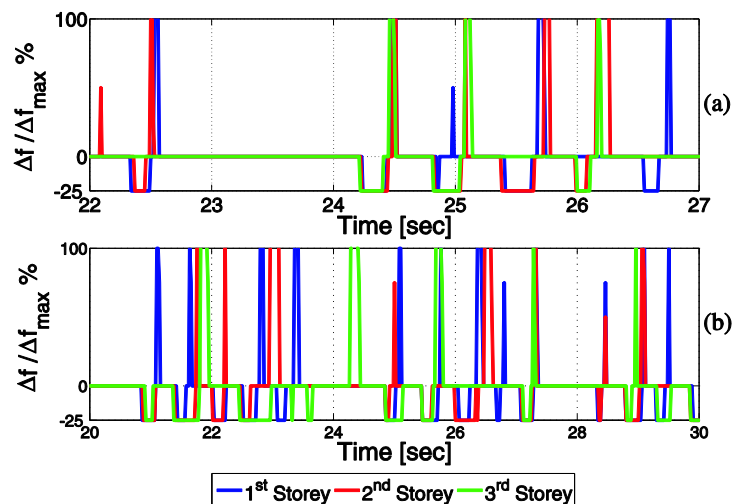


Figure 7.13: *LDFa* control forces time histories: (a) Northridge 1994 and (b) Kobe 1995.

If the energy dissipation approach is used to control the dynamic response of the PT frame, the structure-controller system acts as Multi-Input-Multi-output system (MIMO). In this case, measurements of the control variables (rotations of master connections) are taken at each storey (different input points), processed to obtain the control gains (F_{control}) and then applied at the same input points (Figure 7.14).

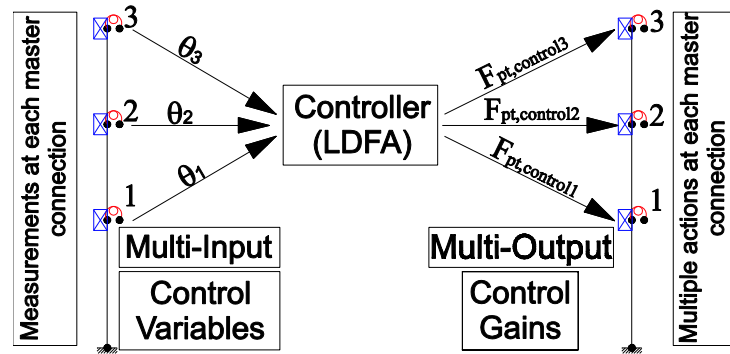


Figure 7.14: Operation of *LDFA* as a MIMO system.

7.3.3. Disadvantages of DB-*LDFA*

Having presented results of the DB-*LDFA*, limitations of the algorithm performance can be determined. A thorough analysis of these results shows the disadvantages of the DB-*LDFA*: (i) uncertainty of the algorithm and (ii) high sensitivity and low robustness.

7.3.3.1. Uncertainty of *LDFA*

Uncertainty of DB-*LDFA* refers to the inability of determining the algorithm parameters that insure the best performance of the algorithm. The flowchart of the DB-*LDFA* (Figure 7.2) shows that the only variable of the algorithm is the rate of varying the PT force in the strands ($\Delta f/\Delta t$), while all the other parameters are pre-set. The results presented earlier showed the response of the frame with ($\Delta f/\Delta t$) as proportional to $(\Delta f/\Delta t)_{max}$. The maximum rate of force increment $(\Delta f/\Delta t)_{max}$ depends only on the motor specifications which can be different for different motors. Also, $(\Delta f/\Delta t)_{max}$ is not related to the structural dimensions or loads and therefore, could not be specified in advance based on the frame properties or expected level of loading.

Even when $(\Delta f/\Delta t)_{max}$ is specified based on the motor specifications, the ratio $(\Delta f/\Delta t)/(\Delta f/\Delta t)_{max}$ that results in the best performance of the DB-*LDFA* could not be determined. The best value of the force increment rate depends on the response of the structure, which is a function of the relationship between the structural characteristics and the characteristics of the earthquake, such as intensity and frequency content. Earthquakes having low frequency and intensity, allow for longer self-centring time of the connection (t_{sc}) and hence, high values of $(\Delta f/\Delta t)_{max}$ may result in better performance of the algorithm.

An approximate method to determine the optimum value of the force increment rate ($\Delta f/\Delta t$) is proposed here. This method is based on the self-centring time which is required to restore the full initial PT force of the connection. This method includes the following steps:

- (i) Specifying the elastic response spectrum for the location (soil type and the PGA),
- (ii) Finding scaled earthquake records that match the elastic response spectrum (Figure 7.15),

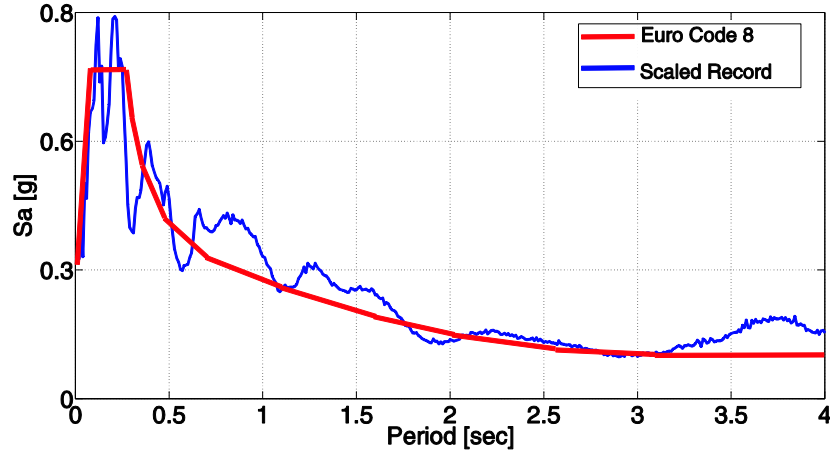


Figure 7.15: Matching scaled records to an elastic response spectrum of Eurocode 8.

- (iii) Simulating the response of passive PT frame under a set of scaled earthquake records to find moment time-histories of the master connections,
- (iv) For each earthquake record, the time required for restoring initial PT force is determined at different points of the moment time-history (t_{sc1} , t_{sc2} , ...) (Figure 7.16),

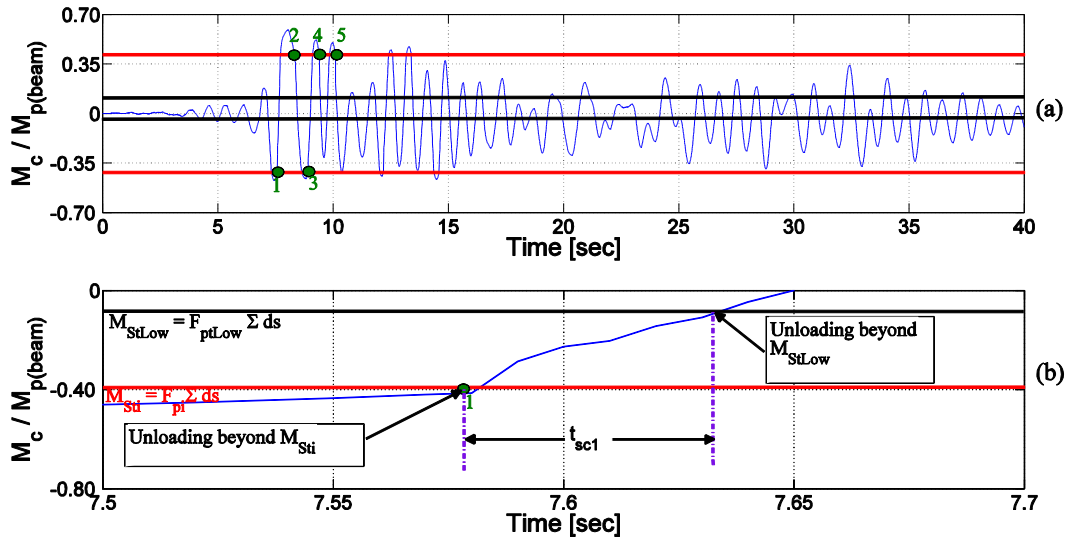


Figure 7.16: Required time for restoring initial PT force: (a) connection moment time-history and (b) finding t_{sci} at each point.

- (v) The time required for restoring initial PT force for this earthquake is:

$$t_{sc} = \min\{t_{sc1}, t_{sc2}, \dots\} \quad (7.8),$$

- (vi) If the force variation is $(\Delta f/\Delta t) = (\Delta f/\Delta t)_{max}$, the time required for restoring initial PT force is:

$$t_{scmax} = \frac{F_{pti} - F_{ptLow}}{(\Delta f/\Delta t)_{max}} \quad (7.9),$$

(vii) The force variation required for this earthquake is given by:

$$\frac{(\Delta f/\Delta t)}{(\Delta f/\Delta t)_{\max}} = \frac{t_{sc}}{t_{sc\max}} \quad (7.10),$$

(viii) The above steps are repeated for different earthquake time-histories, and the lowest value of the control force rate $(\Delta f/\Delta t)$ is selected for the *DB-LDFA*.

7.3.3.2. High Sensitivity and Low Robustness of DB-LDFA

The sensitivity of the control system is measured by the ratio of change in the control output due to the change in the control parameters (Glad and Ljung, 2000). The sensitivity of the *DB-LDFA* is measured by the effect of changing the algorithm parameter $(\Delta f/\Delta t)$ on the response of the controlled frame in terms of deformations.

Figure 7.11 showed that the force increment rate $(\Delta f/\Delta t)$ had a significant impact on the response of the PT frame. Small changes in $\Delta f/\Delta t$, result in large changes in the response of the frame. Also, there is no definite trend of the change in the response due to change of the force variation rate. Therefore, the algorithm can be said to be highly sensitive, and its sensitivity becomes higher for high values of force increments $(\Delta f/\Delta t)$, where in most cases, the response of the controlled frame became significantly higher than the response of the passive frame.

Results of the controlled frame show also that the *DB-LDFA* works better for low-frequency earthquakes where the time allowed for restoring the full initial PT force is long enough. When the exciting earthquake is characterised by high frequency, or the force increment rate is relatively high, the behaviour of the connection in the worst cases is illustrated in Figure 7.17, showing that due to insufficient time for restoring the initial PT forces, the moment carried by the connection rapidly decreases in successive cycles. This indicates low robustness of the algorithm as different loading conditions may result in different behaviour represented by substantial decrease or increase in the connection moment capacity which may lead to intensified response of the frame.

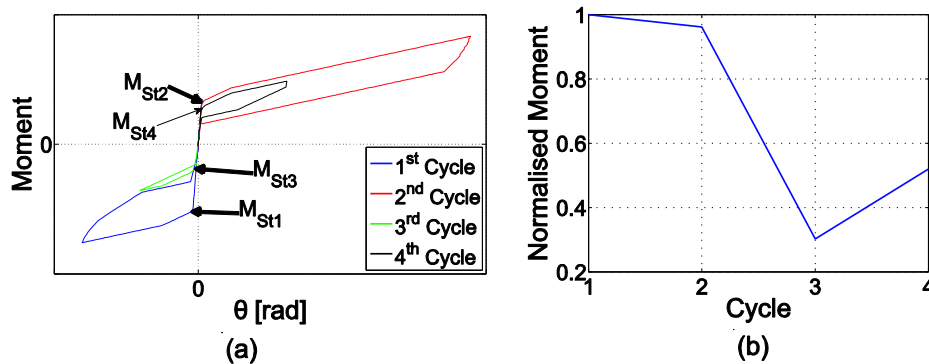


Figure 7.17: Behaviour of connection with large rate of control force increments: (a) moment-rotation relationship and (b) Variation of normalised M_{St} with loading cycles.

7.3.4. Modified DB-LDFA (MDB-LDFA)

7.3.4.1. Concept and Process

Since the *DB-LDFA* is designed to retrieve the full initial post-tensioning force (F_{pti}) when the connection is centred, the algorithm prevents gap opening and consequently, energy dissipation in the connection, when the level of applied moments is reduced due to the natural decay of the earthquake in the late stages of the response. The modification proposed here aims to increase the energy dissipation in the connection in these late loading cycles.

In this modification (Figure 7.18), the connection uses the full PT force at the beginning of the response, up to the first gap opening event (i.e. first large loading cycle). After the inelastic unloading, when the *LDFA* reduces the PT force, the algorithm restores a PT force to a level which is lower than the initial one (capped PT force). Then, the connection keeps working using the reduced, capped PT force (F_{ptc}):

$$F_{ptc} = C_{cap} \times F_{pti} \quad , \quad (7.11)$$

where C_{cap} is the capping ratio ($C_{cap} \leq 1$).

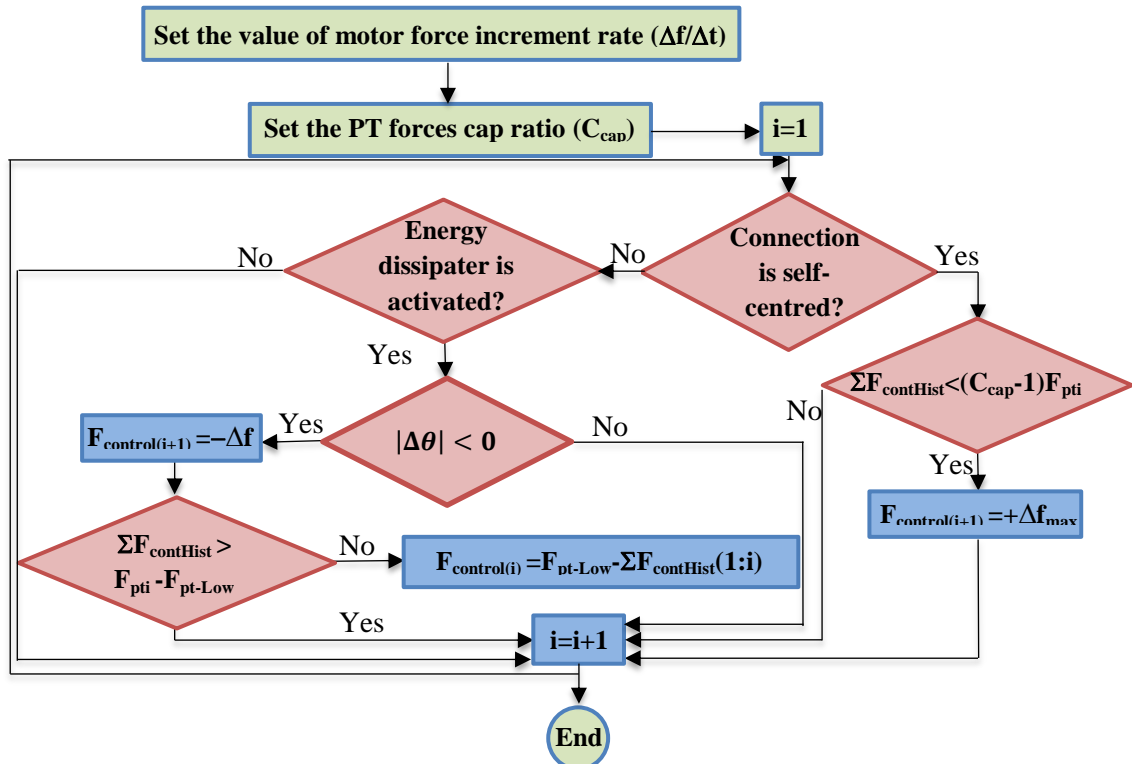


Figure 7.18: Flowchart of the modified deformation-based *LDFA*.

Using the technique shown in Figure 7.18 (capping PT forces in cycles other than the first one) the connection will be able to dissipate more energy when the level of loading becomes lower. Also, the connection will be working using its full moment capacity in the first cycle,

which in most cases imposes the highest moment demand. The idea is to reduce the connection capacity as the demand is reduced, and therefore, to allow for higher energy dissipation in the connection. The modified *DB-LDFA* returns to the original deformation-based *LDFA* when $C_{cap}=1$.

7.3.4.2. Comparison of Results of Modified with Original Deformation-based *LDFA*

The modified *DB-LDFA* with $C_{cap}=0.8$ was applied on the three-storey-two-bay PT steel frame. Results of the *MDB-LDFA* showed better decaying of the frame response in the late stages of loading (Figure 7.19). Maximum and SRSS displacements are similar to those obtained by the *DB-LDFA*.

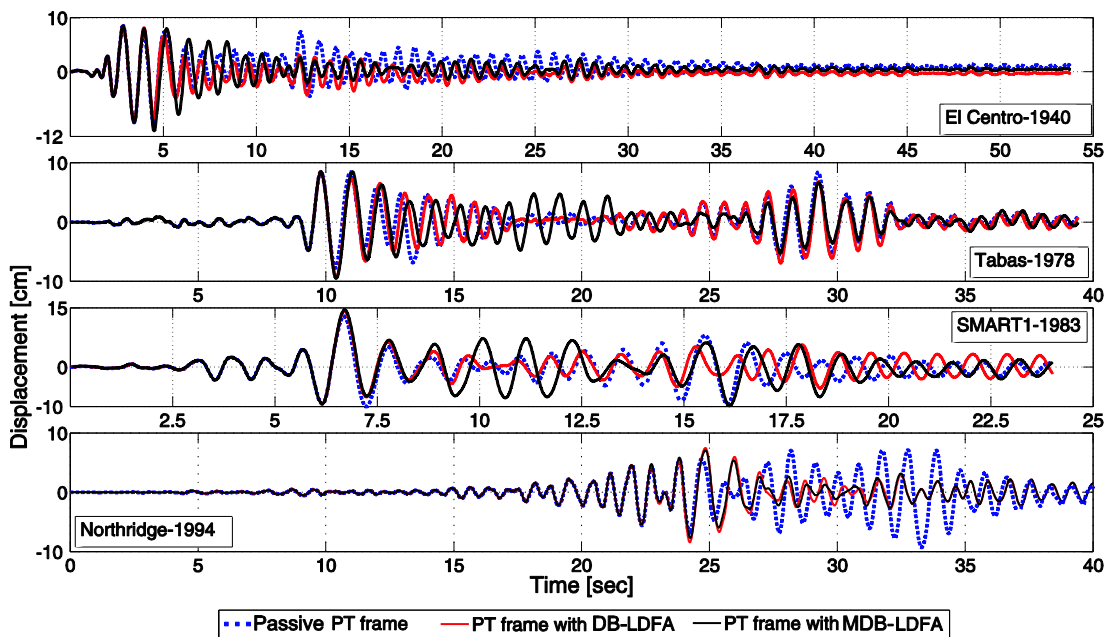


Figure 7.19: PT frame response with *DB-LDFA* and *MDB-LDFA*.

The ability of the *MDB-LDFA* to decay the frame response at the end of the loading is a result of the increased energy dissipation capacity. In the *MDB-LDFA* the connection is forced to dissipate more energy at lower level of demand by lowering the plastic moment of the connection beyond the first cycle (Figure 7.20).

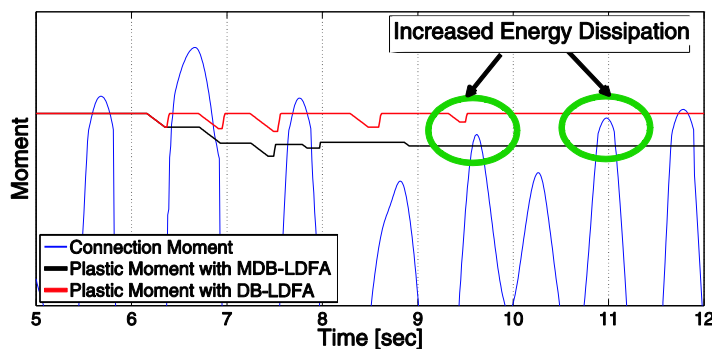


Figure 7.20: Increased energy dissipation in the *MDB-LDFA* (compared with *DB-LDFA*).

Plots of energy dissipated in PT connections (Figure 7.21) show that connections with *MDB-LDFA* dissipate more energy. This is not the case for Northridge earthquake where the energy dissipated in the connections when applying the *MDB-LDFA* is lower than energy dissipated in connections in passive PT frame or frame with *DB-LDFA*.

The displacement histories (Figure 7.19) however, show very little effect of the increase in damping in the later stages, indicating that an increase in energy dissipation may be more effective if applied in the early stages of the response.

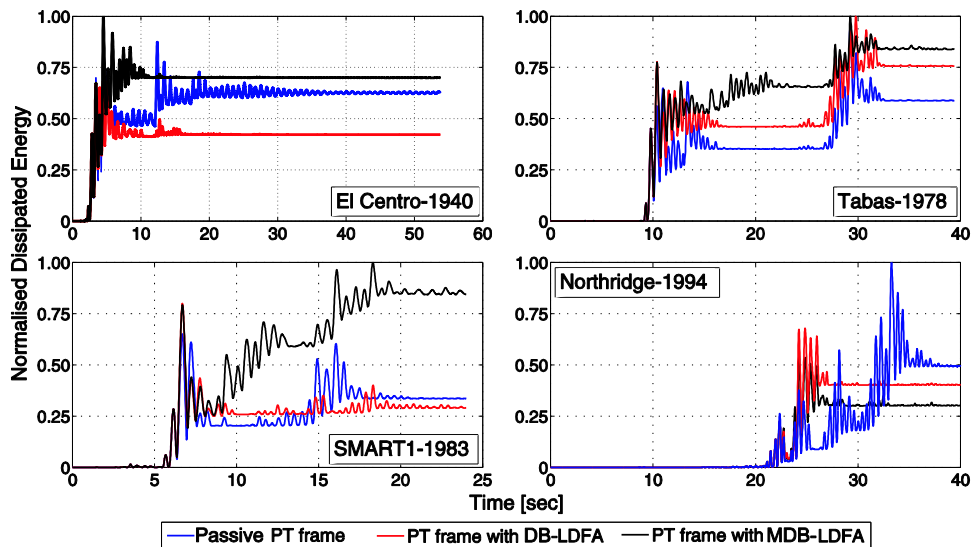


Figure 7.21: Energy dissipated in frame with *DB-LDFA* and *MDB-LDFA*.

7.4. Velocity-Based Loading Direction Feedback Control Algorithm

7.4.1. Operation of the *VB-LDFA*

The velocity-based *LDFA* was considered as a method for increasing the energy dissipation of the connection in the early stages of the response. The concept of the *VB-LDFA* is to interfere with the moment-rotation relationship of the connection before it starts unloading, and yet not to deteriorate the connection moment resisting capacity.

When the deformation-based *LDFA* is applied, forces in the strands are reduced when the connection is unloading, i.e. when absolute values of connection rotations (deformations) are decreasing. In the *VB-LDFA*, PT forces are reduced when the rate of connection rotations (velocity) decreases (Figure 7.22). The reduction of PT forces continues while the connection is unloading. The flowchart of the *VB-LDFA* is presented in Figure 7.23.

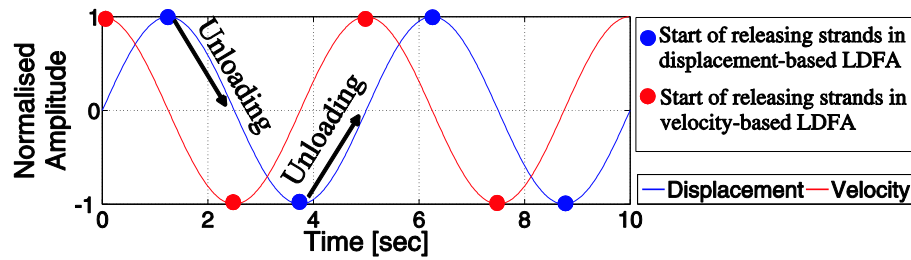


Figure 7.22: Comparison between the deformation-based *LDFA* and the velocity-based *LDFA*.

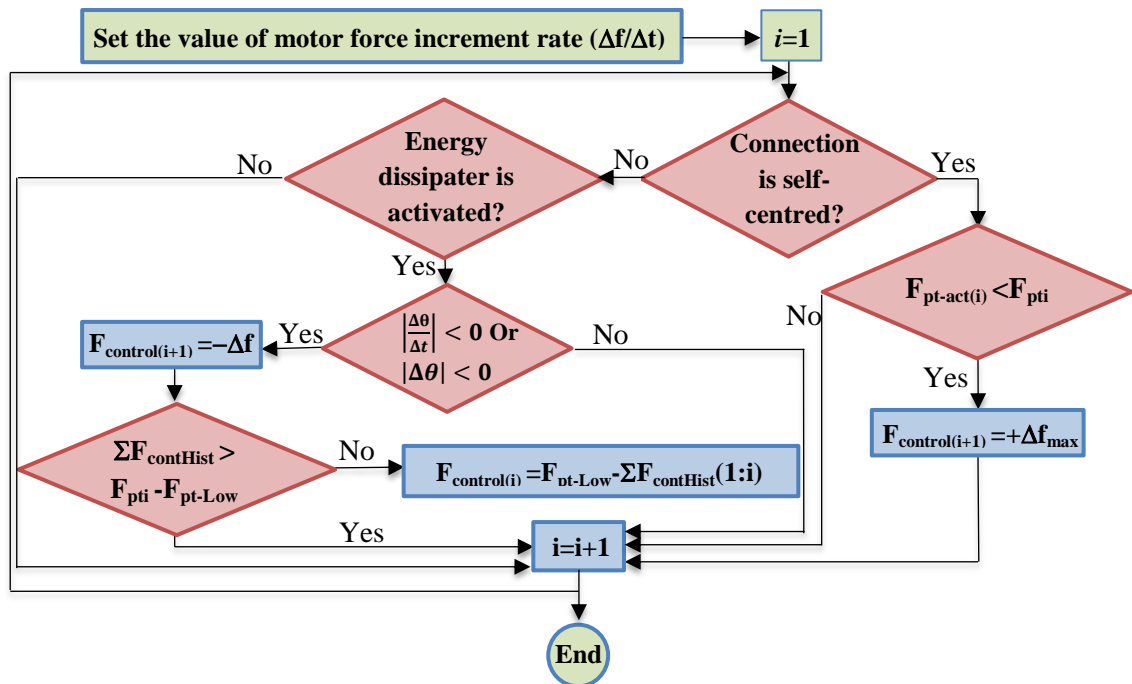


Figure 7.23: Flowchart of the *VB-LDFA*.

7.4.2. Results of the *VB-LDFA*

The results of the *VB-LDFA* (Figure 7.24) show that it improves the frame behaviour in late stages of loading in some, but not in all cases. The velocity-based *LDFA* however does not reduce the SRSS of the frame response comparatively to the deformation-based *LDFA*.

The inability of the *VB-LDFA* of reducing the frame response before the final stages of loading can be traced back to two reasons: (i) reduced capacity of energy dissipation of the frame and (ii) deterioration of the moment-rotation relationship.

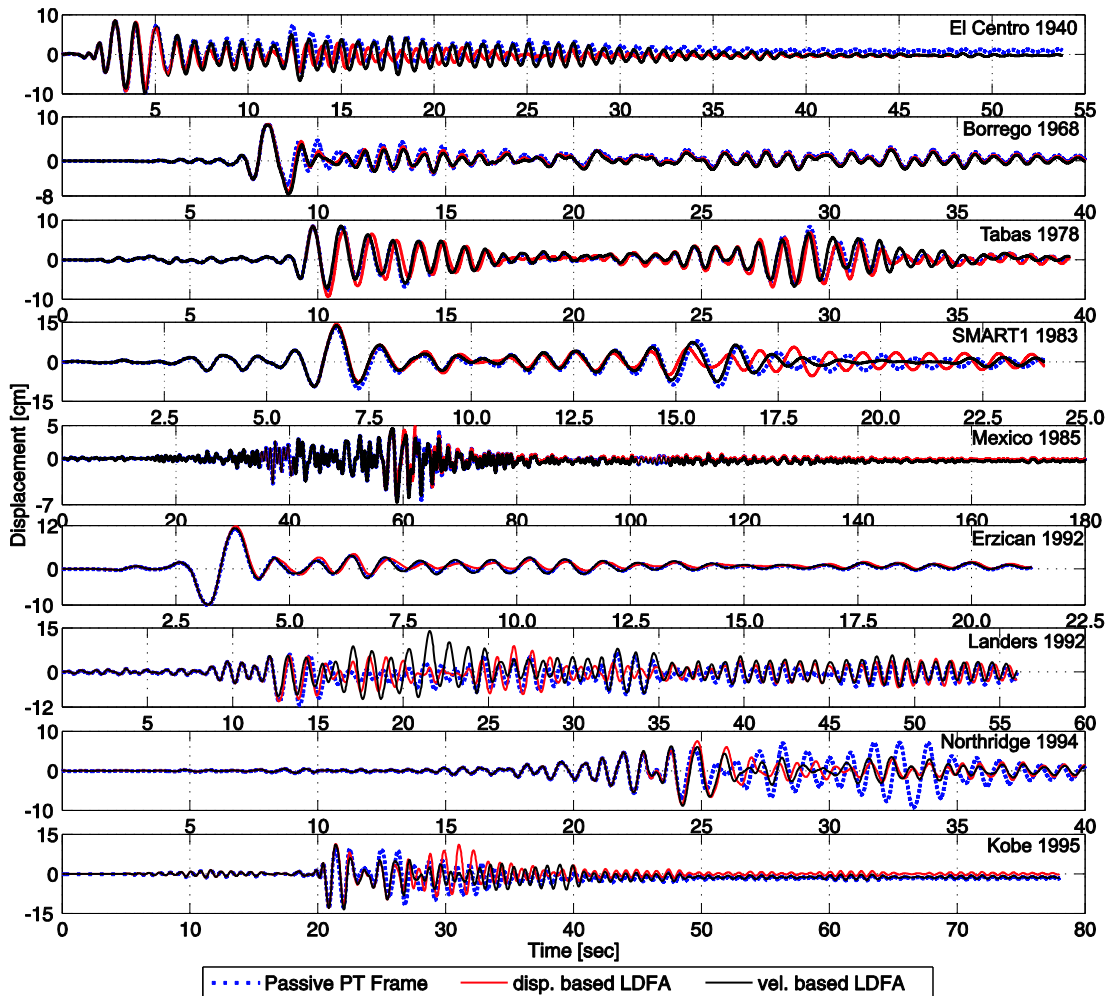


Figure 7.24: Comparison of the PT frames response with velocity and deformation-based *LDFA*.

7.4.2.1. Reduced Capacity of Energy Dissipation of the Frame

Although the velocity-based *LDFA* starts dissipating energy in the early stages of loading, its total dissipated energy is less than these in passive PT frames or PT frames with deformation-based *LDFA* (Figure 7.25).

The reduction in the total dissipated energy is a result of releasing the strands before the connection is unloaded. In the velocity-based *LDFA*, PT forces are reduced when velocity of the connection rotations is reduced and therefore, a significant area of the loop is lost (Figure 7.26). This is illustrated further in Figure 7.27 showing the point where PT forces start reducing. The hatched area in Figure 7.27 is the energy that would be dissipated if passive or deformation-based *LDFA* were used. This area therefore, is the loss in energy dissipation in one loop of the connection loading history which is going to be multiplied several times as the connection experiences several loading cycles. Consequently, total energy dissipated in the velocity-based *LDFA* is significantly reduced which limits the capacity of the algorithm to introduce further reduction in frame displacements in the early stages of loading.

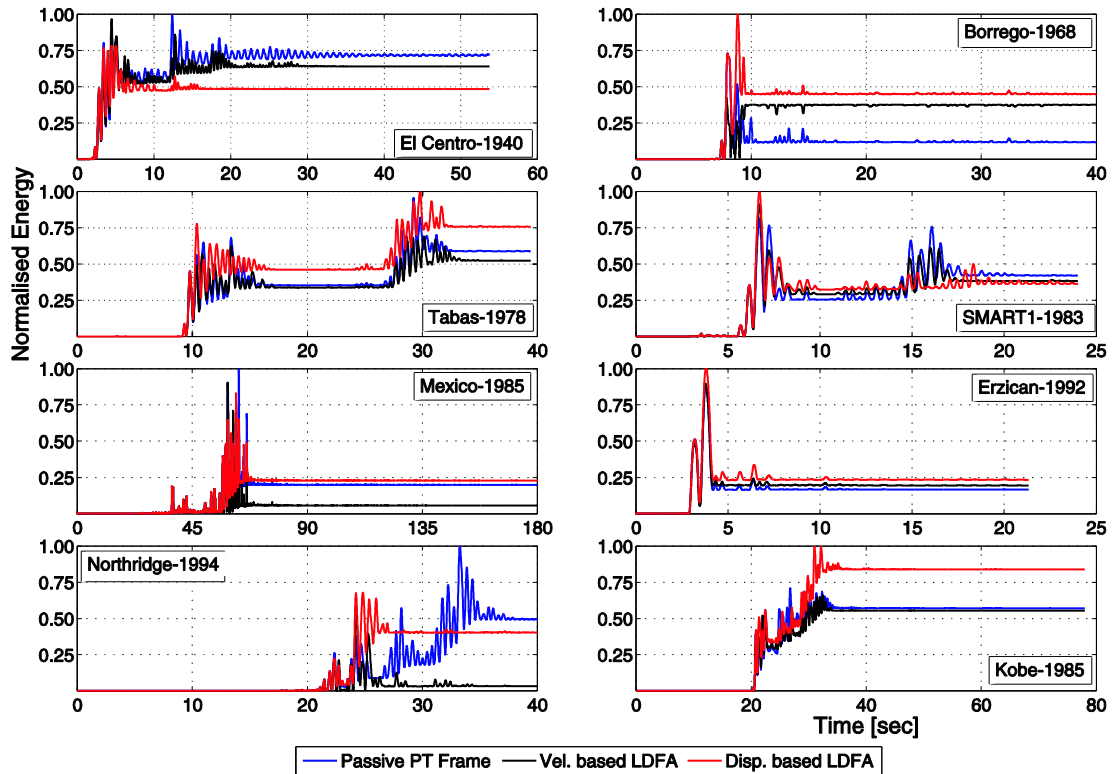


Figure 7.25: Energy dissipation time-history.

7.4.2.2. Deterioration of the Moment-Rotation Relationship

When the velocity-based *LDFA* is applied to post-tensioned connections, PT forces start to release while the connection is still in loading mode (Figure 7.28). Stiffness of the connection prior to releasing PT forces is k_2 , and this stiffness is reduced further when PT forces are reduced. Resultant stiffness of the connection is obtained from adding moments due to: (i) loading the connection which increases tensioning forces in strands and hence increase the connection moment and (ii) releasing PT strands which result in reduction in the connection moment (Figure 7.28). When the reduction of connection moment is greater than the increase, the connection stiffness becomes negative.

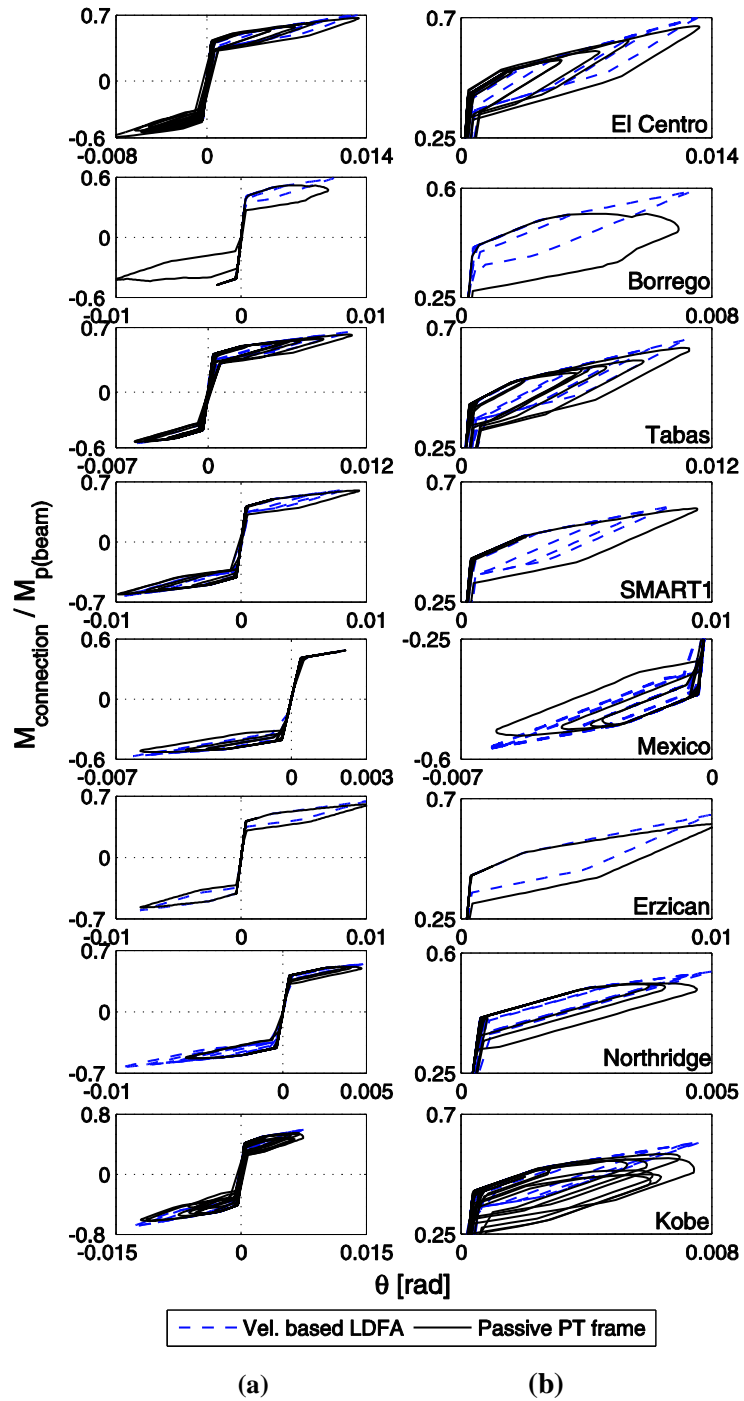


Figure 7.26: Moment-rotation relationships of the master connection of the first storey: (a) complete loop and (b) zoom in.

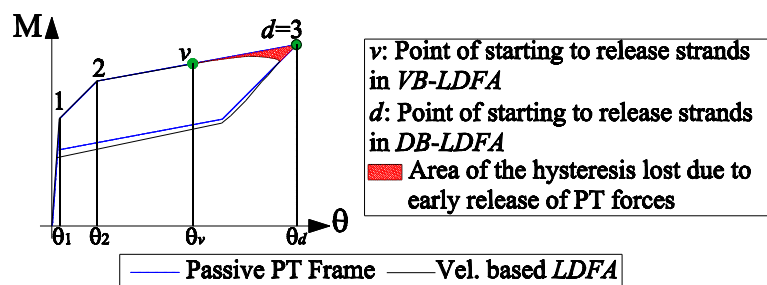


Figure 7.27: Loss of energy dissipation in velocity-based LDFA.

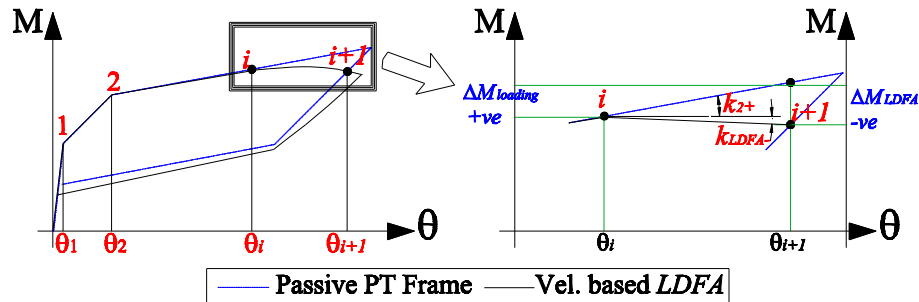


Figure 7.28: Moment reduction and negative stiffness when using the velocity-based *LDFA*.

Negative stiffness of the connection indicates a behaviour in which rotations of the connection increase while its moment capacity is decreasing. As a result, the backbone curve of the connection would be similar to the one shown in Figure 7.29. This behaviour results in deterioration in the connection behaviour leading to low moment capacity of the connection at high level of rotations. Consequently, the velocity based *LDFA* is not an effective approach, as it worsens the energy dissipating behaviour of the connection.

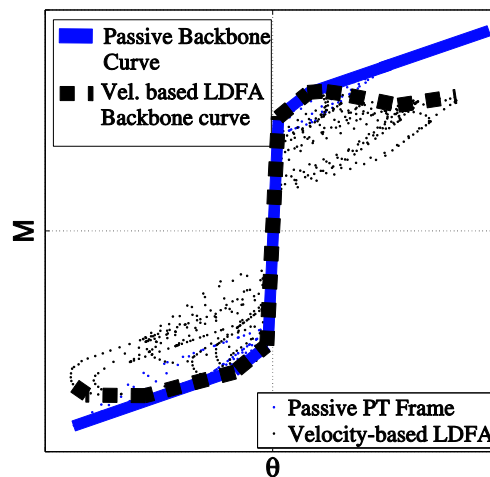


Figure 7.29: Backbone curves for passive and velocity-based *LDFA* controlled frames.

7.5. Concluding Remarks on Energy Dissipation Approach

Control of post-tensioned steel frames using the energy dissipation approach was presented in this chapter. This approach included: (i) deformation-based (DB), (ii) modified deformation-based (MDB) and (iii) velocity-based (VB) loading direction feedback algorithms (*LDFAs*) which are all based on increasing the energy dissipation in the connection (per cycle) achieved by reducing the PT forces during unloading. The difference between the three algorithms is the level of PT forces (DB vs. MDB) or the timing of the reduction of PT forces (DB vs. VB).

The deformation-based *LDFA*, which dissipates energy upon unloading (decrease in the absolute values of connection rotations); showed good and stable behaviour for relatively low-frequency earthquakes. The algorithm was able to increase the dissipated energy upon unloading and restored the full initial post-tensioning forces during the self-centring phase. The behaviour of the connection however, was not as good as expected when the connection was tested under relatively high-frequency earthquakes. This control algorithm is therefore, suitable for post-tensioned steel frames constructed on soft soils or subjected to far field earthquakes where most of high-frequency components of the earthquake are filtered. Also, the deformation-based *LDFA* showed uncertainty, high sensitivity and low robustness as the frame behaviour changes remarkably with small changes in the algorithm parameter.

In order to increase the energy dissipation capacity of the *DB-LDFA*, a modification was proposed by capping PT forces to one smaller than the initial force. This modification increased energy dissipation capacity of the connection but showed that dissipating energy in early stages of loading is sometimes more important than increasing the total dissipated energy.

The velocity-based *LDFA* aims to dissipate energy in early stages of loading by releasing strands when the velocity of the connection rotations starts decreasing. This intervention however was found to have negative effect on the connection ability to dissipate energy as significant parts of the hysteresis were not included in the energy dissipation due to reducing the connection stiffness while loading. In most cases, moment-rotation relationship of the connection deteriorated as a result of the negative stiffness during loading phases.

CHAPTER 8

SEMI-ACTIVE CONTROL OF PT FRAMES USING STIFFNESS CONTROL APPROACH

It was shown in Chapter 6 that PT frames can be softened or kept stiff when varying the initial post-tensioning forces. This feature is used here to present the stiffness control approach of PT steel frames. The concept of the control approach is first introduced, and then, a new control algorithm for controlling the dynamic response of PT frames is proposed. The results of applying the new stiffness-based control algorithm are presented and compared with passive PT frames.

8.1. Basics of Stiffness Control Approach

The purpose of the stiffness control approach is to control the natural frequency of the frame in order to avoid exciting the frame at the frequency of one of its major modes. This concept was first proposed by Kobori et al. (1993) who used active variable stiffness systems to control the seismic response of a three-storey braced frame. Here, the concept is revisited to control the dynamic response of post-tensioned frames using the characteristics of post-tensioned connections.

Moment-rotation relationship of steel post-tensioned beam-column connections naturally supports the stiffness control approach as it is composed of more than one loading phase with different stiffness values. The number of loading stiffness values in the moment-rotation relationship of the connection depends on the energy dissipating device installed in the connection (Figure 8.1). Post-tensioned connections with friction based dissipation mechanism have two stiffness values (pre-slippage and post-slippage). Post-tensioned connections with energy dissipating bars have three stiffness values: pre-gap opening, between gap opening and bars yielding, and post bars yielding. Post-tensioned connections with top and seat dissipating angles have more than three stiffness values based on the

number of plastic hinges forming in the dissipating angles (usually three plastic hinges) (Ricles et al. 2001).

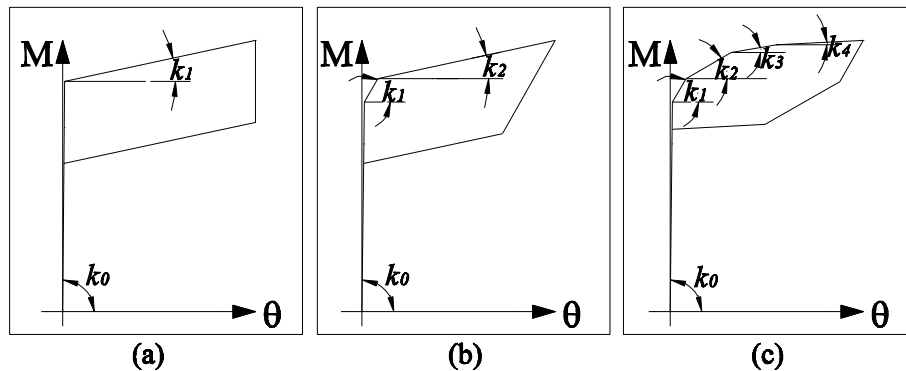


Figure 8.1: Stiffness values for post-tensioned connections with different energy dissipation mechanisms: (a) friction-based energy dissipation, (b) energy dissipating bars and (c) top and seat energy dissipating angles.

During earthquake excitations, stiffness of the connection varies based on the level of loading. At any time, the current stiffness of all connections in the frame governs the tangent stiffness of the frame. By varying the post-tensioning forces of each storey, the gap-opening moment can be controlled, the total stiffness of the frame can be adjusted and the natural frequency of the frame can be shifted to avoid exciting the frame at its principal modes.

Three algorithms were chosen to implement the stiffness control approach: (1) Excitation frequency state feedback (using the ground acceleration), (2) response frequency state feedback (using the acceleration response of the structure) and (3) filtered frequency state feedback (using filtered ground acceleration).

8.2. Excitation Frequency State Feedback Control

Algorithm (EFSFA)

8.2.1. Operation of the Control Algorithm

The purpose of the excitation frequency state feedback control algorithm is to alter the modal properties of post-tensioned frames by softening them so that their natural frequency is shifted away from dominant frequencies of the earthquake. This is performed by analysing the frequency content of the exciting earthquake at regular time intervals. These time intervals are input parameters for the control algorithm.

The first step in this algorithm is determining all stiffness patterns of the frame, which are the control options of the frame. For instance, if beam-column connections in the frame are yield-based with energy dissipating bars, each storey can take three states (for k_0 , k_1 and k_2). However, the range for k_1 is small comparatively to k_0 and k_2 which makes this range

difficult to control and therefore it is not taken into account in the algorithm. Hence, the number of stiffness patterns for each storey is two. Thus, a stiffness pattern is a vector with N_s number of elements. Each element can take the value of 0 or 2. The value of 0 indicates no yielding (connection stiffness is k_0); while the value of 2 indicates yielding (connection stiffness is k_2).

The total number of all stiffness patterns in the frame can be obtained as:

$$S = 2^{N_s}, \quad (8.1)$$

where S is number of possible stiffness patterns of the frame and N_s is number of storeys in the frame.

The same analysis of stiffness patterns applies if the frame is provided with friction-based connections or post-tensioned connection with top and seat angles.

Modal analysis is then performed for each stiffness pattern to determine natural frequencies (f) and modal mass participation ratios (Γ) for the first and the second modes. As a result, stiffness patterns matrix is assembled as illustrated in Table 8.1. It should be noted that these steps of the algorithm are independent from the exciting earthquake.

Pattern	1 st Storey	2 nd Storey	...	N th Storey	First Mode Frequency (f_1)	Second Mode Frequency (f_2)	First Mode Modal Mass Participation (Γ_1)	Second Mode Modal Mass Participation (Γ_2)
1	0	0	0	0	$f_{1,1}$	$f_{1,2}$	$\Gamma_{1,1}$	$\Gamma_{1,2}$
2	2	0	0	0	$f_{2,1}$	$f_{2,2}$	$\Gamma_{2,1}$	$\Gamma_{2,2}$
...
S	2	2	2	2	$f_{s,1}$	$f_{s,2}$	$\Gamma_{s,1}$	$\Gamma_{s,2}$

Table 8.1: Assembly of the stiffness patterns matrix.

The *EFSFA* does not start working immediately after the earthquake excites the structure. It allows for control time (CtrlTime) which is given as an input parameter. During the control time, the *EFSFA* acquires data about the frequency content of the earthquake. Once the control time has passed, the recorded time-history (up to the control time) is analysed using Fourier Transform (in this case FFT) to find its frequency content.

The result of the FT is amplitude spectrum which correlates the frequency to the spectral acceleration. The spectral acceleration is then used to compute the index of weighted frequency content of each stiffness pattern of the frame, calculated by scaling the frequency amplitude of each mode of vibration by its corresponding modal mass participation to obtain an index *FRI*:

$$FR_i = \Gamma_{i,1} \Psi_{i,1} + \Gamma_{i,2} \Psi_{i,2}, \quad (8.2)$$

where FR_i is the index of weighted frequency content of the i^{th} stiffness pattern, $\Gamma_{i,1}$, $\Gamma_{i,2}$ are effective modal mass participation ratios for the first and the second modes of vibration of the i^{th} stiffness pattern and $\Psi_{i,1}$, $\Psi_{i,2}$ are the spectral acceleration amplitude of the first and second modes of vibration of the i^{th} stiffness pattern. In Figure 8.2 is presented an illustration of the calculation of the weighted frequency content.

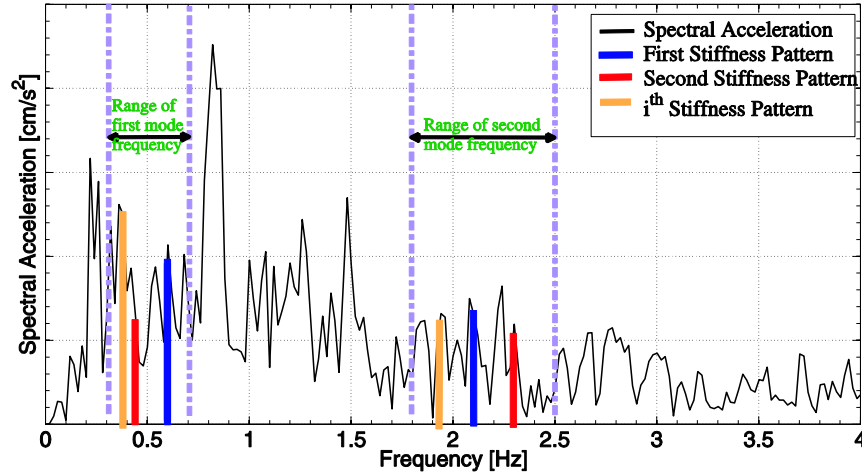


Figure 8.2: Computation of weighted frequency index for each stiffness pattern from the spectral acceleration diagram.

The number of each stiffness pattern (ID) and its index of weighted frequency content (FR_i) are stored in a two-column matrix (*SpecFreq*). The algorithm searches for a stiffness pattern resulting in the minimum index of weighted frequency content from *SpecFreq* matrix. Then, from the stiffness patterns matrix it finds the corresponding stiffness distribution of all storeys. When the required stiffness of the storey from the optimum pattern is k_0 , post-tensioning forces in this storey are increased (tightened) to the upper limit (about 70% of the yielding force of the strands). When the required stiffness of the storey from the optimum pattern is k_2 , post-tensioning forces in the storey are reduced (released) to the lower limit (which satisfies the requirement for full self-centring of the connection).

After every control time interval (*CtrlTime*), the amplitude spectrum of the earthquake is updated, and the operation of the algorithm is repeated. Updating the earthquake record is made by adding the new interval to the earthquake acceleration record for which the previous amplitude spectrum was calculated. Alternatively, Fourier spectra can be calculated segment-by-segment, or by overlapping segments, but extending the acceleration record resulted in a more accurate Fourier spectrum. The process of repeating the algorithm at three successive control intervals is shown in Figure 8.3.

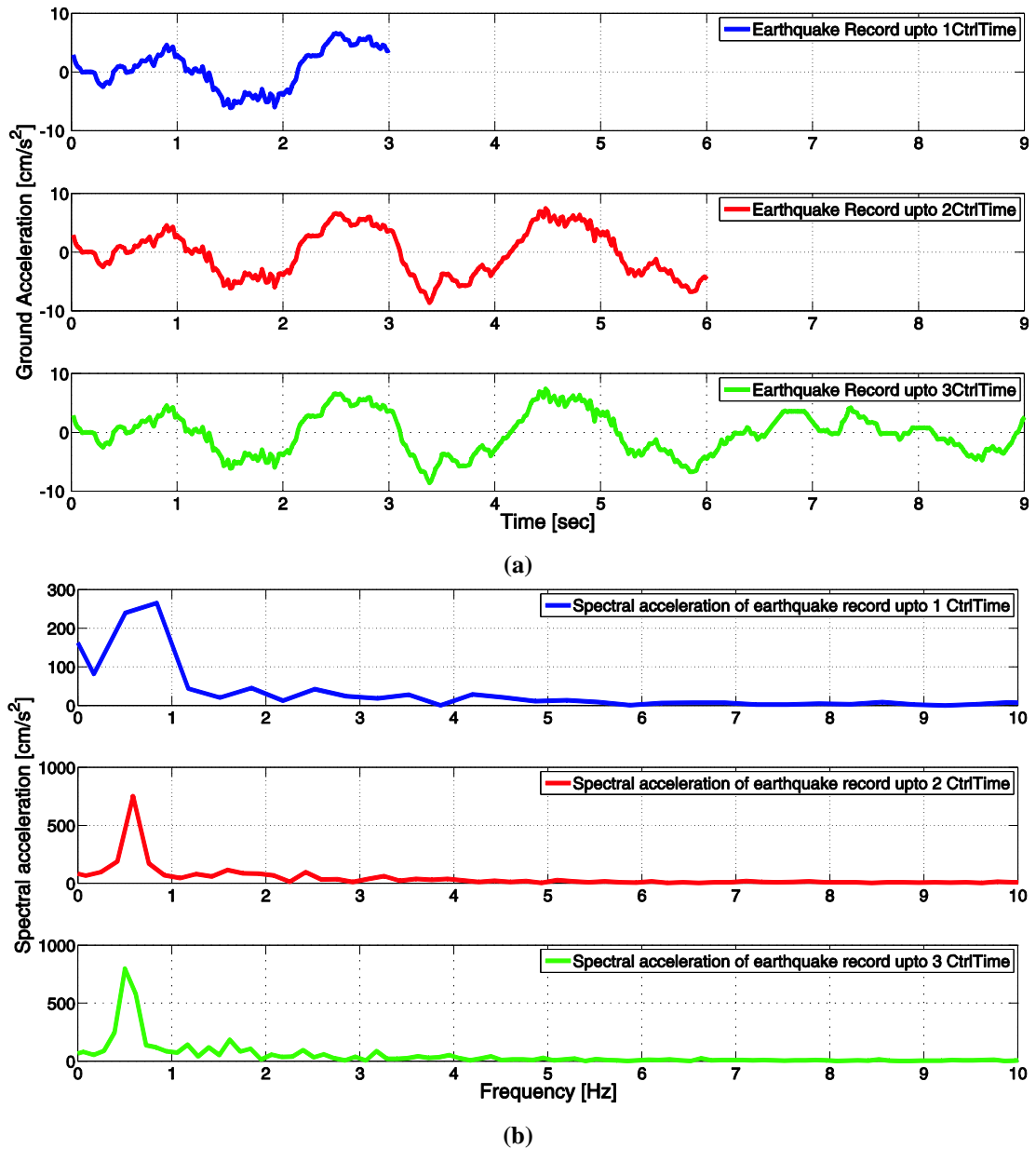


Figure 8.3: Repetition of the excitation frequency state feedback algorithm at every control time interval (CtrlTime = 3 sec in this Figure): (a) progress of the ground acceleration record, and (b) spectral acceleration from Fourier transform.

Since the input data of the Excitation Frequency State Feedback Algorithm (EFSFA) are only the accelerations of the exciting earthquake, this algorithm is an open-loop feedback control algorithm where structure properties are not included in the control algorithm and control gains depend only on analysis of the exciting earthquake. Flowchart of the algorithm is shown in Figure 8.4.

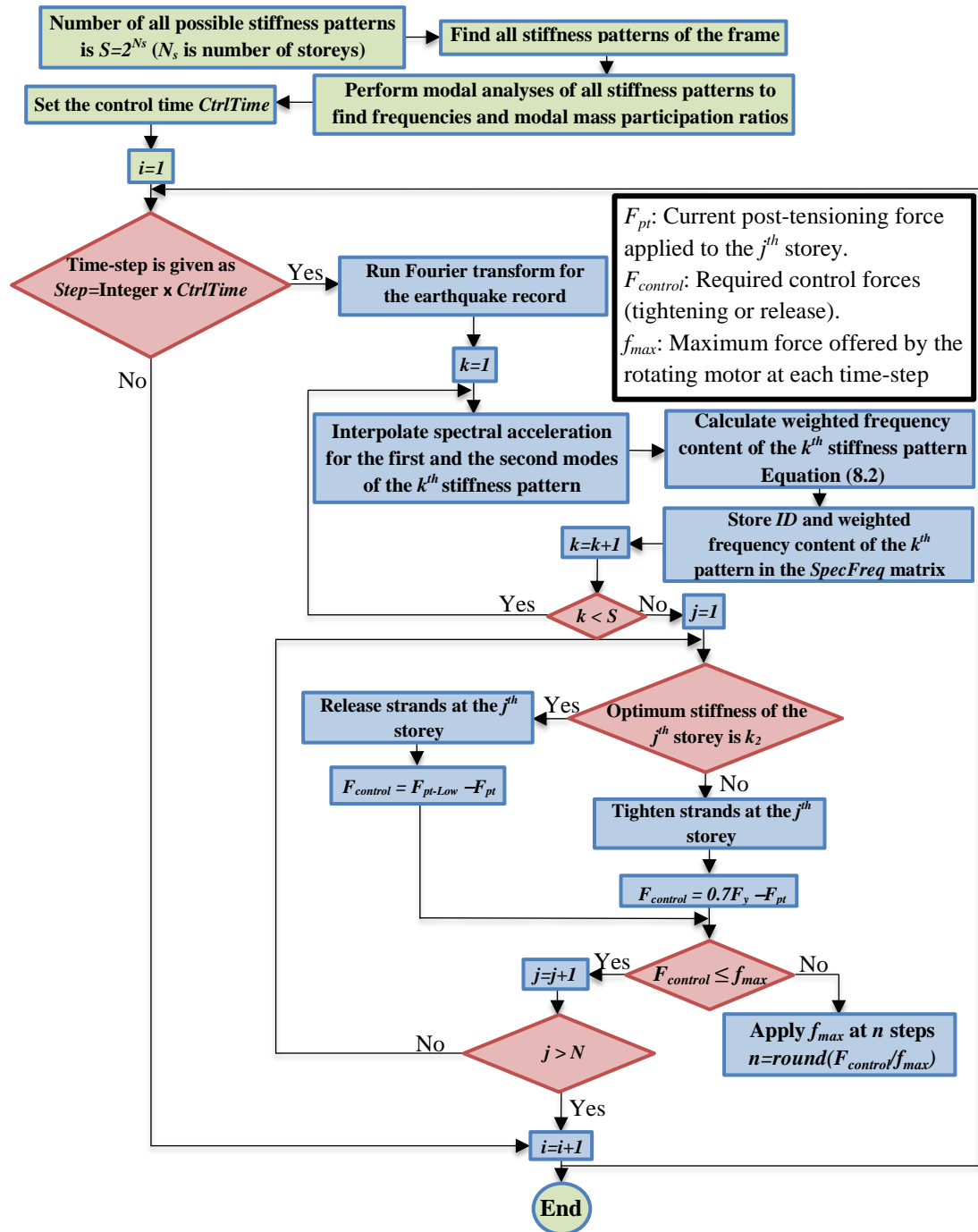


Figure 8.4: Flowchart of the excitation frequency state feedback control algorithm.

8.2.2. Results of the EFSFA Control Algorithm

In order to examine the results of *EFSFA*, a six-storey-one-bay frame was used (Figure 8.5). Each storey was equipped with a rotating motor installed as shown in Figures 5.26 and 5.27 (Section 5.3.2) to allow for controlling post-tensioning forces in strands.

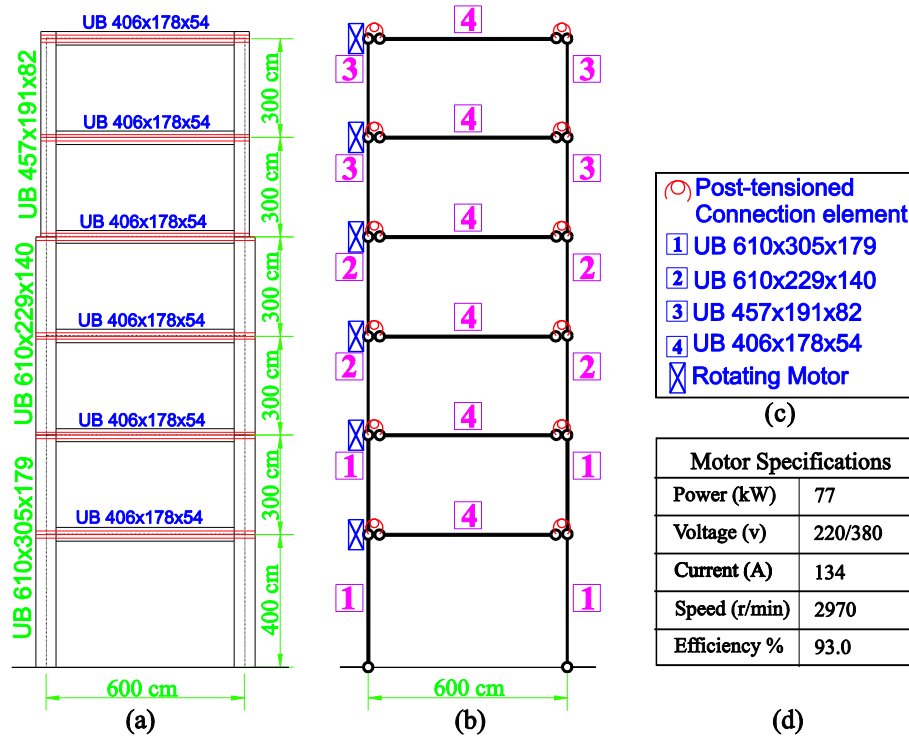


Figure 8.5: Six-storey post-tensioned steel frame: (a) frame geometry and sections, (b) idealised model of the frame, (c) element and section properties and (d) specifications of rotating motor.

The initial post-tensioning forces were taken as 300 kN (about 30% of strands yield force—referred as low initial PT force) which remained constant in the passive system and were varied when the *EFSFA* was applied. Modal properties of the passive frame for the first two modes are presented in Table 8.2. Control time (CtrlTime) in these simulations was 3.0 sec . A comprehensive discussion about control time is presented later on in this chapter.

Mode	f [Hz]	Modal mass participation ratio of first mode %
1	0.66	73.7
2	2.21	14.4

Table 8.2: Modal properties of the PT frame.

Results of the top storey displacements are presented in Figure 8.6 comparing displacements of a passive frame with low PT forces with those resulting from applying the *EFSFA*. It can be noticed that maximum and SRSS displacements are significantly reduced when the *EFSFA* is applied as the structure vibrations were shifted away from frequencies that excited its major modes of vibration.

The biggest reduction in top storey displacements is noticed for Mexico City earthquake. This reduction is investigated by plotting the amplitude spectrum of the earthquake (Figure 8.7), where it can be shown that this earthquake is a low-frequency and the dominant frequency is 0.5 [Hz] . It can also be noticed from the frequency content that there is no significant presence of other frequency components. Therefore, any small change in the

frame modal properties would result in noticeable reduction in the frame response. This means that this approach becomes more effective for specific types of earthquakes which are characterised by velocities similar to low frequency harmonic waves allowing longer times for the algorithm to realise control actions and make changes in the frame modal properties.

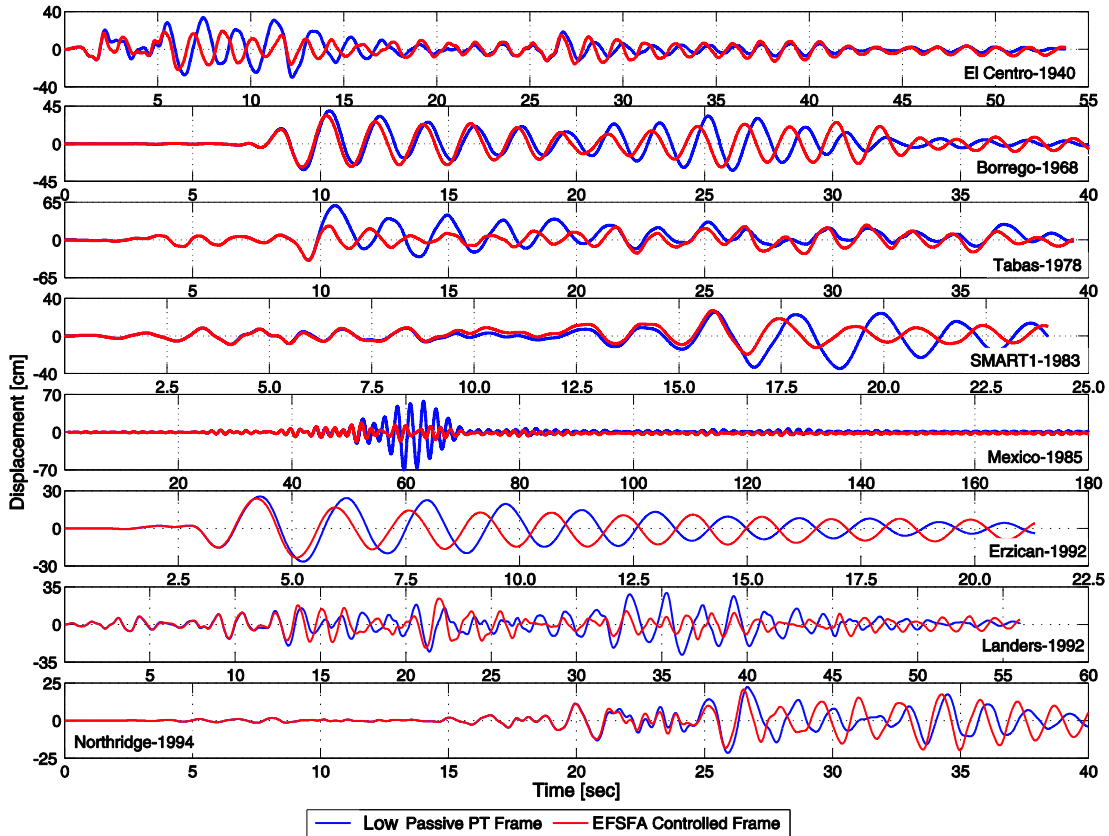


Figure 8.6: Top storey displacements for low passive and *EFSFA*-controlled PT frames.

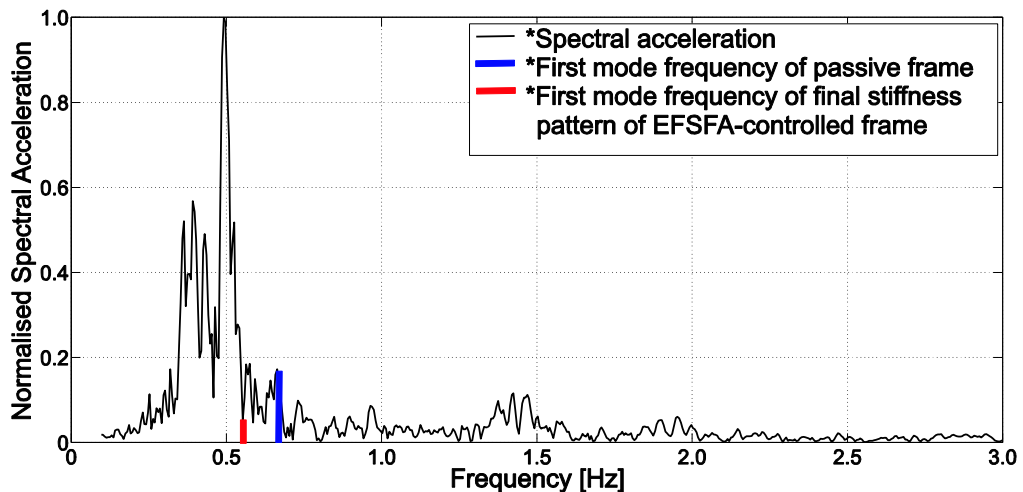


Figure 8.7: Frequency content of Mexico earthquake with first mode frequency of passive and controlled frames.

The final stiffness pattern of the *EFSFA*-controlled frame (Figure 8.7) is found from resultant PT forces distribution at the end of earthquake (Figure 8.8). Resultant PT forces

diagram lead to finding the frame stiffness pattern after the earthquake action from the final value of PT force at each storey. If the final PT force takes a low value in a storey, the final stiffness of this storey is k_2 , whereas it is k_0 if the final PT force is high. The ranges of frequency for different stiffness patterns of the controlled frame are presented in Figure 8.9.

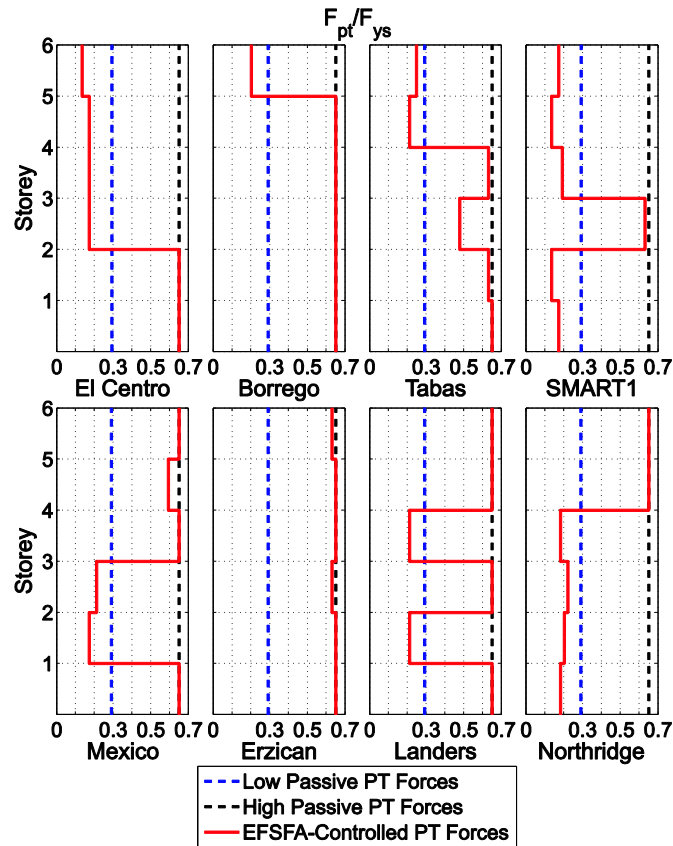


Figure 8.8: Distribution of PT forces in an *EFSFA*-controlled frame at the end of the seismic action.

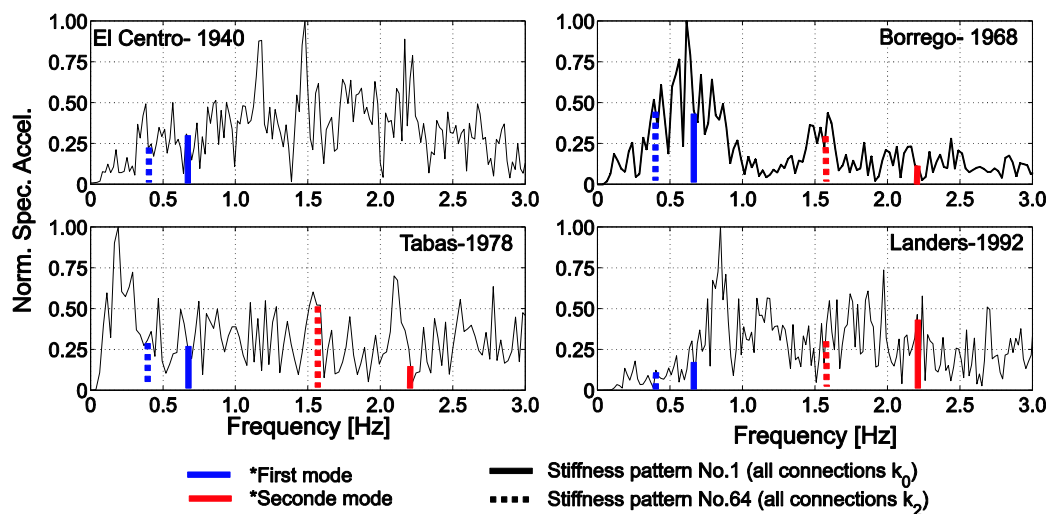


Figure 8.9: Ranges of frequency for different stiffness patterns and earthquakes.

Final PT force graphs show that post-tensioning forces may reach high values (limited to 70% of strands yield force) when the Excitation Frequency State Feedback Algorithm is

used. Hence, the comparison between a frame with low passive PT forces and another one with applied *EFSFA* is not completely fair. A better comparison is provided by plotting results of the *EFSFA*-controlled frame with a passive frame with high initial PT forces ($F_{pti}=0.7F_{ys}$, Figure 8.10) while initial PT forces in the *EFSFA*-controlled frame are as low as 30% of the strands yield force. It can be seen that maximum and SRSS displacements in both frames are similar. The *EFSFA* however reduces the level of PT forces in some storeys (Figure 8.8). This reduction in the resultant PT forces results in a reduction in the moment demand on connected columns. Therefore by applying the *EFSFA*, the achieved control objective is reducing internal forces in columns if frame displacements were not reduced. Biggest reductions in the resultant PT forces are noticed for El-Centro, SMART1 and Northridge earthquakes which are associated with frame displacements similar to those in the passive frame with high initial PT forces.

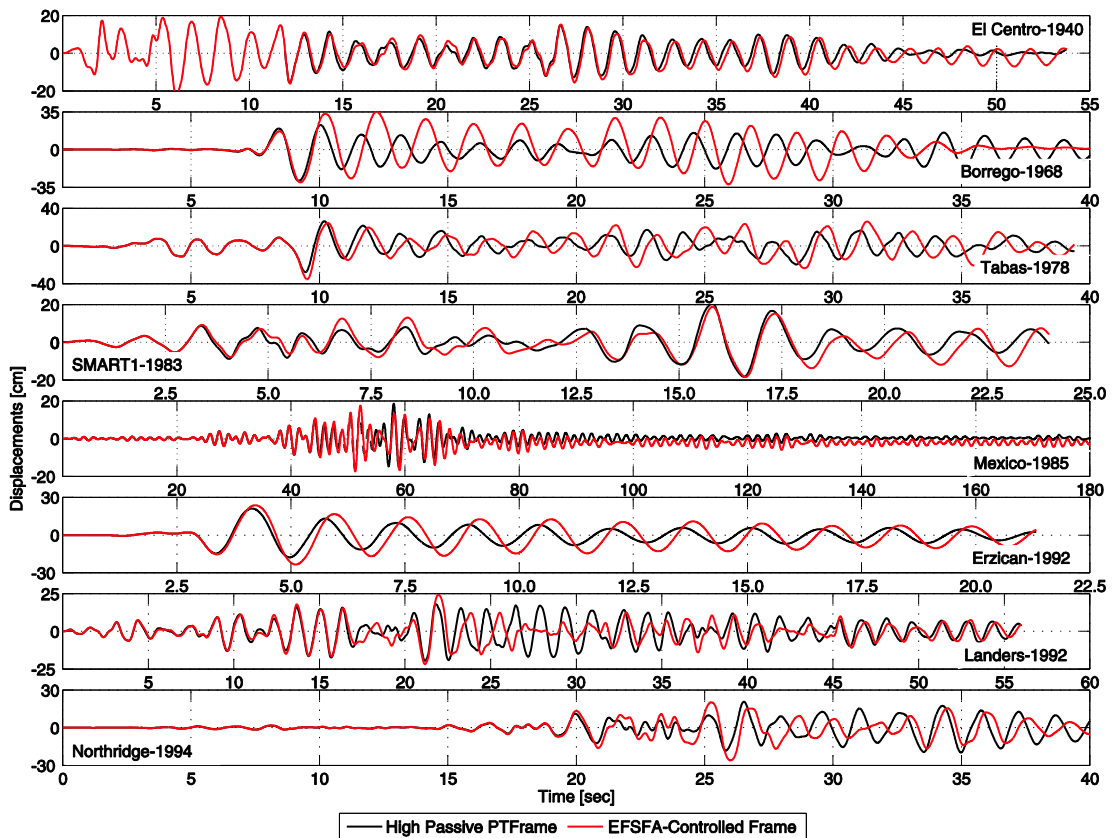


Figure 8.10: Top storey displacements for passive frame with high PT forces and *EFSFA*-controlled PT frames.

It should be noted that applying high initial PT forces does not necessarily result in reduced displacements. When initial PT forces are too high, the stiffness of the frame remains high as well, and the structure behaves elastically. The PT frame in this case might be excited at a major mode of vibration. Figure 8.11 shows an example of negative effect of high PT forces for Northridge earthquake.

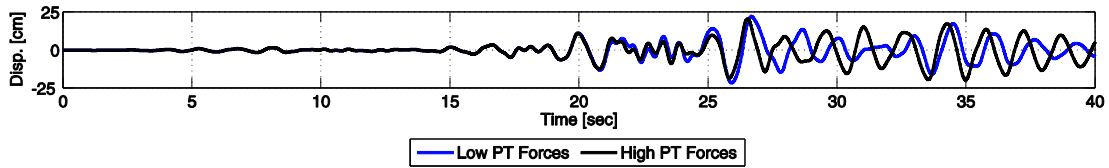


Figure 8.11: Negative effect of high initial PT forces (Northridge earthquake).

The predominant stiffness pattern of the frame during the earthquake is the one that is repeated the most (active most of the time). Figure 8.12 shows the histogram of the selected stiffness patterns, the distribution of PT forces and the frequency of the first mode for the predominant stiffness pattern.

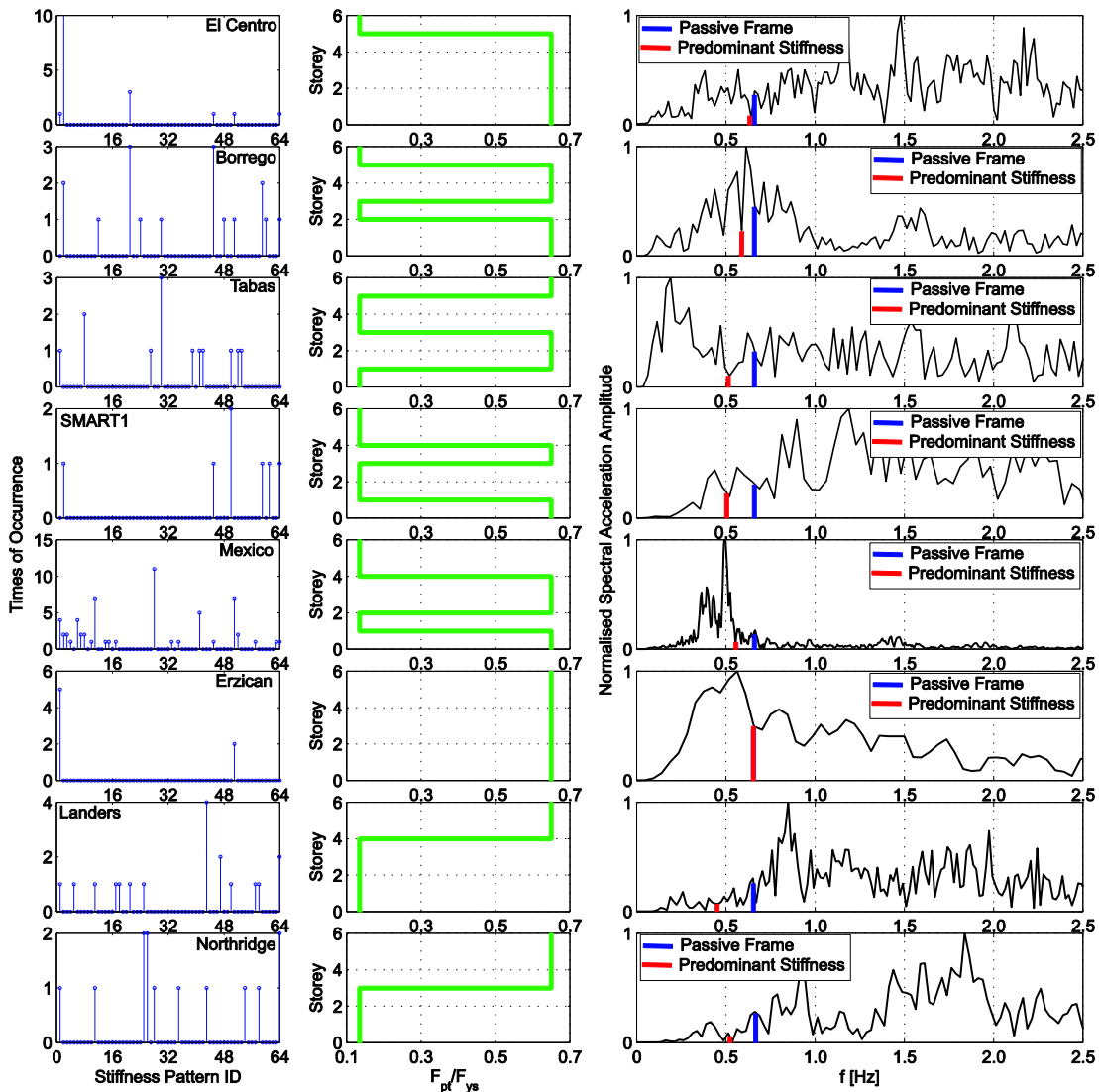


Figure 8.12: Predominant stiffness patterns of the frame for different earthquakes: (a) finding the predominant stiffness pattern, (b) PT forces of the predominant stiffness pattern and (c) first mode frequency of the predominant stiffness pattern.

The main issue of the *EFSFA* is determining the control time interval used in the algorithm. Simulations performed with algorithms with different control times show significant effect

of the selected control time interval on the algorithm performance (Figure 8.13). If the control time is not properly selected, the response of the *EFSFA* frame could be intensified (Borrego, Landers and Northridge earthquakes). On the other hand, good selection of control time may lead to significant reduction in structural displacements as well as internal forces.

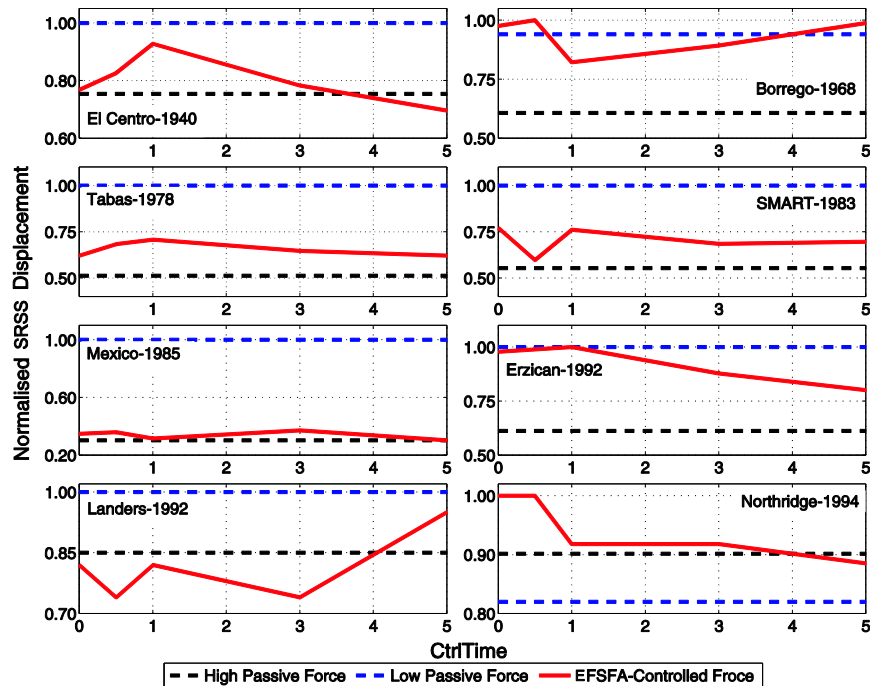


Figure 8.13: Effect of control time interval (CtrlTime) on the *EFSFA* performance.

The effect of the control time interval (CtrlTime) can be analysed from 4 aspects: (i) the *EFSFA* aspect, (ii) the structure damping/stiffness aspect, (iii) the exciting earthquake aspect and (iv) the rotating motor aspect.

(i) Analysis of Control Time from the *EFSFA* Aspect

As presented earlier, the *EFSFA* performs Fourier analysis of the earthquake acceleration after every control interval and based on the analysis results, the stiffness pattern is selected. This means that the Fourier spectrum is updated, taking into account the earthquake acceleration record from the beginning of the seismic action up to the end of the last control interval, resulting in changes in the frequency content with every new interval and, consequently, in changes in the optimal stiffness pattern.

This creates a problem at the beginning of the analysis when the spectrum is calculated for only a few acceleration values (up to $1.0 \cdot \text{CtrlTime}$). As the *EFSFA* performs more and more updates, the results of the analysis become more reliable. This means that the control time interval must be long enough to provide enough data for the first Fourier spectrum to be calculated accurately and to allow a correct selection of the first stiffness pattern. This is particularly important because large earthquake amplitude reversals may occur early. If

wrong stiffness patterns are chosen on the basis of the early spectra, this can lead to magnified response of the structure. Table 8.3 shows how the control time affects the stiffness pattern of the frame after the earthquake. The first column shows final stiffness patterns for $CtrlTime=2dt$, where dt is the time-step of the earthquake acceleration record.

SMART1 earthquake (Table 8.3) is a good example of the effect of control time on selection of stiffness pattern by the *EFSFA*. It can be seen that different control time intervals result in completely different final stiffness patterns (different control forces). The final stiffness pattern for SMART1 earthquake ($CtrlTime = 0.5$ sec) is presented in Table 8.4.

(ii) Analysis of Control Time from the Aspect of Structural Damping/Stiffness

The structural damping becomes more effective when fewer changes are applied to the structure. If more control actions were applied to the frame, it would not have sufficient time to adapt itself and activate its damping. Structural vibrations also need enough time to decay providing that the structural status does not change within this time. Therefore, using short control time in the *EFSFA* might result in structural destabilisation as the structure status changes at short intervals leaving no time for the structure to activate its damping. This is the case for El Centro, Tabas, Erzican, Mexico City and Northridge earthquakes.

On the other hand, too long control times leave the frame with a *late response problem* where the structure changes its stiffness pattern too late at a time that requires different stiffness pattern. This case is presented in Landers earthquake where the best behaviour is achieved for $CtrlTime=3.0$ sec, whereas using $CtrlTime=5.0$ sec results in completely different stiffness pattern that intensifies the frame displacements (Figure 8.14).

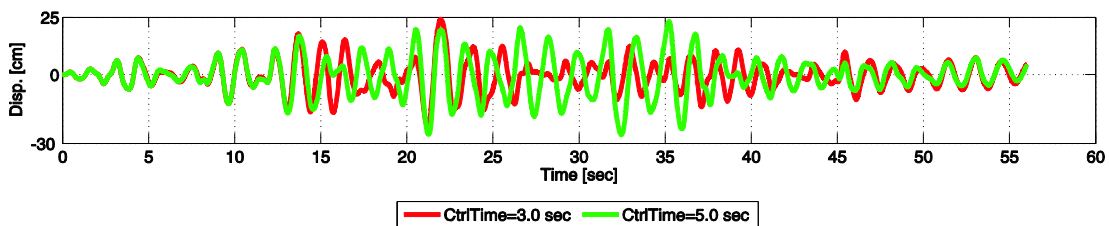


Figure 8.14: Frame response to Landers earthquake for $CtrlTime = 3.0$ sec and $CtrlTime = 5.0$ sec.

(iii) Analysis of Control Time from the Aspect of the Exciting Earthquake

If the frequency content of the exciting earthquake contains several predominant frequencies within the building frequency range, response of the *EFSFA*-controlled frame would be very sensitive to the selected control time. This case is faced for near-field earthquakes or generally for earthquakes with high frequency content. The existence of several predominant frequencies in the frequency content, which appear as peaks in the spectral acceleration plot,

results in two difficulties: (i) reducing the reliability of the running frequency content analysis and (ii) limiting the efficiency of the optimisation process of the *EFSFA*.

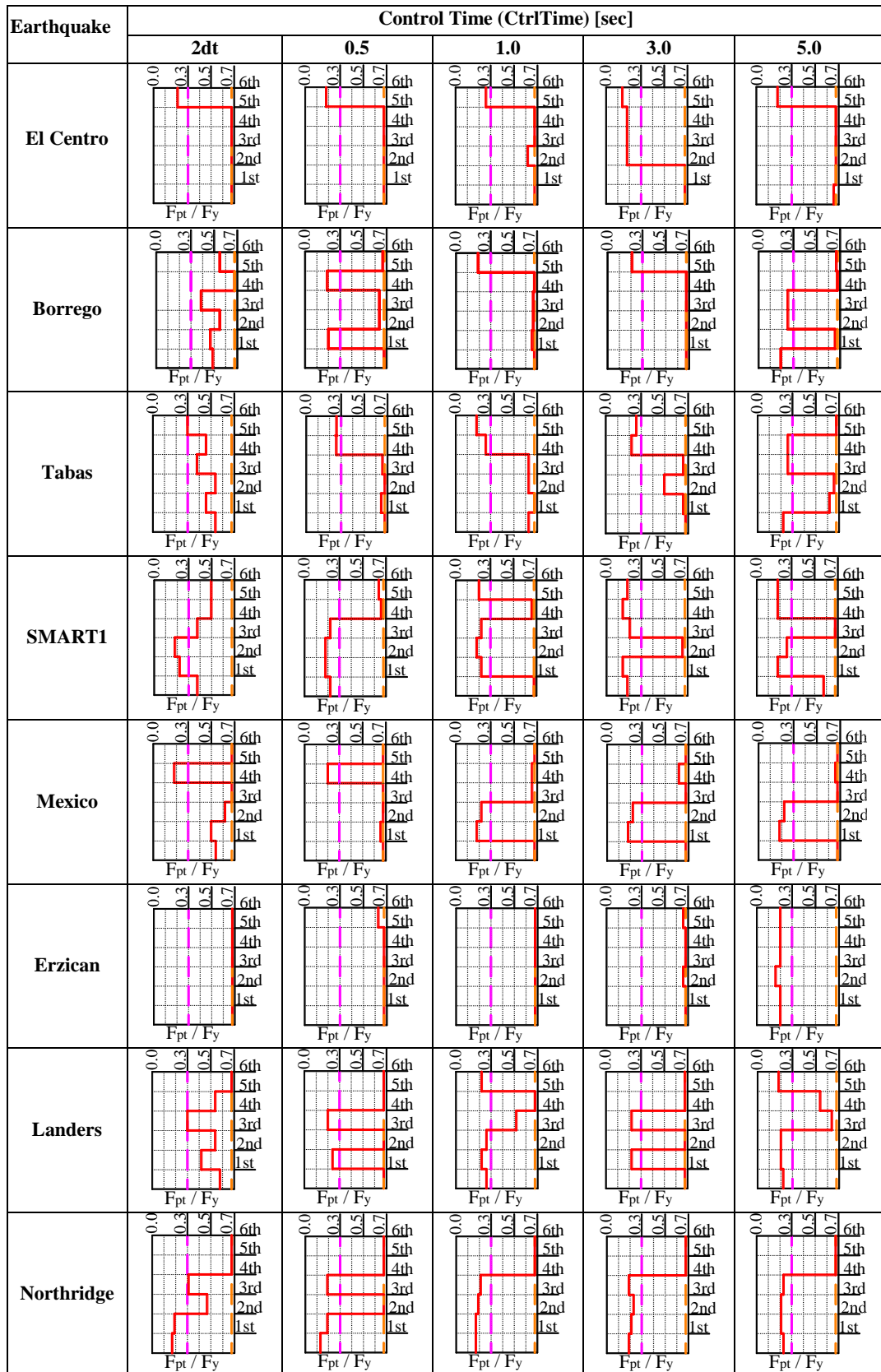


Table 8.3: Effect of the control time on resultant PT forces in the *EFSFA*.

Storey	1 st	2 nd	3 rd	4 th	5 th	6 th
Final Connection Stiffness	k_2	k_2	k_2	k_2	k_0	k_0

Table 8.4: Stiffness pattern after SMART1 earthquake.

The reduction of reliability of the running frequency content analysis is a result of the addition of new frequency component with the new added segment of the earthquake history. The new frequency components might heavily alter results of the frequency content obtained from previous analyses. When significant changes are imposed to the frequency content, the stiffness pattern becomes different. The longer the control time, the more frequency components could be added to the frequency content and as a result the stiffness pattern would never stabilise as an optimal pattern. Figure 8.15 shows changes on running frequency content of Northridge earthquake where it can be seen that when the analysis included the record up to 3.0 sec, the major frequency component was at about 3.5 Hz which is higher than natural frequency of the second mode of all stiffness patterns. New low-frequency peaks were added for analyses of the record up to 6.0 sec and 9.0 sec. This made stiffness pattern selected for the first analysis no longer valid.

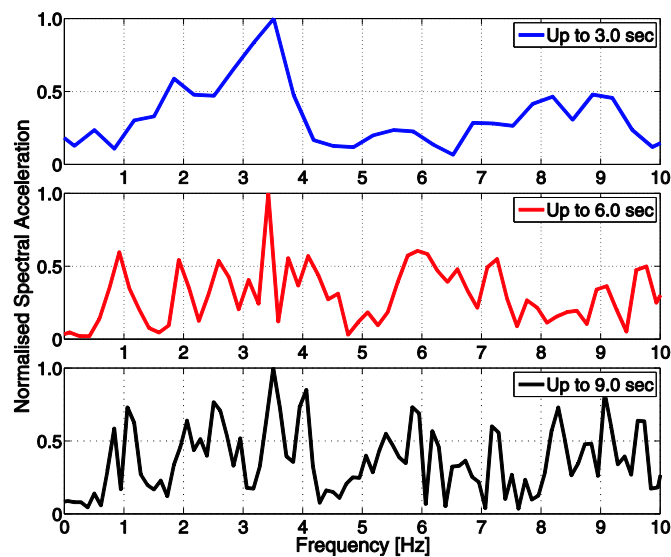


Figure 8.15: Development of the spectral acceleration results for Northridge earthquake.

This effect can again be seen in Figure 8.16 which shows the development of the frequency content with every control time interval associated with the optimum stiffness pattern (target stiffness pattern) for SMART1 earthquake.

When the frequency content of the earthquake contains several peaks within the frequency range of the structure, the optimisation process may lead to wrong stiffness patterns as results of the weighted spectral acceleration would be very similar. Also, the change of the stiffness pattern may cause jumping of the frame frequency from one peak to another when the minimum is in between two peaks.

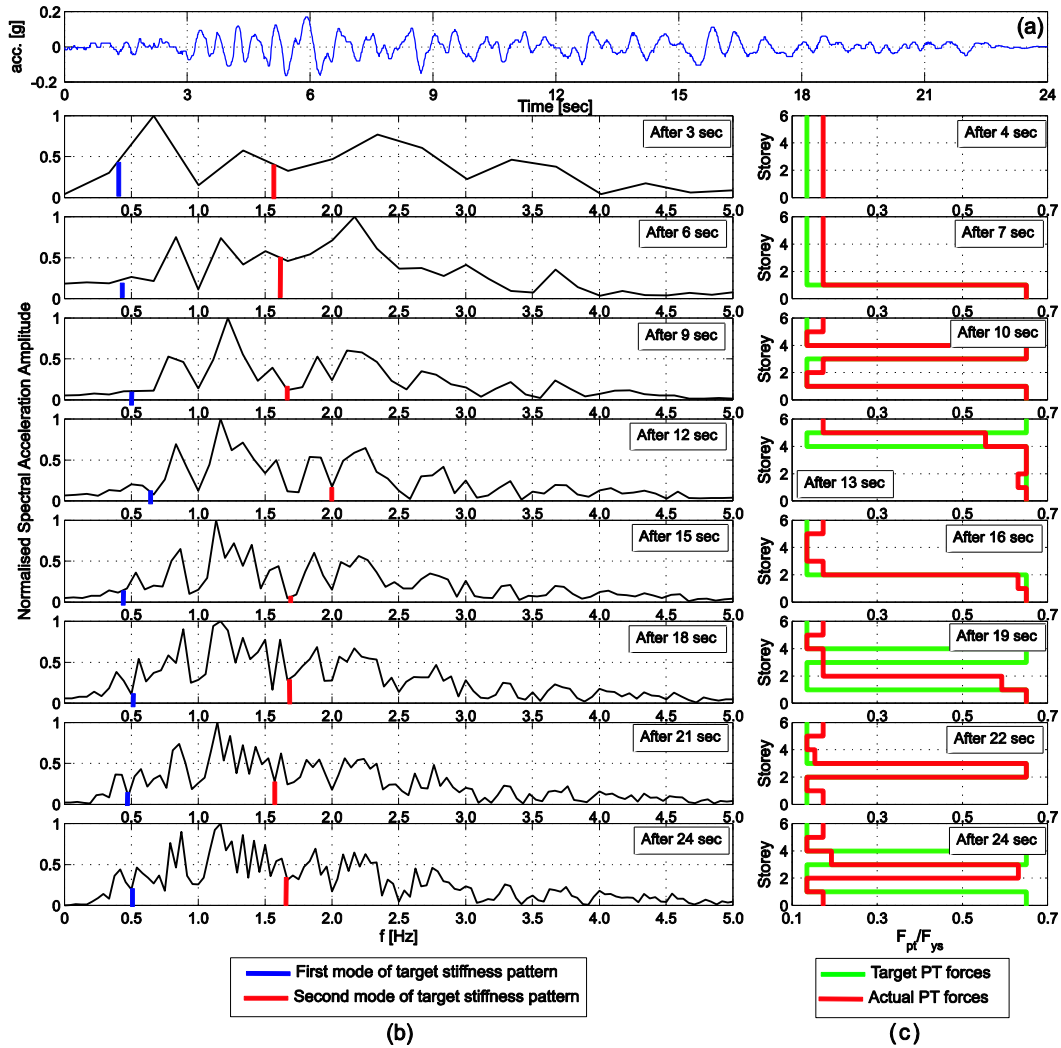


Figure 8.16: Development of frequency content and PT forces pattern for SMART1 earthquake: (a) earthquake time history, (b) updates of frequency content with time and (c) development of PT forces (actual and target).

The type of the exciting earthquake therefore significantly influences the selection of the control time interval. Earthquakes with several frequency peaks require longer control time to increase the reliability of the frequency content; whereas those with fewer peaks may show good response to the *EFSFA* when shorter control time intervals are used.

(iv) Analysis of Control Time from the Aspect of the Rotating Motor

Post-tensioning forces in each storey of the *EFSFA*-controlled frames switch their values between high and low forces when the stiffness pattern is changed. PT forces are changed by using rotating motors which cannot perform the changes instantly. Time required to switch between high and low PT forces (T_{switch}) is obtained from:

$$T_{switch} = \frac{|F_{ptHigh} - F_{ptLow}|}{(\Delta f / \Delta t)_{max}}, \quad (8.3)$$

where F_{ptHigh} is the upper limit of post-tensioning forces, F_{ptLow} is the lower limit of post-tensioning forces and $(\Delta f / \Delta t)_{max}$ is the maximum rate of increment in control force offered by

the rotating motor. Control time of the *EFSSFA* should therefore be long enough to allow for the rotating motor to switch between F_{ptHigh} and F_{ptLow} . If the control time was shorter than T_{switch} , the frame would not have sufficient time to achieve the required stiffness pattern. In this case, the resultant PT forces may become neither low nor high and the required stiffness patterns could not be achieved.

This effect can be seen in Figure 8.16 where the target PT forces are different from the actual PT forces. To quantify the difference between the target and the actual forces, two indices are used:

$$J_1 = \frac{\sum |F_{pt-act} - F_{pt-tar}|}{\sum F_{pt-tar}}, \quad (8.4)$$

$$J_2 = \frac{STD|F_{pt-act} - F_{pt-tar}|}{\sum F_{pt-tar}}, \quad (8.5)$$

The first index (J_1) represents the total difference between target and actual post-tensioning forces whereas the second index (J_2) represents the distribution of the differences over the storeys of the frame. The lower the value of these indices is, the smaller the difference is. Table 8.5 presents the value of J_1 and J_2 for SMART1 earthquake.

Time (sec)	J_1	J_2
4.0	0.285	0.000
7.0	0.145	0.011
10.0	0.042	0.010
13.0	0.023	0.062
16.0	0.031	0.009
19.0	0.031	0.115
22.0	0.087	0.015
24.0	0.218	0.127

Table 8.5: Indices of difference between target and actual PT forces.

It can be concluded that control time interval of the *EFSSFA* should be long enough to increase reliability of the running frequency analysis, include major frequency components, allow stabilising the structure damping, and allow for the motors to achieve the required force levels. The intervals should be short enough however so the structure does not experience late response. Hence, determining the best control time for the *EFSSFA*-controlled frame is a very complex and interactive process that needs further research.

8.3. Response Frequency State Feedback Algorithm (RFSFA)

8.3.1. Concept and Operation of the RFSFA

Since results of the *EFSSFA* control algorithm were found to be very sensitive to the type and the frequency content of the exciting earthquake, the **Response Frequency State Feedback**

Algorithm (RFSFA) was introduced as an attempt to reduce the effects of the frequency changes of the earthquake. In the *RFSFA*, frequency analysis is performed on accumulated response vector instead of the earthquake record. The *RFSFA* is a closed-loop control algorithm where control gains (F_{control}) are decided based only on response of the controlled system. The analysed response vector in the *RFSFA* was selected as the acceleration of the top-storey as shown in the flowchart of the *RFSFA* (Figure 8.17).

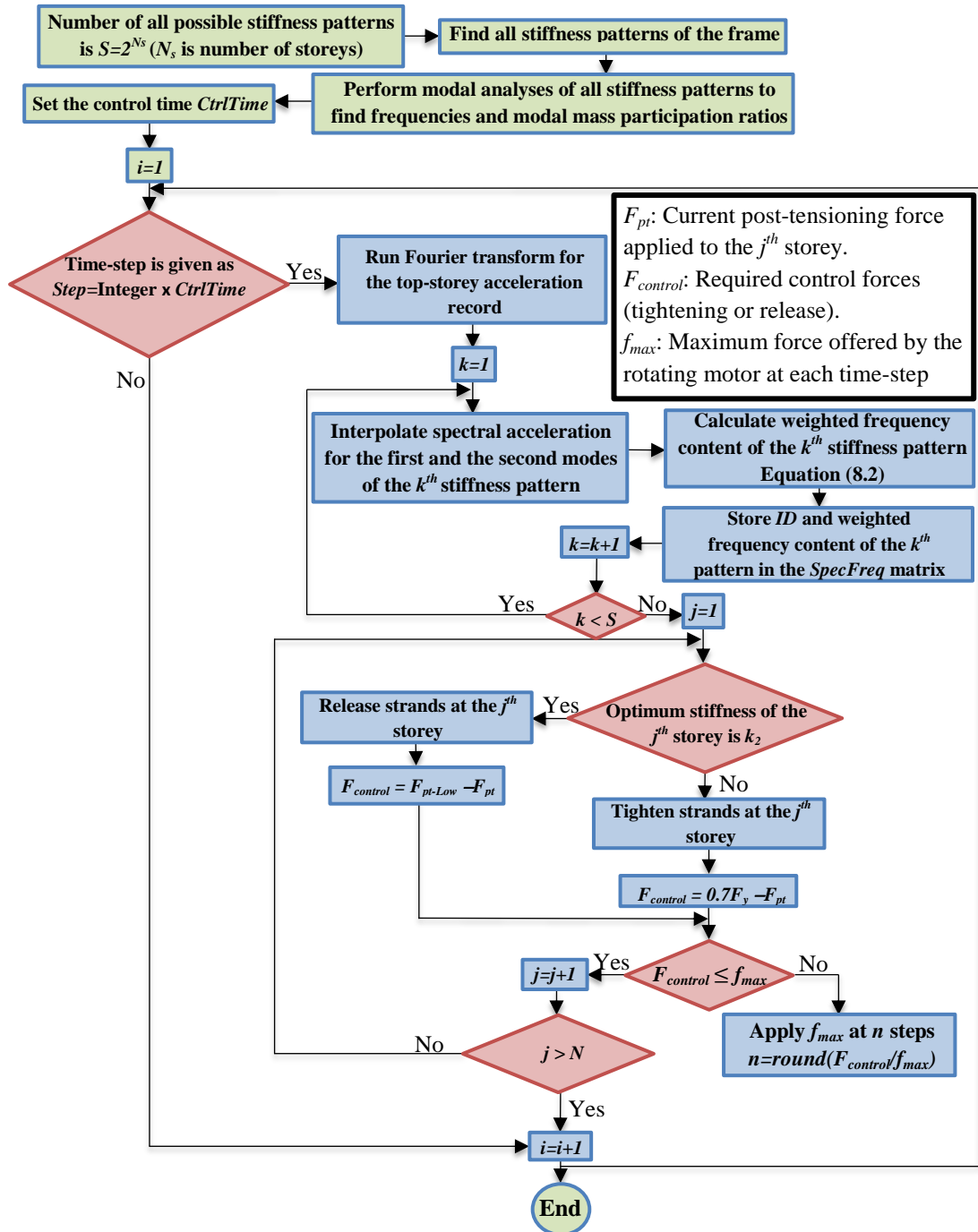


Figure 8.17: Flowchart of the response frequency state feedback control algorithm.

If the *RFSFA* is used instead of the *EFSFA*, two improvements are expected to be achieved: (i) reducing the effect of earthquake characteristics on the algorithm performance, (ii) incorporating frame properties in deciding the algorithm gains.

Effects of the earthquake characteristics are reduced when using the *RFSFA* as spectral acceleration of the response does not include the frequency components which have a minor effect of the frame response. It is shown in Figure 8.18 that the spectral amplitudes of the response at frequencies between the two modes of the structure are lower than the corresponding excitation amplitudes. Thus, the structure in this case acts as a filter of the earthquake record. The reliability and efficiency of the control algorithm increase by reducing the effects of high frequency components of the excitation that have little effect on the response of the frame.

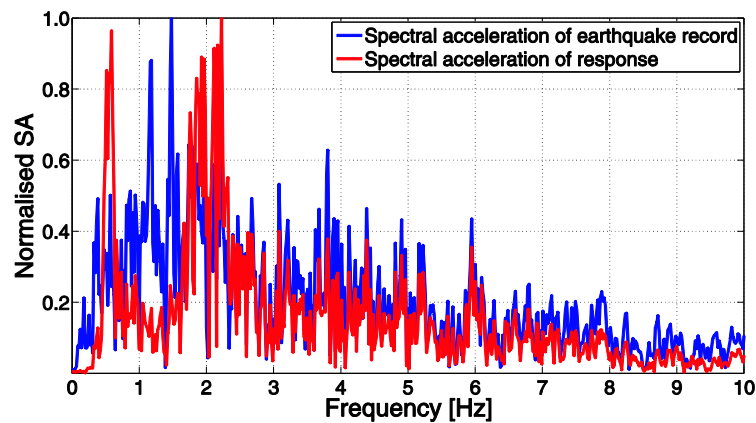


Figure 8.18: Spectral accelerations of earthquake and response (El Centro).

The *RFSFA* allows inclusion of the structure modal properties in optimising stiffness patterns and determining control gains of the algorithm. Frequency content of the response acceleration shows peaks at frequencies of the natural modes and reduces values of the spectral acceleration at frequencies that do not correspond to any mode of vibration. This is shown in Figure 8.18 (red graph) where the first peak in the response spectrum occurs at about $f=0.6$ Hz, which is the natural frequency of the first mode and the second peak at about $f=2.0$ Hz, which is the natural frequency of the second mode of the passive PT frame. The spectral acceleration amplitudes of the response are significantly reduced from those of the earthquake record between $f=0.6$ Hz and $f=2.0$ Hz where there are no major modes of vibration despite the fact that the predominant frequencies of the earthquake are between 1.1 Hz and 1.5 Hz. Therefore, normalised frequency content of the frame would be similar for a range of different earthquakes (Figure 8.19).

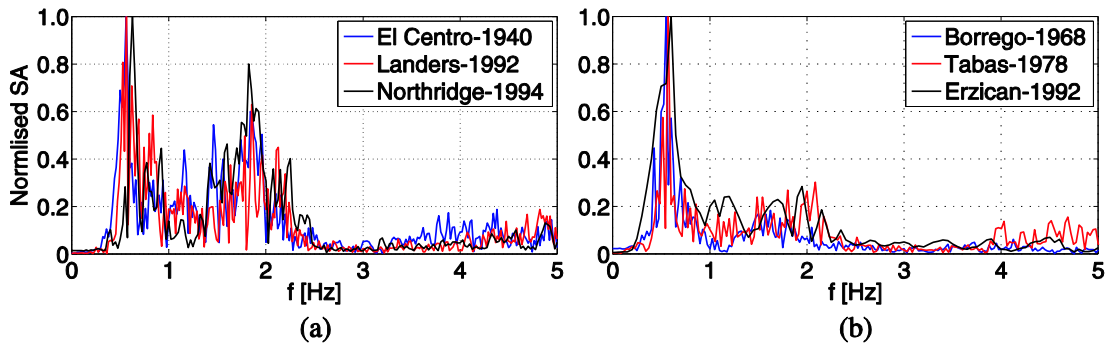


Figure 8.19: Frequency content of response acceleration: (a) high effect of second mode and (b) low effect of second mode.

8.3.2. Results of the *RFSFA*

Results of the *RFSFA* showed that this algorithm reduced the frame displacements when relatively long control time was used (Figure 8.20). In most cases, the best performance of the *RFSFA* corresponded to $CtrlTime = 3.0$ sec \sim 5.0 sec. Displacements of the *RFSFA* however, were not significantly reduced from those achieved with the *EFSFA* control.

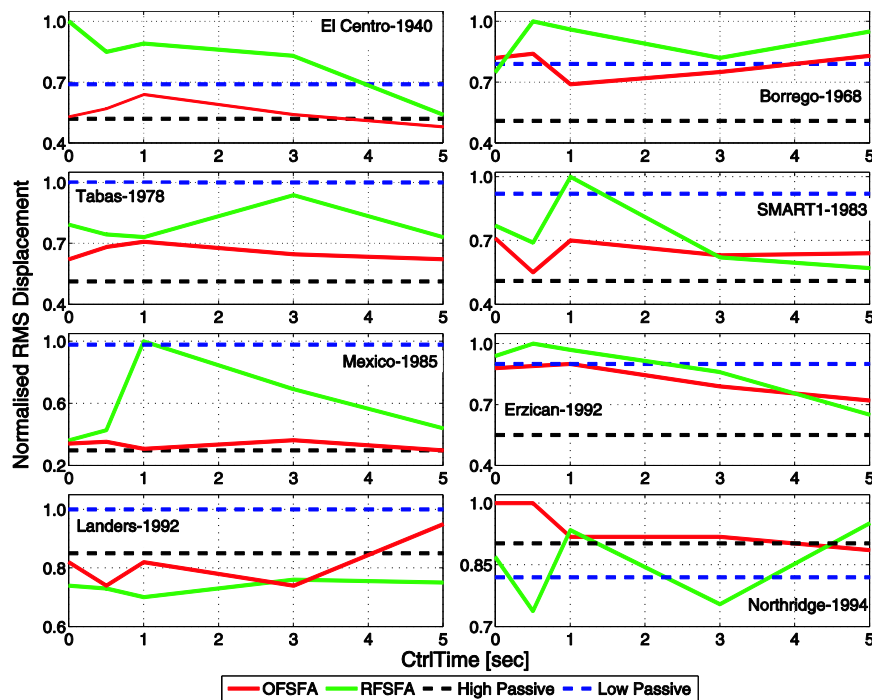


Figure 8.20: Effect of control time on the *RFSFA* performance.

Except for Northridge and Landers earthquakes, the general performance of the *EFSFA* was better than *RFSFA*. Displacements from the *RFSFA* for $CtrlTime = 5.0$ sec were similar or reduced from *EFSFA*. Despite the fact that these displacements were not very reduced, they indicated that relatively long control time would result in acceptable behaviour of the *RFSFA*.

Sensitivity of the *RFSFA* was higher than the *EFSFA* as its behaviour showed very unstable behaviour for different earthquakes. This is because the frequency content of the *EFSFA*-controlled frame represents the exciting earthquake as changing stiffness pattern of the frame does not affect the frequency content of earthquake. In *RFSFA*, the frequency content represents different states of the frame as the frame status (stiffness pattern) may change every control time. Therefore, frequency content of the frame response up to k control times is composed of the frequency content of up to k different states of the frame (different patterns) which explains the instability of the *RFSFA*.

Also, robustness of the *RFSFA* seemed to be very low as it did not show steady performance for different earthquakes. The algorithm showed very good performance for Landers earthquake, whereas its performance was worse for El-Centro, Borrego and Mexico City earthquakes. Efficiency of the algorithm was significantly affected by the control time for other earthquakes.

Results of the *RFSFA* and the *EFSFA* at CtrlTime= 1.0 sec for Mexico City and Landers earthquake (Figure 8.20) were interesting. For Mexico City earthquake, displacements of the *RFSFA* frame were significantly higher from those of the *EFSFA*, whereas for Landers earthquake they were significantly reduced. To investigate the reason of this performance, frequency content for the two earthquakes is plotted with the frequency content of the response acceleration and the final stiffness patterns (Figure 8.21).

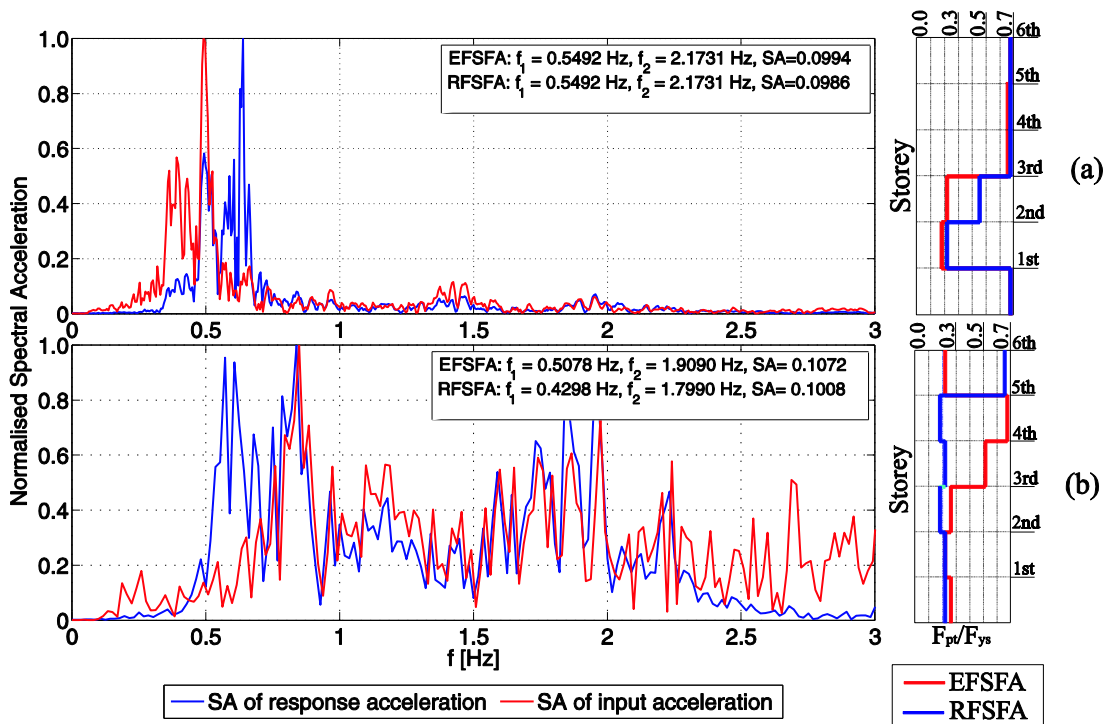


Figure 8.21: Frequency content of input and response accelerations with their final stiffness patterns: (a) Mexico City earthquake and (b) Landers earthquake.

Figure 8.21 shows that the structure subjected to Landers earthquake avoids the first (low frequency) peak of the excitation, which results in reduced displacements in the response. This is not the case for the Mexico City earthquake where the structure amplifies the low frequency content of the excitation, resulting in large response displacements. It should be noted that the structure amplifies specific frequencies corresponding to its stiffness patterns which may match the minima of the spectral acceleration of the excitation. Also, the range of frequencies that is offered by PT frames is relatively narrow. Therefore, change in the stiffness pattern of the frame may not result in improvement in its behaviour if it shifts the frame from a peak in the frequency content to another one.

The final PT forces in the *RFSFA*-controlled frame indicate that applying the *RFSFA* reduces the post-tensioning forces in the frame and therefore, reduces the moment demand on the columns (Figure 8.22). In most cases, the predominant stiffness pattern was the one with lowest PT forces (yield of all PT connections) with $f_i=0.4$ Hz. It can be seen that PT forces of the *RFSFA*-controlled frame are significantly lower than the corresponding forces of the *EFSFA*-controlled frame while the displacements resulted from applying the *RFSFA* are not significantly larger than those resulted from applying the *EFSFA*. Therefore, the *RFSFA* was able to reduce the force demand on the frame while keeping acceptable level of displacements.

8.4. Filtered Excitation Frequency State Feedback

Algorithm (FEFSFA)

8.4.1. Changes from the *EFSFA*

Results of the *EFSFA* showed high sensitivity to the earthquake type and frequency content. Frequency contents of exciting earthquakes showed frequent variations of the spectral acceleration with frequency. On the other hand, the frequency content of the *RFSFA* was not consistent as it included the frequency content from the acceleration response of frame with different stiffness patterns (different modal properties).

The **Filtered Excitation Frequency State Feedback Algorithm (FEFSFA)** attempts to maintain advantages of the *EFSFA* and the *RFSFA* and eliminate their disadvantages. The *FEFSFA* uses the frequency content of the exciting earthquake as it is a consistent analysis of the earthquake records, but it tries to reduce its sensitivity by filtering high frequency components.

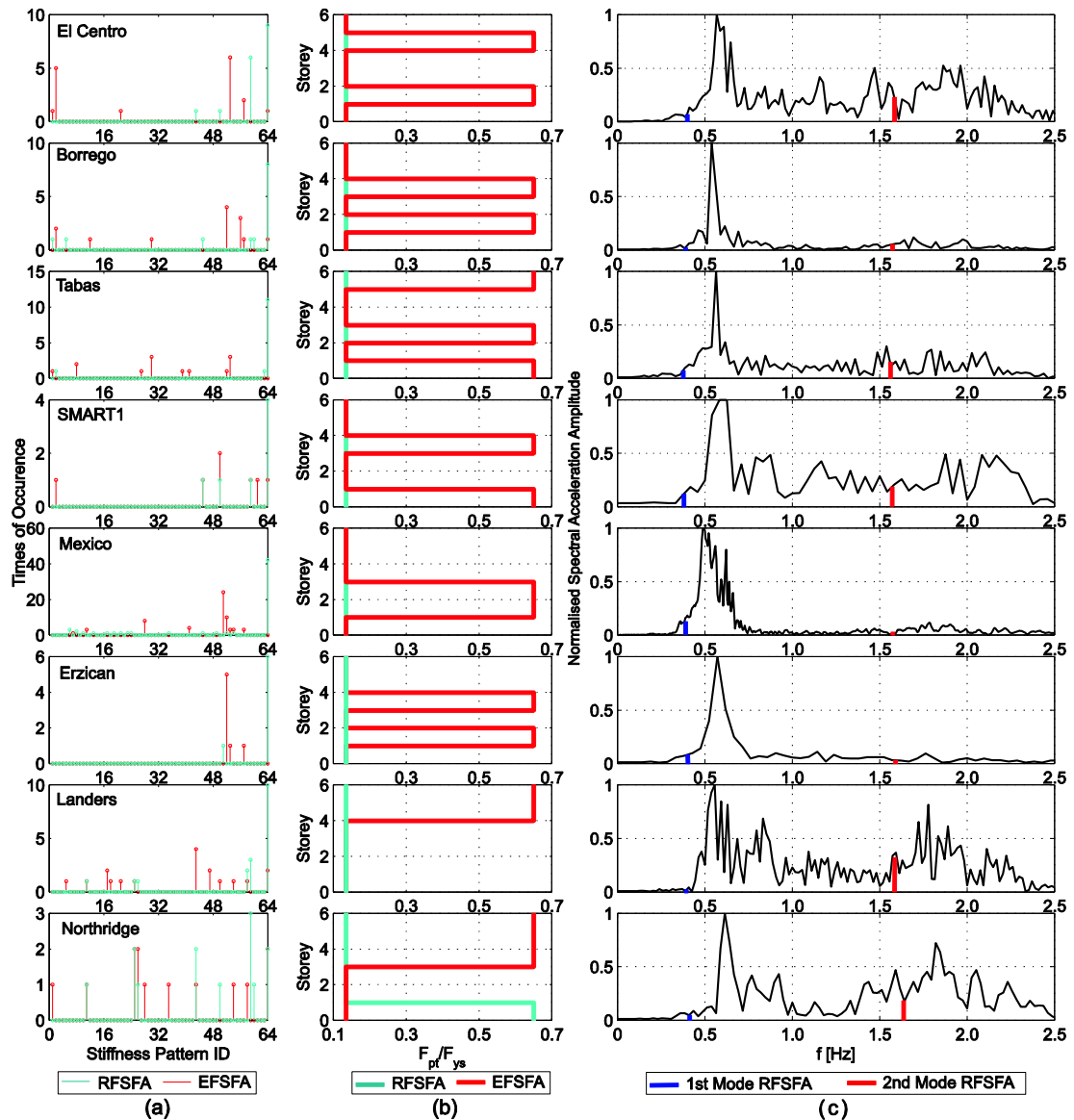


Figure 8.22: Predominant stiffness patterns of the *RFSFA*-controlled frame for different earthquakes: (a) finding the predominant stiffness pattern, (b) PT forces of the predominant stiffness pattern and (c) first and second mode frequency of the predominant stiffness pattern.

To proceed with the *FEFSFA*, the earthquake record segments (within the control time intervals) are filtered using a low-pass filter. If elliptic filter is used in the algorithm, input data of the filter are: (i) order of the filter (n), (ii) frequency of band-pass edge (W_p), (iii) normalised magnitude at the cut-off frequency (R_p) and (iv) slope of the filter (R_s) (Figure 8.23).

If the filter used in the *FEFSFA* is elliptic of 2^{nd} order with $R_p = 0.1f_s$, where f_s is the sampling rate of the exciting earthquake, band-pass frequency was 20% greater than the highest second mode frequency of all stiffness patterns, and slope of the filter $R_s=0.5$, filtered signal and frequency content for Landers earthquake would be as shown in Figure 8.24. Flowchart of the *FEFSFA* is shown in Figure 8.25.

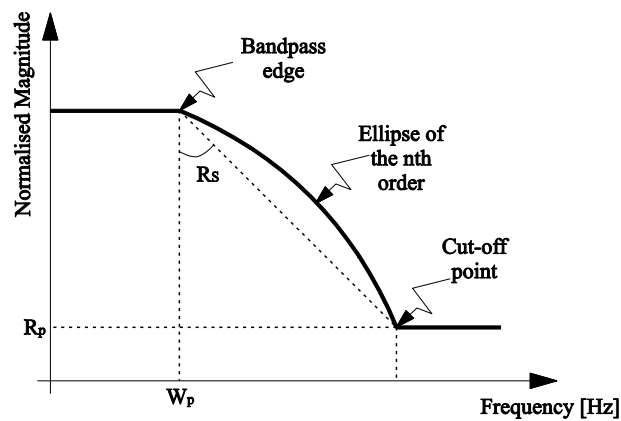


Figure 8.23: Design and input data of low-pass filter.

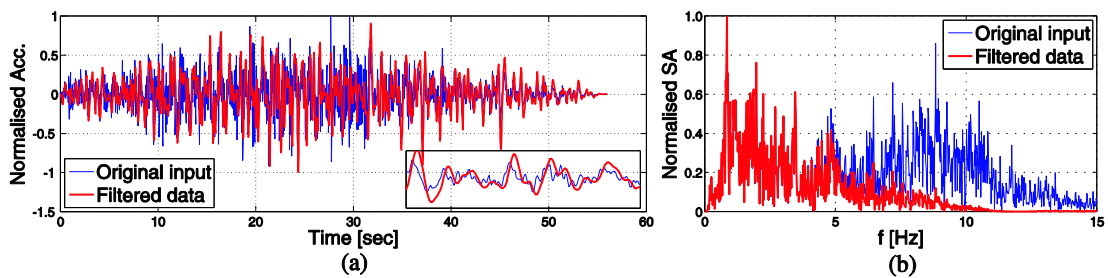


Figure 8.24: Applying low-pass filter on exciting earthquake (Input: Landers): (a) earthquake time-histories and (b) spectral accelerations.

8.4.2. Results of the *FEFSFA*

Simulations of the six-storey frame with applied *FEFSFA* showed that results were similar to those obtained from the *EFSFA* with relatively long control time intervals used in the algorithm (Figure 8.26). These results indicated that applying the filter did not significantly affect the efficiency of the *EFSFA*. The *FEFSFA* however showed less sensitivity to the chosen control time as shown for Borrego, Mexico City and Landers earthquakes.

Similarity in results of the *EFSFA* and the *FEFSFA* indicated that weighted frequency and final stiffness patterns of the two algorithms are very similar (Figure 8.27). This similarity is a result of filtering frequencies that are higher than the frequency of the second mode. These high frequencies do not contribute to the optimisation process as both *EFSFA* and *FEFSFA* use only the first and the second mode frequencies. Eliminating the effect of higher modes is reasonable in low to mid-high frames as their contribution to the total mass participation is less than 10%. In high and very high frames, contribution of higher modes is significantly greater, and therefore, if the *EFSFA* and *FEFSFA* algorithms are used in high to very high buildings, they have to be modified to include the effect of modes higher than the second mode.

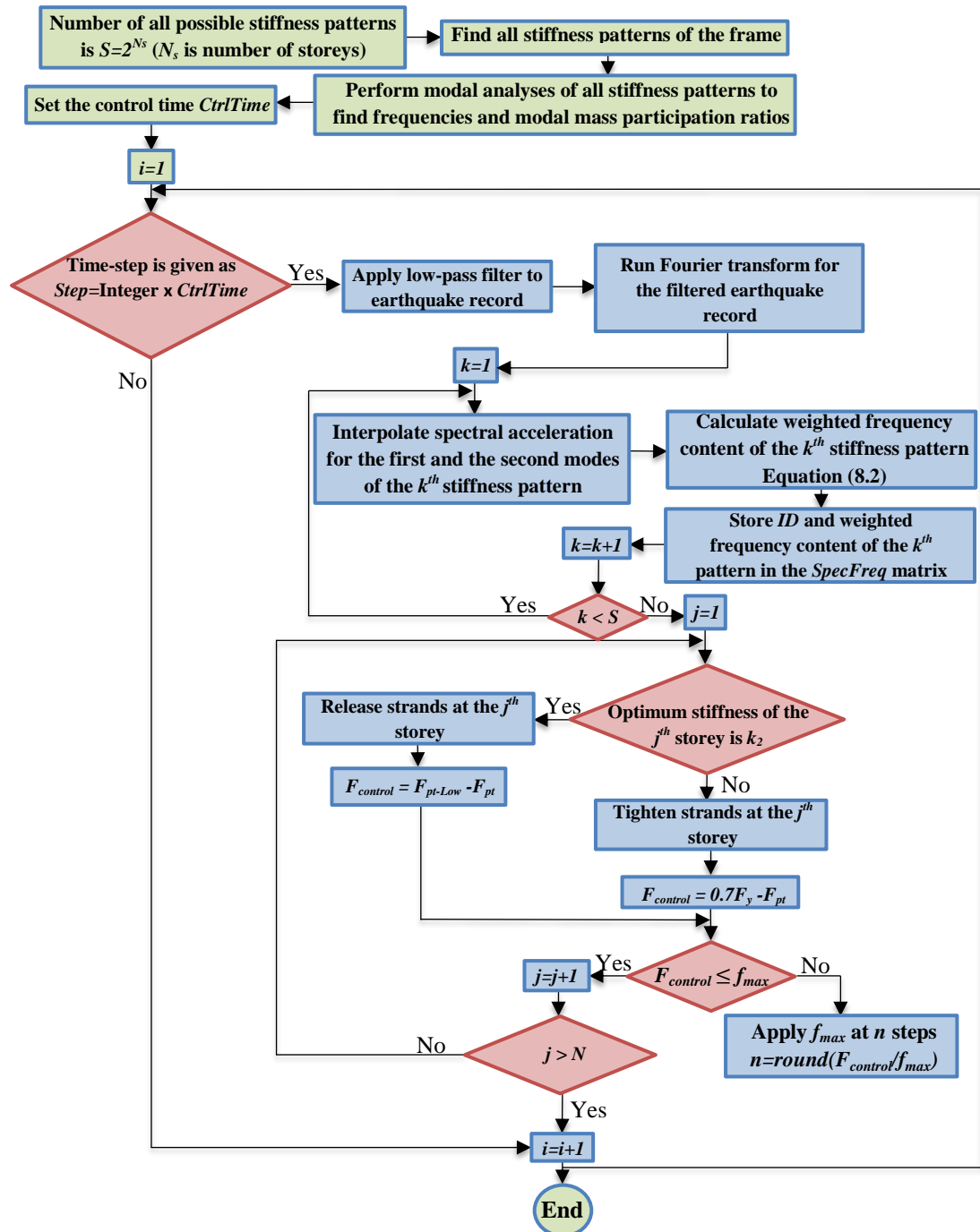


Figure 8.25: Flowchart of the filtered excitation frequency state feedback control algorithm.

It should be noted that since the weighted frequency content of the FEFSFA includes only the first and the second modes of vibration, and as long as $w_p > f_2$ (maximum frequency of the second mode in any possible stiffness pattern), the filter parameters w_p , R_p and R_s will have a minor effect on the algorithm results. The slope of the filter (R_s) however should not be too steep as this would result in a leakage in the frequency content of the recorded signal. The leakage would be a result of eliminating high number of points which have high frequency components resulting in reduced number of elements in the signal record. This affects the accuracy of the algorithm because of the reduced accuracy in the spectral

acceleration results. It is worth reminding that the Fourier Transform was derived originally with an assumption that the signal is continuous and infinite. Therefore, shortening the duration of the signal as well as reducing the number of elements in the discretised signal would severely influence the results of the frequency analysis.

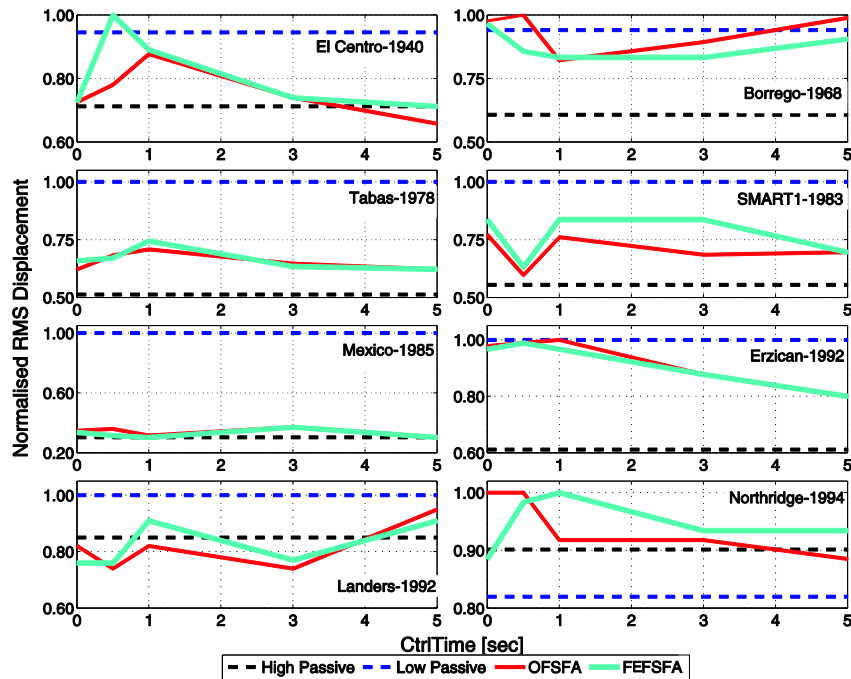


Figure 8.26: Effect of control time on the FEFSFA performance.

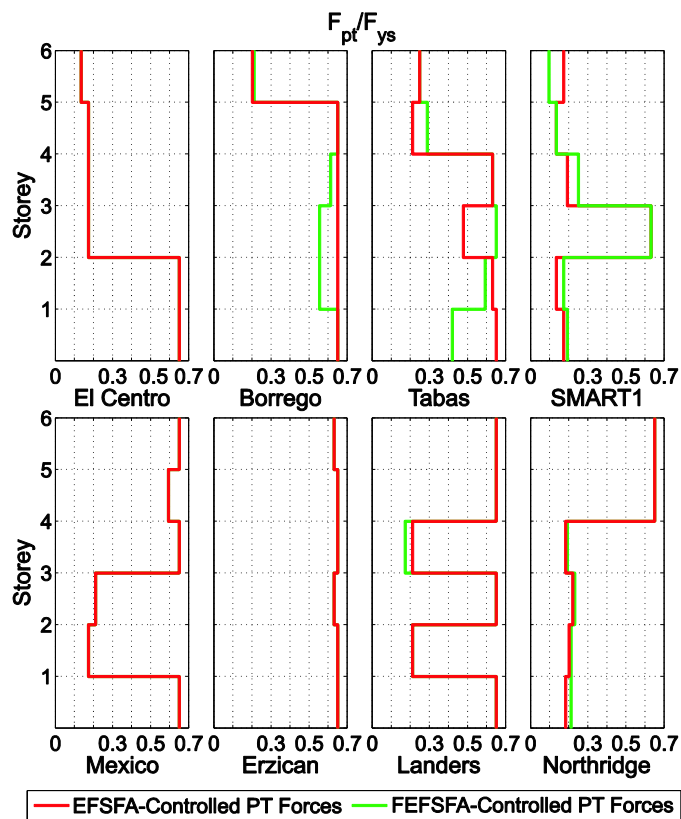


Figure 8.27: Similarity in final stiffness pattern between EFSFA and FEFSFA.

8.5. Stiffness Control Approach using Active Variable Stiffness System

The work done by Kobori et al. 1993 was the first to use the stiffness control approach to suppress the dynamic response of a three-storey steel braced frame. The aim of his work was to reach a non-resonant situation of the frame by varying the stiffness of the frame.

Although the active variable stiffness system used by Kobori et al. 1993 was designed only for braced frames and it had no relation with controlling post-tensioned steel frames, the overall idea was to select the optimum stiffness type (stiffness pattern) of the frame as shown in Figure 8.28.

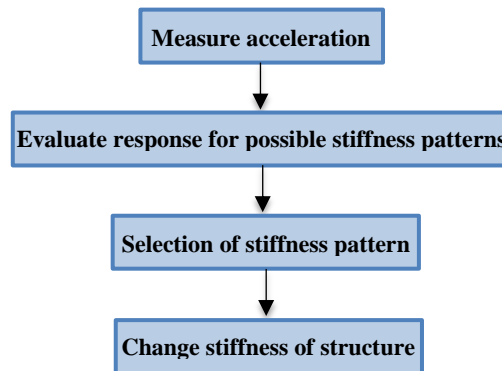


Figure 8.28: Control algorithm proposed by Kobori et al. 1993.

The main difference between Kobori's work and the work proposed in this thesis is the algorithm adopted to select the optimum stiffness pattern at each time interval. While the Frequency State Feedback algorithms use the frequency content to decide the optimum stiffness of the frame, Kobori et al. (1993) used some evaluative indices to evaluate the response of each possible stiffness pattern. These indices employed some coefficients which were not deterministic as their values were based on simulations of the structural response under several earthquakes with different characteristics.

Also, in order to avoid control complications resulted from having several possible stiffness patterns, Kobori et al. 1993 used only three stiffness patterns instead of eight which is the number of possible stiffness patterns for a three-storey frame. No information was given for the eliminated stiffness patterns and the method of selecting only three of them. This elimination would significantly affect the accuracy of the control algorithm if used for structures with higher number of storeys.

Time intervals used in Kobori experiments was 4 msec which is relatively short time for the structure to stabilise with every new stiffness pattern. Using this short control time intervals, this algorithm cannot be used for realistic control of multi-storey frames, as the time needed

for motors to achieve the forces required for the different stiffness patterns would be significantly longer. Most importantly, the work did not provide any information of the effect of the control time intervals on the efficiency of the control algorithm which significantly magnified the maximum displacement response of the frame when subjected to the 2nd February 1992 earthquake (Figure 8.29).

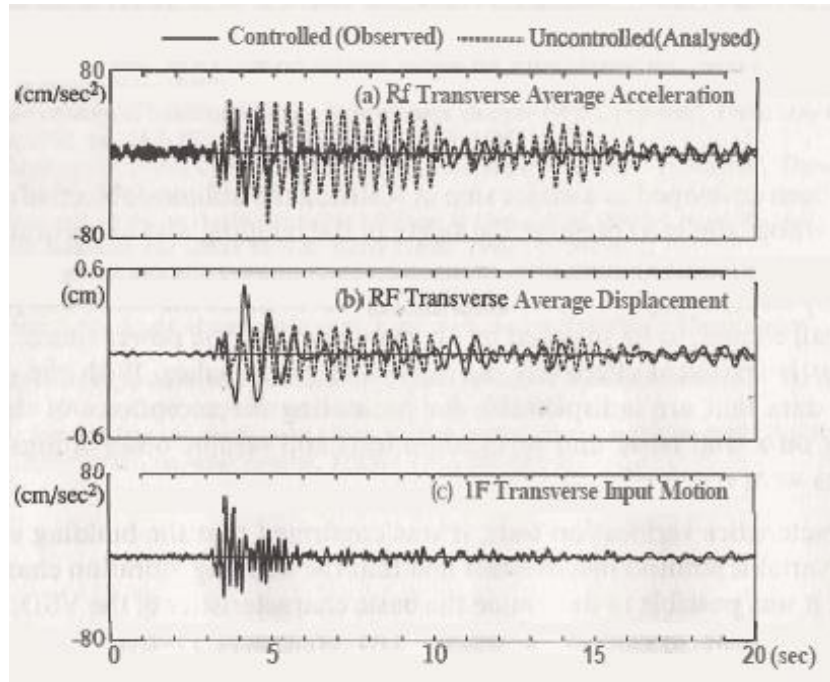


Figure 8.29: Control effect under the 2 February 1992 earthquake (Kobori et al. 1993).

8.6. Centralisation of Stiffness-Based Control Algorithms

Centralised control refers to controlling the whole structure using one main computer. Centralised control systems introduce better control for relatively short to medium high structures where the response of any storey cannot be separated from the adjacent ones.

The stiffness control approach is a centralised control approach where the structure responds to one control action to change a property of the structure (i.e. natural frequency). In this approach, post-tensioning forces in master connections work together and form specific patterns of loading or unloading. It is shown in Figure 8.30 that control forces of each storey are arranged in separate sets, comprising extended constant levels and successions of increments, which can be positive or negative. Each set represents control forces needed by the storey to change its stiffness (k_0 to k_2 or k_2 to k_0). If the increment is negative, the storey switches its stiffness from k_0 to k_2 and vice versa. These sets are synchronised in stiffness-based control algorithm as force increments at different storeys start exactly at the same

time. The sets are synchronised as a result of one control action, such as “change stiffness pattern from pattern I to pattern J ”. This control action contains the required PT forces for all storeys of the target stiffness pattern as well as the differences in PT forces between the current and required stiffness pattern. It can be seen that control forces of the 1st, 2nd, 5th and 6th storeys are synchronised during the first set (from 16.0 sec to 21.5 sec). While the 3rd and 4th storeys are synchronised during the second set (from 15.0 sec to 21.5 sec).

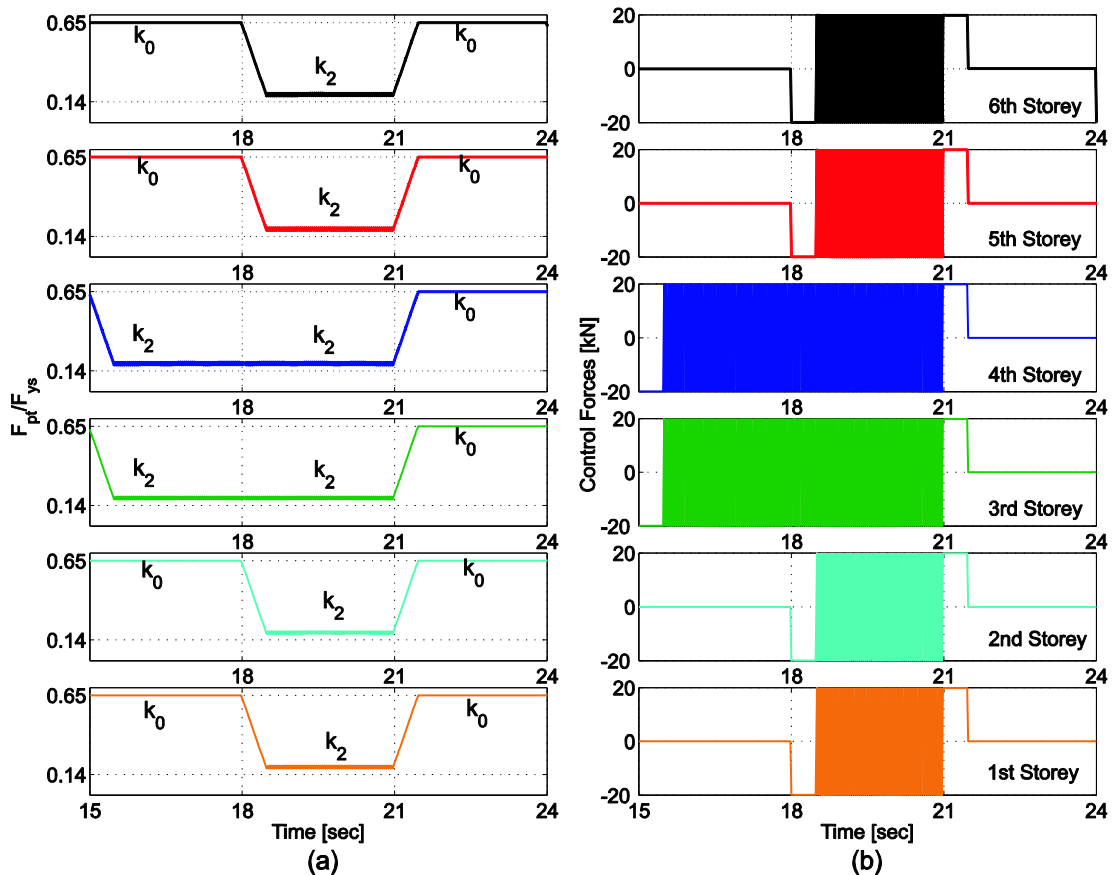


Figure 8.30: Centralisation of control forces in stiffness control algorithms: (a) PT forces and switching between k_0 and k_2 and (b) control forces time-histories for the EFSFA (input: Mexico City earthquake).

Structures with stiffness-based control algorithms can be considered as Single-Input-Multi-Output systems (SIMO). The input of the control algorithm is one measurement which can be acceleration of the earthquake or the response acceleration, whereas the output is control force acting at each storey (Figure 8.31). Although the control gains could be different for different storeys, they are all combined in one vector which is the output of the controller. Therefore, the output of the controller is not k separate values; it is a single vector including k values.

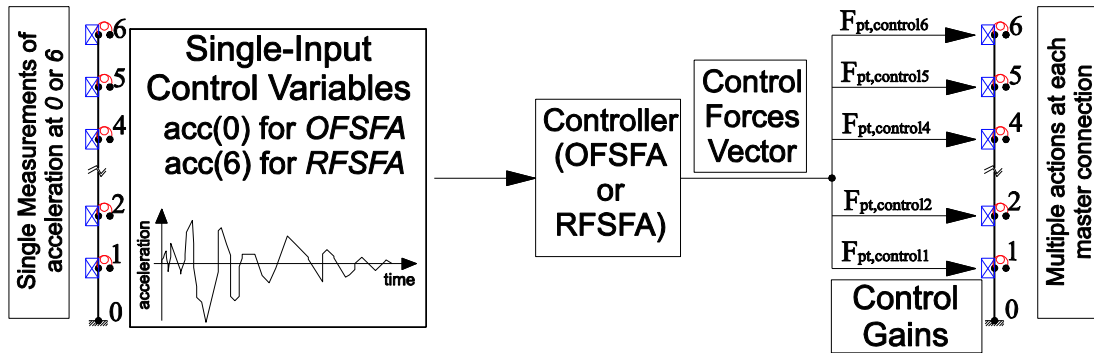


Figure 8.31: Operation of stiffness-based control algorithms as SIMO systems.

8.7. Concluding Remarks on Stiffness Control Approach

In this chapter were presented stiffness-based control algorithms for controlling the dynamic response of PT steel frames. All algorithms were based on performing Fourier analysis of the acceleration records at specific constant time intervals (control time), defined as an input parameter for the algorithms.

The Excitation Frequency State Feedback Algorithm (EFSFA) performed Fourier analysis of the earthquake record (e.g. recorded at the foundation). The results of frame response simulations with applied *EFSFA* showed that this algorithm reduced the displacements of a passive post-tensioned frame with low post-tensioning forces. When compared with a passive frame with high post-tensioning forces, the *EFSFA*-controlled frame showed reduced moment demand on columns as PT forces were reduced in some storeys.

The key element of the algorithm to achieve good performance was the selection of control time interval. The selection of control time depended on few factors including earthquake and frame characteristics, the rotating motor properties and the control algorithm. The *EFSFA* control showed high sensitivity and potential instability with different control times. In order to reduce the effect of different factors on the control time, two improvements were proposed: (i) replacing the earthquake record by the frame acceleration response and (ii) applying a low-pass filter on the earthquake record before processing it.

The response acceleration of the frame was used in the Response Frequency State Feedback Algorithm (RFSFA) instead of the earthquake record. In this case, the frequency contents of the input signal were similar for different earthquakes, showing peaks at the vibration modes of the frame which reduced the sensitivity of the controller to the frequency content of the control signal. The running acceleration spectrum (updated with every new control interval) however was not consistent as it was affected by the changes in frame stiffness patterns.

Filtering the earthquake record before processing it using Fourier analysis was introduced to avoid the inconsistency in the frequency content resulting from the RFSFA, and smooth out the frequency content of the earthquake record. The filter eliminated the high-frequency components from the earthquake record and reduced the instability, but the displacements of the Filtered Frequency State Feedback Algorithm (FEFSFA) were similar to those obtained from the EFSFA.

It can be concluded that stiffness control approach results in significant reduction of either displacements or internal forces in PT frames, provided that the control parameters are well selected. The main control parameters in the algorithms presented in this chapter is the control time interval. Optimum values of the control time need further investigation of different factors influencing the algorithm efficiency.

CHAPTER 9

SEMI-ACTIVE CONTROL OF PT FRAMES USING DEFORMATION REGULATION CONTROL APPROACH

In addition to adjusting the energy dissipation capacity and stiffness of the PT frames, post-tensioning forces can work as a regulator of the frame displacements. In this chapter are presented the concept of the deformation regulation control and the application of this approach in a control algorithm (Uniform Inter-storey Drift Algorithm - UIDA). Results, characteristics and possible improvements of this control algorithm are also discussed.

9.1. Basics of the Deformation Regulation Control Approach

The purpose of the deformation regulation approach is redistributing and organising the structural deformations over the structure. This will save the structure from having concentrated response (displacements) at one storey while other storeys are not affected. This can cause concentration of internal forces and damage in a limited number of structural elements and eventually lead to a soft storey mechanism.

In a well-designed multi-storey structure, the ratios between strength and demand (over-strength ratios) in the elements are supposed to be distributed evenly over all storeys. However, this is not achievable for passively controlled systems as the response of any frame depends also on the properties of the earthquake excitation. Therefore, the deformation regulation approach aims at rearranging the internal forces in the elements in the structure (demand), so that the over-strength ratios are evenly distributed, regardless of the properties of the exciting earthquake.

9.2. Uniform Inter-Storey Drift Algorithm (UIDA)

9.2.1. Operation of the Control Algorithm

In this control algorithm, post-tensioning forces are redistributed over the frame in order to regulate the peak values of inter-storey drift. The regulation of the inter-storey drift aims to provide an even distribution of all inter-storey drifts so there is no concentration in internal forces in one storey.

The first step in this control algorithm is determining the drift threshold at which the algorithm is activated. Drift threshold (**Thr**), defined as a ratio of storey height, is used as input in the algorithm. The inter-storey drift threshold **Thr** is a column vector with number of elements equal to the number of the storeys in the frame (one threshold values is assigned to each storey).

The operation of the *UIDA* is in three stages: (i) activation, (ii) control action, (iii) deactivation.

- (i) Activation: The algorithm is activated whenever the following two conditions are satisfied: (a) any of the inter-storey drifts has exceeded the threshold given for that storey and (b) at least one inter-storey drift has reached a peak value. The algorithm starts assembling a column vector (**PeakCode**) every time one inter-storey drift exceeds the threshold. The values of the **PeakCode** vector are 0 if the storey drift has not reached a peak or 1 if it has reached a peak. The algorithm is activated when at least one of the **PeakCode** values becomes 1.
- (ii) Control Action: When the control algorithm is activated, it computes the average inter-storey drift of all drifts in each control time step. For storeys with inter-storey drifts less than the average value, the post-tensioning forces are decreased (strands are released). For storeys with inter-storey drifts higher than the average value, the post-tensioning forces are increased (strands are tightened). The amount of increase or decrease of post-tensioning force in j^{th} storey can be obtained from:

$$F_{\text{control},j} = \frac{D_j - D_{av}}{D_{av}} F_{\text{pt},j}, \quad (9.1)$$

where $F_{\text{control},j}$ is the amount of control force that needs to be applied to reach the desired PT force, D_j is inter-storey drift, D_{av} is average of the inter-storey drifts of all storeys, and $F_{\text{pt},j}$ is post-tensioning force applied to the storey, all recorded at the moment of activation. Control force $F_{\text{control},j}$ is applied at a rate determined by the characteristics of the rotating motor, which means that a period of time is needed to complete the control action. If a new activation event occurs during this time, the

control action is interrupted and the algorithm starts a new control sequence (new control forces are calculated).

- (iii) **Deactivation:** If the control action is completed (desired PT forces are achieved), and all values of the **PeakCode** vector are 0, the algorithm is deactivated and PT forces remain unchanged until the algorithm is activated again.

As the input data of the control algorithm are only inter-storey drifts of the frame, and properties or accelerations of the excitation do not affect the algorithm outputs, the *UIDA* can be classified as a close-loop control algorithm. Figure 9.1 illustrates the operation and Figure 9.2 shows the flowchart of the Uniform Inter-storey Drift Algorithm.

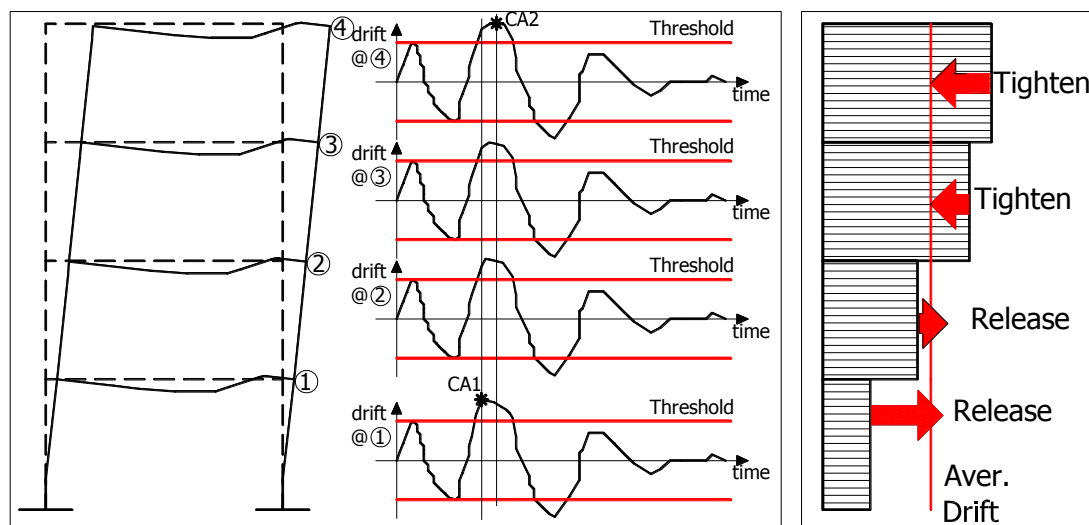


Figure 9.1: Illustration of the operation of Uniform Drift Distribution control algorithm (CA1: activation of the algorithm, CA2: new control forces calculated before completion of CA1 sequence).

9.2.2. Results of the *UIDA*

The behaviour of a structure controlled by *UIDA* was simulated by using the six-storey post-tensioned steel frame (Figure 8.5- Chapter 8). Since the level of the initial post-tensioning forces changes when the *UIDA* is applied, results of the *UIDA*-controlled frame are compared with the results obtained for a passive PT frame with different levels of passive post-tensioning forces. The low post-tensioning force ($F_{pt} = 0.3 F_{ys}$) is used as initial PT force of the *UIDA*-controlled frame. Then the *UIDA*-controlled frame is compared with passive PT frames with high post-tensioning forces determined from the highest level of PT forces reached when applying the *UIDA*. The only input parameter of the *UIDA* is the drift threshold (Thr) at which the algorithm starts performing. The value of $Thr = 0.005$ was used in the initial simulations, and this value is discussed later in this chapter. A comparison of the top storey displacement between the *UIDA*-controlled frame and the passive frame with low PT forces ($F_{pt} = 0.3 F_{ys}$) is presented in Figure 9.3.

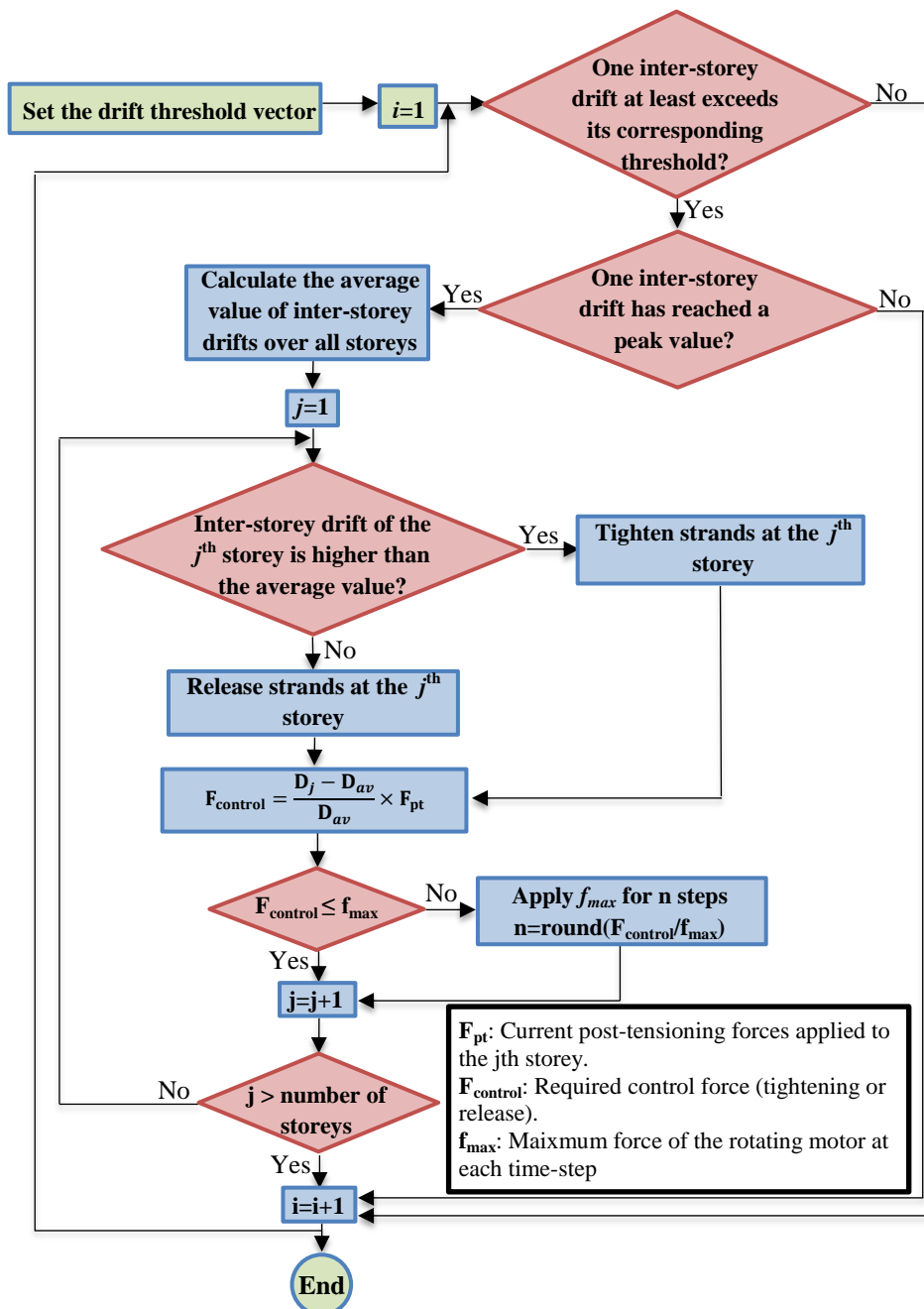


Figure 9.2: Flowchart of the uniform inter-storey drift control algorithm.

Since the operation of the *UIDA* does not depend on the global frame characteristics such as stiffness and energy dissipation capacity, displacements of the frame could be increased when applying the algorithm as it changes the frame stiffness by increasing the PT forces in some storeys while reducing them in other storeys. Therefore, although reducing the top storey displacement is not an explicit objective of the *UIDA*, it is highly important to check these displacements to ensure that the algorithm does not result in magnifying the frame response. When the top storey displacements of the *UIDA*-controlled frame are reduced this could be simply a result of the increased PT forces in some storeys (Figure 9.3). This

increase in PT forces is shown in Figure 9.4 where the resultant post-tensioning forces in each storey are plotted. Resultant PT forces show that the *UIDA* tends to increase the post-tensioning forces in the second, third, fourth and fifth storeys whereas it reduces the post-tensioning forces in the top and the bottom storeys.

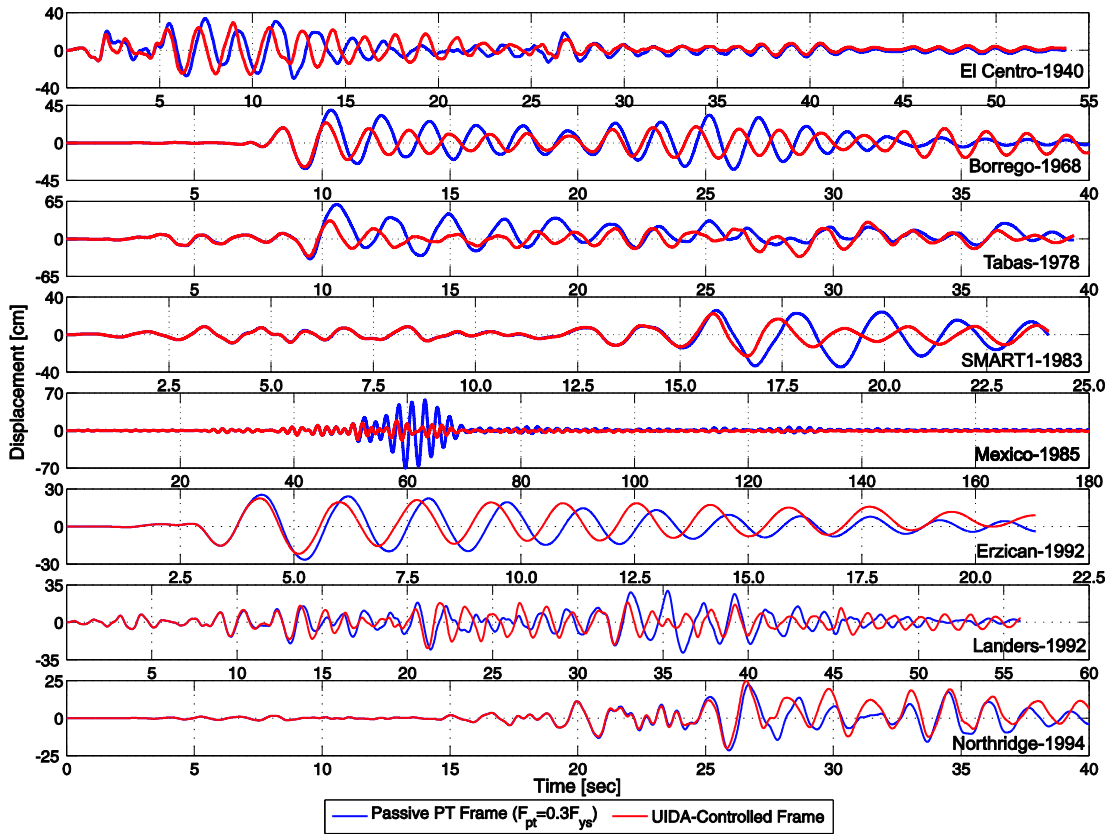


Figure 9.3: Top storey displacements for passive and *UIDA*-controlled PT frames.

Results shown in Figure 9.4 suggest that the first and the top storey experience less inter-storey drift than other storeys and hence, the *UIDA* tends to reduce their PT forces in order to increase their inter-storey drifts and equalise them with the inter-storey drifts of the other storeys. The resultant PT forces show similar patterns for all earthquakes for this frame, but there are some differences in the final value of the resultant force. These can be explained by taking into account different factors. One of these factors is the effect of different modes of vibration on the frame response. This effect can explain the higher resultant PT forces in the top storey under Borrego than those of the Mexico City earthquake. In these cases, the second mode of vibration shows higher contribution to the total response of the frame under Borrego than under Mexico City earthquake (Figure 9.5).

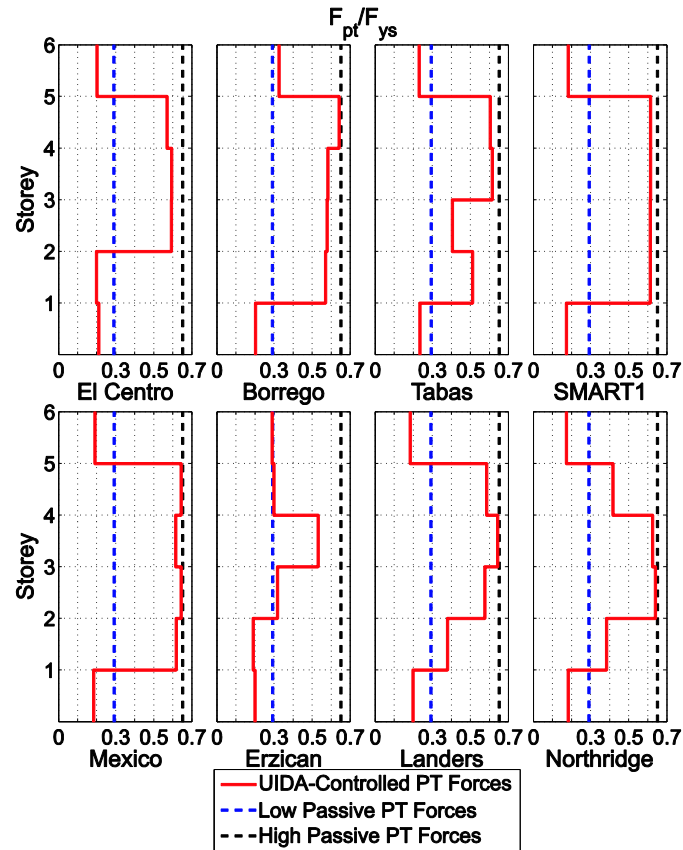


Figure 9.4: Resultant PT forces in *UIDA*-controlled frame.

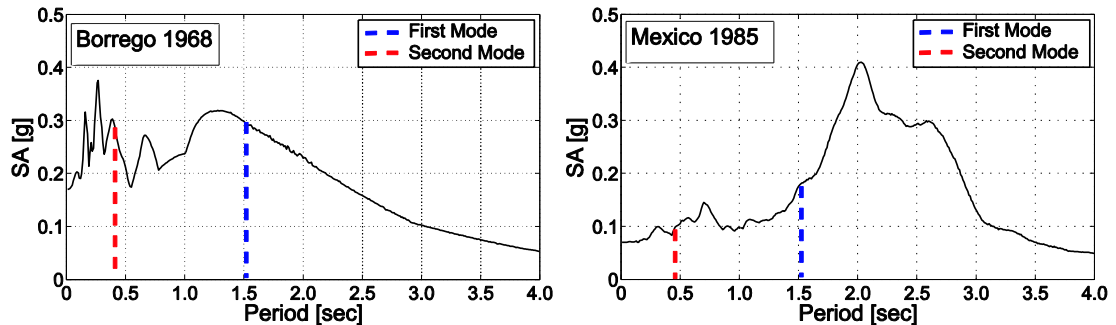


Figure 9.5: Response spectra of Borrego and Mexico City earthquakes.

Since the post-tensioning forces in the *UIDA*-controlled frame reach high level in some storeys, comparison of the results between the *UIDA*-controlled frame and the passive frame with low initial PT forces is not appropriate as it compares two frames with different levels of post-tensioning. In order to obtain a better comparison, the maximum post-tensioning forces reached when applying the *UIDA* are applied as passive forces, constant for all storeys.

The comparison between the top storey displacement of the passive frame with high forces ($0.7 F_{ys}$) and the *UIDA*-controlled frame (Figure 9.6) show that the *UIDA*-controlled frame can achieve behaviour similar to the behaviour of a passive frame with high post-tensioning forces. The reduction in the top storey displacements of the *UIDA*-controlled frame is

associated with a reduction in the moment demand on the columns of storeys with low resultant PT forces. This means that a frame with *UIDA* can exhibit top storey displacements similar to those resulted from a passive PT frame with high post-tensioning forces with reduced internal forces in some storeys in the frame.

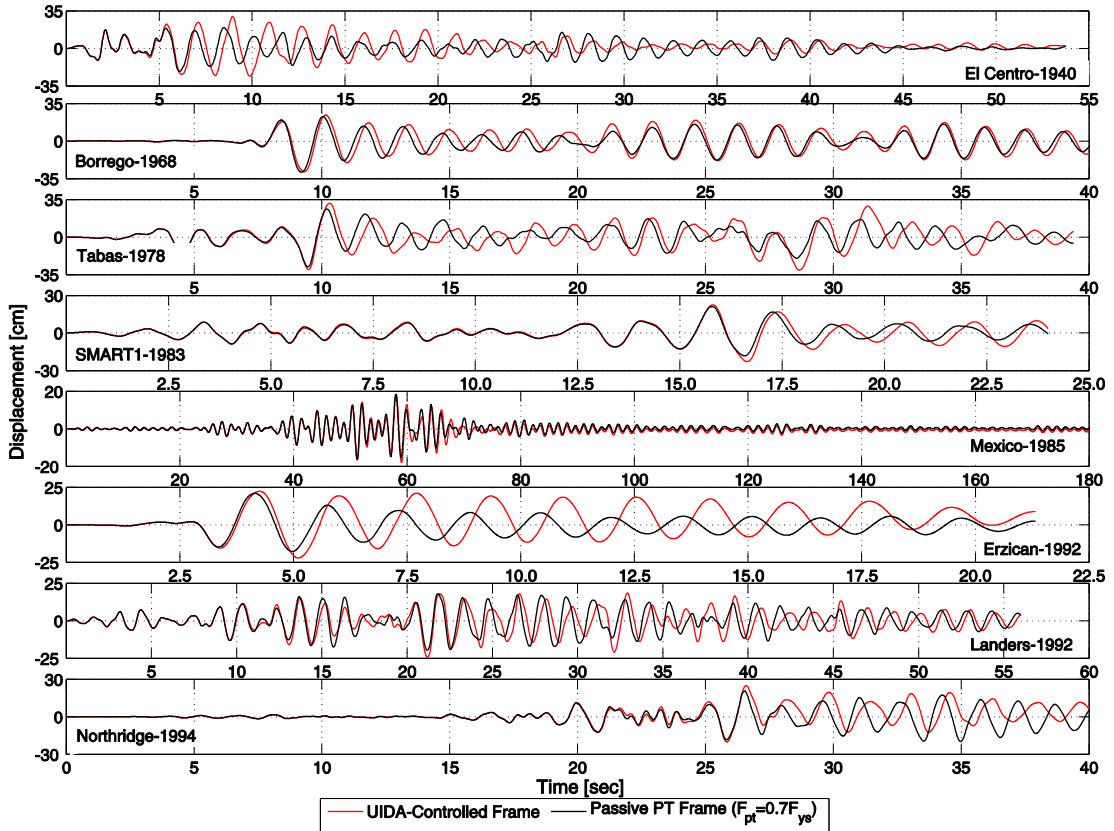


Figure 9.6: Top storey displacements for passive frame with high initial PT forces and the *UIDA*-controlled PT frame.

In addition to the good performance of the *UIDA* in controlling the top storey displacement of the PT frame, differences in the maximum inter-storey drift are also reduced when the *UIDA* is applied, which is the main objective of this algorithm. The standard deviation of these drifts (Figure 9.7) shows that *UIDA* results in a more uniform distribution of maximum inter-storey drift of the frame, compared with both passive frames (with low and high PT forces). Even when the frame with low passive forces showed better distribution of inter-storey drifts than the one with high passive forces (as in Erzican earthquake); the *UIDA*-controlled frame showed even better distribution. These results show that the algorithm was able to achieve the control objective with PT forces lower than those in the passive frame with high PT forces.

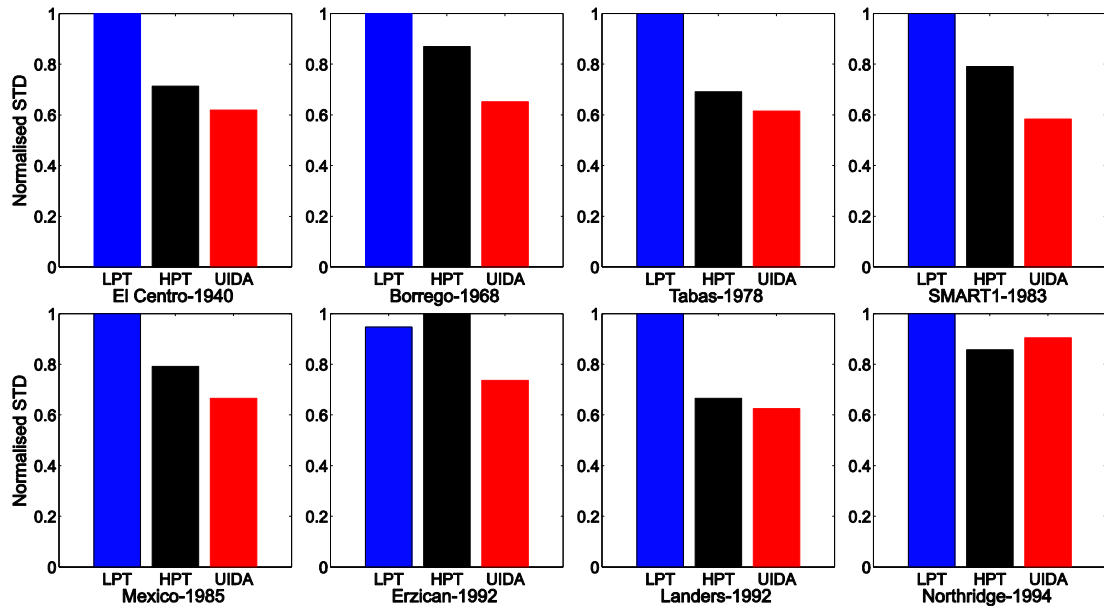


Figure 9.7: Standard deviations of the normalised inter-storey drifts.

9.2.3. Effect of the Drift Threshold on the Algorithm Performance

It was shown in Figure 9.2 that the only parameter that affects the Uniform Inter-storey Drift Algorithm is the drift threshold (Thr) at which the algorithm starts working. In the previous simulations, the value of Thr was assumed to be 0.005 . This value was chosen by simulating the frame response with applied $UIDA$ at different levels of the drift threshold. The response of the frame was simulated for $Thr = 0.002, 0.005, 0.01$ and 0.015 as shown in Figure 9.8.

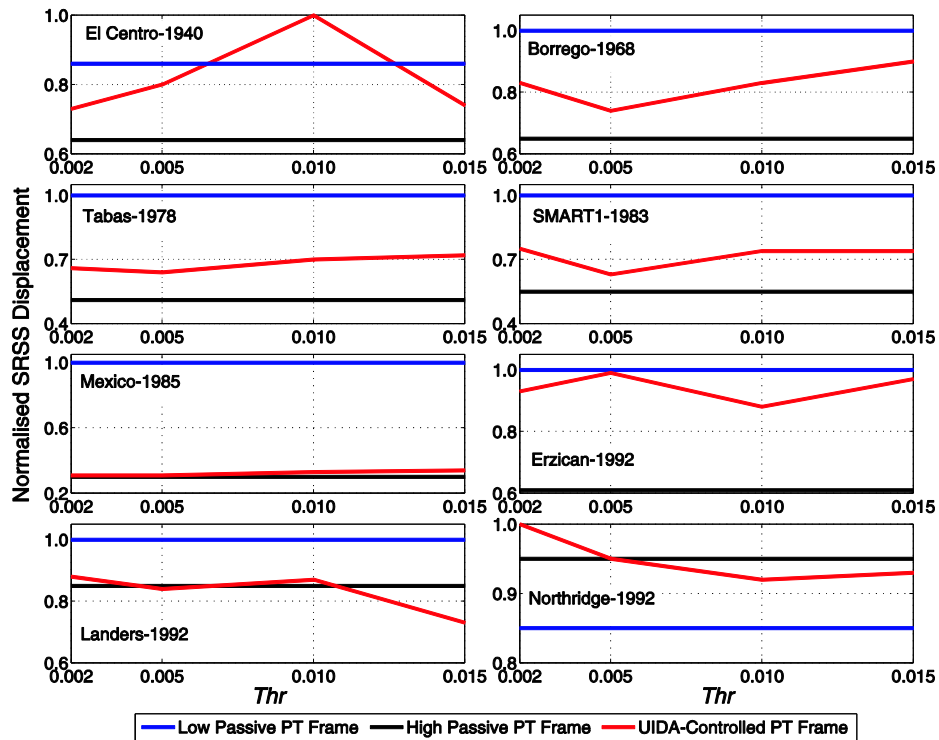


Figure 9.8: Effect of the drift threshold on the PT frame response.

The drift threshold shows a significant effect on the *UIDA* performance, which indicates a relatively high sensitivity of the algorithm to this value. Generally, the response is relatively high when the drift threshold is very small (Borrego, Tabas, SMART1, Landers and Northridge earthquakes) or very large (Borrego, Tabas, SMART1, Erzican, and Northridge earthquakes).

When the value of the drift threshold is relatively small, the *UIDA* is activated at low levels of vibration and post-tensioning forces are changed accordingly. Initial vibrations however, do not include the main frequency components of the earthquake. Hence, the PT forces are changed without detecting the correct position of the maximum inter-storey drifts of the frame. This would result in control forces that are different from those resulting in the desirable performance of the *UIDA* (Figure 9.9). On the other hand, when the drift threshold was too high, the algorithm was activated too late, when most of the vibration peaks have passed. When the threshold was $Thr=0.005$, the algorithm showed acceptable performance for all earthquakes. This value was the inter-storey drift ratio at which the inelastic phase of the connection started, which means that limited inelastic deformations were allowed before the *UIDA* started operating.

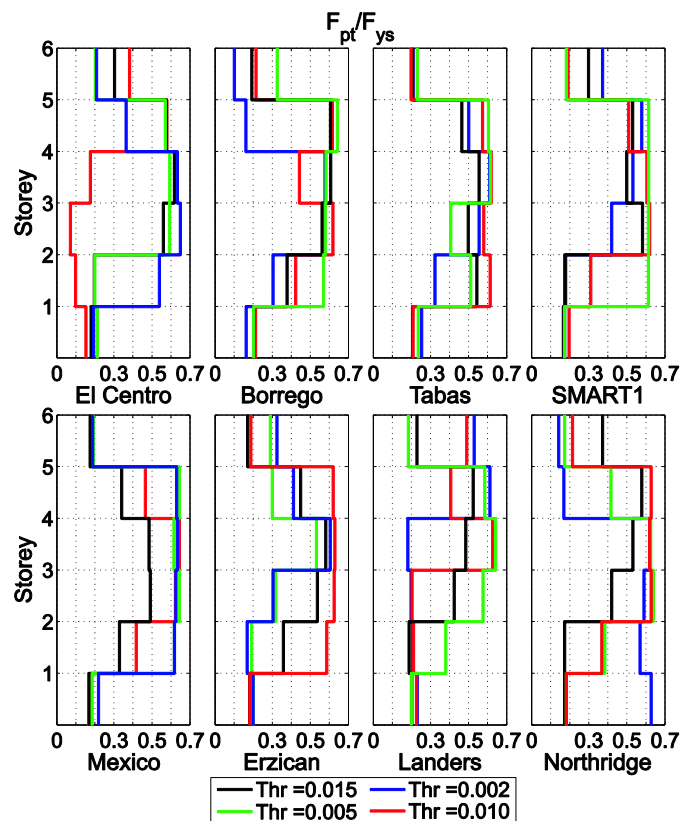


Figure 9.9: Effect of the drift threshold value on resultant PT forces.

Deeper insight into the effect of the drift threshold value can be achieved by investigating the standard deviation of the normalised inter-storey drifts at each level of Thr (Figure 9.10).

The results show that with the exception of El Centro and Northridge, the algorithm performed well for $Thr=0.005$. These simulations indicate that the best value of drift threshold is the one at which the connection enters its inelastic phase.

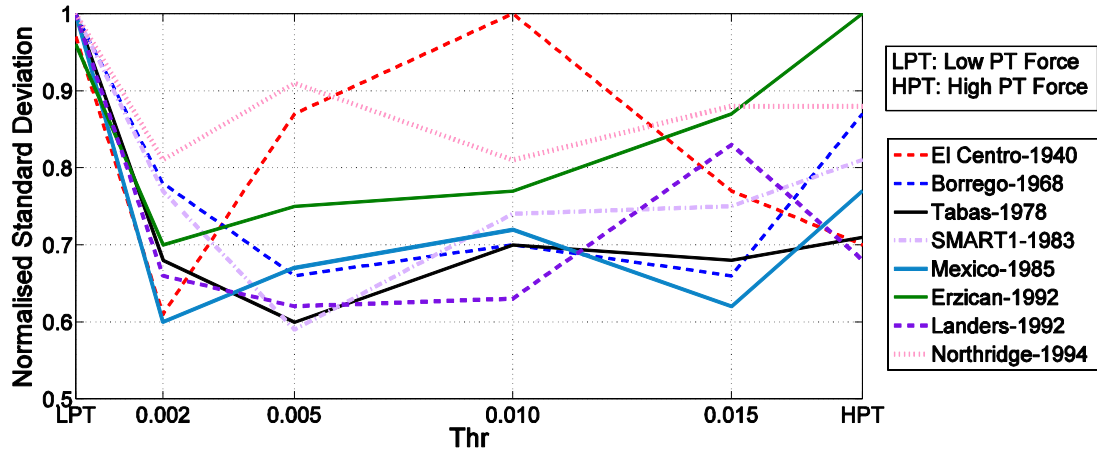
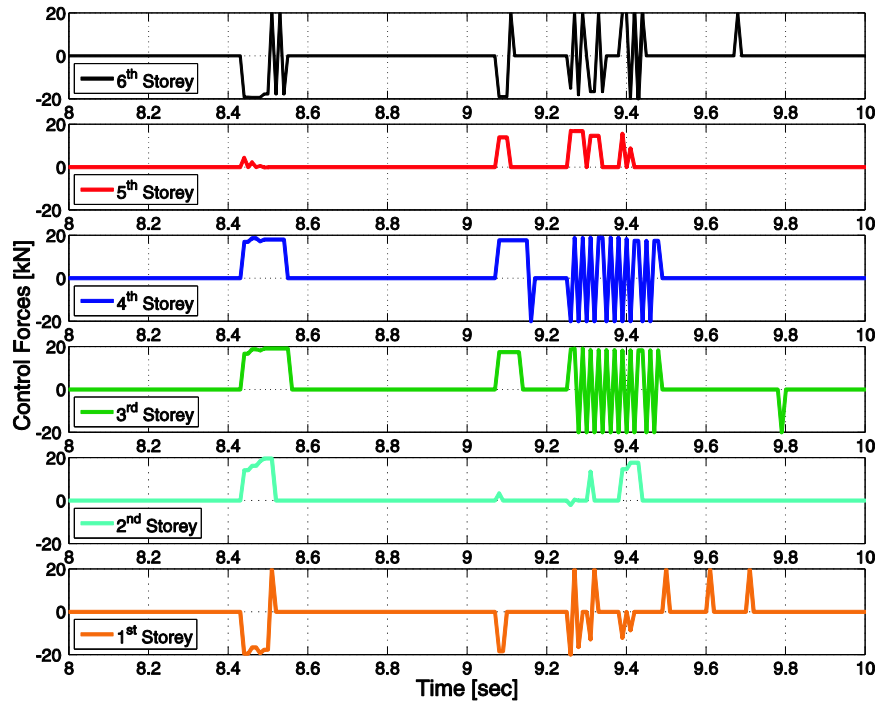
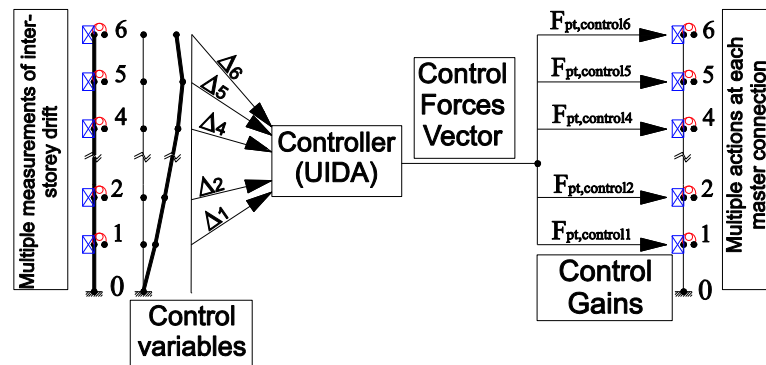


Figure 9.10: Effect of the drift threshold value on the standard deviation of inter-storey drifts.

9.2.4. Centralisation of Control Forces in *UIDA*

When the *UIDA* is applied to a PT frame, every change in control forces of all storeys is made by one action from the control computer. This control action is based on the position of all inter-storey drifts at a given time. This is done by finding the average inter-storey drift and modifying the post-tensioning forces in all storeys accordingly. Since all control forces are given by one action, the *UIDA* is classified as centralised control algorithm. Control forces in this algorithm are synchronised for different storeys (Figure 9.11). The control force histories (Figure 9.11) show that all sets of control forces start at the same time which indicates that all control forces act simultaneously. In the intervals where control forces are applied only to few storeys, the drifts in the other storeys are close to the average drifts and no action is required by the algorithm.

The *UIDA* can also be thought as a Multi-Input-Multi-Output system (MIMO) where input data (input variables) are the inter-storey drift (a vector of multiple elements) and the output data (control gains) of the algorithm is a vector of control forces which also comprises multiple elements (Figure 9.12).

Figure 9.11: Control forces in *UIDA*.Figure 9.12: Operation of the *UIDA* as MIMO systems.

9.2.5. Development of PT forces in *UIDA*

Figure 9.13 shows the development of post-tensioning forces in the *UIDA*-controlled frame. The results presented here show a comparison of PT forces after the first, second and third set of control forces with the final (resultant) distribution. It can be seen that in most cases the distribution of the PT forces after the first set is similar to the final distribution. This suggests that the algorithm tends to apply the correct force distribution after the first control interval, with the forces in the subsequent sets cancelling each other, oscillating about the initial distribution. Figure 9.13 also indicates that from the early stages of the response the *UIDA* is able to detect the dominant position of inter-storey drifts and modify the distribution of PT forces of all storeys accordingly. This characteristic can be used to simplify the *UIDA* and obtain a simplified version of this algorithm.

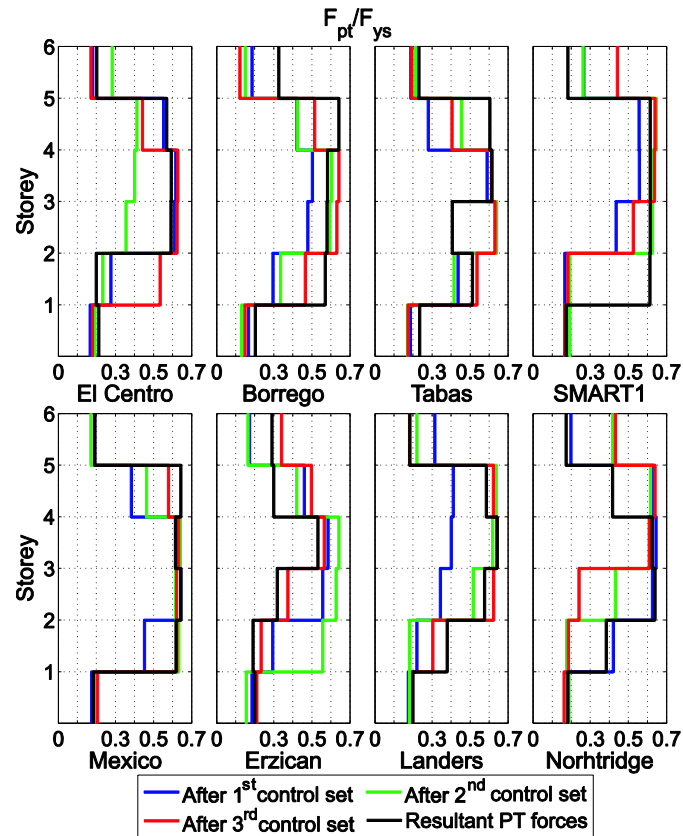


Figure 9.13: Development of PT forces in UIDA.

9.3. Simplified Uniform Inter-Storey Drift Algorithm (SUIDA)

9.3.1. Operation of the SUIDA

The *SUIDA* is a modified algorithm from the Uniform Inter-storey Drift Algorithm which aims to simplify the action required from the rotating motors in the *UIDA*. Based on the findings of section 9.2.5, the *SUIDA* utilises the fact that post-tensioning forces after the first set take a similar distribution with that of the final forces. Therefore, the *SUIDA* acts only once during the earthquake to modify the PT forces and then it remains inactive.

In the Simplified Uniform Inter-storey Drift Algorithm, the frame remains passive before the first control set (before reaching the drift threshold of the algorithm). Then the first set of control forces is applied by tightening the strands in some storeys and releasing them in other storeys. After achieving the required distribution of PT forces, the algorithm is deactivated and the structure remains passive for the rest of the seismic action. The period of active control action during the earthquake is very short in comparison to the periods of passive behaviour. Hence, this algorithm can be classified as Adaptive Passive system, where the structure starts from an initial passive state and adapts itself to another (final) passive state.

The adaptation depends only on the external forces in the early stages of the seismic action and the given drift threshold.

In order to deactivate the *SUIDA* after performing the first set of post-tensioning forces, extra conditions are added to the *UIDA*. These conditions constrain the application of control forces after the first set. The first condition is to ensure that the control set has been completed for all storeys:

$$\{\mathbf{F}_{\text{control}(i)}\} = \{\mathbf{0}\}, \quad (9.2)$$

where $\{\mathbf{F}_{\text{control}(i)}\}$ is the vector of control forces at time-step i . This condition however, is not sufficient by itself as it might be satisfied before the first set or between the sets. Therefore, another condition is required to ensure that the first set has been completed. This condition can be obtained from:

$$\Sigma \mathbf{F}_{\text{control}} \neq \mathbf{0}, \quad (9.3)$$

where $\Sigma \mathbf{F}_{\text{control}}$ is the sum of the control forces from the beginning of the seismic action. This condition should be satisfied at each storey. Introducing conditions 9.2 and 9.3 in the operation of the *SUIDA* is shown in flowchart of the algorithm (Figure 9.14).

9.3.2. Results of the of the *SUIDA*

Results of the *SUIDA* were simulated by using the six-storey post-tensioned steel frame (Figure 8.5- Chapter 8). The initial post-tensioning forces were assumed to be equal in all storeys ($F_{\text{pti}} = 0.3F_{\text{ys}}$). The results of the *SUIDA* are compared with those of the passive frame with $F_{\text{pt}}=0.3F_{\text{ys}}$ and the passive frame with F_{pt} equal to the highest value of post-tensioning reached by the control algorithm.

In Figure 9.15 is presented a comparison between the top storey displacements of the *SUIDA*-controlled frame with low initial forces and two passive frames with low and high post-tensioning forces. It can be seen in this figure that the *SUIDA* does not offer significant reduction of the top storey displacements from those obtained with the passive frame with low post-tensioning forces. Therefore the simplification offered by the *SUIDA* is at the expense of the reduced efficiency of the algorithm, when compared to the *UIDA*. However, the algorithm changes the distribution of the PT forces of the passive frame (Figure 9.16) without increasing the response of the frame. In terms of top storey displacements, the *SUIDA* results are between those of a passive frame with low and high PT forces (closer to low PT forces).

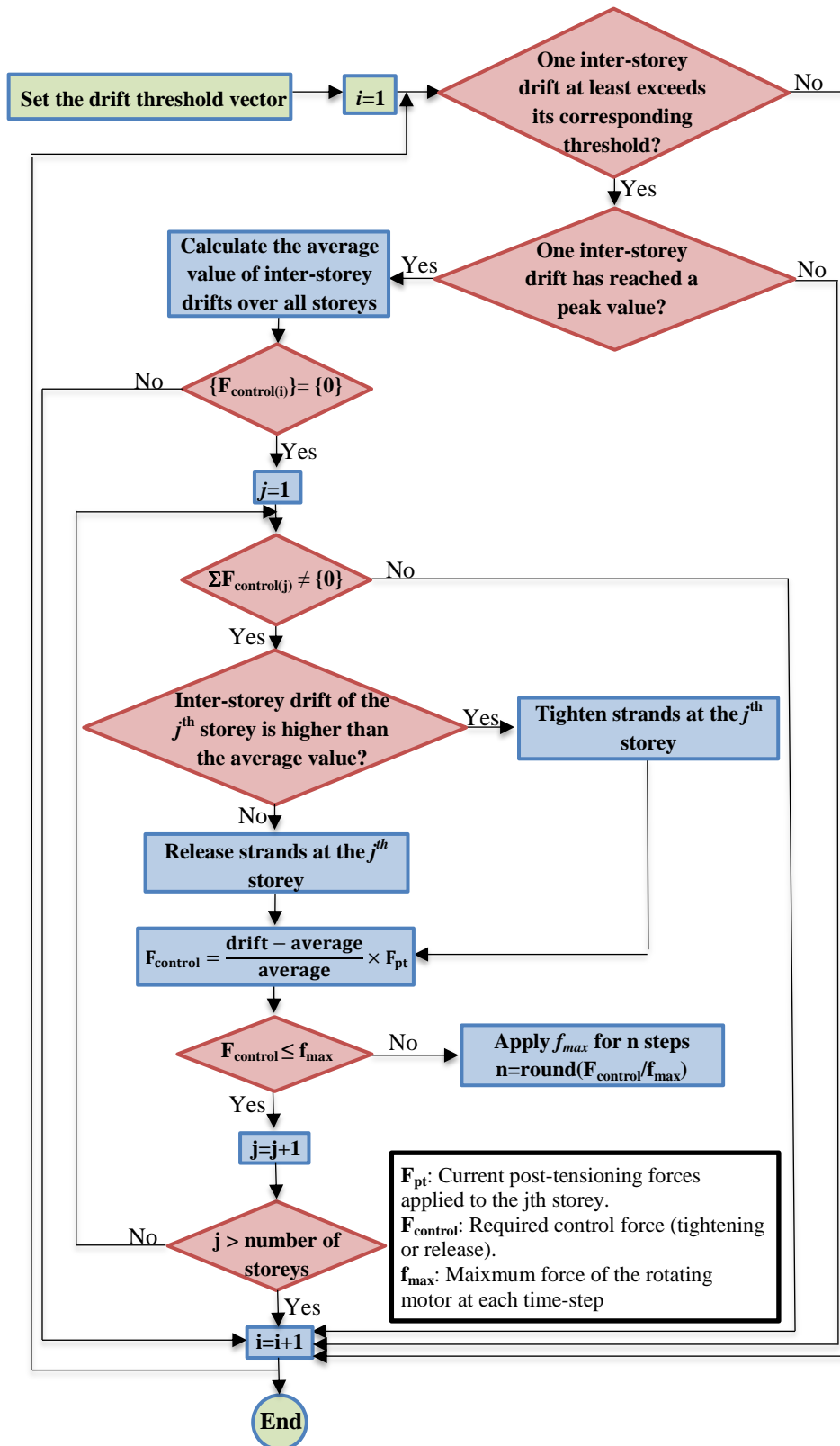


Figure 9.14: Flowchart of the simplified uniform inter-storey drift control algorithm.

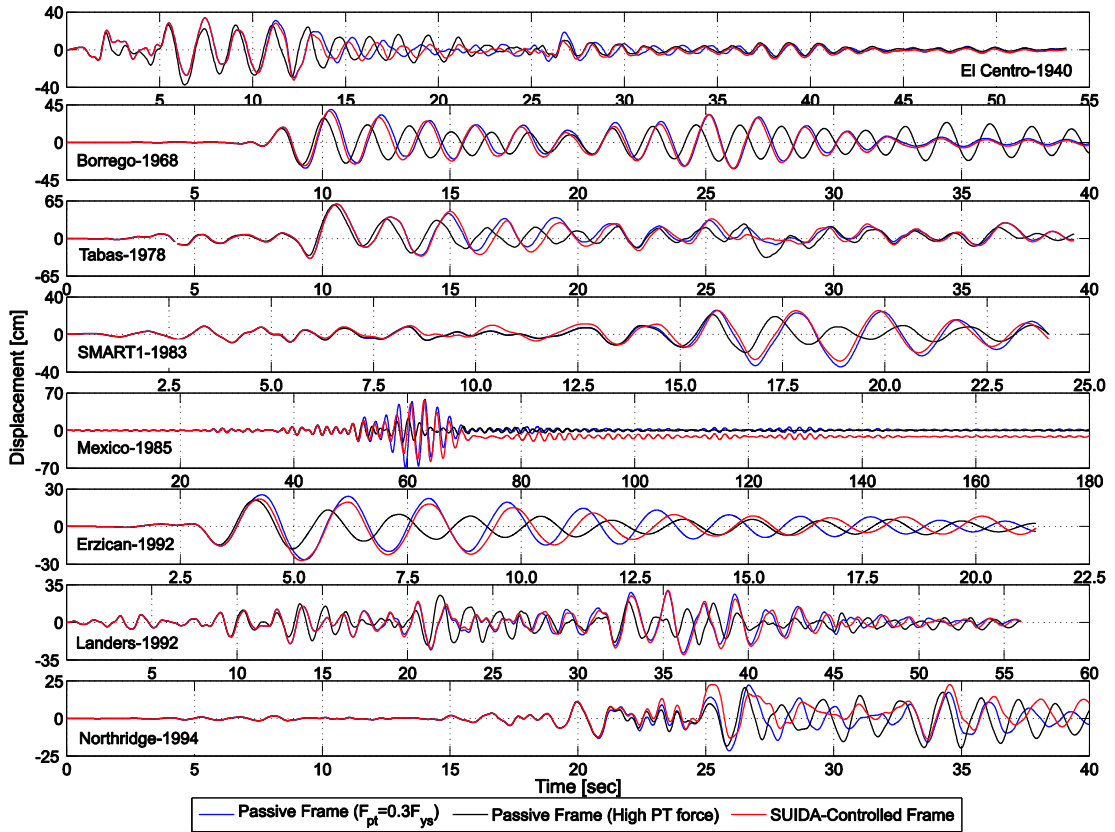


Figure 9.15: Top storey displacements for passive frames with low and high initial PT forces and the SUIDA-controlled PT frame.

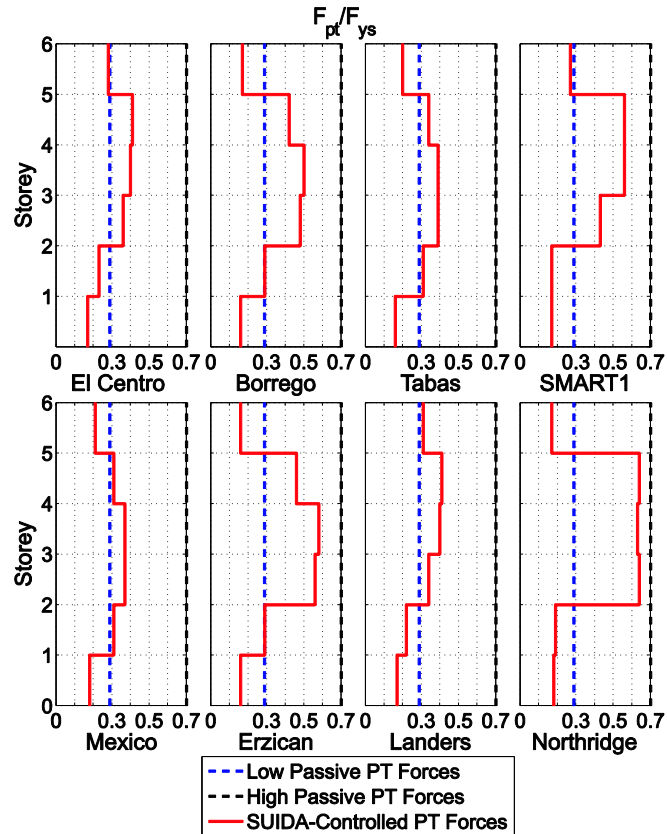


Figure 9.16: Resultant PT forces in SUIDA-controlled frame.

Reducing the top storey displacements is not the main objective of the *SUIDA*, and therefore, investigating its effect on the uniformity of inter-storey drifts is required for further assessment of its efficiency. This assessment is performed by comparing the standard deviation of maximum inter-storey drifts (Figure 9.17).

Figure 9.17 shows that *SUIDA* offers a small reduction in the normalised standard deviation (STD) of maximum inter-storey drifts from a passive frame with either low or high PT forces. In most cases, the response of the *SUIDA*-controlled frame was between the response of the passive frame with low and high post-tensioning forces. In some cases however, the *SUIDA* did not show any reduction in the STD (El Centro earthquake) or resulted in higher STD value (Northridge earthquake) indicating a negative effect of the re-distribution of PT forces.

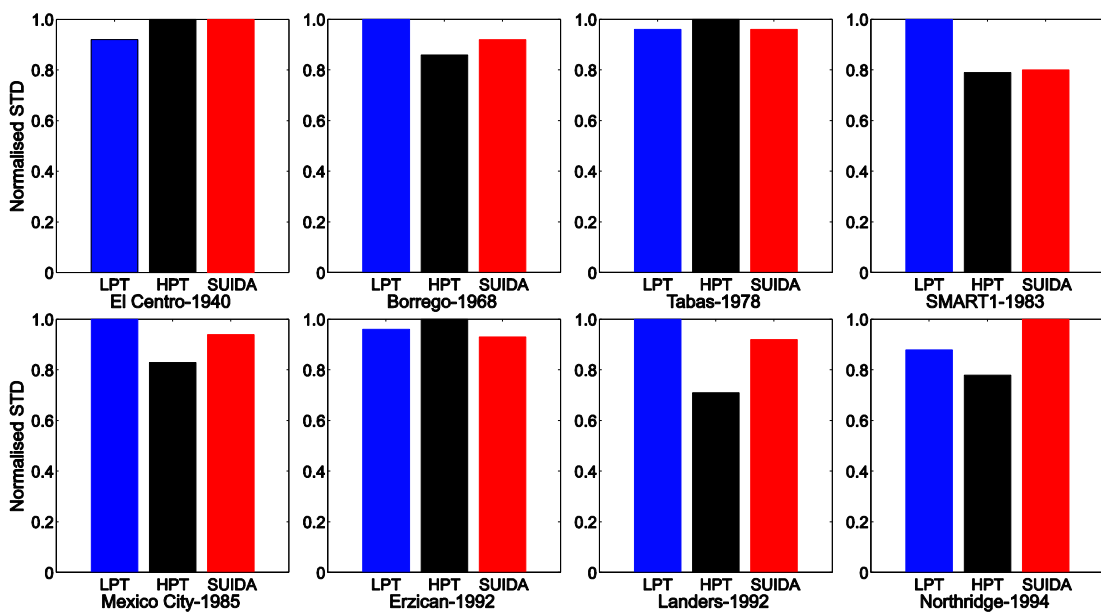


Figure 9.17: Normalised standard deviation of maximum inter-storey drifts for low passive forces, high passive forces and *SUIDA*-controlled forces.

This comparison shows that the *simplified* version of the Uniform Inter-storey Drift Algorithm, which was proposed in order to simplify the operation of the algorithm, results in a reduction in its efficiency. Although the distribution of the PT forces after the first set was similar to the resultant distribution, the latter sets seem to have a continuous effect on balancing the inter-storey drift despite that their effect on the resultant distribution of PT forces was relatively small.

9.4. Concluding Remarks on Deformation Regulation Approach

In this chapter was presented a control approach based on deformation regulation of post-tensioned steel frames. The basic idea of this approach was to provide a more uniform distribution of deformations along the height of the structure during the earthquake excitation. Since the inter-storey drifts determine the internal forces in structural elements, they were chosen as a control parameter to implement the deformation regulation control approach in control algorithms.

The Uniform Inter-storey Drift Algorithm (UIDA) was proposed based on the deformation regulation control approach. The main objective of the algorithm was to produce uniform maximum inter-storey drifts of the frame. This objective was achieved when providing the algorithm with a proper value for the drift threshold (Thr) at which the algorithm starts operating. Simulations of the algorithm performance indicated that the algorithm was generally most effective for $Thr=0.005$ which is the drift ratio at which the post-tensioned connections enter their inelastic phase.

An investigation of control forces time-history and comparing the development of PT forces indicated that the distribution of PT forces after the first set of control forces was similar to the final distribution of PT forces. This feature was used to propose a Simplified Uniform Inter-storey Drift Algorithm (SUIDA) as a version of the UIDA. The aim of the *SUIDA* was to produce uniform maximum inter-storey drift with minimum control action. *SUIDA* was designed to perform only one set of control forces and then it was deactivated resulting in an adaptive passive system. The efficiency of the *SUIDA* however was significantly lower than the original *UIDA*.

Despite the fact that *SUIDA* did not offer very good behaviour in comparison to the *UIDA*; it has the potential to be improved by adding a certain limited number of sets of control forces to the algorithm. Limiting the number of sets of the control forces can be used in order to reduce the control actions (thereby increasing its reliability), but also to improve its efficiency.

CHAPTER 10

SUMMARY, CONCLUSIONS AND RECOMMENDATIONS FOR FUTURE WORK

In this chapter is presented a summary of the results obtained from simulations of response of PT frames using passive control and various semi-active control approaches (Chapters 5-9). The summary is divided in two parts: (i) summary of passively controlled PT frames and (ii) summary of semi-actively controlled PT frames. In each section is presented the original contribution to the field of post-tensioned steel frames carried out in this research.

Also, in this chapter are presented the conclusions drawn from the work carried out in this research. These conclusions are then used as a basis for recommendations for future work on seismic behaviour of passive and semi-active post-tensioned steel frames.

10.1. Summary of Results

10.1.1. Summary of Work on Passively Controlled PT Frames

This section summarises the new work included in this thesis which contribute to the work already carried out on post-tensioned steel frames with passive systems.

10.1.1.1. Integrated Post-tensioned Connection Model (IPTC)

A new computational model for simple representation and incorporation of post-tensioned connections was presented in Chapter 5. The Integrated Post-tensioned Connection element (IPTC) is a two-node, six-DOF element with linear behaviour when subjected to axial and shear forces, and complex nonlinear moment-rotation behaviour. This element is able to simulate all phases of the rotational behaviour of the post-tensioned connection in addition to providing direct information about the tension forces in the strands. The element is simple and easy to incorporate in a frame analysis program and yet able to simulate all important events in the post-tensioned connections including gap-opening and self-centring of the connection.

Practical details of the connection element were proposed for both passive and semi-active control systems. The key detail of the post-tensioned connection is the geometry of the slotted holes that are provided in the shear tab to facilitate the rotation of the connection without obstruction or bearing action of the bolts in the beam web. Also proposed are specifications of the rotating motor shown in the connection detail of semi-active control systems.

10.1.1.2. Simulations of PT Frames Response with Large Selection of Earthquakes and Different Levels of PT Forces

The response of the passive PT frames was simulated for a broad range of earthquake characteristics that have not been presented in the literature (Chapter 6). The characteristics of earthquake excitations are usually investigated only in terms of peak ground acceleration (PGA), frequency content and duration. Results here show that the distribution of large reversals (amplitudes) during the seismic action (shape of the earthquake envelope) is also an important factor in the PT frame response. Three types of the earthquake envelopes were investigated:

- (i) Exponential envelope which is characterised by large amplitudes in the early stages of the seismic action and followed by long decaying phase. The maximum deformations of PT frames in response to this type of earthquake envelopes cannot be reduced easily as there is no time to activate the passive system to dissipate energy and damp the response.
- (ii) Stationary envelope where the acceleration amplitudes are consistently distributed over the earthquake duration. This type of earthquakes may magnify the response of the PT frame and the response can be improved by either large energy dissipation or by changes in the stiffness (and consequently, natural frequency of the structure). Passive systems have low energy dissipation (flag-shaped hysteresis) and limited stiffness-changing capability. Under some earthquakes the gap opening may result in reducing the response frequency of the structure to coincide with the predominant frequency of the seismic input, leading to further dynamic magnification.
- (iii) Trapezoidal envelope is characterised by gradual ascending accelerations followed by a flat phase and finally a decaying part. This type helps the passive system to build up its energy dissipation and therefore, it results in significant reduction of the response in the late stages of the earthquake which include the largest acceleration amplitudes.

The response of PT frames using different levels of post-tensioning forces was also investigated by push over analyses to assess the effect of PT forces level on the development of failure modes. This investigation indicated that the level of post-tensioning force has a

significant impact on the frame behaviour. The non-linear dynamic response simulations showed that the effects of the PT force level on the response were higher for some earthquakes than others and hence, the research was directed toward investigating the use of semi-active control systems.

10.1.2. Summary of Results of Semi-Active Control of PT Frames

In chapters 7 to 9 is presented a new approach in the control of seismic response of PT frames by introducing semi-active control of post-tensioning forces of the strands. Three different approaches were considered for semi-active control of PT frames: (i) energy dissipation approach, (ii) stiffness control approach and (iii) deformation regulation control approach.

The energy dissipation approach is very popular in the literature as a semi-active technique to increase the energy dissipation capacity of the structure and help it to improve its seismic response. In this research, a new control algorithm was proposed to increase the energy dissipation capacity of PT frames based on the loading direction of the PT connection.

The stiffness control approach has also been proposed in previous research work and investigated for braced frames and truss structures. The main part of any algorithm based on the stiffness control approach is the stiffness selection algorithm. In this research, a new stiffness selection algorithm is proposed based on Fourier analysis of either the earthquake record or the frame response, during the seismic action.

Finally, a completely new control approach was also proposed to regulate the deformation of PT frames along all storeys. In this approach, the main objective is not necessarily to reduce the inter-storey drifts of all floors, but to create a uniform distribution of the maximum frame deformations. This regulation is achieved by reducing the inter-storey drifts in some storeys while increasing them in the other storeys. The aim of this control approach is a better distribution of internal forces in the elements throughout the structure.

When the response of semi-actively controlled PT frames is assessed, the reference cases are passive post-tensioned frames and all response results are normalised to the response of passive PT frames. Since the main objective of all control approaches is to reduce the frame displacements, the maximum displacement and the SRSS of displacements for the top storey are adopted as general indices for assessing the effectiveness of all control approaches. Different other indices (forces, inter-storey drifts and energy dissipation values) have also been used and are presented for each control approach.

10.1.2.1. Summary of Energy Dissipation Approach Results

In the energy dissipation control approach, three versions of the loading direction feedback algorithm were introduced: (a) deformation-based loading direction feedback algorithm (DB-LDFA) with final post-tensioning force equal to the initial one and control actions based on the rotation feedback of the PT connections, (b) modified deformation-based loading direction feedback algorithm (MDB-LDFA) with final PT force proportional to the initial one and (c) velocity-based loading direction feedback with control actions based on the rotation rate feedback of the PT connections. In addition to the top storey maximum displacements and SRSS of top storey displacements history (Table 10.1 and Figure 10.1), the energy dissipation ratios are used as another index to correlate the relationship between energy dissipation and displacements of the frames.

Earthquake	$\Delta_{\max}/\Delta_{\max(\text{passive})}$			SRSS/SRSS _(passive)			E/E _(passive)		
	DB	MDB	VB	MDB	MDB	VB	DB	MDB	VB
El Centro	0.96	1.13	1.05	0.79	0.91	1.02	0.67	1.11	0.89
Borrego	1.00	1.00	0.98	0.92	0.95	0.87	3.86	5.16	3.23
Tabas	1.10	1.02	1.00	1.03	1.12	1.01	1.29	1.43	0.89
SMART1	1.11	1.12	1.07	0.92	1.15	0.91	0.87	2.44	0.91
Mexico	0.90	1.02	1.05	0.96	1.00	1.04	1.15	2.25	0.30
Erzican	1.06	1.28	1.02	1.04	1.38	1.02	2.57	3.37	1.18
Landers	0.89	1.20	1.23	0.97	1.30	1.22	1.43	2.89	1.92
Northridge	0.91	0.82	0.94	0.70	0.67	0.69	0.82	0.62	0.07
Kobe	1.00	1.06	1.05	0.91	1.43	0.88	1.47	2.70	0.97

Table 10.1: Summary of loading direction feedback algorithms results: DB: deformation-based, MDB: modified deformation-based and VB: velocity based.

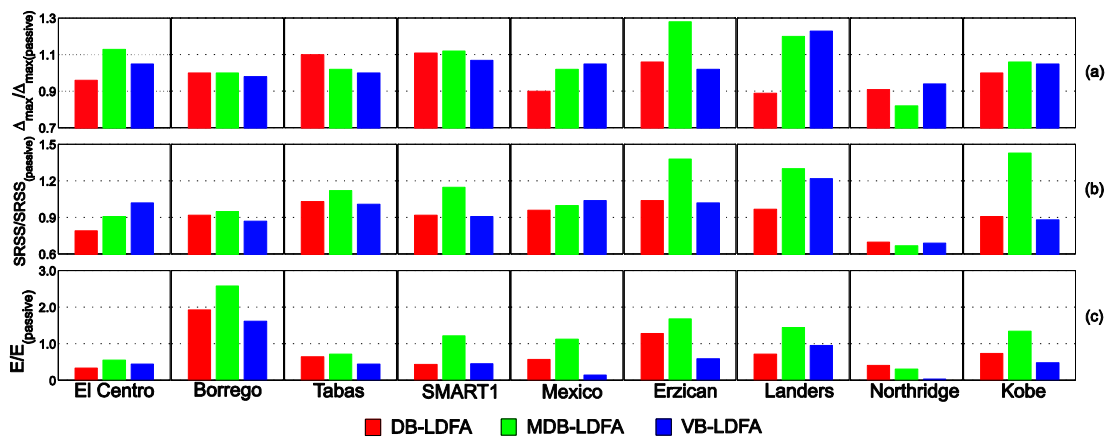


Figure 10.1: Response of LDFA-controlled PT frame normalised to response of passive PT frames: (a) top storey maximum displacements, (b) SRSS of top storey displacements and (c) energy dissipation.

Table 10.1 and Figure 10.1 show that response of the DB-LDFA-controlled frame is in general better than the MDB-LDFA-controlled and the VB-LDFA-controlled frames. The MDB-LDFA dissipated significantly higher energy without reducing the frame displacements. This dissipated energy is a result of larger amplitudes of the response. On the

other hand, the *VB-LDFA* shows results similar to those obtained from the *DB-LDFA* despite that its dissipated energy is much lower than the dissipated energy using the *MDB-LDFA* and the *DB-LDFA*. This is a result of forcing the frame to dissipate more energy in early stages of loading.

In general, it can be noticed that all algorithms proposed for the energy dissipation approach could not offer a significant reduction in frame deformations. The largest reduction in the maximum top storey displacements was 18% and the largest reduction in the SRSS of top storey displacements was 33%, both obtained for the Northridge earthquake. Also, as control algorithms based on energy dissipation approach take time to dissipate more energy than passive frames, they cannot reduce the maximum displacements occurring in early stages of the seismic excitation, which are typical for most earthquake excitations. Therefore, it can be concluded that it is not efficient to rely only on energy dissipation to control the frame response.

10.1.2.2. Summary of Stiffness Control Approach Results

In the three algorithms based on stiffness control (Chapter 8) the Fourier analysis was adopted as a methodology for choosing the optimum stiffness pattern of the frame. The only difference between the different algorithms was the choice of input signal that was analysed and used for the selection of the stiffness pattern. The three control algorithms are: (i) Excitation Frequency State Feedback Algorithm (EFSFA) where the input is the earthquake acceleration record, (ii) Response Frequency State Feedback Algorithm (RFSFA) in which the input is the acceleration time-history of the top storey and (iii) Filtered Frequency State Feedback Algorithm (FEFSFA) where the input is the filtered acceleration record of the excitation.

As a result of applying different stiffness patterns on the frame during the seismic action, control algorithms based on the stiffness control approach result in final pattern of PT forces that is different from the initial one. Therefore, the comparison of the controlled frame results is made first against the passive frame with a PT force distribution equal to the initial one (Table 10.2, Figure 10.2), then against a passive frame with a constant, uniformly distributed PT force equal to the highest force reached at any floor of the controlled frame. In the latter case, a comparison between the resultant element forces in the passive and the controlled frames is presented to assess the effect of the control algorithms on the moment demand on the columns in each storey (Table 10.3).

It can be noticed from Tables 10.2, 10.3 and Figure 10.2 that the different control algorithms of the stiffness control approach show good performance in reducing both the frame top

storey displacements and the moment demand on columns. The best performance in terms of displacements is achieved using the EFSFA (open-loop control), reducing the displacements of the low-PT passive system by up to 70% for Mexico City and between 20% and 40% for most of the other earthquakes (Figure 10.3), with Northridge as the only excitation for which this approach was not effective.

Earthquake	$\Delta_{max}/\Delta_{max(passive)}$			SRSS/SRSS _(passive)		
	EFSFA	RFSFA	FEFSFA	EFSFA	RFSFA	FEFSFA
El Centro	0.64	0.76	0.76	0.70	0.78	0.76
Borrego	0.71	0.84	0.84	0.95	1.04	0.87
Tabas	0.67	0.62	0.68	0.71	0.73	0.74
SMART1	0.53	0.75	0.58	0.60	0.75	0.63
Mexico	0.30	0.30	0.28	0.36	0.44	0.31
Erzican	0.79	0.79	0.79	0.80	0.72	0.80
Landers	0.73	0.67	0.80	0.74	0.73	0.76
Northridge	1.16	0.96	0.98	1.12	0.92	1.14

Table 10.2: Deformations of the frames controlled by stiffness control approach algorithms compared to a passive frame with low initial PT force.

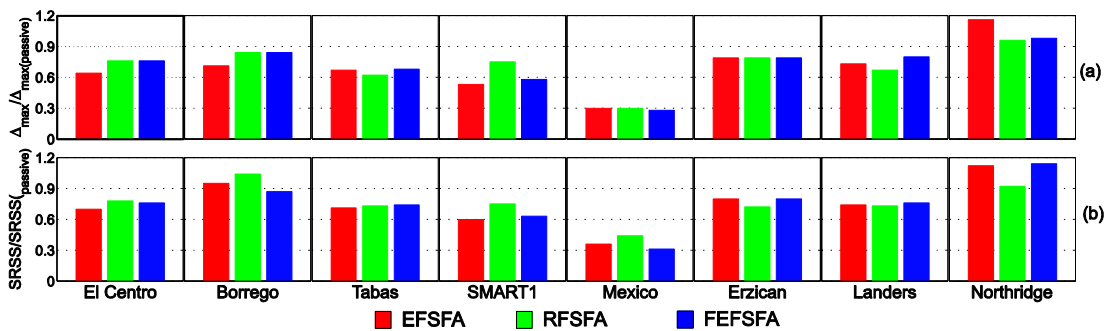


Figure 10.2: Deformations of frames controlled by stiffness control approach algorithms compared to a passive frame with low initial PT force.

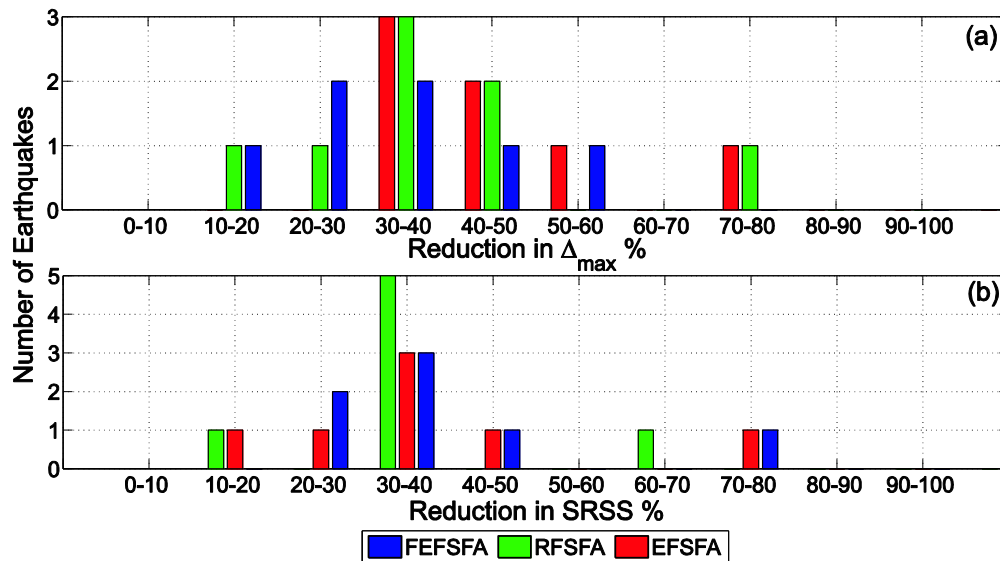


Figure 10.3: Distribution of reduction of top storey displacements: (a) reduction in maximum displacement and (b) reduction in SRSS of displacements.

Earthquake	$\Delta_{max}/\Delta_{max(passive)} -$ Top Storey			SRSS/SRSS _(passive) - Top Storey			F _{pt} /F _{pt(passive)}			Storey
	E	R	F	E	R	F	E	R	F	
El Centro	1.00	1.20	1.20	0.92	1.04	1.00	0.97	0.27	1.00	1 st
							1.00	0.33	1.00	2 nd
							1.00	0.38	1.00	3 rd
							1.00	0.33	1.00	4 th
							1.00	0.27	1.00	5 th
							0.27	0.27	0.24	6 th
Borrego	1.16	1.14	1.14	1.47	1.61	1.37	1.00	0.30	1.00	1 st
							1.00	0.30	0.85	2 nd
							1.00	0.27	0.85	3 rd
							1.00	0.38	0.94	4 th
							1.00	0.41	1.00	5 th
							0.31	0.38	0.33	6 th
Tabas	1.35	1.40	1.19	1.33	1.45	1.31	1.00	0.38	1.00	1 st
							0.94	0.35	0.82	2 nd
							1.00	0.38	1.00	3 rd
							0.97	0.44	0.82	4 th
							0.38	0.44	0.38	5 th
							0.38	0.85	0.33	6 th
SMART1	0.89	1.23	0.95	1.08	1.35	1.14	0.32	0.33	0.32	1 st
							0.27	0.38	0.27	2 nd
							0.27	0.97	0.27	3 rd
							0.33	0.33	0.33	4 th
							0.97	0.15	0.97	5 th
							0.94	0.27	0.97	6 th
Mexico City	1.12	1.13	1.08	1.19	1.44	1.04	1.00	0.97	0.94	1 st
							0.97	1.00	0.97	2 nd
							1.00	0.27	1.00	3 rd
							1.00	0.30	1.00	4 th
							0.29	0.21	0.29	5 th
							1.00	0.33	1.00	6 th
Erzican	1.00	1.00	1.00	1.31	1.18	1.31	0.30	0.24	0.30	1 st
							0.30	0.30	0.30	2 nd
							0.24	0.30	0.24	3 rd
							0.30	0.18	0.30	4 th
							0.30	0.24	0.30	5 th
							0.30	0.18	0.30	6 th
Landers	1.11	1.01	1.20	0.87	0.86	0.89	1.00	0.38	1.00	1 st
							0.35	0.35	0.35	2 nd
							1.00	0.41	1.00	3 rd
							0.29	0.38	0.35	4 th
							1.00	0.30	1.00	5 th
							1.00	1.00	1.00	6 th
Northridge	1.25	1.04	1.05	1.02	0.84	1.04	0.28	0.21	0.33	1 st
							0.31	0.21	0.33	2 nd
							0.34	0.21	0.35	3 rd
							0.28	0.18	0.30	4 th
							1.00	1.00	1.00	5 th
							1.00	1.00	1.00	6 th

Table 10.3: Results of the stiffness control approach algorithms compared to passive frame with high initial PT force; E: EFSFA, R: RFSFA, F: FEFSFA.

The RFSFA (close-loop control) resulted in similar (or slightly higher) displacements compared with the passive frame with high PT forces, but the moment demand on the frame columns was significantly reduced (by up to 55%, considering the maximum PT forces distribution).

Efficient stiffness control can be obtained only if the control time intervals of the algorithms are chosen carefully. In general, these results suggest that the stiffness control approach offers a good potential for reducing the dynamic response of PT frames.

10.1.2.3. Summary of Deformation Regulation Control Approach Results

Two control algorithms were proposed in the deformation regulation control approach: (i) Uniform Inter-storey Drift Algorithm (UIDA) and (ii) Simplified Uniform Inter-storey Algorithm (SUIDA). The two algorithms aim to regulate the distribution of inter-storey drifts along the height of the frame. The latter algorithm aims to simplify the operation and increase the reliability of the control by performing only one set of control forces.

In addition to investigating the effects of deformation regulation control on the frame top storey displacements, the standard deviation of all unit-normalised inter-storey drifts is investigated as an index for assessing the performance of the two algorithms. The response of the controlled frames is compared with a PT frame with low passive forces (Table 10.4, Figure 10.4). In Figure 10.5 is presented the distribution of reduction of top storey displacements in the semi-active controlled frame in normalised to the corresponding passive PT frame with low PT force.

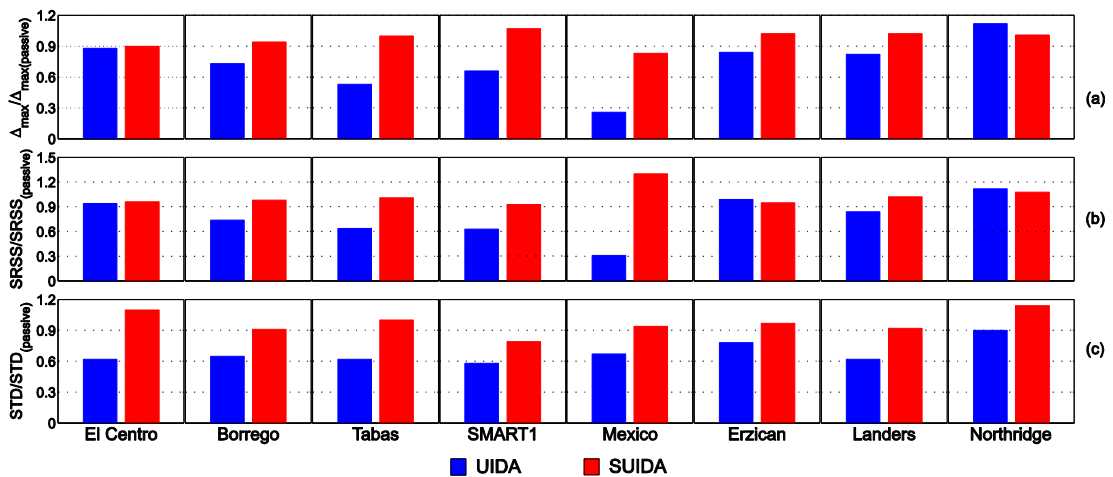


Figure 10.4: Response of deformation regulation controlled PT frame normalised to response of passive frame with low PT force: (a) top storey maximum displacements, (b) SRSS of top storey displacements and (c) standard deviation of inter-storey drifts.

Earthquake	$\Delta_{\max}/\Delta_{\max(\text{passive})}$		SRSS/SRSS _(passive)		STD/STD _(passive)	
	UIDA	SUIDA	UIDA	SUIDA	UIDA	SUIDA
El Centro	0.88	0.90	0.94	0.96	0.62	1.10
Borrego	0.73	0.94	0.74	0.98	0.65	0.91
Tabas	0.53	1.00	0.64	1.01	0.62	1.00
SMART1	0.66	1.07	0.63	0.93	0.58	0.79
Mexico	0.26	0.83	0.31	1.30	0.67	0.94
Erzican	0.84	1.02	0.99	0.95	0.78	0.97
Landers	0.82	1.02	0.84	1.02	0.62	0.92
Northridge	1.12	1.01	1.12	1.08	0.90	1.14

Table 10.4: Results of the deformation regulation control algorithms compared to passive frame with low PT force.

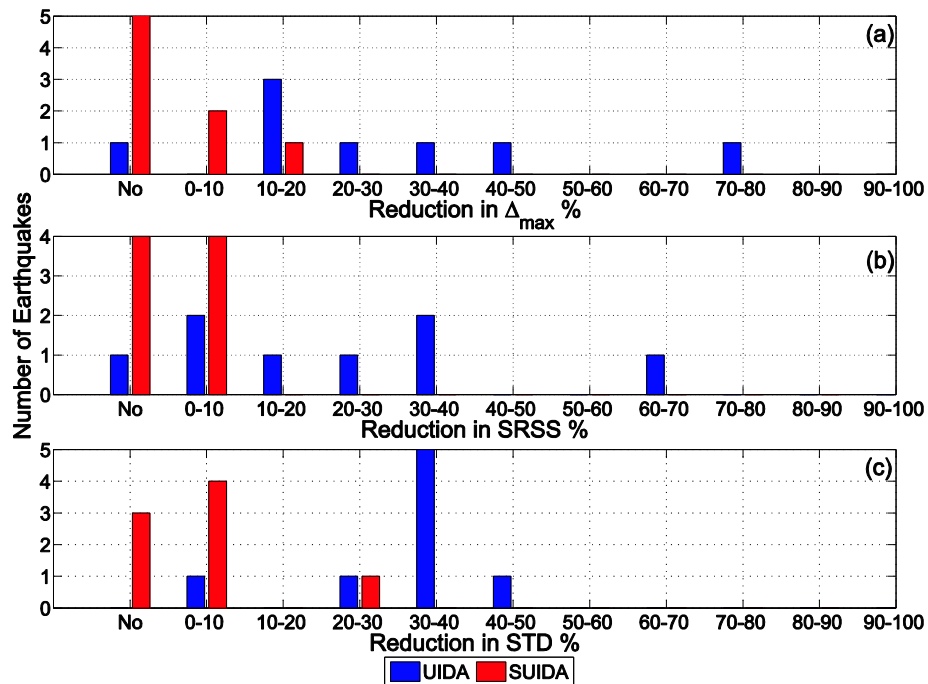


Figure 10.5: Distribution of reduction of top storey displacements in UIDA and SUIDA-controlled frame: (a) reduction in maximum displacement, (b) reduction in SRSS of displacements and (c) Reduction in standard deviation.

Table 10.5 and Figure 10.6 present top storey displacements of semi-actively controlled frame normalised to the passive frame with PT forces equal to the highest forces reached by the control algorithms.

Earthquake	$\Delta_{\max}/\Delta_{\max(\text{passive})}$		SRSS/SRSS _(passive)		STD/STD _(passive)	
	UIDA	SUIDA	UIDA	SUIDA	UIDA	SUIDA
El Centro	1.39	1.00	1.24	0.94	0.87	1.09
Borrego	0.99	1.29	1.14	1.08	0.75	1.07
Tabas	1.13	1.55	1.25	1.20	0.89	0.96
SMART1	1.08	1.34	1.15	1.55	0.74	1.01
Mexico	1.00	2.66	1.03	3.70	0.84	1.13
Erzican	1.07	1.29	1.62	1.56	0.74	0.93
Landers	1.24	1.18	0.99	1.22	0.94	1.30
Northridge	1.21	1.09	1.00	0.97	1.06	1.28

Table 10.5: Results of the deformation regulation control algorithms compared to passive frame with high PT force.

Results shown in Tables 10.4 and 10.5 and Figures 10.4, 10.5 and 10.6 indicate that the *UIDA* offers: (i) significant reduction in the peak displacements of the frame (20-70%) compared to low-PT passive frame, (ii) no reduction in displacement compared to high-PT passive frame, and (iii) better regulation of inter-storey drift than either of the passive frames (30-40% compared to low-PT, and 10-20%, compared to high-PT passive). It should be noted that the final PT forces in the *UIDA*-controlled frame are lower than those in the high-PT frame. This means that the *UIDA* reduce the moment demand on frame columns (up to 55% in some storeys depending on the initial PT force) and regulate inter-storey drift.

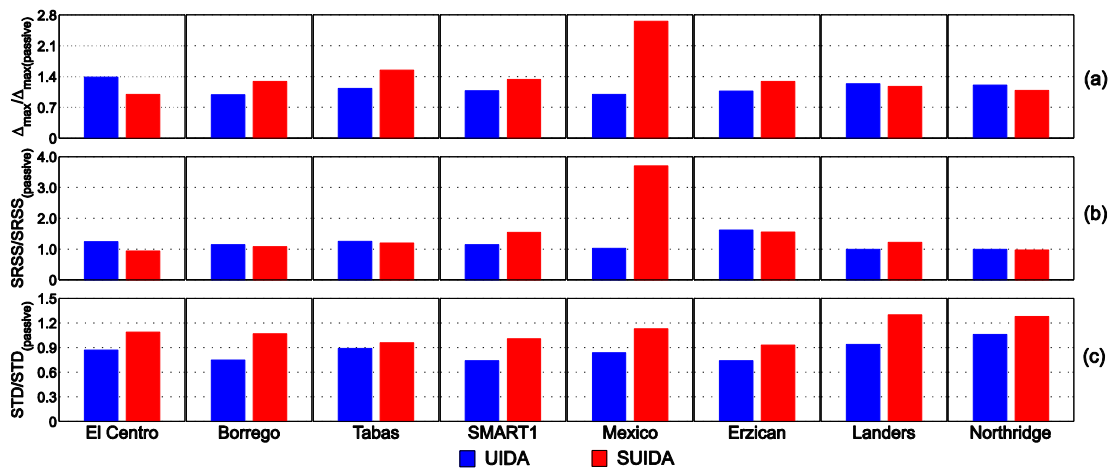


Figure 10.6: Response of deformation regulation controlled PT frame normalised to response of passive frame with high PT force: (a) top storey maximum displacements, (b) SRSS of top storey displacements and (c) standard deviation of inter-storey drifts.

The simplified version of the *UIDA* was less efficient than the original *UIDA* algorithm (Tables 10.4 and 10.5). This implies that simplifying the operation (one adaptation) would affect the efficiency of the control. The *SUIDA* however can be used as a reference point for balancing the algorithm efficiency and the reliability or complexity of the control software/hardware.

10.2. Conclusions

This research included original work on seismic behaviour of PT frames with passive and semi-active control systems: (i) a new integrated post-tensioned connection element (IPTC), (ii) simulating the response of PT frames with wide selections of seismic excitations, (iii) incorporation of semi-active control in controlling the seismic behaviour of PT frames, (iv) a new control algorithm (LDFA) for increasing the energy dissipation capacity of PT frames, (v) a new stiffness selection algorithm in the stiffness control approach and (vi) an entirely new approach for regulating maximum deformations of PT frames through minimising the differences in inter-storey drift.

Several conclusions can be drawn from the modelling and simulations of the seismic response of passive and semi-active post-tensioned frames:

- Post-tensioned steel frames offer seismic response that is superior to the seismic response of conventional moment resisting frames in terms of reducing the residual displacements and damage in the frame elements but not in the amount of energy dissipation. Conventional MRFs can dissipate significantly higher energy in the early stages of the earthquake which results in damping of the response in the later stages. The dissipated energy in conventional MRFs however is a result of permanent damage in the frame elements (plastic hinges). In passive PT frames acceptable levels of response (deformations) can be achieved without damage to the frame elements (without plastic hinges).
- Seismic response of passive post-tensioned steel frames is heavily dependent on the connection parameters F_{pt} (post-tensioning force) and β (energy dissipation factor). When these parameters are selected correctly, post-tensioned steel frames exhibit very good dynamic behaviour under seismic actions. However, the values of these two parameters (and consequently the response of passive PT frames) are very sensitive to the characteristics of the seismic excitation and therefore cannot be considered as a propitious solution for improving the seismic response of these structures.
- The structure and components of the post-tensioned steel frames make them versatile and give a potential to apply semi-active control without adding new structural elements to the frame. Semi-active control can be used to correct the major deficiency of passive PT frames: the sensitivity of F_{pt} and β to the characteristics of the excitations. The aim of the semi-active control is to correct F_{pt} (and consequently β) during the seismic action. Hence, the performance of the different control approaches in this research is always compared with that of corresponding passive PT frames (frame with the same level of maximum passive PT forces).
- Controlling the dynamic behaviour of post-tensioned steel frames by increasing their energy dissipation capacity is not sufficient to effectively reduce the frame response. The energy dissipation control approach proposed here did not reduce peak displacements and the results were very dependent on the type of the seismic excitation. This approach can be used successfully only for post-tensioned steel frames subjected to low frequency earthquakes such as those constructed on soft soils or subjected to far field earthquakes, where the maximum top storey displacements can be reduced up to 18%.

- Semi-active control of structures based on avoiding a resonant state during the earthquake is a good approach for reducing structural response. The feedback algorithms proposed here demonstrated that this approach can be used to improve the dynamic response of post-tensioned steel frames effectively (typically 30-40% reduction in top storey displacement, and 70% reduction of top storey displacement for Mexico City earthquake). Compared to passive PT frames, the stiffness control approach offers acceptable response deformations at significantly reduced force demand on the frame elements (typically between 50 and 70% reduction of initial PT force).
- Controlled post-tensioning forces in the strands can be used to create a more uniform distribution of deformations through all storeys of the frame. When the post-tensioning forces are semi-actively controlled to achieve certain distribution over all storeys, they result in more uniform distribution of inter-storey drifts than the distribution of drifts in passive frames with high post-tensioning forces. This results in a better distribution of internal forces in the elements of the structure in all storeys (typical reduction of the standard deviation of inter-storey drifts by 30-40%).

10.3. Recommendations for Future Work

Based on the conclusions from this research, the work on this field can be continued in the following directions:

- Improving the model of the Integrated Post-tensioned Connection (IPTC) to provide a better representation of the axial stiffness of the connection in the post-yielding/slipping phase. This model should consider the reduction in the axial stiffness of the connection due to gap-opening and yielding/ slipping of the energy dissipaters. Also, the effects of the beam shortening and the diaphragm action should be included in the improved model.
- Upgrading the IPTC model to include other energy dissipaters such as top and seat angles or the newly developed pin hourglass-shaped energy dissipaters.
- Investigating optimum distributions of passive PT forces over all storeys that are suitable for different types of PT frames and seismic locations to improve the seismic behaviour of passively controlled PT frames.
- Carrying out robustness analyses of the proposed control algorithms for better determination of the control parameters and their corresponding ranges of action. Special investigations should be directed to specifying the appropriate control time in the stiffness-based control algorithms based on mathematical and practical studies of the algorithms' factors.

- Investigating other forms of force variation to improve the performance of Uniform Inter-storey Drift Algorithms, and performing computational cost analysis to obtain the optimum number of sets of control forces that result in the optimum point of performance.
- Extending the control algorithms proposed in this thesis (especially the frequency state feedback and uniform inter-storey drift distribution algorithms) to other types of structures such as braced frames with semi-active devices.
- Verifying the simulated behaviour by shaking table (or other dynamic) experiments on reduced scale PT structures equipped with systems for semi-active control.

References

- Abdel-Rohman M. and Leipholz H.H. (1979), "A general approach to active structural control". Journal of the Engineering Mechanics Division, ASCE, 105(6), 1007-1923.
- Aiken I, Nims D, Whittaker A, and Kelly J. (1993), "Testing of Passive Energy Dissipation Systems". Earthquake Spectra. 9(3).
- American Institute of Steel Construction (AISC). (1994), "Load and Resistance Factor Design Manual of Steel Construction", Second Edition, Volume II, Connections, Part 10, American Institute of Steel Construction, Chicago, Illinois.
- Arfiadi, Y, and Hadi, M N S. (2000), "Passive and active control of three-dimensional buildings". Earthquake Engineering & Structural Dynamics. 29(3), 377-396.
- Aydinoğlu M, and Fahjan Y. (2003), "A unified formulation of the piecewise exact method for inelastic seismic demand analysis including the *P*-delta effect". Earthquake Engineering & Structural Dynamics. 32(6), 871-890.
- Bhardwaj M, and Datta T. (2006), "Semiactive Fuzzy Control of the Seismic Response of Building Frames". Journal of Structural Engineering, 132(5), 791-799.
- Bitaraf M, Ozbulut O, Hurlebaus S, Barroso L. (2010), "Application of Semi-Active Control Strategies for Seismic Protection of Buildings with MR Dampers". Engineering Structures, 32, 3040-3047.
- Borgan W L. (1991), "Modern Control Theory" Prentice Hall, Englewood Cliffs, New Jersey.
- Bruneau M. (2004), "Seismic Retrofit of Steel Structures", VIII Mexican Symposium on Earthquake Engineering, Tlaxcala, Mexico, September 2004. Available at: http://www.eng.buffalo.edu/~bruneau/Bruneau_VIIISNIS.pdf
- Bruneau M, Engelhardt M, Filiatrault M, Goel M, Itani M, Hajar J, Leon R, Ricles J, Stojadinovic B and Uang C. (2005), "Review of selected recent research on US seismic design and retrofit strategies for steel structures". Earthquake Engineering and Structural Dynamics, 7, 103-114.
- Carr A J. (2007) "Ruaumoko Manual"- Volume 1, Theory. University of Canterbury, New Zealand, available at: <http://www.ruaumoko.co.nz/manuals/RuaumokoTheory.pdf>
- Castro J, Elghazouli A, and Izzuddin B. (2005), "Modelling of the panel zone in steel and composite moment frames". Engineering Structures. 27(1), 129-144.
- Chae Y, Ricles J, and Sause R. (2013), "Large-Scale Experimental Studies of Structural Control Algorithms for Structures with Magnetorheological Dampers Using Real-Time Hybrid Simulation". Journal of Structural Engineering. 139(7), 1215-1226.

-
- Cheng F. (2001), "Matrix Analysis of Structural Dynamics, Applications and Earthquake Engineering". Chapter 9, "Various Hysteresis Models and Nonlinear Response Analysis". New York, MARCEL DEKKER, INC.
- Chopra A.K. (1995), "DYNAMICS OF STRUCTURES: Theory and Applications to Earthquake Engineering". Chapter 15, "Numerical Evaluation of Dynamic Response". New Jersey, PRENTICE HALL.
- Chou C, Wang Y, and Chen J. (2008), "Seismic design and behaviour of post-tensioned steel connections including effects of a composite slab". *Engineering Structures*. 30(11), 3014-3023.
- Chou C, and Lai Y. (2009), "Post-tensioned self-centering moment connections with beam bottom flange energy dissipaters". *Journal of Constructional Steel Research*, 65(10-11), 1931-1941.
- Christopoulos C, Filiatrualt A, Uang C, and Folz B. (2002^a), "Post-tensioned Energy Dissipating Connections for Moment-Resisting Steel Frames". *Journal of Structural Engineering*, 128(9), 1111-1120.
- Christopoulos C, Filiatrualt A, and Folz B. (2002^b), "Seismic Response of Self-centring Hysteretic SDOF Systems". *Earthquake Engineering and Structural Dynamics*, 31(5), 1131-1150.
- Christopoulos C. (2004), "Frequency Response of Flag-Shaped Single Degree-of-Freedom Hysteretic Systems". *Journal of Engineering Mechanics*, 130(8), 894-903.
- Christopoulos C, Tremblay R, Kim H and Lacerte M. (2008), "Self-Centering Energy Dissipative Bracing System for the Seismic Resistance of Structures: Development and Validation". *Journal of Structural Engineering*, 134(1), 96-107.
- Constantinou, M C, Soong, T T, and Dargush, G F (1998). "Passive energy dissipation systems for structural design and retrofit". MCEER Monograph Series, No.1, Multidisciplinary Center for Earthquake Engineering Research, Buffalo, N.Y.
- Datta T.K. (2003), "A State-of-the-Art Review on Active Control of Structures". *ISET Journal of Earthquake Technology*, 40(1), 1-17.
- Datta T K, (2010), "Seismic Analysis of Structures". Chapter 9, "Seismic Control of Structures". John Wiley & Sons (Asia) Pte Ltd, Singapore.
- Deylami A. and Shiravand M.R. (2008), "The Experimental Study on Built-up Column Seismic Resistant Moment Connections Using Side Plates". The 14th World Conference on Earthquake Engineering October 12-17, 2008, Beijing, China. Available at: http://www.iitk.ac.in/nicee/wcee/article/14_05-05-0059.pdf
- Di Sarno L and Elnashai A. (2002), "Seismic Retrofitting of Steel and Composite Building Structures". Mid-America Earthquake Centre, University of Illinois at Urbana-Champaign. Available at: http://mae.cee.illinois.edu/documents/cd_rom_series/02-01/Report02-01.pdf

-
- Dimopoulos A, Karavasilis T, Vasdravellis G, and Uy B. (2013), “Seismic design, modelling and assessment of self-centering steel frames using post-tensioned connections with web hourglass shape pins”. *Bulletin of Earthquake Engineering*, in press.
- Djajakesukma S, Samali B, Nguyen H. (2002), “Study of a semi-active stiffness damper under various earthquake inputs”. *Earthquake Engineering and Structural Dynamics*, 31(10), 1757-1776.
- Dobossy M, Garlock M, and VanMarcke M. (2006) “Comparison of Two Self-Centering Steel Moment Frame Modelling Techniques: Explicit Gap Models and Non-Linear Rotational Spring Models”. 4th International Conference on Earthquake Engineering, Taipei, Taiwan, October 12-13, 2006. Paper No.101.
- Dolce M and Cardone D. (2001), “Mechanical behaviour of shape memory alloys for seismic applications 2: Austenitic NiTi wires subjected to tension”. *International Journal of Mechanical Sciences*, 43(11), 2657–2677.
- Doyle J, Francis B, Tannenbaum A. (1990), “Feedback Control Theory”. Macmillan Publishing Co. New York.
- Duerr K, Tesfamariam S, Wickramasinghe V, and Grewal A. (2013), “Variable Stiffness Smart Structure System to mitigate Seismic Induced Building Damages”. *Earthquake Engineering and Structural Dynamics*, 42, 221-237.
- Dyke S J. (1996), “Acceleration Feedback Control Strategies for Active and Semi-Active Systems: Modeling, Algorithm Development and Experimental Verification”. PhD Dissertation, University of Norte Dame, Norte Dame.
- Dyke S J, Spencer Jr. B F, Sain M K, and Charlson J D. (1996^a), “Seismic Response Reduction Using Multiple Magneto-rheological Dampers”. *Proceedings of the IFAC world Congress, San Francisco CA, June 30 – July 5*.
- Dyke S J, Spencer Jr. B F, Sain M K, and Charlson J D. (1996^b), “Modeling and Control of Magnetorheological Dampers for Seismic Response Reduction”. *Smart Materials and Structures*. 5, 565 – 575.
- Dyke S J and Spencer Jr. B F. (1997), “A Comparison of Semi-Active Control Strategies for the MR Damper”. *Proceedings of the IASTED International Conference. Intelligent Information Systems. The Bahamas, Dec 8-10, 1997*.
- Eljajeh Y. (2010), “Seismic Behaviour of Passively Controlled Eccentric Braced Frames with Self-Centring Systems”. MSc Dissertation, University of Sheffield.
- Eurocode 2. (2004), “Design of concrete structures- Part 1-1: General rules and rules for buildings”. BS EN 1992-1-1:2004.
- Eurocode 8. (2004), “Design of structures for earthquake resistance- Part 1: General rules, seismic actions and rules for buildings”. BS EN 1998-1:2004.
- Engelhardt M, and Husain A. (1993), “Cyclic-Loading Performance of Welded Flange-Bolted Web Connections”. *Journal of Structural Engineering*. 119 (12), 3537-3550.

-
- Engelhardt M, and Sabol T. (1998), "Reinforcing of Steel Moment Connections with Cover Plates: Benefits and Limitations". *Engineering Structures*. 20(4-6), 510-520.
- Esposito M. (2008), "PTED Beam-to-Column Connections for Steel Moment Resisting Frames: Structural Identification Based on Numerical Analyses", PhD Thesis, Università degli Studi di Napoli Federico II, Naples, Italy.
- Federal Emergency Management Agency (FEMA). (2000), "Recommended Seismic Design Criteria for New Steel Moment-Frame Buildings". FEMA, Rep. No. 350, Washington, D.C.
- Federal Emergency Management Agency (FEMA). (2000), "Recommended Seismic Evaluation and Upgrade Criteria for Existing Welded Steel Moment-Frame Buildings", FEMA, Rep. No. 351, Washington, D.C.
- Federal Emergency Management Agency (FEMA). (2000), "State of the Art on Connection Performance". FEMA, Rep. No. 355 D, Washington, D.C.
- Federal Emergency Management Agency (FEMA). (2006), "Next-Generation Performance-Based Seismic Design Guidelines; Program Plan for New and Existing Buildings". FEMA, Rep. No. 445, Washington, D.C.
- Garlock M, Sause R, and Ricles J. (2007), "Behaviour and Design of Posttensioned Steel Frame Systems". *Journal of Structural Engineering*. 133(3), 389-399.
- Garlock M and Li J. (2008), "Steel self-centering moment frames with collector beam floor diaphragms". *Journal of Constructional Steel Research*. 64(5), 526-538.
- Garlock M, Ricles J, and Sause R. (2008), "Influence of design parameters on seismic response of post-tensioned steel MRF systems". *Engineering Structures*, 30(4), 1037-1047.
- Glad T and Ljung L. (2000), "Control Theory: Multivariable and Nonlinear Methods". Chapter 6, "The Closed Loop System". New York, Taylor & Francis
- Horvat D, Barak P and Rabins M. (1983), "Semi-active Versus Passive or Active Tuned Mass Dampers for Structural Control". *Journal of Engineering Mechanics*, 109(3), 691-705.
- Houghton D.L. (1997), "Prototype Cyclic Testing of the Side-Plate Moment Connection System". Northridge Earthquake Research Conference Los Angeles, California. Available at: http://www.sideplate.com/tech_papers/Prototype%20Cyclic%20Testing%20of%20the%20SidePlate%20Moment%20Connection%20System.pdf
- Hu J, and Leon R. (2011), "Analyses and evaluations for composite-moment frames with SMA PR-CFT connections". *Nonlinear Dynamics*, 65, 433-455.
- Hu J, Choi E, and Leon R. (2011), "Design, analysis and application of innovative composite PR connections between steel beams and CFT columns". *Smart Materials and Structures*, 20, 1-15.

-
- Inaude J A. (1997), “Modulated Homogenous Friction: A Semi-Active Damping Strategy”. *Earthquake Engineering and Structural Dynamics*, 26(3), 361–376.
- Iskhakov I, and Ribakov Y. (2008), “Seismic Response of Semi-Active Friction-Damped Reinforced Concrete Structures with Self-Variable Stiffness”. *The Structural Design of Tall and Special Buildings*, 17, 351-365.
- Janke L, Czaderski C, Motavalli M, and Ruth J. (2005), “Applications of shape memory alloys in civil engineering structures – Overview, limits and new ideas”. *Materials and Structures*, 38, 578-592.
- Jinping Q, and Hui L. (2009), “Design approaches for active, semi-active and passive control systems based on analysis of characteristics of active control forces”. *Earthquake Engineering and Engineering Vibration*, 8(4), 493-506.
- Karavasilis T. (2010), “High-Performance Seismic-Resistant Steel Frame Equipped with Self-Centering Viscous Damping Devices”. *SECED - Society for Earthquake and Civil Engineering Dynamics -Young Engineers Conference – 2010*.
- Karavasilis T, Blakeborough T, and Williams M. (2011), “Development of nonlinear analytical model and seismic analysis of steel frame with self-centering devices and viscoelastic dampers”. *Computers and Structures*, 89, 1232-1240.
- Karavasilis T and Seo C. (2011), “Seismic structural and non-structural performance evaluation of highly damped self-centering and conventional systems”. *Engineering Structures*, 33(8), 2248-2258.
- Kim H and Christopoulos C. (2008) “Friction Damped Posttensioned Self-Centering Steel Moment-Resisting Frames”. *Journal of Structural Engineering*. 134(11), 1768–1779.
- Kim H and Christopoulos C. (2009) “Numerical models and ductile ultimate deformation response of post-tensioned self-centring moment connections”. *Earthquake Engineering and Structural Dynamics*. 38(1), 1–21.
- Kobori T, Takahashi M, Nasu T, Niwa N and Ogasawara K. (1993), “Seismic response controlled structure with active variable stiffness system”. *Earthquake Engineering and Structural Dynamics*. 22(11), 925-941.
- Krawinkler H, Bertero V, and Popov E. (1971), “Inelastic Behaviour of Steel Beam-to-Column Sub-assemblages”. *EERC Report 71-7*, University of California, Berkeley.
- Krawinkler H, and Popov E. (1982), “Seismic Behaviour of Moment Connections and Joints”. *Journal of the Structural Division; Proceedings of the American Society of Civil Engineers*. 108(2), 373-391.
- Kurata N, Kobori T, and Koshika N. (2002), “Performance-based design with semi-active structural control technique”. *Earthquake Engineering and Structural Dynamics*. 31, 445-458.

-
- Lane J.S, Ferri A.A, and Heck B.S. (1992), "Vibration Control Using Semi-Active Friction Damping". Friction-Induced Vibration, Chatter, Squeal, and Chaos, American Society of Mechanical Engineers, Design Engineering Division (49), 165-171.
- Latour M, Pilosu V and Rizzano G. (2012), "Experimental Behaviour of Friction T-Stub Beam-to-Column Joints Under Cyclic Loads". 7th International Workshop on Connections in Steel Structures. Timișoara 30 May - 02 June 2012. Available at: http://www.ct.upt.ro/connections/files/Session%203_Connections%20for%20seismic%20effects/6_M.%20Latour,%20V.%20Pilosu,%20G.%20Rizzano_Experimental%20behaviour%20of%20friction%20T-stub%20beam-to-column%20joints%20under%20cyclic%20loads.pdf [Accessed on 4th April 2013].
- Leitmann G. (1994), "Semi-active Control for Vibration Attenuation". Journal of Intelligent Material Systems and Structures, 5(6), 841 - 846.
- Li S, Liu K, Zhang N, Tam M, and Yang F. (2001), "Multi-level design model and genetic algorithm for structural control system optimization". Earthquake Engineering and Structural Dynamics, 30(6), 927-942.
- Lin Ying-C, Ricles J, and Sause R. (2008), "Earthquake Simulation on a Self-Centering Steel Moment Resisting Frame with Web Friction Devices". The 14th World Conference on Earthquake Engineering, Beijing, China, October 12-17, 2008. Available at: http://www.nees.lehigh.edu/wordpress/uploads/2010/12/sc-mrf-14WCEE_SC-MRF_YCL.pdf
- Lu L. (2004), "Semi-active modal control for seismic structures with variable friction dampers". Engineering Structures, 26(4), 437-454.
- Mahmoodi (1969) "Structural Dampers". Journal of Structural Division, ASCE, 95(8), 1661-1672.
- Markis N and McMahon S. (1996), "Structural control with controllable fluid dampers: design and implementation issues". Proceedings of Second International Workshop on Structural Control, Hong Kong, 311-322.
- McClamroch N H and Gavin H P. (1995), "Closed Loop Structural Control Using Electro-rheological Dampers". Proceedings of the American Control Conference. Seattle, Washington, 4173 - 4177.
- Nemir D, Lin Y and Osegueda R. (1994), "Semi-active Motion Control Using Variable Stiffness". Journal of Structural Engineering, 120(4), 1291- 1306.
- Ng C and Xu Y. (2007), "Semi-active control of a building complex with variable friction dampers". Engineering Structures, 29(6), 1209-1225.
- Nishitani A and Inoue Y. (2001), "Overview of the application of active/semi-active control to building structures in Japan". Earthquake Engineering and Structural Dynamics. 30, 1565–1574.

- Nishitani A, Nitta Y, and Ikeda Y. (2003), "Semi-active Structural Control Based on Variable Slip-Force Level Dampers". *Journal of Structural Engineering*, 129(7), 933-940.
- Nishitani A. (2008), "Structural Control: Overview and Fundamentals". Available at: http://bridge.tongji.edu.cn/APSS2011/LECTURES/AUG%2015/August%2015%20-%20PDF_summerschool.pdf
- Ocel J, DesRoches R, Leon R, Hess G, Krumme R, Hayes J, and Sweeney S. (2004), "Steel Beam-Column Connections Using Shape Memory Alloys". *Journal of Structural Engineering*. 130(5), 732-740.
- Otsuka K, and Wayman C M. (1999), "Shape Memory Materials". Cambridge University Press.
- Popov E, and Pinkney R. (1969), "Cyclic Yield Reversals in Steel Building Connections". *Journal of Structural Division*. 95(3), 327-353.
- Popov E, and Stephen R. (1970), "Cyclic Loading of Full Size Steel Connections". EERC Report 70-3, University of California, Berkeley.
- Powel G.H. (1993), "DRAIN-2DX Element Description and User Guide for Element Type01, Type02, Type04, Type06, Type09, and Type15".
- Prakash V, Powel G.H, and Campbell S (1993), "DRAIN-2DX Base Program Description and User Guide".
- Priestley MJN. (1996), "Seismic design philosophy for precast concrete frames". *Structural Engineering International*. 6(1), 25- 31.
- Regents of the University of California. (2000), "PEER Strong Motion Database". Available at: <http://peer.berkeley.edu/smcat/search.html> [Accessed 7th February 2013].
- Ricles J, Sause R, Garlock M, and Zhao C. (2001), "Posttensioned Seismic-Resistant Connections for Steel Frames". *Journal of Structural Engineering*. 127(2), 113-121.
- Ricles J, Mao C, Lu L, and Fisher J. (2002^a), "Inelastic Cyclic Testing of Welded Unreinforced Moment Connections". *Journal of Structural Engineering*, 128(4), 429-440.
- Ricles J, Sause R, Peng S and Lu L. (2002^b), "Experimental Evaluation of Earthquake Resistant Posttensioned Steel Connections". *Journal of Structural Engineering*, 128(7), 850-859.
- Roeder C. (2002^a), "General Issues Influencing Connection Performance". *Journal of Structural Engineering*, 128(4), 420-428.
- Roeder C. (2002^b), "Connection Performance for Seismic Design of Steel Moment Frames". *Journal of Structural Engineering*, 128(4), 517-525.
- Rojas P, Ricles J, and Sause R. (2004), "Seismic Response and Design of Post-tensioned Steel Moment Resisting Frames with Friction Components". 13th World Conference on Earthquake Engineering. Vancouver, B.C., Canada. Paper No. 1603.

- Rojas P, Ricles J, and Sause R. (2005), "Seismic Performance of Post-tensioned Steel Moment Resisting Frames with Friction Devices". *Journal of Structural Engineering*, 131(4), 529-540.
- Rustighi E, Brennan, M. J., and Mace, B. R. (2005), "A shape memory alloy adaptive tuned vibration absorber: design and implementation". *Smart Materials and Structures*, 14, 19-28.
- SAC Steel Project (SAC). (1994), "Proceeding of the invitational workshop on steel seismic issues." Rep. No SAC 94-01, SAC Steel Project, Sacramento, California.
- Sadek F, and Mohraz B. (1998), "Semiactive Control Algorithms for Structures with Variable Dampers". *Journal of Engineering Mechanics*, 124(9), 981-990.
- Sause R, Ricles J, Garlock M, VanMarcke E, Peh Li-S, and Lin J. (2005), "Self-centering Seismic-Resistant Steel Frame Systems: Overview of Past and Current Research", NEES@ Lehigh Publications. Available at: http://www.nees.lehigh.edu/wordpress/uploads/2010/12/SC_Systems_Overview_Abstract_US-Taiwan_Workshop_on_Self-Centering_Structural_Systems.pdf
- Schneider S, and Teeraparbowng I. (2002), "Inelastic Behaviour of Bolted Flange Plate Connections". *Journal of Structural Engineering*, 128(4), 492-500.
- Schurter K, and Roschke P. (2001), "Neuro-fuzzy control of structures using acceleration feedback". *Smart Materials and Structures*, 10, 770-779.
- Shing P, Dixon M, Kermiche N, Su R, and Frangopol D. (1996), "Control of Building Vibrations with Active/Passive Devices". *Earthquake Engineering and Structural Dynamics*, 25(10), 1019-1039.
- Song G, Ma N and Li H-N. (2006), "Applications of shape memory alloys in civil structures". *Engineering Structures*, 28(9), 1266-1274.
- Speicher M, Hodgson D, DesRoches R, and Leon R. (2009), "Shape Memory Alloy Tension/Compression Device for Seismic Retrofit of Buildings". *Journal of Materials Engineering and Performance*, 18(5-6), 746-753.
- Speicher M, DesRoches R, and Leon R. (2011), "Experimental results of a NiTi shape memory alloy (SMA)-based recentering beam-column connection". *Engineering Structures*, 33(9), 2448-2457.
- Spencer Jr B F, Dyke S J, and Deoskar H S. (1998), "Benchmark Problems in Structural Control Part I: Active Mass Driver System". *Earthquake Engineering and Structural Dynamics*, 27(11), 1127-1139.
- Spencer Jr B F, Dyke S J, Sain M K, and Charlson J D. (1997). "Phenomenological Model of a Magneto-rheological Damper". *Journal of Engineering Mechanics*, ASCE, 123(3), 230-238.
- Spencer Jr B F and Nagarajaiah S. (2003). "State of the Art of Structural Control". *Journal of Structural Engineering* 129(7), 845-856.

-
- Swensen S. (2008), "Design of Self-Centering Moment Resisting Frame and Experimental Loading System", NEES@ Lehigh Publications, 2008. Available at: http://nees.org/site/oldnees/filedir_2/swensen_Research_Paper.pdf
- Symans M and Constantinou M. (1995), "Development and experimental study of semi-active fluid damping devices for seismic protection of structures". Report No. NCEER 95-0011, National Centre for Earthquake Engineering Research, Buffalo, NY.
- Symans M D, and Constantinou, M C. (1999), "Semi-active control systems for seismic protection of structures: a state-of-the-art review". *Engineering Structures*, 21(6), 469-487.
- Tsai K, Chou C, Lin C, Chen P, and Jhang S. (2008), "Seismic self-centering steel beam-to-column moment connections using bolted friction devices". *Earthquake Engineering and Structural Dynamics*, 37(4), 627-645.
- Uang C, Yu Q, Noel S and Gross J. (2000), "Cyclic Testing OF Steel Moment Connections Rehabilitated with RBS or Welded Haunch". *Journal of Structural Engineering*, 126(1), 57-68.
- Vasdravellis G, Karavasilis T, Uy B. (2013^a), "Large-Scale Experimental Validation of Steel Posttensioned Connections with Web Hourglass Pins". *Journal of Structural Engineering*, 139(6), 1033-1042
- Vasdravellis G, Karavasilis T, Uy B. (2013^b), "Finite element models and cyclic behavior of self-centering steel post-tensioned connections with web hourglass pins". *Engineering Structures*, 52, 1-16.
- Walsh K, Abdullah M, and Moore C. (2008), "Control of Civil Structures Using a Semiactive Stiffness System Based on Variable Amplification". *Journal of Structural Engineering*, 134(7), 1246-1251.
- Wang D. (2004), "Seismic Response of Steel Framed Hospital Buildings with Self-Centering Systems", MCCER Buffalo publication, in Student Research Accomplishments Volume: 2004-2005. Available at: <http://mceer.buffalo.edu/publications/resaccom/06-sp04/pdf/03wang.pdf>
- Weber F, Feltrin G, and Huth O. (2006), "SAMCO Final Report 2006 F05 Guidelines for Structural Control". Structural Engineering Research Laboratory, Swiss Federal Laboratories for Materials Testing and Research, Dübendorf, Switzerland.
- Williams K, Chiu G, and Bernhard R. (2002), "Adaptive-passive absorbers using shape-memory alloys". *Journal of Sound and Vibration*, 249(5), 835-848.
- Wilson C, and Abdullah M. (2010), "Structural Vibration Reduction using Self-tuning Fuzzy Control of Magnetorheological Dampers". *Bulletin of Earthquake Engineering*, 8, 1037-1054.

- Wolski M, Ricles J, and Sause R. (2009), “Experimental Study of a Self-Centering Beam–Column Connection with Bottom Flange Friction Device”. *Journal of Structural Engineering*, 135(5), 479-488.
- Xu Z D, Shen Y P, and Gou Y Q. (2003), “Semi-active control of structures incorporated with magneto-rheological dampers using neural networks”. *Journal of Smart Materials and Structures*, 12(1), 80-87.
- Yang C, DesRoches R, Leon R. (2010), “Design and analysis of braced frames with shape memory alloy and energy-absorbing hybrid devices”. *Engineering Structures*, 32 (2), 498-507.
- Yao J. (1972). “Concept of Structural Control”. *Journal of Structural Division*, 98 (1972), 1567–1574.
- Zhou L, Chang C, Wang L. (2003), “Adaptive Fuzzy Control for Nonlinear Building Magnetorheological Damper System”. *Journal of Structural Engineering*, 129(7), 905-913.

Appendix A

FASAC V2.5: FRAME ANALYSIS WITH SEMI-ACTIVE CONTROL- GUIDANCE OF INPUT FILE

Input data of FASAC-2D are read from (Fasac_input.m) module. To start a new project, copy the content of the FASAC folder and edit the input file (Fasac_input.m) to fit the geometry, material characteristics and element properties of the frame.

A.1. Input File (Fasac_input.m)

Fasac_input.m is a script that can be modified as an input file for FASAC-2D.

A.1.1. Geometric Properties

Geometry of the frame is considered in the matrix of coordinates (**Coor**). The input of this matrix is the (x, z) coordinates of all nodes of the frame.

A.1.2. Element Connectivity Array and Element Type

Element connectivity in the frame is considered in the connectivity matrix (**Connectivity**). The input of the matrix is presented in Table A.1.

Column	Variable	Notes
1	Elementnum	Sequence of the element.
2	i	Start node.
3	j	End node
4	Type	Type of the element ¹ .
5	endi	Freedom of end (i) - 1: framed, 2: pinned.
6	endj	Freedom of end (j) - 1: framed, 2: pinned.

Table A.1: Connectivity matrix.

¹ Element types considered in this version are: (i) Element Type 1- Beam-Column Element, (ii) Element Type 2- Bar element (truss element), (iii) Element Type 3- Post-tensioned connection element and (iv) Element Type 6- Simple connection element.

A.1.3. Non-Connection Element Properties

Properties of Non-connection elements are considered in the properties matrix (Prop). The input of this matrix is presented in Table A.2.

Column	Variable	Notes
1	Elementnum	Sequence of the element.
2	E	Modulus of elasticity [F/L ²]
3	A	Area of cross section [L ²].
4	I	Moment of inertia of the section [L ⁴].
5	Mp	Plastic Moment of the section [F.L].
6	Np	Plastic normal force of the section [F].
7	P	Ratio of the post-yield stiffness to the initial stiffness of the element.
8	Beta	β coefficient of Rayleigh damping

Table A.2: Terms of Prop matrix.

A.1.4. Properties of Post-tensioned Connection Elements

Properties of post-tensioned connection elements are input in three matrices: (i) Type of energy dissipating and (ii) Properties of energy dissipater.

A.1.4.1. Type of energy dissipating (EnDisType):

Column	Variable	Notes
1	CESeq	Connection Element Sequence
2	EDType	Energy dissipation type: 1. Yielding: Energy Dissipating Bars. 2. Friction: Friction Dissipating Device

Table A.3: Energy dissipation type of PT connection.

A.1.4.2. Properties of Energy Dissipater (DissProp):

A ten-column matrix is use to input the properties of energy dissipater (Table A.3).

Column	Variable	Notes
1	ConSeq	Sequence of the connection.
2	Db	Depth of the adjacent beam.
3	Eb	Modulus of elasticity of energy dissipating bars.
4	fyb	Yield stress of energy dissipating bars.
5	Fyed	Slip force of energy dissipating device.
6	Lb	Length of energy dissipating bars.
7	dia	Diameter of energy dissipating bars.
8	alphaEb2	Ratio of post-yield stiffness to the initial stiffness of energy dissipating bars
9	C	Friction stiffness ratio ² .
10	FricLoc	Location of friction device: 1. Installed at Flanges. 2. Installed at Web.

Table A.4: Properties of energy dissipater in post-tensioned connection elements.

A.1.4.3. Properties of Strands (StrandProp):

An eight-column matrix is used to input the properties of the post-tensioned strands at each connection (Table A.5).

Column	Variable	Notes
1	-	Sequence of the connection number.
2	NoS	Number of strands.
3	Es	Modulus of elasticity of strands.
4	fys	Yield stress of strands.
5	As	Area section of one strand.
6	Ls	Length of the strand (half of the adjacent beam span).
7	Fpti	Initial post-tensioning force.

Table A.5: Properties of strands in post-tensioned connection elements

A.1.5. Properties of Simple Connection Elements

Properties of the simple connection elements are input in a five-column matrix (ConnProp) as given in Table A.6.

Column	Variable	Notes
1	CSeq	
2	K0	
3	K1/k0	
4	Dir	
5	SimFyCon	

Table A.6: Input data of simple connection elements.

A.1.6. Nodal Masses

Nodal masses are considered in the nodal masses matrix (Mass). The input of this matrix is given in Table A.7.

Column	Variable	Notes
1	M	Mass of the node.
2	Fx	Factor of the mass in x direction.
3	Fy	Factor of the mass in y direction.
4	Fr	Factor of the mass in rotation.

Table A.7: Input of nodal masses matrix.

² C: Friction stiffness ratio is a factor assigned to approximate the pre-slippage stiffness of the friction device. The actual pre-slippage stiffness should be infinite, but this will result in numerical errors and convergence difficulties. Also this factor is used to approximate deformations of the connection at slippage. Assigning zero causes numerical problems.

A.1.7. Mass Coefficient of Rayleigh Damping

This is to input the value of α in Rayleigh damping (Damping is proportional to stiffness and mass).

A.1.8. Boundary Conditions (Restrains)

The matrix (Restrains) is used to input the boundary conditions of the frame. Table A.8 lists the terms of this matrix.

Column	Variable	Notes
1	Nodesnum	Node number.
2	x	1: Restrained in X direction, 0: Free in X direction.
3	z	1: Restrained in Z direction, 0: Free in Z direction.
4	R	1: Restrained in rotation, 0: Free in rotation.

Table A.8: Terms of (Restrains) Matrix.

A.1.9. External Forces

External Forces are applied using (Force) matrix. Terms of this matrix are shown in Table A.9.

Column	Variable	Notes
1	Nodesnum	Number of node on which the force is applied.
2	Fx	Load in X direction.
3	Fz	Load in Y direction.
4	M	Moment applied on the node.

Table A.9: External Forces Matrix.

A.1.10. Analysis Type

The variable *Analysis* stands for the analysis type (Table A.10).

Value of <i>Analysis</i>	Analysis Type
1	Static analysis
2	Dynamic analysis
3	Static pushover analysis

Table A.10: Types and input of *Analysis*.

The variable *DynLin* stands for the linearity of dynamic analysis (Table A.11).

Value of <i>DynLin</i>	Analysis Type
1	Linear dynamic analysis
2	Nonlinear dynamic analysis

Table A.11: Types and input of *DynLin*.

A.1.11. Dynamic Analysis Input Data

A.1.11.1. Earthquake Excitation for the Dynamic Analysis

The variable *Quake* is used to select the earthquake excitation (Table A.12). A set of earthquake records are included in the program folder (other records can be imported and used).

Quake	Earthquake Record
1	Loma-Prieta -1989
2	Kobe -1995
3	Mexico City-1985
4	Northridge -1994
5	Parkfield-2004
6	Borrego Mountain-1968
7	Landers- 1992
8	El Centro-1940
9	Imperial Valley-1979
10	Erzican -1992
11	Tabas- 1978
12	SMART1-1983
13	Artificial earthquake

Table A.12: Earthquake records in FASAC-2D.

The earthquake record is scaled using the *PGA* variable.

A.1.11.2. Analysis of Earthquake Record

FASAC-2D offers analysing the earthquake record by finding its response spectrum using the piecewise exact method (Aydinoğlu and Fahjan, 2003), or performing frequency analysis using Fast Fourier Transform (FFT) as shown in Table A.13.

Variable	Notes
<i>Resp</i>	Computation of response spectrum-0: do not compute, 1: compute.
<i>TnInitial</i>	Initial period of the spectrum.
<i>TnFinal</i>	Final period of the spectrum.
<i>stepTn</i>	Increment in period in spectrum computation.
<i>damp</i>	Damping Ratio of the response spectrum
<i>Freq</i>	Computation of frequency content-0: do not compute, 1: compute.

Table A.13: Analysis of earthquake records in FASAC-2D.

A.1.12. Dynamic Analysis Parameters

Parameters of the dynamic analysis in FASAC-2D are presented in Table A.14.

Variable	Notes
<i>Dt</i>	Integration time-step
<i>alfa, deltaa</i>	Newmark integration parameters
<i>iter</i>	Maximum number of iterations in a time-step for nonlinear analysis.

Table A.14: Parameters of nonlinear dynamic analysis in FASAC-2D.

A.1.13. Pushover Analysis Input Data

Input data for pushover analysis in FASAC-2D are presented in Table A.15.

Variable	Notes
<i>LoadPat</i>	Load pattern of the analysis- 1: rectangular 2: triangular.
<i>LoadMax</i>	Maximum load in the analysis (load-control)
<i>LoadStep</i>	Increment in the lateral load.
<i>PBD</i>	Performance Based Design analysis: 0: analysis is stopped when the maximum displacement (rotation) is reached. 2: analysis is continued until the maximum load is reached.
<i>ThetaLim</i>	Maximum rotation (or displacement).

Table A.15: Input data of nonlinear static pushover analysis in FASAC-2D.

A.1.14. Plot Deformed Shape for Static Analysis

The variable (*PlotDeformed*) states the selection to plot the deformed shape of static analysis or not. Setting *PlotDeformed* (1) plots the deformed shape; or to (2) otherwise. The variable *magfac* stands for the magnification factor of the deformed shape.

A.1.15. Parameters of Semi-Active Control

Control parameters in FASAC-2D are presented in Table A.16.

Variable	Notes
<i>Control</i>	0. No control, 1. Apply semi-active control
<i>CtrlStrat</i>	Control strategy (control algorithm)- Table A.17
<i>CtrlTime</i>	Control time interval (for <i>CtrlStrat</i> =1,5,6,7 and 8)
<i>Filter</i>	Applying low-pass filter (for <i>CtrlStrat</i> =5 to 8) 0: Don't apply filter, 1: apply filter.
<i>FreqAnalyse</i>	Type of analysing the frequency content (for <i>CtrlStrat</i> =5 to 8). 1. Short control time with overlapping periods. 2. Continuous Frequency Content.
<i>OverLapTime</i>	OverLapping Time (for <i>CtrlStrat</i> =5 to 8 and <i>FreqAnalyse</i> =1).
<i>forceInc</i>	Control force increment in each time step (for <i>CtrlStrat</i> =2, 3).
<i>fmax</i>	Maximum force increment in each time step (for <i>CtrlStrat</i> =2, 3).
<i>threshold</i>	Threshold of inter-storey drift ration (for <i>CtrlStrat</i> =4).

Table A.16: Control parameters in FASAC-2D.

Control strategies (algorithms) developed in this version of FASAC-2D are presented in Table A.17.

CtrlStrat	Notes
<i>1</i>	Control time feedback.
<i>2</i>	Displacement-based loading direction feedback (DB-LDFA).
<i>3</i>	Velocity-based loading direction feedback (VB-LDFA).
<i>4</i>	Uniform inter-storey drifts (UIDA).
<i>5</i>	Optimal frequency state feedback (OFSFA).
<i>6</i>	Frequency state feedback with threshold.
<i>7</i>	Response frequency state feedback (RFSFA).
<i>8</i>	Response spectrum feedback (RSFA)
<i>9</i>	Frequency response function feedback (FRFFA)
<i>13</i>	Lazy uniform inter-storey drift (LUIDA).

Table A.17: Control strategies in FASAC-2D.

Appendix B

MATLAB SCRIPTS OF CONTROL ALGORITHMS

B.1. Energy Dissipation Approach

```
% Loading Direction Feedback
% MATLAB script to apply Loading Direction control strategy
%-----
for dd=1:ns
    FcontHist=Fcontrol(dd,1:Step);
    if abs(ConRot(ConMaster(dd),Step+1)) > th2(ConMaster(dd),Step+1) &&...
        abs(ConRot(ConMaster(dd),Step+1)) < abs(ConRot(ConMaster(dd),Step))
        Fcontrol(dd,Step+1)=-f;
    elseif abs(ConRot(ConMaster(dd),Step+1)) < 0.9*th1(ConMaster(dd),2)
        if sum(FcontHist) < (cap-1)*Fpt(1,ConMaster(dd),1);
            % Number of Steps for changing the force
            Chan(dd,Step+1)=abs(sum(FcontHist));
            if Chan(dd,Step+1) >= fmax
                Fcontrol(dd,Step+1)=fmax;
            elseif Chan(dd,Step+1) < fmax
                Fcontrol(dd,Step+1)=Chan(dd,Step+1);
            end
        end
    end
end

for slgr=ConGroup(dd,:)
    Fpt(:,slgr,Step+1)=Fcontrol(dd,Step+1)+Fpt(:,slgr,Step)+ ...
        Es(slgr,1)*As(slgr,1)*(delta_st(:,slgr,Step+1)- ...
        delta_st(:,slgr,Step))/Ls(slgr,1);
end
FcontHist=Fcontrol(dd,1:Step+1);
for grslave=ConGroup(dd,:)
    % Check that the actual Post-tensioning Force is greater than the
    % Least self-centring force (FptLow)
    if min(Fpt(:,grslave,Step+1)) <= FptLow(grslave)
        Fcontrol(dd,Step+1)=0;
    end
    if sum(FcontHist) <= (FptLow(grslave)-max(Fpt(:,grslave,Step+1)))
        if abs(ConRot(ConMaster(dd),Step+1)) < th1(ConMaster(dd),2)
            Fcontrol(dd,Step+1)=fmax;
        else Fcontrol(dd,Step+1)=0;
        end
    end
end
```

```

% Check that forces in the strands do not exceed the 70% of the
% Yield force
if max(Fpt(:,grslave,Step+1))>=0.7*Fys(grslave)
    Fcontrol(dd,Step+1)=-fmax;
end
Fpt(:,grslave,Step+1)=Fcontrol(dd,Step+1)+Fpt(:,grslave,Step)+...
    Es(grslave)*As(grslave)*(delta_st(:,grslave,Step+1)-...
    delta_st(:,grslave,Step))/Ls(grslave);
FcontHist=Fcontrol(dd,1:Step+1);

M1(grslave,Step+1)=ds(:,grslave)^(Fpt(:,grslave,1)+sum(FcontHist));
th1(grslave,Step+1)=M1(grslave,Step+1)/kpt0(grslave,1);

M2(grslave,Step+1)=M1(grslave,Step+1)+kpt1(grslave,1)* ...
    (theta_y(grslave,1)-th1(grslave,Step+1));
th2(grslave,Step+1) =theta_y(grslave,1);
end
end

% Loading Direction Feedback (Velocity Based)
% MATLAB script to apply velocity based Loading Direction
% Feedback control strategy
%-----
for dd=1:ns
    FcontHist=Fcontrol(dd,1:Step);
    if abs(ConRot(ConMaster(dd),Step+1))> th2(ConMaster(dd),Step+1)&&...
        abs(DConRot(ConMaster(dd),Step)< ...
            abs(DConRot(ConMaster(dd),Step-1))
            Fcontrol(dd,Step+1)=-f;
    elseif abs(ConRot(ConMaster(dd),Step+1))<0.9*th1(ConMaster(dd),2)
        if sum(FcontHist)<(cap-1)*Fpt(1,ConMaster(dd),1);
            % Number of Steps for changing the force
            Chan(dd,Step+1)=abs(sum(FcontHist));
            if Chan(dd,Step+1)>=fmax
                Fcontrol(dd,Step+1)=fmax;
            elseif Chan(dd,Step+1)< fmax
                Fcontrol(dd,Step+1)=Chan(dd,Step+1);
            end
        end
    end
    for slgr=ConGroup(dd,:)
        Fpt(:,slgr,Step+1)=Fcontrol(dd,Step+1)+Fpt(:,slgr,Step)+ ...
            Es(slgr,1)*As(slgr,1)*(delta_st(:,slgr,Step+1)- ...
            delta_st(:,slgr,Step))/Ls(slgr,1);
    end
    FcontHist=Fcontrol(dd,1:Step+1);
    for grslave=ConGroup(dd,:)
        % Check that the actual Post-tensioning Force is greater than the least
        % self-centring force (FptLow)
        if min(Fpt(:,grslave,Step+1))<= FptLow(grslave)
            Fcontrol(dd,Step+1)=0;
        end
        if sum(FcontHist)<=(FptLow(grslave)-max(Fpt(:,grslave,Step+1)))
            if abs(ConRot(ConMaster(dd),Step+1))<th1(ConMaster(dd),2)

```

```

        Fcontrol(dd, Step+1)=fmax;
    else Fcontrol(dd, Step+1)=0;
    end
end
% Check that forces in strands do not exceed 70% of the Yield force
if max(Fpt(:, grslave, Step+1))>=0.7*Fys(grslave)
    Fcontrol(dd, Step+1)=-fmax;
end
Fpt(:, grslave, Step+1)=Fcontrol(dd, Step+1)+Fpt(:, grslave, Step)+...
    Es(grslave)*As(grslave)*(delta_st(:, grslave, Step+1)-...
    delta_st(:, grslave, Step))/Ls(grslave);
FcontHist=Fcontrol(dd, 1:Step+1);

M1(grslave, Step+1)=ds(:, grslave)'*(Fpt(:, grslave, 1)+sum(FcontHist));
th1(grslave, Step+1)=M1(grslave, Step+1)/kpt0(grslave, 1);

M2(grslave, Step+1)=M1(grslave, Step+1)+kpt1(grslave, 1)* ...
    (theta_y(grslave, 1)-th1(grslave, Step+1));
th2(grslave, Step+1) =theta_y(grslave, 1);
end
end

```

B.2. Stiffness Control Approach

% Frequency Analysis

% MATLAB Script to analyse the frequency content of the

% running earthquake

```

%-----
fs=1/dt; % Sampling Rate
nsteps=CtrlTime/Dt; % Number of steps within the control time
% Coninuous Frequency Content
freqRec=Hfreq+1;
if CtrlStrat==6 % (Optimal Frequency State Feedback Algorithm)
    if isempty(find(ConRot(:, 1:Step)>th1(:, 1:Step), 1))==0
        if rem(Step, nsteps)==0
            VFourier=v(1:Step/StepRat); % Portion of the earthquake
            % record to perform Fourier transform
            fs = 1/dt;
            nss=length(VFourier);
            f=fs*linspace(0, 1, nss);
            FreqCon=fft(VFourier, nss);
            FreqCon=abs(FreqCon);
            FreqArr=[f' FreqCon];
        end
        if Filter ==1 % (Activate Filter)
            % Design of the Low-Pass Filter (2nd order filter)
            % cut-off frequency
            cut_freq=max(Patterns(:, 9))*1.2/(fs/2);
            [bfilt, afilt]=ellip(2, 0.5, 1, cut_freq, 'low');
            VFourier=filter(bfilt, afilt, VFourier);
        end
    end
else
    if rem(Step, nsteps)==0
        if CtrlStrat==7 % (Response Frequency State Feedback Algorithm)

```

```

        VFourier=accResp(1:Step)'; % Portion of the response acceleration
        %                               to perform Fourier transform
    else VFourier=v(1:Step/StepRat); % Portion of the earthquake record
        %                               to perform Fourier transform
    end
    if Filter ==1
        % Design of the Low-Pass Filter (2nd order filter)
        % cut-off frequency
        cut_freq=max(Patterns(:,9))*1.2/(fs/2);
        [bfilt,afilt]=ellip(2,0.5,20,cut_freq,'low');
        VFourier=filter(bfilt,afilt,VFourier);
    end
    fs = 1/dt;
    nss=length(VFourier);
    f=fs*linspace(0,1,nss);
    FreqCon=fft(VFourier,nss);
    FreqCon=abs(FreqCon);
    FreqArr=[f' FreqCon];
end
end

```

% Pattern Optimisation

**% MATLAB script to optimise the stiffness patterns for the
% minimum frequency content**

```

%-----
for i3=1:PatR
    if rem(Step,nsteps)==0
        fn1(i3)=Patterns(i3,PatC-3); % Natural frequency of the 1st mode for
        %                               the (i3)th stiffness Pattern
        fn2(i3)=Patterns(i3,PatC-2); % Natural frequency of the 2nd mode for
        %                               the (i3)th stiffness Pattern
        Lmod1(i3)=Patterns(i3,PatC-1); % Effective participation factor of the
        %                               1st mode for the (i3)th stiffness
        %                               Pattern
        Lmod2(i3)=Patterns(i3,PatC); % Effective participation factor of the
        %                               2nd mode for the (i3)th stiffness
        %                               Pattern
    end
    %-----
    % Interpolate 1st and 2nd frequencies of the pattern
    % 1st frequency
    Content1(i3) = interp1(FreqArr(:,1),FreqArr(:,2),fn1(i3));
    % 2nd frequency
    Content2(i3) = interp1(FreqArr(:,1),FreqArr(:,2),fn2(i3));
    % Total frequency content
    TotalContent(i3)= Lmod1(i3)*Content1(i3)+Lmod2(i3)*Content2(i3);
end
OptimumPattern=find(TotalContent==min(TotalContent),1);
% Optimum stiffness pattern
OptStiff=Patterns(OptimumPattern,2:PatC-4)';

```

```

% Excitation Frequency State Feedback
% MATLAB Script to apply the Excitation Frequency State
% Feedback control strategy
%-----
Frequency_Analysis; % Invoke MATLAB script to analyse the frequency content
%                   of the running earthquake
Pattern_Optimisation; % Invoke MATLAB script to optimise the stiffness
%                   patterns for the minimum frequency content
for k3=1:ns % (number of storeys)
    if OptStiff(k3)==0
        Chan(k3,Step+1)= 0.65*Fys(ConMaster(k3))-(Fpt(1,ConMaster(k3),1)+...
            sum(Fcontrol(k3,1:Step)));
        if abs(Chan(k3,Step+1))<fmax
            Fcontrol(k3,Step+1)=Chan(k3,Step+1);
        elseif abs(Chan(k3,Step+1))>fmax
            % Number of Steps for changing the force
            if abs(round(Chan(k3,Step+1)/fmax)) >= ...
                abs(Chan(k3,Step+1)/fmax)
                stepnum=abs(round(Chan(k3,Step+1)/fmax));
            else stepnum=abs(round(Chan(k3,Step+1)/fmax))+1;
            end
            for costep=1:stepnum
                Fcontrol(k3,Step+costep)=Chan(k3,Step+1)/stepnum;
            end
        end
    elseif OptStiff(k3)==2
        Chan(k3,Step+1)= FptLow(ConMaster(k3))-(Fpt(1,ConMaster(k3),1)+...
            sum(Fcontrol(k3,1:Step)));
        if abs(Chan(k3,Step+1))<fmax
            Fcontrol(k3,Step+1)=Chan(k3,Step+1);
        elseif abs(Chan(k3,Step+1))>fmax
            % Number of Steps for changing the force
            if abs(round(Chan(k3,Step+1)/fmax)) >=abs(Chan(k3,Step+1)/fmax)
                stepnum=abs(round(Chan(k3,Step+1)/fmax));
            else stepnum=abs(round(Chan(k3,Step+1)/fmax))+1;
            end
            for costep=1:stepnum
                Fcontrol(k3,Step+costep)=Chan(k3,Step+1)/stepnum;
            end
        end
    end
end
for k3=1:ns
    for slgr=ConGroup(k3,:)
        Fpt(:,slgr,Step+1)=Fcontrol(k3,Step+1)+Fpt(:,slgr,Step)+...
            Es(slgr,1)*As(slgr,1)*(delta_st(:,slgr,Step+1)- ...
                delta_st(:,slgr,Step))/Ls(slgr,1);
    end
    FcontHist=Fcontrol(k3,1:Step+1);
    for grslave=ConGroup(k3,:)
        % Check that the actual Post-tensioning Force is greater than the
        % least self-centring force (FptLow)
        if min(Fpt(:,grslave,Step+1))< FptLow(grslave)
            Fcontrol(k3,Step+1)=+fmax;
        end
        if sum(FcontHist)<(FptLow(grslave)-max(Fpt(:,grslave,Step+1)))
            Fcontrol(k3,Step+1)=+fmax;
        end
        % Check that forces in the strands do not exceed the 70% of the
        % Yield force
        if max(Fpt(:,grslave,Step+1))>0.7*Fys(grslave)
            Fcontrol(k3,Step+1)= -fmax;
        end
    end
end

```

```

Fpt(:,grslave,Step+1)=Fcontrol(k3,Step+1)+Fpt(:,grslave,Step)+...
    Es(grslave)*As(grslave)*(delta_st(:,grslave,Step+1)-...
    delta_st(:,grslave,Step))/Ls(grslave);
FcontHist=Fcontrol(k3,1:Step+1);

M1(grslave,Step+1)=ds(:,grslave)'+(Fpt(:,grslave,1)+sum(FcontHist));
th1(grslave,Step+1)=M1(grslave,Step+1)/kpt0(grslave,1);

M2(grslave,Step+1)=M1(grslave,Step+1)+kpt1(grslave,1)* ...
    (theta_y(grslave,1)-th1(grslave,Step+1));
th2(grslave,Step+1) =theta_y(grslave,1);
end
end

```

B.3. Deformation Regulation Approach

```

% Uniform Inter-storey Drift
% MATLAB script to apply Uniform Inter-storey Drift strategy
%-----
for dd=1:ns
    if dd==1
        height(dd)= Coor(Connectivity(Beamnum+Barnum+ConMaster(dd),2),3);
        drift(dd,Step+1)=u(3*Connectivity(Beamnum+Barnum+ConMaster(dd),2)
            ... -2,Step+1);
    else height(dd)= Coor(Connectivity(Beamnum+Barnum+ConMaster(dd),2),3)-
        ...Coor(Connectivity(Beamnum+Barnum+ConMaster(dd-1),2),3);
        drift(dd,Step+1) = u(3*Connectivity(Beamnum+Barnum+ConMaster(dd),2)-
            ... 2,Step+1)-u(3*Connectivity(Beamnum+Barnum+ConMaster(dd-1),2)-
            ... 2,Step+1);
    end
    driftRat(dd,Step+1)=drift(dd,Step+1)/height(dd);
    if abs(driftRat(dd,Step+1))>treshold
        if abs(drift(dd,Step))>abs(drift(dd,Step+1)) && ...
            abs(drift(dd,Step))> abs(drift(dd,Step-1))
            Peakcode(dd,Step)=1;
        end
    end
end
if isempty(find(Peakcode(:,Step)==1, 1))==0
    aver=sum(driftRat(:,Step+1))/ns;
    % Linear Multiplication
    for dd=1:ns
        Chan(dd,Step+1)=((driftRat(dd,Step+1)-aver)/aver)* ...
            (Fpt(1,ConMaster(dd),1)+sum(Fcontrol(dd,1:Step)));
        if abs(Chan(dd,Step+1))<fmax
            Fcontrol(dd,Step+1)=Chan(dd,Step+1);
        elseif abs(Chan(dd,Step+1))>fmax
            % Number of Steps for changing the force
            if abs(round(Chan(dd,Step+1)/fmax)) >=...
                abs(Chan(dd,Step+1)/fmax)
                stepnum=abs(round(Chan(dd,Step+1)/fmax));
            else stepnum=abs(round(Chan(dd,Step+1)/fmax))+1;
            end
            for costep=1:stepnum
                Fcontrol(dd,Step+costep)=Chan(dd,Step+1)/stepnum;
            end
        end
    end
end
end
end

```



```

for dd=1:ns
    for slgr=ConGroup(dd,:)
        Fpt(:,slgr,Step+1)=Fcontrol(dd,Step+1)+Fpt(:,slgr,Step)+ ...
            Es(slgr,1)*As(slgr,1)*(delta_st(:,slgr,Step+1)- ...
                delta_st(:,slgr,Step))/Ls(slgr,1);
    end
    FcontHist=Fcontrol(dd,1:Step+1);
    for grslave=ConGroup(dd,:)
        % Check that the actual Post-tensioning Force is greater than the
        % least self-centring force (FptLow)
        if min(Fpt(:,grslave,Step+1))< FptLow(grslave)
            Fcontrol(dd,Step+1)=+fmax;
        end
        if sum(FcontHist)<(FptLow(grslave)-max(Fpt(:,grslave,Step+1)))
            Fcontrol(dd,Step+1)=+fmax;
        end
        % Check that forces in the strands do not exceed the 70% of the
        % Yield force
        if max(Fpt(:,grslave,Step+1))>0.65*Fys(grslave)
            Fcontrol(dd,Step+1)= -fmax;
        end
        Fpt(:,grslave,Step+1)=Fcontrol(dd,Step+1)+Fpt(:,grslave,Step)+...
            Es(grslave)*As(grslave)*(delta_st(:,grslave,Step+1)-...
                delta_st(:,grslave,Step))/Ls(grslave);
        FcontHist=Fcontrol(dd,1:Step+1);
        M1(grslave,Step+1)=ds(:,grslave) '* (Fpt(:,grslave,1)+sum(FcontHist));
        th1(grslave,Step+1)=M1(grslave,Step+1)/kpt0(grslave,1);

        M2(grslave,Step+1)=M1(grslave,Step+1)+kpt1(grslave,1)* ...
            (theta_y(grslave,1)-th1(grslave,Step+1));
        th2(grslave,Step+1) =theta_y(grslave,1);
    end
end
end

```

```

% Simplified Uniform Inter-storey Drift (LUIDA)
% MATLAB script to apply the Simplified Uniform Inter-storey
% Drift algorithm
%-----
for dd=1:ns
    if dd==1
        height(dd)= Coor(Connectivity(Beamnum+Barnum+ConMaster(dd),2),3);
        drift(dd,Step+1)=u(3*Connectivity(Beamnum+Barnum+ConMaster(dd),2)
            ... -2,Step+1);
    else
        height(dd)= Coor(Connectivity(Beamnum+Barnum+ConMaster(dd),2),3)-
            ...Coor(Connectivity(Beamnum+Barnum+ConMaster(dd-1),2),3);
        drift(dd,Step+1) = u(3*Connectivity(Beamnum+Barnum+ConMaster(dd),2)-
            ... 2,Step+1)-u(3*Connectivity(Beamnum+Barnum+ConMaster(dd-1),2)-
            ... 2,Step+1);
    end
    driftRat(dd,Step+1)=drift(dd,Step+1)/height(dd);
    if abs(driftRat(dd,Step+1))>treshold
        if abs(drift(dd,Step))>abs(drift(dd,Step+1)) && ...
            abs(drift(dd,Step))> abs(drift(dd,Step-1))
            Peakcode(dd,Step)=1;
        end
    end
end
end
if isempty(find(Peakcode(:,Step)==1, 1))==0
    aver=sum(driftRat(:,Step+1))/ns;
    % Linear Multiplication
    for dd=1:ns
        Chan(dd,Step+1)=((driftRat(dd,Step+1)- ...aver)/aver)* ...
            (Fpt(1,ConMaster(dd),1)+sum(Fcontrol(dd,1:Step)));
        if abs(Chan(dd,Step+1))<fmax
            Fcontrol(dd,Step+1)=Chan(dd,Step+1);
        elseif abs(Chan(dd,Step+1))>fmax
            % Number of Steps for changing the force

```

```

        if abs(round(Chan(dd, Step+1)/fmax)) >=abs (Chan(dd, Step+1)/fmax)
            stepnum=abs(round(Chan(dd, Step+1)/fmax));
        else stepnum=abs(round(Chan(dd, Step+1)/fmax))+1;
        end
        for costep=1:stepnum
            Fcontrol(dd, Step+costep)=Chan(dd, Step+1)/stepnum;
        end
    end
end
end
if Fcontrol(:, Step)==0
    if sum(Fcontrol(:, 1:Step)')~=0
        Fcontrol(:, Step+1)=0;
    end
end
for dd=1:ns
    for slgr=ConGroup(dd, :)
        Fpt(:, slgr, Step+1)=Fcontrol(dd, Step+1)+Fpt(:, slgr, Step)+Es(slgr, 1)*...
            As(slgr, 1)*(delta_st(:, slgr, Step+1)-delta_st(:, slgr, Step))/ ...
            Ls(slgr, 1);
    end
    FcontHist=Fcontrol(dd, 1:Step+1);
    for grslave=ConGroup(dd, :)
        % Check that the actual Post-tensioning Force is greater than the
        % least self-centring force (FptLow)
        if min(Fpt(:, grslave, Step+1)) < FptLow(grslave)
            Fcontrol(dd, Step+1)=+0;
        end
        if sum(FcontHist) < (FptLow(grslave)-max(Fpt(:, grslave, Step+1)))
            Fcontrol(dd, Step+1)=+0;
        end
        % Check that forces in the strands do not exceed the 70% of the
        % Yield force
        if max(Fpt(:, grslave, Step+1)) > 0.65*Fys(grslave)
            Fcontrol(dd, Step+1)= -0;
        end
        Fpt(:, grslave, Step+1)=Fcontrol(dd, Step+1)+Fpt(:, grslave, Step)+...
            Es(grslave)*As(grslave)*(delta_st(:, grslave, Step+1)-...
            delta_st(:, grslave, Step))/Ls(grslave);
        FcontHist=Fcontrol(dd, 1:Step+1);

        M1(grslave, Step+1)=ds(:, grslave)'*(Fpt(:, grslave, 1)+sum(FcontHist));
        th1(grslave, Step+1)=M1(grslave, Step+1)/kpt0(grslave, 1);

        M2(grslave, Step+1)=M1(grslave, Step+1)+kpt1(grslave, 1)* ...
            (theta_y(grslave, 1)-th1(grslave, Step+1));
        th2(grslave, Step+1) =theta_y(grslave, 1);
    end
end
end

```

Appendix C

ACCELERATION RESPONSE OF CONTROLLED PT FRAMES

The main body of this thesis presented results of the displacement response of passive and semi-active control of PT frames. Since the acceleration response of the structure is an important response that affects the non-structural elements, it should be investigated and cannot be neglected. In this appendix are summarised the acceleration response results of controlled PT frames.

C.1. Passive PT Frames

In this section is presented a summary of acceleration response of passively controlled PT frames. These results include the effect of post-tensioning forces on the acceleration of the frame and a comparison between the acceleration response of a conventional MRF and a passive PT frame. Displacement response of these frames was presented in Chapter 6.

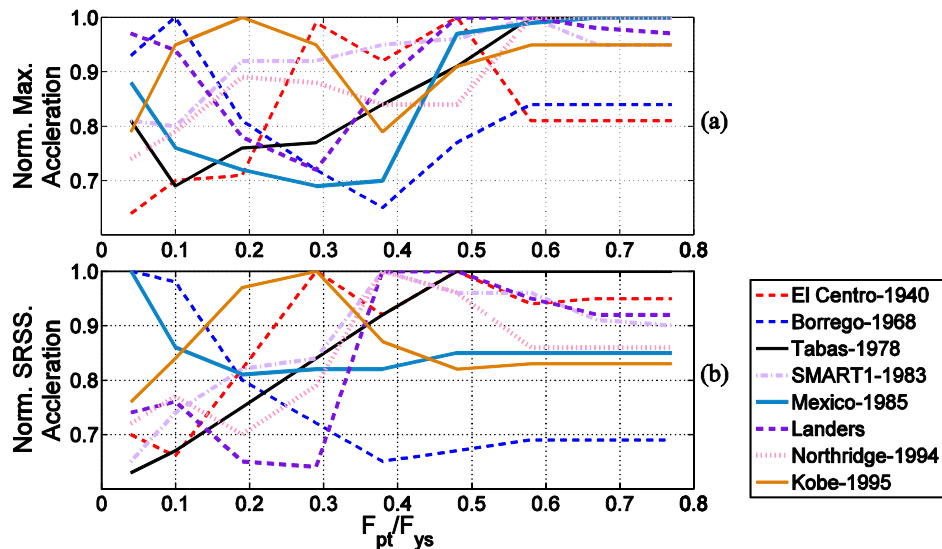


Figure C.1: Effects of variation in post-tensioning forces on frame acceleration response. (a) Normalised maximum 3rd storey acceleration and (b) normalised SRSS of 3rd storey acceleration.

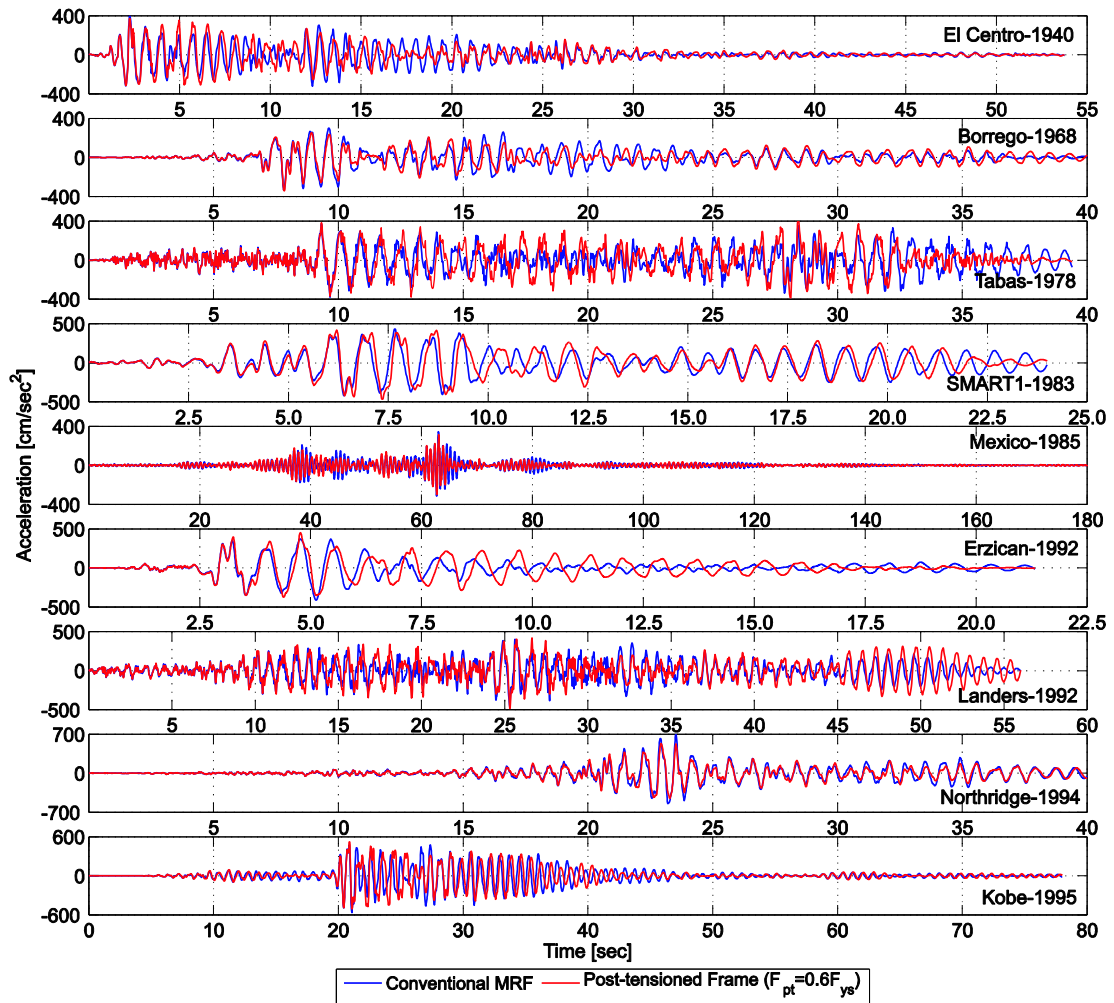


Figure C.2: Comparison of top storey acceleration for PT frame and conventional MRF.

C.2. Semi-Active Control of PT Frames Using Energy Dissipation Control Approach

In this section is presented a summary of the acceleration response resulted from applying the semi-active control on PT frames using energy dissipation control approach. These results include the three energy-based control algorithms introduced in the thesis: (i) displacement-based loading direction feedback algorithm (DB-LDFA), (ii) modified displacement-based loading direction feedback algorithm (MDB-LDFA) and (iii) velocity-based loading direction feedback algorithm (VB-LDFA).

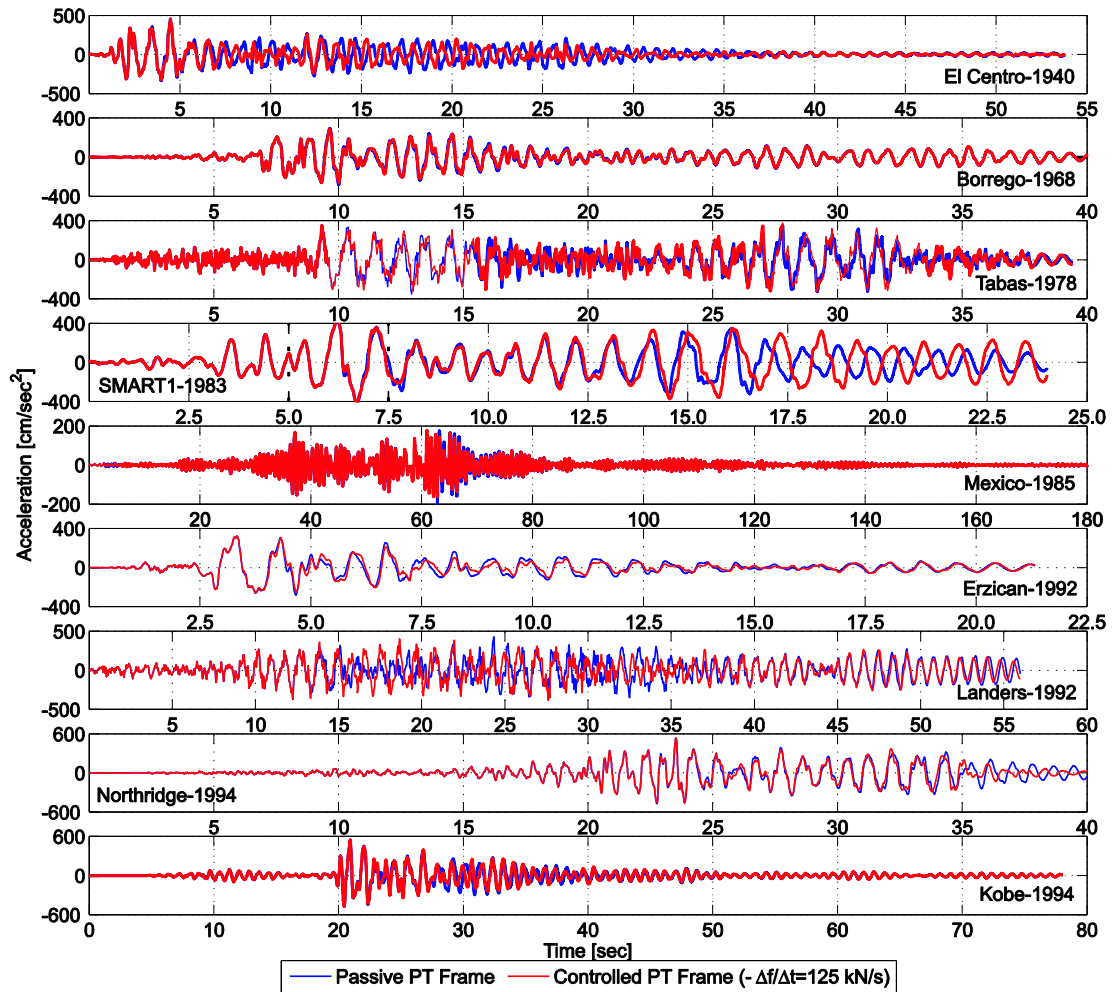


Figure C.3: Top storey acceleration time histories.

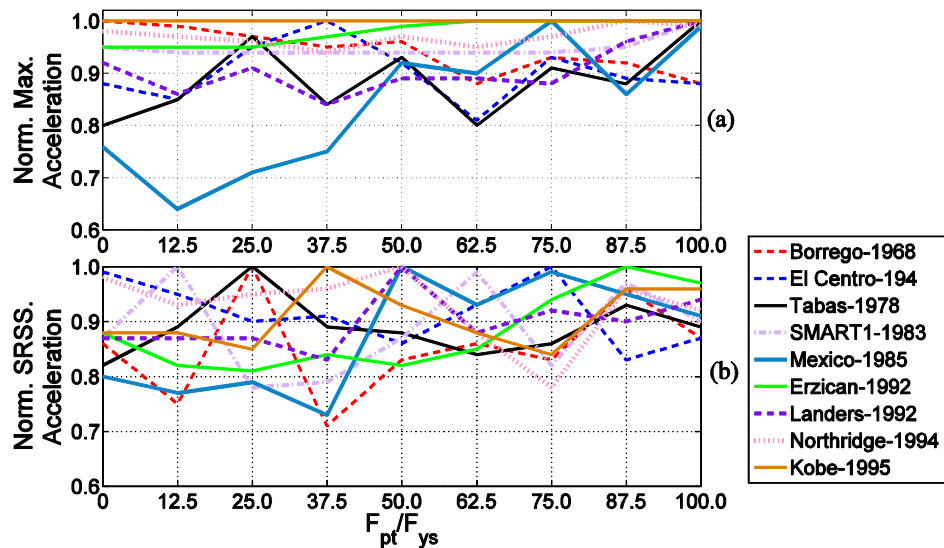


Figure C.4: Effect of control force rate on frame behaviour: (a) maximum top storey acceleration and (b) SRSS of top storey acceleration.

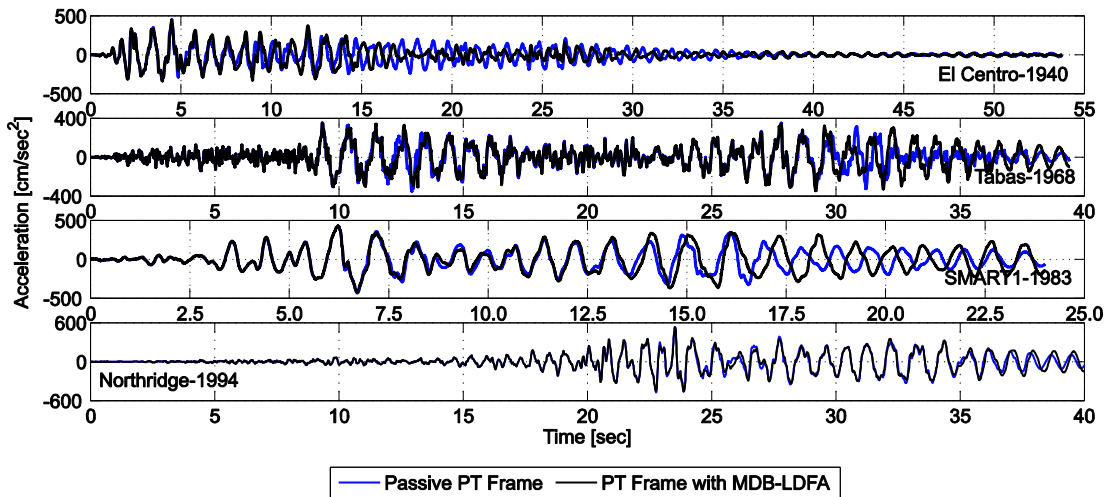


Figure C.5: PT frame response with *MDB-LDFA*.

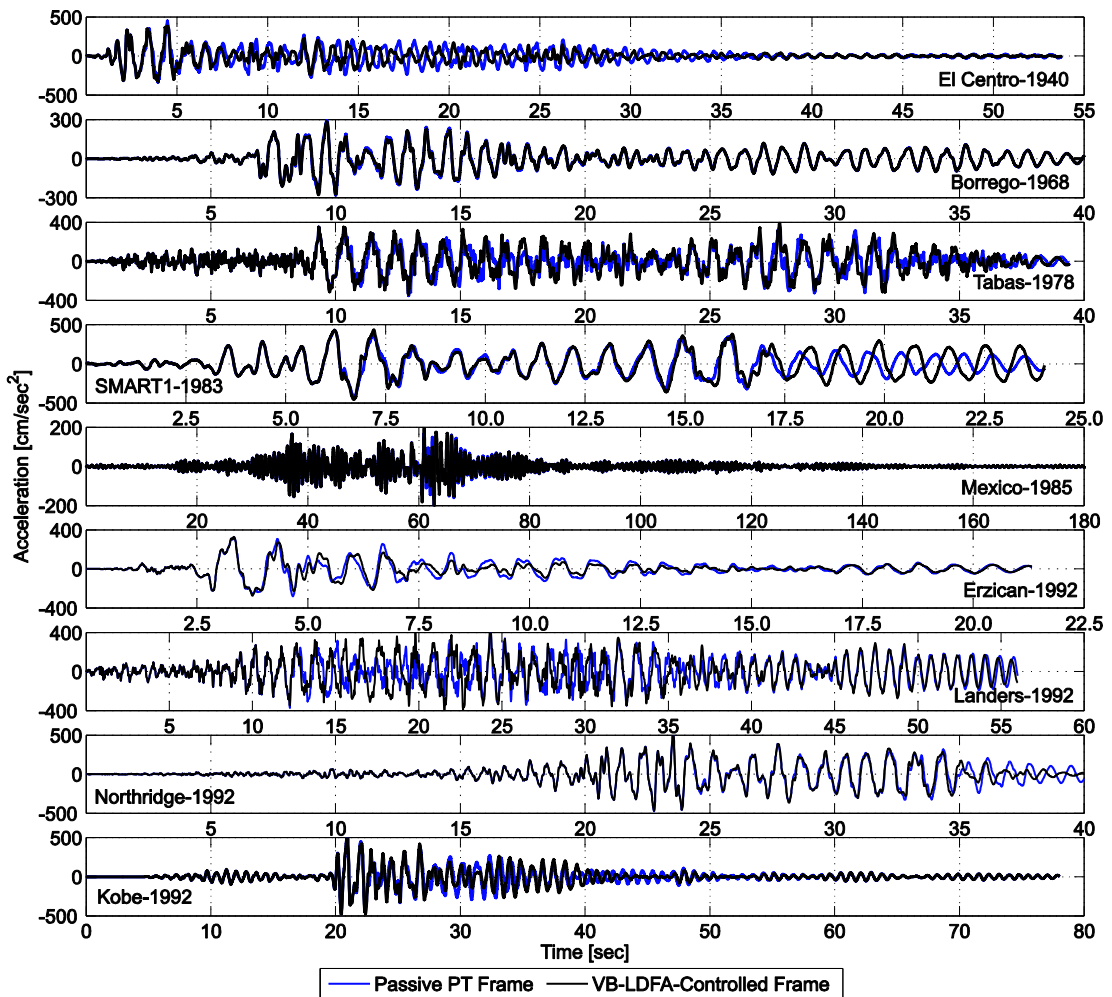


Figure C.6: Acceleration response of passive *VB-LDFA*-controlled PT frames.

C.3. Semi-Active Control of PT Frames Using Stiffness Control Approach

In this section are presented acceleration response results obtained from applying the stiffness control algorithms on post-tensioned steel frames. These results include three control algorithms classified based on the input signal: (i) excitation frequency state feedback algorithm (EFSFA), (ii) response frequency state feedback algorithm (RFSFA) and (iii) filtered excitation frequency state feedback algorithm (FEFSFA).

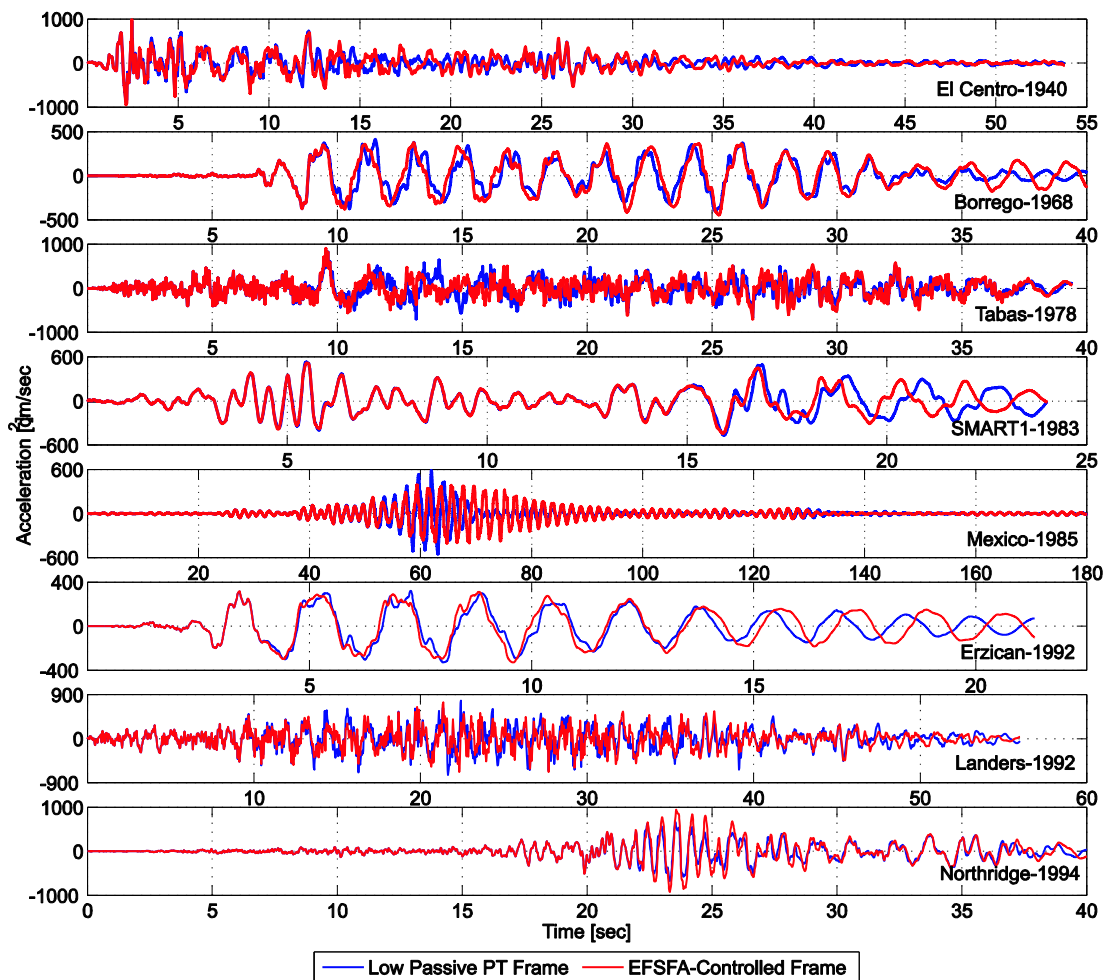


Figure C.7: Top storey acceleration for low passive and *EFSFA*-controlled PT frames (CtrlTime=3.0 sec).

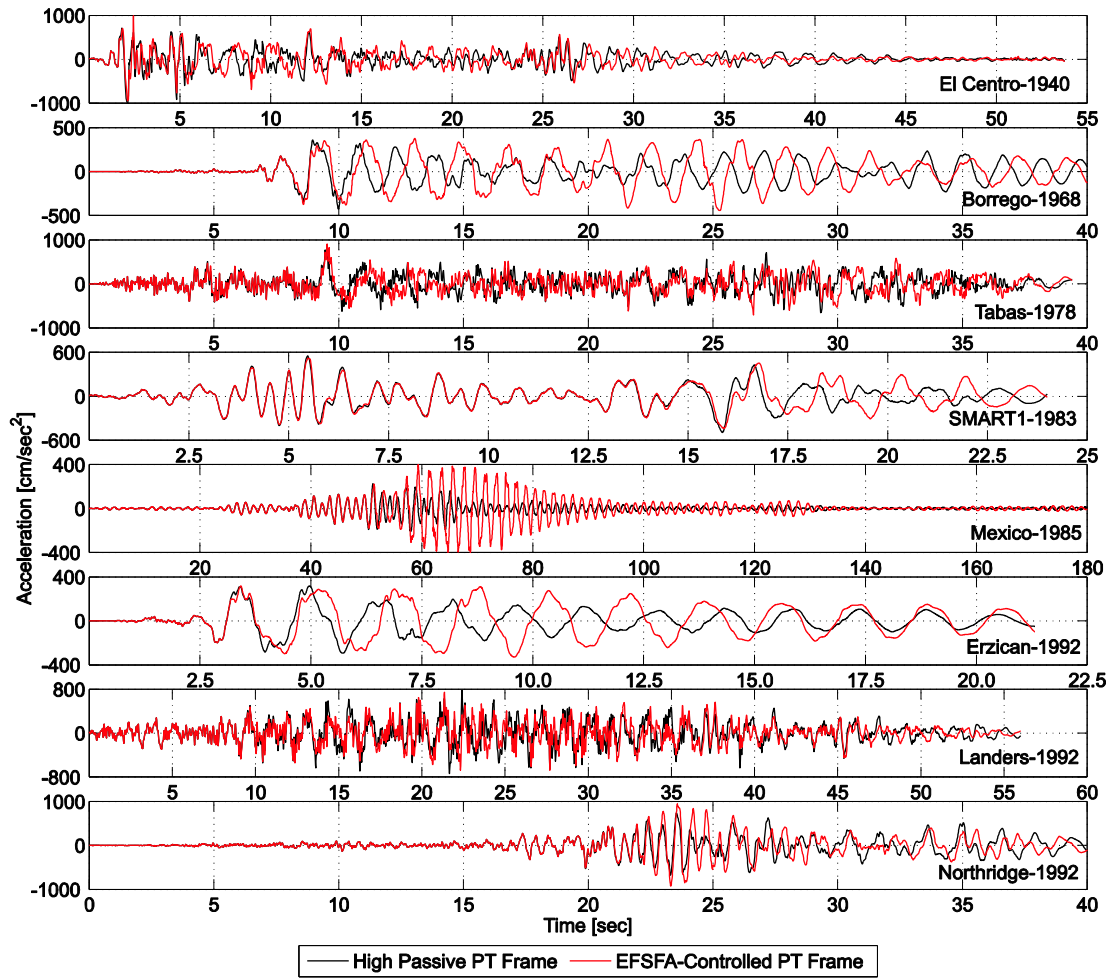


Figure C.8: Top storey acceleration for high passive and *EFSFA*-controlled PT frames (CtrlTime=3.0 sec).

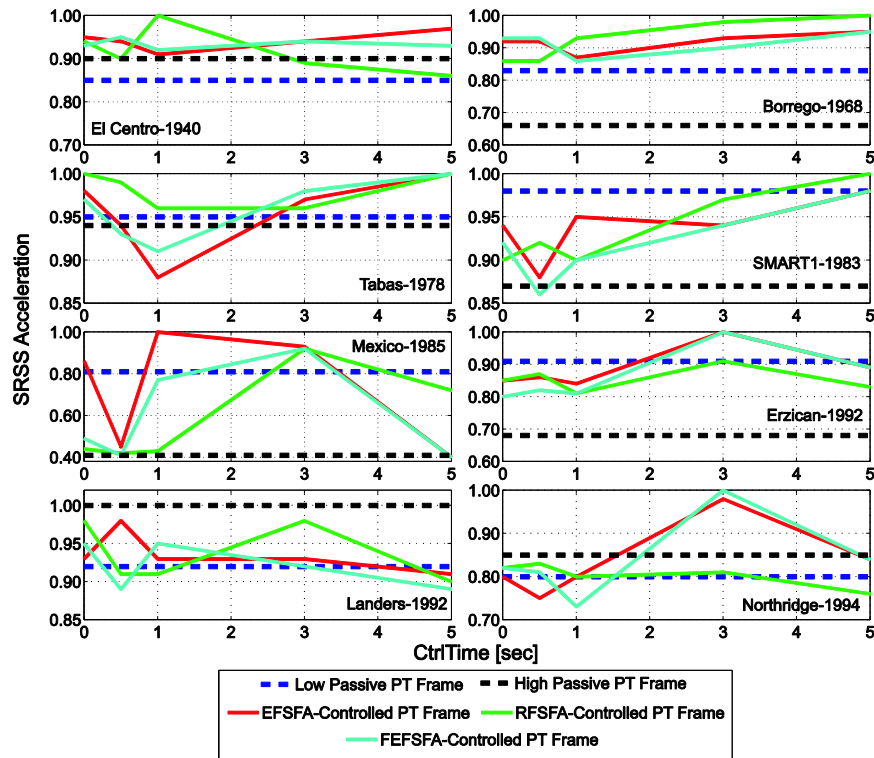


Figure C.9: Effect of control time interval (CtrlTime) on the performance of stiffness control algorithms.

C.3. Semi-Active Control of PT Frames Using Deformation Regulation Control Approach

In this section are presented results of the acceleration response obtained from applying the deformation regulation control approach on PT steel frames. These results include the acceleration response of UIDA-controlled frame compared with the acceleration results of passive PT frame with low and high post-tensioning forces. The effect of the drift threshold (Thr) on the acceleration response is also presented. In addition, results of the acceleration response obtained from applying the Simplified Uniform Inter-storey Drift Algorithm (UIDA) on the six-storey PT frame are presented.

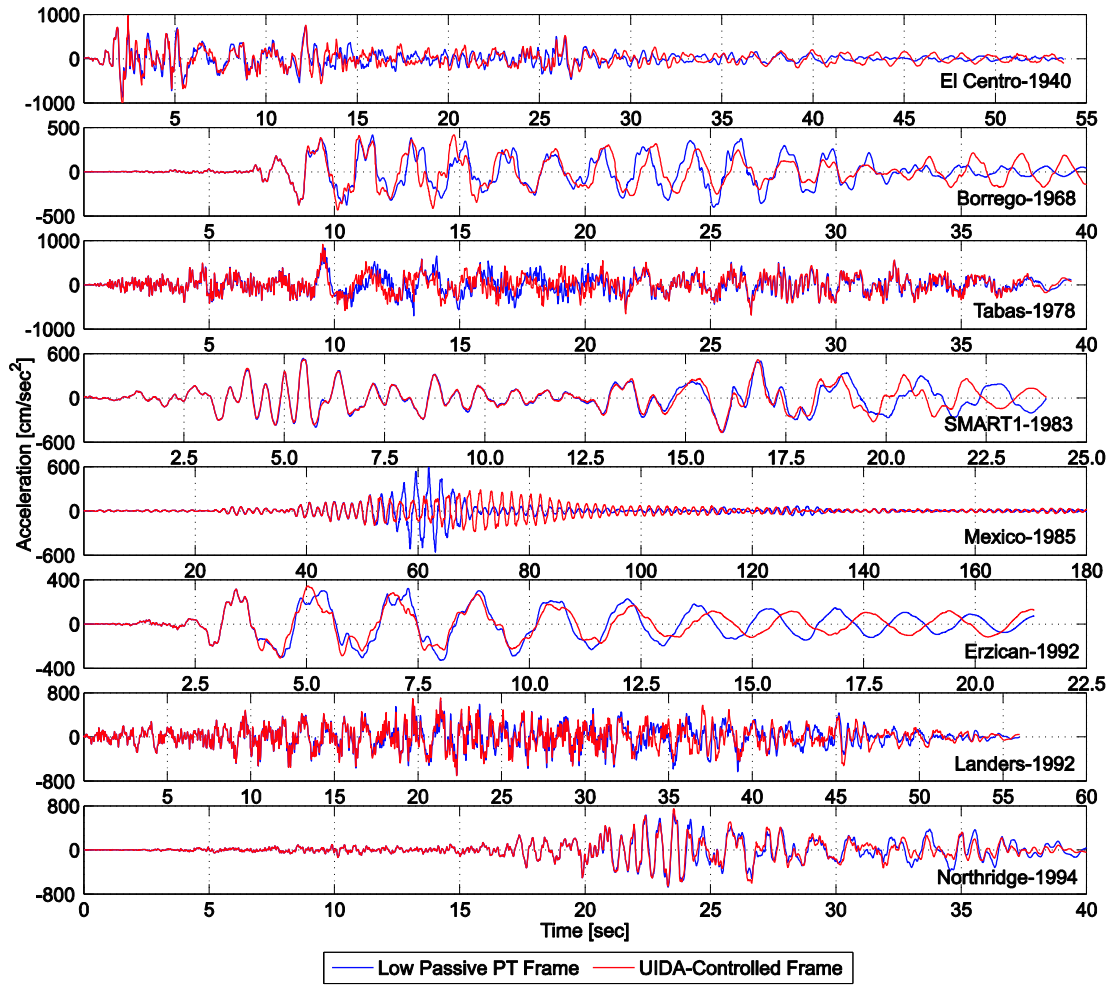


Figure C.10: Top storey acceleration for low passive and *UIDA*-controlled PT frames (Thr=0.005).

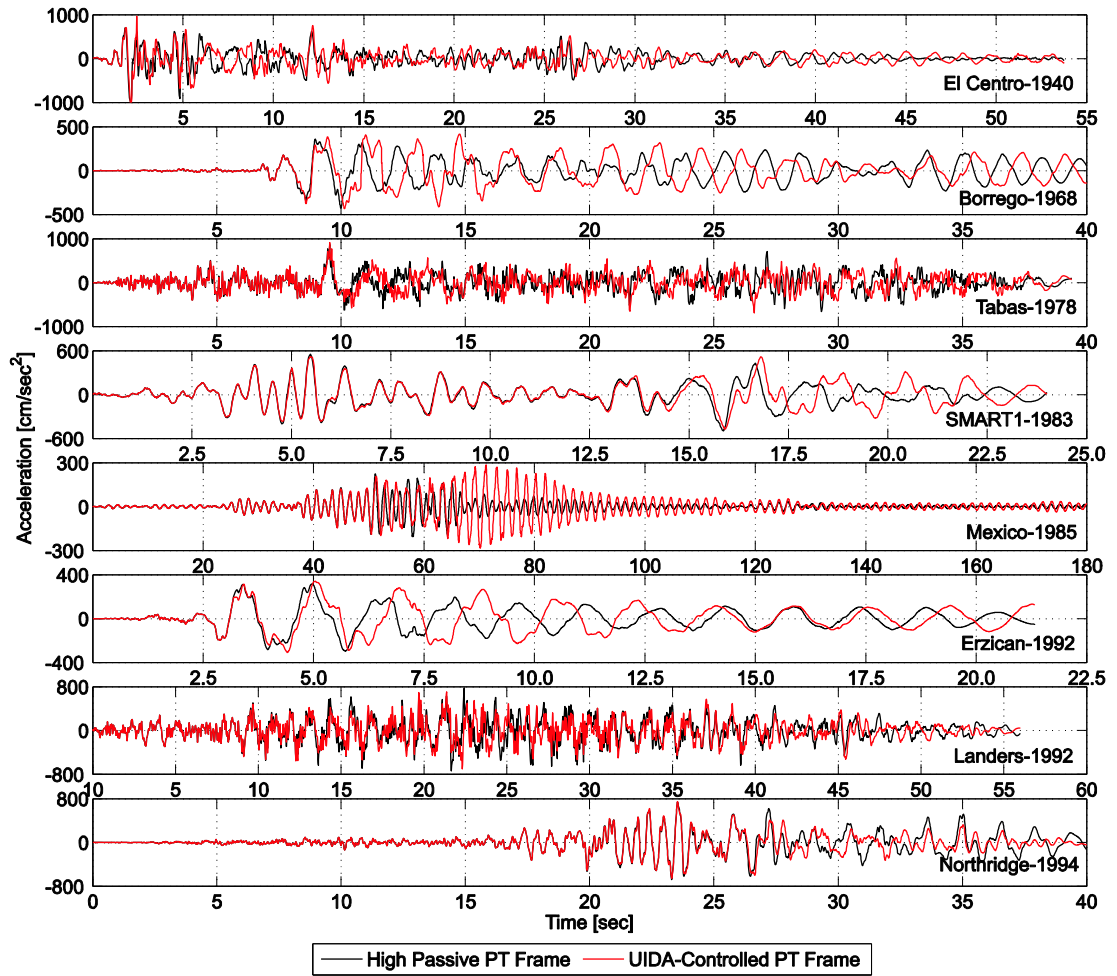


Figure C.11: Top storey acceleration for high passive and *UIDA*-controlled PT frames ($Thr=0.005$).

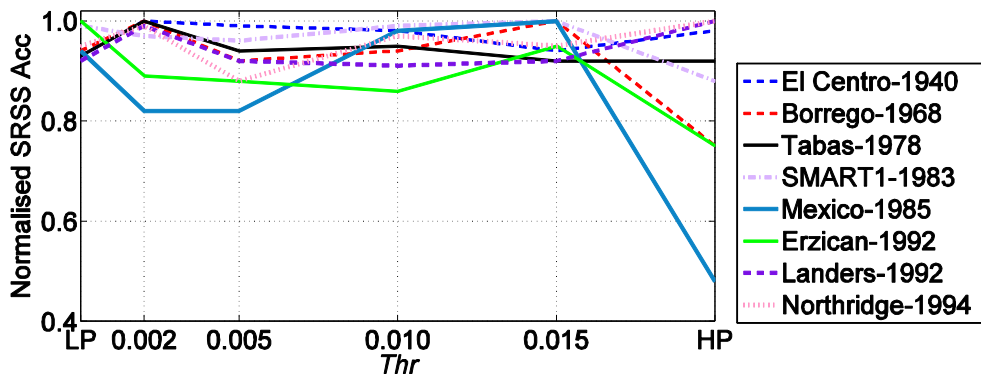


Figure C.12: Effect of the drift threshold on the top storey acceleration.

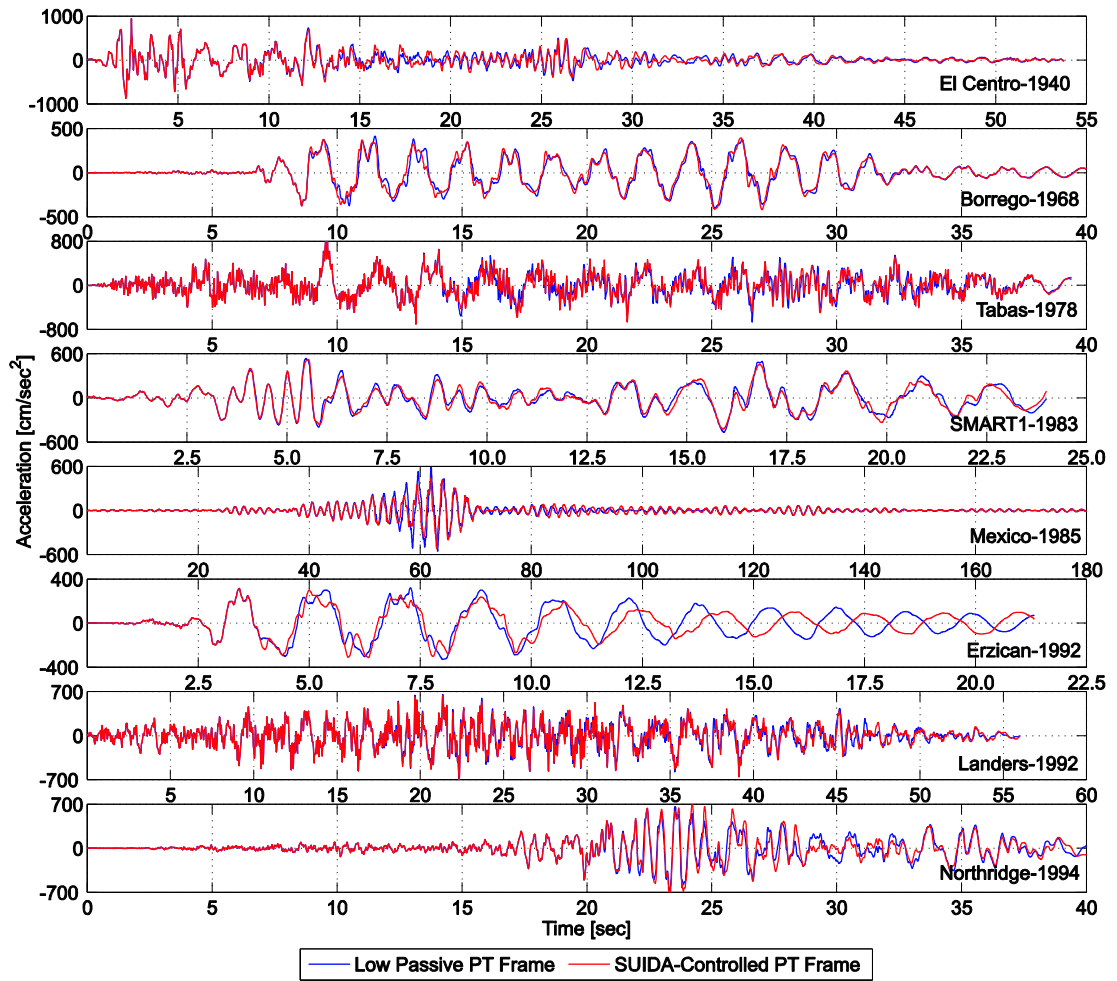


Figure C.13: Top storey acceleration for low passive and *SUIDA*-controlled PT frames (Thr=0.005).

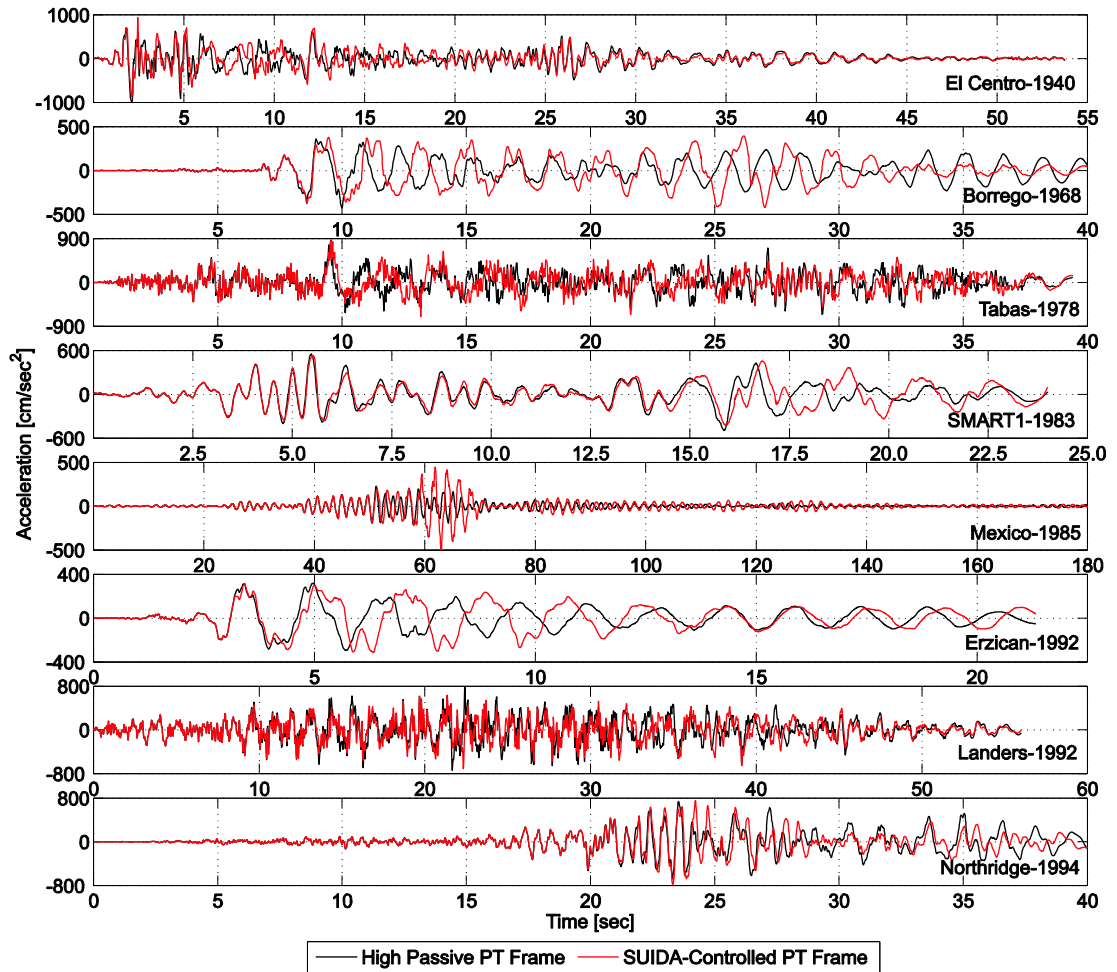


Figure C.14: Top storey acceleration for high passive and *SUIDA*-controlled PT frames (Thr=0.005).